This is to certify that the

dissertation entitled

ELECTRON SPIN ECHO ENVELOPE MODULATION STUDIES OF SOME TRANSITION METAL MODEL COMPLEXES

presented by

HONG IN LEE

has been accepted towards fulfillment
of the requirements for

PH.D degree in CHEMISTRY

JOHN L. McCRACKEN

John L McCracken

Major professor

Date 7/6/94

ABSTRACT

ELECTRON SPIN ECHO ENVELOPE MODULATION STUDIES OI SOME TRANSITION METAL MODEL COMPLEXES

By

Hong In Lee

Two different lines of pulsed-EPR experiments linked by t common theme of further developing electron spin echo envelo modulation (ESEEM) methods for the determination of structure abo paramagnetic centers in randomly ordered samples are described. The fi set of measurements involve the extension of a recently developed fo pulse ESEEM method to measure the proton hyperfine couplings strongly bound water ligands to paramagnetic transition ions. The secc project involves the use of standard ESEEM methods to characterize solution structures of some Cu(II)-pteridine complexes.

Four-pulse ESEEM studies aimed at characterizing the hyperf interactions between protons of axially bound water molecules and nickel ion of $Ni(III)(CN)_4(H_2O)_2^-$ were carried out. Because the liga hyperfine coupling of the strongly bound water protons to Ni(III) characterized by a large anisotropic interaction, an ESEEM feature at sum combination frequency, $\nu_\alpha+\nu_\beta$, that shows pronounced shifts fr twice the proton Larmor frequency is observed. Theoretical simulation

the magnetic field dependence of the $\nu_\alpha+\nu_\beta$ lineshapes and frequency shift from the twice the Larmor frequency gave an effective Ni-H dipole-dipol distance of 2.33±0.03 Å and a θ_n, the orientation for the principal axi system of the ^1H hyperfine coupling tensor with respect to the g_3 axis c the Ni(III) g-tensor, of 18±3°. The τ-suppression behavior of the $\nu_\alpha+\nu$ lineshape at a fixed magnetic field position was used to place more exac constraints on the isotropic hyperfine coupling constant than possible with simple two-pulse approach. An isotropic hyperfine coupling constant c 2.5±0.5 MHz was found for the bound axial water protons.

Four-pulse ESEEM studies aimed at characterizing hyperfin interactions between protons of equatorially and axially bound wate molecules and the copper ion of $Cu(II)(H_2O)_6^{2+}$ were carried ou Theoretical simulation of the magnetic field dependence of the proton sur combination lineshape revealed an effective Cu-H distance of 2.49 Å, an showed that θ_N, the angle between the principal axis of the ligan hyperfine tensor and the g_3 of the Cu(II) electron g-tensor, can b discribed by a distribution of values ranging from 71° to 90°. An isotropi hyperfine coupling constant of ≤ 4 MHz for the equatorially bound wate protons was estimated. Attempts were made to distinguish the sur combination peaks of the axially bound water protons by using the τ suppression behavior of the four-pulse ESEEM spectra. It was found tha the intensities and lineshapes of the sum combination peaks of the axia protons are relatively well developed and distinguished from the sur combination peaks of the equatorial protons when τ is around values give by n/νI (n=integer). Simulation of the frequency shift of the axial proto sum combination peaks *vs.* magnetic field strength yielded an effective Cu

H distance of 3.05 Å, θ_N of 11° and an isotropic hyperfine coupling of ≤ MHz.

ESEEM measurements were also used to characterize the ligation o pteridine ligands to Cu(II) in a variety of complexes prepared in aqueou and non-aqueous solvents. These studies were aimed at understanding th structural relationship between the Cu(II) and pterin cofactors i Phenylalanine Hydroxylase (PAH) from *Chromobacterium Violaceum*. Fo the model compound, $Cu(II)(ethp)_2(H_2O)_2$ (ethp = 2-ethylthio-4 hydroxypterin), X-ray crystallographic studies showed bidentat coordination of ethp through O-4 and N-5. ESEEM spectra obtained fo this compound show intense, sharp peaks at 0.6, 2.4, 3.0 MHz and a broa peak at 5.4 MHz. The spectrum is indicative of two identically coupled ^{14} nuclei and is assigned to N-3 of the coordinated ethp ligands. Simila spectra were obtained for a Cu(II)-folic acid (FA) complex at pH=9.5 i aqueous media. ESEEM studies of compounds where mixed equatoria axial ligation of the pterin moiety show little or no ^{14}N contributions i their ESEEM spectra. Examples of a complex of this type includ Cu(II)(bpy)(PC) where N-5 is equatorially bound while O-4 is axiall coordinated (PC = 6-carboxy pterin). Because the ^{14}N ESEEM respons from equatorially coordinated pterin is intense and the peaks occur in spectral region where there would be little interference from the protei the experimental results are most consistent with a mixed equatorial-axi ligation of this cofactor at the Cu(II) site of PAH.

To My Parents and Wife

ACKNOWLEDGMENT

Somebody said, "Life is a voyage." I feel that I am finishing a portion of the voyage. For the last five years Prof. John McCracken has been my private captain. Without his brilliant guidance and support I might not have finished the voyage. I would like to express my deep thanks to Prof. John McCracken, my captain. Also I would like to thank my committee members, Prof. G. Babcock, Prof. C. K. Chang, and Prof. M. Kanatzidis. I would like to thank Prof. J. Jackson, Prof. R. Cukier, and Prof. J. Yesinowski for their help. I would like to thank my colleagues, Dr. Kurt Warncke, Michelle Mac, Kerry Reidy, Gyorgy Filep, and Vladimir Bouchev for their help and discussions.

I would like to give my heartful thanks to my parents and sisters for their endless love. Special thanks should be given to my wife and daughter for their love and ability to create happiness.

LIST OF CONTENTS

LIST OF TABLES

LIST OF FIGURES

LIST OF ABBREVIATIONS

bpy	2,2'-bipyridine
CW	Continuous Wave
DEER	Double Electron Electron Resonance
dien	Diethylenetriamine
ENDOR	Electron Nuclear Double Resonance
EPR	Electron Paramagnetic Resonance
ESE	Electron Spin Echo
ethp	2-ethylthio-4-hydroxypterin
ESE-ENDOR	Electron Spin Echo Detected-ENDOR
ESE-EPR	Electron Spin Echo Detected-EPR
ESEEM	Electron Spin Echo Envelope Modulation
FA	Folic acid
FID	Free Induction Decay
FT	Fourier Transformation
FWHM	Full Width at Half Maximum
HFI	Hyperfine Interaction
HYSCORE	Hyperfine Sublevel Correlation Spectroscopy
MW	Microwave
NQI	Nuclear Quadrupole Interaction
NZI	Nuclear Zeeman Interaction
PAH	Phenylalanine Hydroxylase

PAS	Principal Axis System
PC	6-carboxy pterin
TPP	Tetraphenylporphyrin
TWT	Travelling Wave Tube

I. INTRODUCTION

Although nuclear spin echoes resulting from the application resonant radio frequency pulses were first reported by Hahn in 1950,[1] t application of pulse methods to electron spin resonance has been slow develop. Reasons for this slow development included the lack of fast digit electronics, required to generate electron spin echoes using microwa (MW) pulses, and restrictions imposed by microwave pulse bandwidt Most of the early experiments utilized ESE to measure electron sp relaxation times.[2] Nuclear modulations of the electron spin echo amplitu were unexpectedly observed by two independent groups during these ear experiments on electron spin relaxation.[3,4] Further experimental a theoretical studies of these nuclear modulation effects, commonly referr to as electron spin echo envelope modulation (ESEEM), showed that t modulation depths and frequencies are related to the electron-nucle couplings.[5-8] Many technical problems in MW pulse generation and da collection have been solved within the past 15 years. As a result, electr paramagnetic resonance (EPR) studies utilizing MW pulse techniques a being rapidly developed to open a new renaissance in the study paramagnetic species.[9-11] Several different pulse sequences and da collection schemes have been developed for pulsed-EPR spectroscop Each scheme has its own characteristics and applications depending on t types of radical centers and the desired information.[12]

Theoretical studies have revealed that electron spin echo envelo modulation effects are observed when the nuclear hyperfine states a quantized along effective fields that differ between electron spin manifol In other words, when the hyperfine interactions between unpaired electr and magnetic nuclei contain anisotropic couplings, the high-field nucl hyperfine eigenstates are mixed so that all EPR transitions ($\Delta M_S=\pm$ $\Delta M_I=0$) between α and β electron spin manifolds can simultaneously occ in response to a resonant MW pulse. The resulting interferences betwe the EPR transitions give rise to nuclear modulation effects. The effecti frequency width of the fourier transform components of the MW puls used in ESEEM experiments depend on the pulse width and are genera ca. 80 MHz . Therefore, only weak hyperfine interactions (< 40 MHz) a observed in ESEEM making it complementary to conventional CW-EI where small hyperfine couplings are not resolved due to inhomogeneo line broadening. ESEEM can be applied to not only crystalline samples b also randomly oriented powder or glassy paramagnetic compound Because ESEEM spectra are most sensitive to anisotropic hyperfi interactions between magnetic nuclei and the unpaired electron, th provide structural information about the paramagnetic center.

Two-pulse and three-pulse or stimulated echo ESEEM are mo routine pulsed-EPR methods and have been very well studied. Two-pul ESEEM measurements are carried out with a $\pi/2$-τ-π pulse sequence whe τ is the time interval between the first and second MW pulses. Electr spin echoes are produced at a time, τ, after the second pulse. In a two-pul ESEEM experiment, echo intensities are recorded as a function of the ti interval, τ. The stimulated echo is generated at time τ after the third pul of a three $\pi/2$ pulse sequence ($\pi/2$-τ-$\pi/2$-T-$\pi/2$). The echo amplitudes a

collected as a function of T, the time interval between the second and third pulses. The spectral resolution of stimulated ESEEM is generally better than that of two-pulse ESEEM because the decay time of two-pulse echo is restricted by the relatively short phase memory time (T_M) while the stimulated echo decay is determined by the electron spin-lattice relaxation time, T_1, or nuclear spin-spin relaxation time, T_{2n}. In ESEEM experiments, the choice of pulse scheme depends on the purpose of the experiment. Even though the stimulated ESEEM experiment has better resolution, the spectra suffer from τ- suppression effects which cause distortion of the ESEEM lineshapes. However, the suppression effect can be used to suppress unwanted echo modulations and identify correlations between peaks. In two pulse ESEEM, the lineshapes are not distorted, but the spectral resolution is limited as mentioned above. The two-pulse scheme is applicable when the hyperfine interaction is strongly anisotropic. Two-pulse ESEEM spectra have sum ($\nu_\alpha+\nu_\beta$) and difference ($\nu_\alpha-\nu_\beta$) combination bands as well as fundamental frequencies (ν_α, ν_β), while stimulated ESEEM experiments show only the fundamental frequencies. For the case of strong anisotropic hyperfine coupling, the fundamental bands are spread over a wide frequency range for randomly oriented samples, making them difficult to detect. The peak positions of the sum combination bands are directly related to the anisotropic portion of the hyperfine interactions, and have a narrow linewidth making them easy to detect. The two-pulse sequence can be most useful for such cases.[13,14]

A Four-pulse ($\pi/2$-τ-$\pi/2$-T/2-π-T/2-$\pi/2$) ESEEM method has also been suggested recently.[15] In this experiment, a π-pulse is inserted in the middle of the second and third pulses of the three-pulse ESEEM sequence and the time domain ESEEM data are collected as a function of T, the time

interval between the second and fourth pulses. Here, sum ($\nu_\alpha+\nu_\beta$) and difference ($\nu_\alpha-\nu_\beta$) combination bands are also found, but with improved spectral resolution because the spin coherences decay by a T_1 process as in a stimulated echo experiment. Few results from four-pulse experiments have been reported.[16] For detection of the combination bands, four-pulse experiments have the advantage of better spectral resolution when compared to two-pulse ESEEM results. Also, the τ-suppression behavior of the four-pulse echo modulation experiment can give more information. A problem in using the four-pulse scheme is echo amplitude diffusion. As the number of pulses increases, so does the number of unwanted two- and three-pulse echoes. These additional echoes lead to loss of four-pulse echo intensity. As a result, relatively high concentrations or increased signal averaging is required.[16] Another problem of four-pulse ESEEM measurements is that the stimulated echo made of the first, second and fourth pulses occurs at the same position and phase of four-pulse echo. Hence, four-pulse ESEEM data always contains some stimulated echo modulation data.[15]

Two-dimensional (2D) ESEEM experiments can be carried out using three-pulse or four-pulse sequences.[17,18] 2D ESEEM experiments provide information about the correlation between nuclear hyperfine lines belonging to the same paramagnetic center and the relative signs of hyperfine couplings. In the three-pulse 2D ESEEM experiment, time domain data are collected in τ and T time axes for the $\pi/2$-τ-$\pi/2$-T-$\pi/2$ pulse sequence. Four-pulse 2D ESEEM or hyperfine sublevel correlation (HYSCORE) spectroscopy is performed with a $\pi/2$-τ-$\pi/2$-t_1-π-t_2-$\pi/2$ pulse sequence. The data are collected as a function of t_1 and t_2. In the three-pulse 2D experiments, the echo decay rates on the τ and T axes are

determined by the phase memory time (T_M) and spin-lattice relaxation ti (T_1), respectively. Therefore, linewidths along the τ axis are severe broadened. In the HYSCORE experiment, spectral resolution along t_1 a t_2 axes are the same because the echo amplitude decays are determined T_1. However, the HYSCORE experiments can suffer from the suppression effects while three-pulse 2D experiments are free of t distortion. There are few publications concerning the application of ESEEM methods to paramagnetic samples.[19] The main reason for this the data collection time to produce a 2D spectrum. A new detection sche using coherent "Raman Beat" detection is expected to provide solution this problem.[20]

This thesis will present the applications of ESEEM to some transiti metal ion complexes. In chapter II, the basic principles of electron sp echo formation and the ESEEM experiment will be explained. T quantum mechanical formalism of ESEEM will be derived in chapter I In chapter IV, the pulsed-EPR spectrometer which was used in t research will be described with an emphasis on modifications made perform the experiments described in chapters V and VI. In chapter angle selection four-pulse ESEEM studies of bis-aq tetracyanonickelate(III) $[Ni(III)(CN)_4(H_2O)_2^-]$ will be discussed characterize the hyperfine interactions between the axially bound wa protons and the nickel ion. In chapter VI, the hyperfine interactions equatorially and axially bound water protons in $Cu(II)(H_2O)_6^{2+}$ will distinguished using four-pulse ESEEM experiments. In chapter VII, thr pulse ESEEM studies of copper-pterin complexes as a model complexes the Cu(II) site of Phenylalanine Hydroxylase (PAH) fr

Chromobacterium Violaceum[21] will be described to understand structural relationship between Cu(II) and the pterin cofactor.

References

1. E. L. Hahn, *Phys. Rev.*, **80**, 580 (1950).
2. K. D. Bowers, and W. B. Mims, *Phys. Rev.*, **115**, 285 (1959).
3. W. B. Mims, K. Nassau, and J. D. McGee, *Phys. Rev.*, **123**, 205 (1961).
4. J. A. Cowen, and D. E. Kaplan, *Phys. Rev.*, **115**, 285 (1959).
5. L.G. Rowan, E. L. Hahn, and W. B, Mims, *Phys. Rev.*, **A137**, 6 (1965).
6. D. Grischkowsky, and S. R. Hartmann, *Phys. Rev.*, **B2**, 60 (196
7. W. B. Mims, *Phys. Rev.*, **B5**, 2409 (1972).
8. W. B. Mims, *Phys. Rev.*, **B6**, 3543 (1972).
9. L. Kevan, and M. Bowman, Ed., in *Modern Pulsed and Continuo Wave Electron Spin Resonance*, John Wiley & Sons, New York (1990).
10. A. J. Hoff, Ed., in *Advanced EPR*, Elsevier, Amsterdam (1989).
11. C. P. Keijers, E. J. Reijerse, and J. Schmidt, Ed., in *Pulsed EPR* North-Holland, Amsterdam (1989).
12. A. Schweiger, *Angew. Chem. Int. Ed. Engl*, **30**, 265 (1991).
13. A. V. Astashkin, S. A. Dikanov, and Yu. D. Tsvetkov, *Chem. Ph Lett.*, **136**, 204 (1987).
14. E. J. Reijerse, and S. A. Dikanov, *J. Chem. Phys.*, **95**, 836 (199
15. C. Gemperle, G. Abeli, A, Schweiger, and R. R. Ernst, *J. Magn. Reson.*, **88**, 241 (1990).
16. A. M. Tryshkin, S. A. Dikanov, and D. Goldfarb, *J. Magn. Reso* **A105**, 271 (1993).
17. R. P. J. Merks, and R. de Beer, *J. Phys. Chem.*, **83**, 3319 (1979
18. P. Höfer, A. Grupp, H. Nebenführ, and M. Mehring, *Chem. Phy Lett.*, **132**, 279 (1986).
19. P. Höfer, *Bruker Report*, **118**, 1 (1993).
20. M. K. Bowman, *Israel J. Chem.*, **32**, 339 (1992).
21. S. O. Pember, J. J. Villafranca, and S. J. Benkovic, *Biochemistr* **25**, 6611 (1986).

II. BASIC PRINCIPLES OF ELECTRON SPIN ECHO ENVELOPE MODULATION

1. Basic Principles of Electron Spin Echo (ESE)

1-1. Two-Pulse Spin Echo

Two-pulse spin echoes were first observed for nuclear spins usin $\pi/2$-τ-$\pi/2$ pulse sequence by Hahn.[1] Later, a more idealized two-pu sequence of $\pi/2$-τ-π was described by Carr and Purcell.[2] The formatio spin echoes can be explained using a magnetization vector model.

In a static external magnetic field, the magnetic moments of unpa electron spins are aligned either antiparallel or parallel to the external f according to their spin states, α or β, respectively. The populations of states follow the Boltzmann distribution law. For electrons, the β spin s is more stable resulting in a total magnetization, **M**, parallel to the exte field direction. When a linearly polarized MW is applied to the system, a torque is applied to the magnetization and it is turned into plane perpendicular to the external magnetic field direction. This line polarized MW magnetic field can be represented in the rotating fram letting one of two circular polarized components of the MW be along x-axis of rotating frame with frequency of ω_1 [$B_1(r)$ in Fig. II-1]. Ther field $B_1(r)$ is time-independent. The other component $B_1(l)$ has a freque

of $-2\omega_1$ in the rotating frame but has little effect on a magnetic reson experiment. From now on, X,Y and Z indicate axes of the labora frame and x, y, and z indicate the axes of the rotating frame.

In this rotating frame, when a short and intense MW pulse, w center frequency, ω_o, and bandwidth cover the precession frequency r of the individual spin magnetic moments that contribute to magnetization, is applied, the magnetization vector, **M**, is deflected the external field direction due to the torque between the time indepen MW field of the rotating frame and the magnetization vector. The ang deflection ,or flip angle, is given by $\theta_{flip}=\omega_1 t_p=\gamma_e B_1 t_p$. Here, t_p is the p width, γ_e is the gyromagnetic ratio for an electron, and B_1 is the magn field amplitude of the applied MW pulse. The relationship between applied MW power and the B_1 field depends on the cavity or sample pr

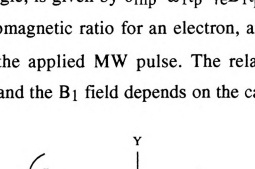

Figure II-1. Resolution of a linearly polarized microwave field into circularly polarized components, $B_1(r)$ and $B_1(l)$. X, Y and x, y denote laboratory and the rotating frames, respectively.

If one choose a 90° pulse, the magnetization vector ends up along y-axis of the rotating frame immediately after the pulse is turned off [II-2 (a)]. Because of inhomogeneity in external and internal magn

fields, the individual electron spin magnetic moments precess about the z-axis with the frequencies of ω-ω_o. If one installs the detection system along the y-axis of the rotating coordinate, the amplitude of the total transverse magnetization decays rapidly (Free Induction Decay: FID) [Fig. II-2 (b)]. After a time τ a 180° pulse is applied about the x-axis so that the each magnetization vector is turned into the -y direction [Fig. II-2 (c)]. The precession behavior of each vector component or spin packet remains the same as before the

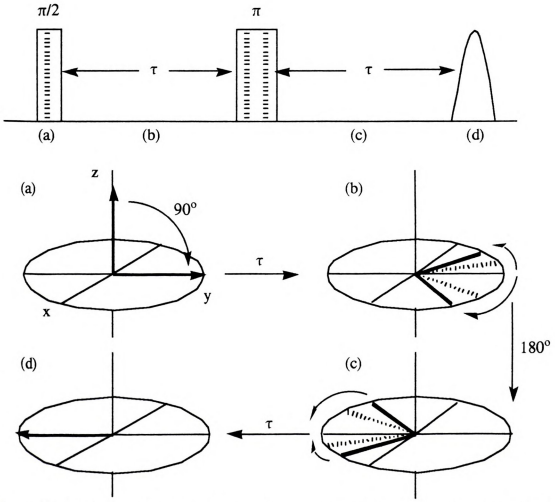

Figure II-2. Two-pulse spin echo sequence and formation of spin echo in the rotating frame.

refocussing pulse. Hence, all magnetization vectors are aligned along the direction at time τ after the second pulse to build up a "spin echo" [Fig. 2 (d)].

The amplitude of the two-pulse spin echo is a function of τ, the ti interval between the first and second MW pulses. During τ, t magnetization is in the xy plane so that relaxation processes are due to sp spin relaxation. The decay rate of the two-pulse electron spin ec amplitude can be represented by a phase memory time, T_M. T_M is , in pa a function of the spin-spin relaxation time, T_2, which corresponds to t time during which individual spin packets maintain their phases in t diffused pattern of Figure II-2 (b).

1-2. Three-Pulse Spin Echo (Stimulated Spin Echo)

Three-pulse or stimulated spin echoes are produced by a $\pi/2$-τ-π T-$\pi/2$ pulse sequence. The spin echo is formed along the -y direction of t rotating frame as depicted in Fig. II-3. The formation of the spin echo c be easily explained by following the behavior of a component of the to magnetization vector **M**.

The character of the magnetization after the first pulse is the same in the two-pulse spin echo sequence. At time τ after the first pulse component $\delta\mathbf{M}$ of the total transverse magnetization **M** makes an angle $(\omega-\omega_o)\tau$ with respect to the y-axis [Fig. II-3 (a)]. Here, ω_o is the M pulse frequency and ω is the precession frequency of the component δ the laboratory field axis (Z-axis). The second 90° MW pulse, applied alo the x-axis at time τ after the first pulse, brings $\delta\mathbf{M}$ into the xz pla making an angle between $\delta\mathbf{M}$ and the -z-axis of $(\omega-\omega_o)\tau$ [Fig. II-3 (b)].

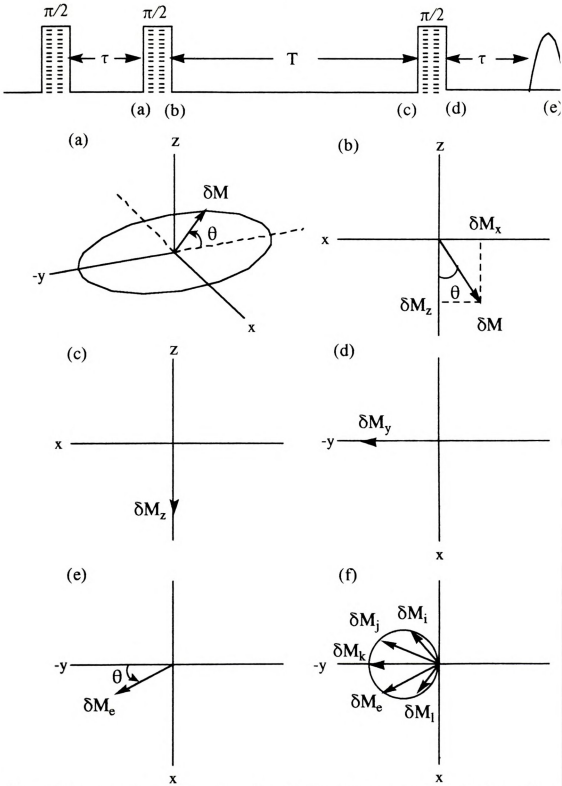

Figure II-3. Three-pulse or stimulated spin echo sequence and formation spin echo.

At this moment, $\delta\mathbf{M}$ can be resolved into two components, a transverse component, δM_x, and a longitudinal component, δM_z. The transverse magnetization δM_x makes a spin echo of $\pi/2$-τ-$\pi/2$, so called "eight ball", at time τ after the second pulse. The "eight ball spin echo" was described by Hahn in his original discovery of the spin echo.[1] The longitudinal magnetization δM_z begins decaying on the z-axis by spin-lattice relaxation process [Fig. II-3 (c)]. The third $\pi/2$ pulse applied at time T after the second pulse torques δM_z leaving it along the -y-axis to generate a transverse magnetization component δM_y [Fig. II-3 (d)]. Assuming that there is no decay and the magnitude of $\delta\mathbf{M}$ is unity, the projection of δM_y along the -y direction is $\cos(\omega-\omega_o)\tau$ at this moment. After the third pulse is turned off, the magnetization component δM_y starts precessing about the z-axis with the frequency of $\omega-\omega_o$. At an arbitrary time t after the third pulse, the magnetization component δM_e is located at the angle of $(\omega-\omega_o)t$ from the -y-axis [Fig. II-3 (e)] and a projection along the -y-axis of $\cos\{(\omega-\omega_o)\tau\}\cos\{(\omega-\omega_o)t\}$. Until now, we have considered only one component of the total magnetization. The total magnetization M_y along the -y direction at this time t can be estimated as the integration of $\cos\{(\omega-\omega_o)\tau\}\cos\{(\omega-\omega_o)t\}$ over the range of ω. Assuming the width of ω is $2\Delta\omega$ and the distribution function of ω is constant over the considered range ($f(\omega)=1$),

$$M_y=\int_{\omega_o-\Delta\omega}^{\omega_o+\Delta\omega}\cos\{(\omega-\omega_o)\tau\}\cos\{(\omega-\omega_o)t\}d\omega. \qquad \text{[II-1]}$$

The timing for the maximum transverse magnetization M_y is obtained
satisfying the condition, $\partial M_y/\partial t=0$.

$$\frac{\partial M_y}{\partial t}=\frac{-(\tau-t)^2\sin\{\Delta\omega(\tau+t)\}+\Delta\omega(\tau+t)(\tau-t)^2\cos\{\Delta\omega(\tau+t)\}}{(\tau+t)^2(\tau-t)^2}$$
$$+\frac{-(\tau+t)^2\sin\{\Delta\omega(\tau-t)\}-\Delta\omega(\tau-t)(\tau+t)^2\cos\{\Delta\omega(\tau-t)\}}{(\tau+t)^2(\tau-t)^2}. \quad \text{[II-2]}$$

Therefore, when $t=\tau$ for $t>0$, the $\partial M_y/\partial t=0$ condition is satisfied and
total magnetization along the -y-axis is maximized to form the three-pu
or stimulated spin echo. At the time of spin echo formation, the compon
δM_e of the total magnetization can be divided into two components, x an
components, $\delta M_{e,x}$, and $\delta M_{e,y}$. Their sizes along x and y axes are given
$\delta M_{e,x}=\cos\{(\omega-\omega_o)\tau\}\sin\{(\omega-\omega_o)\tau\}$ and $\delta M_{e,y}=-\cos^2\{(\omega-\omega_o)\tau$
respectively. Hence, the relationship between $\delta M_{e,x}$ and $\delta M_{e,y}$ is obtain
as

$$[\delta M_{e,x}]^2 + [\delta M_{e,y} + 1/2]^2=1/2. \quad \text{[II-3]}$$

Therefore, when the stimulated spin echo is formed all the individual sp
moment vectors of the total magnetization are placed on the circ
expressed by Eq. II-3 [Fig. II-3 (f)], which results in echo formation alo
the -y direction.

The amplitude of the stimulated echo is a function of τ, the ti
interval between the first and second pulses, and T, the time interv
between the second and third pulses. During τ, the magnetization dephas
in the xy plane so that the decay rate should follow the phase memory ti

T_M as in the two-pulse spin echo sequence. The second $\pi/2$ pulse serves t
store the precession frequency offsets $(\omega-\omega_o)$ of each spin packet as
longitudinal magnetization which forms the stimulated echo. Because th
amplitudes of these longitudinal magnetization components are governed b
a relatively slow spin-lattice, T_1, relaxation time, the overall the decay ra
of the amplitude of the stimulated echo is reduced.

1-3. Four-Pulse Spin Echo

The four-pulse spin echo sequence and the formation of the fou
pulse echo are similar to that described above for the three-pulse spin ech
Here, a π pulse is inserted between the second and third $\pi/2$-pulses wi
overall pulse sequence being $\pi/2$-τ-$\pi/2$-T/2-π-T/2-$\pi/2$. The four-pulse sp
echo is formed at time τ after the fourth pulse.

Fig. II-4 shows the pulse sequence and a vector diagram for th
formation of the four-pulse spin echo. Following the description given f
Fig. II-3, we focus on a spin packet with an electron spin magnet
moment, located along the -z-axis with z-projection of $\cos(\omega-\omega_o)$
immediately following the second $\pi/2$ pulse [Fig. II-4 (a)]. By applying th
π pulse at T/2 after the second pulse, the longitudinal component δM_z o
the magnetization turns into the z-axis [Fig. II-4 (b)]. This component goe
to y-axis by the fourth pulse of $\pi/2$ which is applied at time T/2 after thi
pulse [Fig. II-4 (c)]. Immediately after the fourth pulse, the transvers
component δM_y precesses about the z-axis with a frequency of $\omega-\omega_o$. I
analogy to the formation of the stimulated spin echo, the tot
magnetization along the y-axis is maximized at time τ after the fourth puls
forming the four-pulse spin echo [Fig. II-4 (d)-(e)]. Here, the spin echo

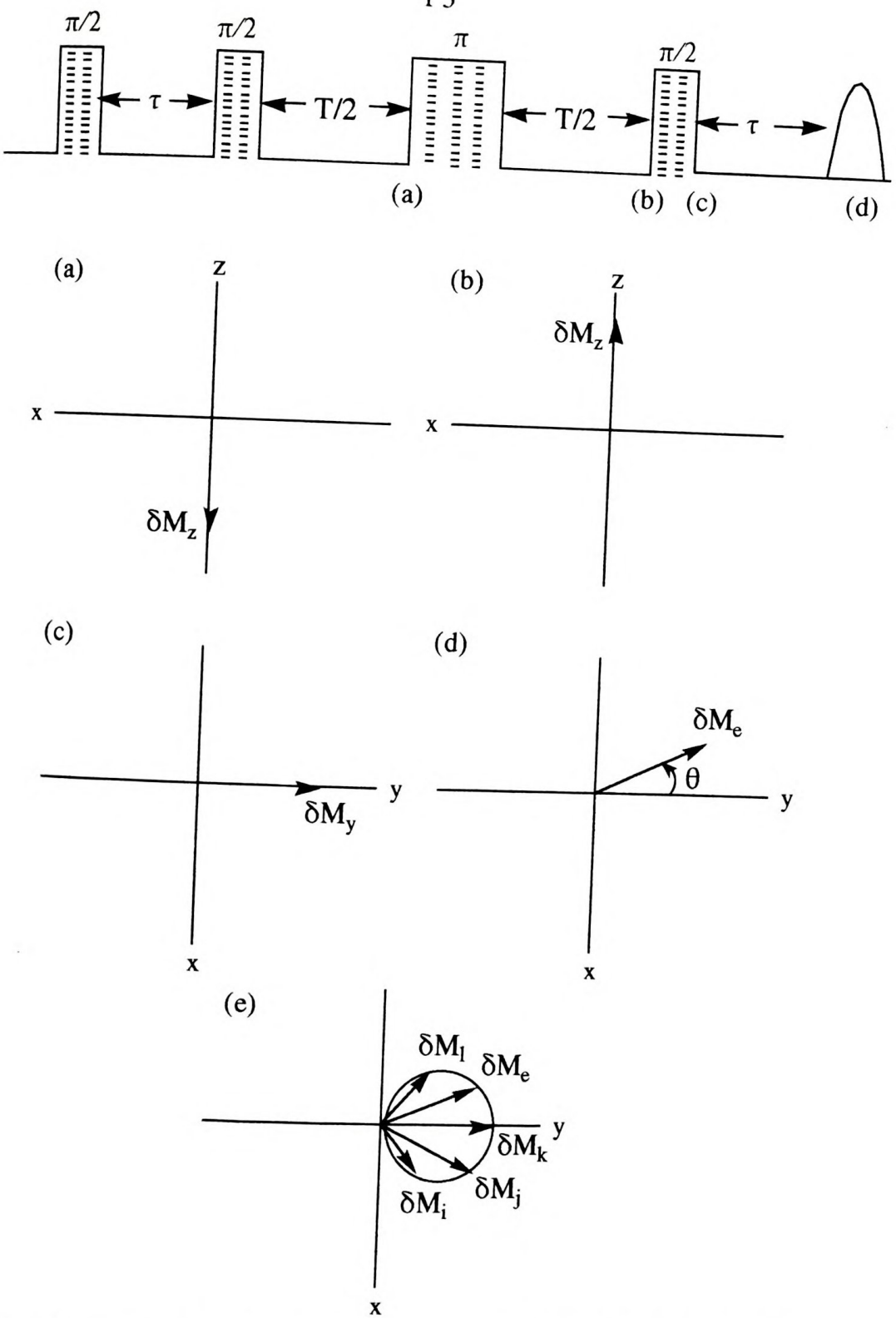

Figure II-4. Four-pulse spin echo sequence and formation of spin echo.

produced along the y-axis in contrast to the two-pulse and the three-pu spin echoes where echoes are formed along the -y-axis. The decay rate the amplitude of the four-pulse spin echo is determined by both T_M and as in the stimulated echo because the magnetization is stored on the plane for the time τ and along the z-axis during T.

2. Basic Principles of Electron Spin Echo Envelope Modulation (ESEEM

ESEEM experiments are carried out by measuring the integra intensity of electron spin echoes as a function of the time intervals betw pulses. The modulation frequencies and depths reflect the hyperf couplings between electron and nuclear spins and ,in some cases, nucl quadrupole interactions.[3-8] The modulation effect occurs when allowed semiforbidden EPR transitions are simultaneously excited by a MW pu with enough bandwidth to cover the transition energies. Interfere between the EPR transitions results in the nuclear frequencies wh appear as modulations of the electron spin echo decay envelope. So, ESEEM can be applied only to samples where this "branching" in energy level scheme occurs.

ESEEM spectra generated by Fourier transformation are analog to electron nuclear double resonance (ENDOR) spectra because both sh the nuclear hyperfine frequencies. The intensity of ESEEM frequenc depend on the product of EPR transition probabilities and the number nuclei coupled to the electron spin. In contrast, the amplitude of ENDOR peak depends on a balance of electron and nuclear relaxat processes in addition to these factors. In practice, these techniques complimentary to each other.[14]

2-1. Two-Pulse ESEEM

In the two-pulse ESEEM experiment, the echo intensity is
as a function of τ, the time interval between the pulses [Fig.
modulation of the electron spin echo can be explained semiclassic
spin system consisting of a single unpaired electron spin (S=1/2)
an I=1/2 nucleus, the hyperfine energy levels are split as in Fig. I

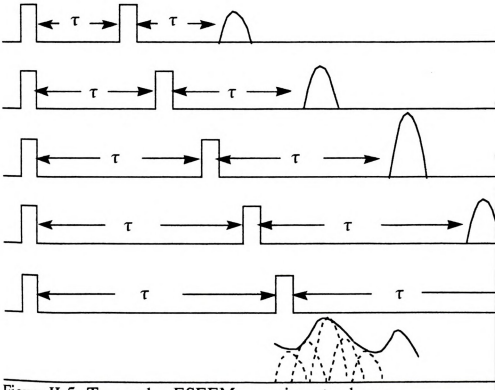

Figure II-5. Two-pulse ESEEM experiment scheme

Assuming that the energy levels within each electron spin ma
admixtures of the high-field nuclear states that are a conse

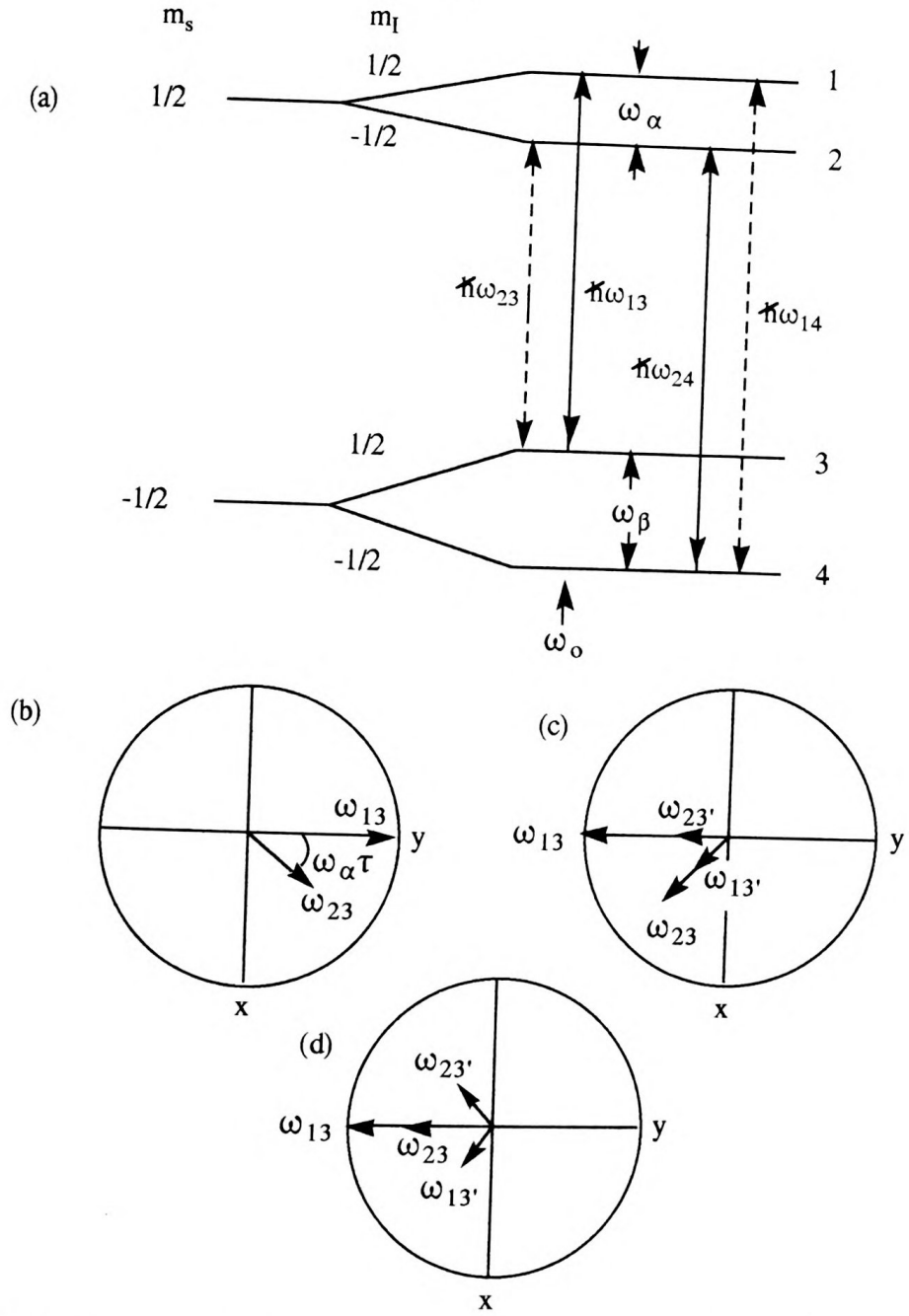

Figure II-6. Nuclear modulation effect of two-pulse electron spin echo. (a) Energy level diagram for I=1/2 nucleus coupled to S=1/2 electron spin. (b)-(d) Behavior of magnetization of the allowed and the semiforbidden spin packets during two-pulse sequence.

anisotropic hyperfine couplings, all four EPR transitions, 1-3, 2-4, 2-3, and 1-4, are allowed. If the Fourier frequency range of the MW pulse is wide enough, all four transitions are excited simultaneously. Letting the MW frequency correspond to the energy difference between levels 1 and 3 ($\omega_o=\omega_{13}$) in Fig. II-6, the modulation effect can be explained using the magnetization vectors corresponding to the 1-3 and 2-3 transitions. If the first $\pi/2$ pulse is directed along the x-axis, the vectors for the 1-3 and 2-3 transitions point along the y-axis of the rotation frame which has the frequency of ω_o with respect to the laboratory frame. Letting the transition probabilities of 1-3 and 2-3 be $|I_{13}|^2$ and $|I_{23}|^2$, the magnitudes of the vectors, ω_{13} and ω_{23}, correspond to their transition probabilities. After the pulse is turned off, the vector ω_{23} precesses about z axis with frequency of $\omega_{23}-\omega_{13}$ which is the hyperfine frequency of the α electron spin state, ω_α. At time τ after the first pulse, the vector ω_{23} makes the angle $\omega_\alpha\tau$ with y-axis [Fig. II-6 (b)]. At this time, a π pulse is applied along the x-axis. This torques the magnetization vectors, ω_{13} and ω_{23}, to the -y direction. The π pulse also generates new vectors, $\omega_{13'}$ and $\omega_{23'}$, along ω_{23} and ω_{13} directions due to the "branching of the transitions" [Fig. II-6 (c)]. The length of the vector $\omega_{13'}$ is the product of the transition probabilities of 2-3 and 1-3 transitions, i.e., $|I_{23}|^2|I_{13}|^2$. By analogy, the magnitudes of the vectors, $\omega_{23'}$, ω_{13}, and ω_{23}, are $|I_{13}|^2|I_{23}|^2$, $|I_{13}|^4$ and $|I_{23}|^4$, respectively. During the second evolution time, ω_{13} and $\omega_{13'}$ remain stationary while ω_{23} and $\omega_{23'}$ precess with an angular velocity of ω_α. At the moment of the spin echo, ω_{13} and ω_{23} are refocused on the -y-axis and $\omega_{23'}$ and $\omega_{13'}$ make an angle of $\omega_\alpha\tau$ with respect to this axis [Fig. II-6 (d)]. Since we detect the magnitude of the total magnetization along the

-y-direction, the amplitude of the echo signal which is produced by t
transitions, ω_{13} and ω_{23}, will be given by

$$E(\omega_{13},\omega_{23},\tau)= |I_{13}|^4 + |I_{23}|^4 + 2|I_{13}|^2|I_{23}|^2\cos\omega_\alpha\tau. \qquad [II\text{-}4]$$

In Eq. II-4, we can see two components of the echo amplitude. One is a
component which is not modulated and the other is an a.c component whi
is modulated at a frequency of ω_α. The above mechanism of the nucl
modulation effect can be applied to all other "branching" combinations
the energy level diagram of Fig. II-6. Because $|I_{13}|^2 = |I_{24}|^2 = |I_a|^2$ a
$|I_{14}|^2 = |I_{23}|^2 = |I_f|^2$, the overall normalized amplitude of the two-pulse s
echo is expressed by[4]

$$E(\tau)=1\text{-}k/4\{2\text{-}2\cos(\omega_\alpha\tau)\text{-}2\cos(\omega_\beta\tau)+\cos(\omega_-\tau)+\cos(\omega_+\tau)]. \qquad [II\text{-}5]$$

Here, $k = 4|I_a|^2|I_f|^2$, $\omega_- = \omega_\alpha-\omega_\beta$, and $\omega_+ = \omega_\alpha+\omega_\beta$. As seen in Eq. II
the two-pulse echo amplitude is modulated by sum, ω_+, and difference,
combination frequencies as well as the fundamental frequencies, ω_α a
ω_β. The modulation amplitude is determined by the depth parameter, k.

Including the decay rate of the echo amplitude, $V(\tau)$, the total e
amplitude is given by

$$E_{tot}(\tau) = V(\tau)E(\tau). \qquad [II\text{-}6]$$

As described in the previous section, the decay rate of the two-pulse ech
determined by the phase memory time, T_M. During the evolution time
the electron spin coherences which give rise to the modulation also de

with the phase memory time. Hence, the decay rates of the d.c ampli and the a.c amplitude of the two-pulse echo are the same. In a solid, T only a few microseconds so that the linewidths of two-pulse ESEEM p are severely broadened.

In ESEEM experiments, the echo signal can not be recorded about one hundred nanoseconds after the final pulse due to cavity-ring This time is called the dead time, t_D. During the dead time, the microv pulse power in the cavity is so high that the echo signal can not be detec The dead time determines the minimum value of τ that can be used i ESEEM experiment. The affect of the dead time on ESEEM experim can be very serious. For example, if the dead time is 200 nanoseconds the echo signal persists for only 2 microseconds (a typical T_M), freque domain spectra derived from Fourier transformation can be seve distorted. To reduce the dead time or the effect of the dead time, sev instrumental,[15-17] mathematical,[18-20] pulse sequence,[21,22] detection[23,24] methods have been proposed.

2-2. Three-Pulse ESEEM

In three-Pulse ESEEM experiments, the stimulated echo signa recorded as a function of T, the time interval between the second and third $\pi/2$ pulses, with τ being fixed for a given measurement [Fig. I Here, the first pulse generates the electron spin coherence as in the t pulse scheme. The second pulse transfers the electron spin coherence to nuclear spin coherence. During the time T, nuclear spin coherences developed. The third pulse takes these nuclear spin coherences back to electron spin coherence which is detected. Hence, the three-pulse ESE

has only the fundamental frequencies, ω_α an ω_β, without the combina frequencies.

For the S=1/2, I=1/2 system [Fig. II-6 (a)], the echo amplitud expressed by[4]

$$E(\tau,T)=1-k/4[\{1-\cos(\omega_\alpha\tau)\}\{1-\cos(\omega_\beta(\tau+T))\} +\{1-\cos(\omega_\beta\tau)\}\{1-\cos(\omega_\alpha(\tau+T))\}]. \quad [II-7]$$

As expected, only the fundamental frequencies are shown in Eq. II-7. modulation amplitudes of the nuclear frequencies depend on not only modulation depth parameter, k, but also the time interval, τ, between the

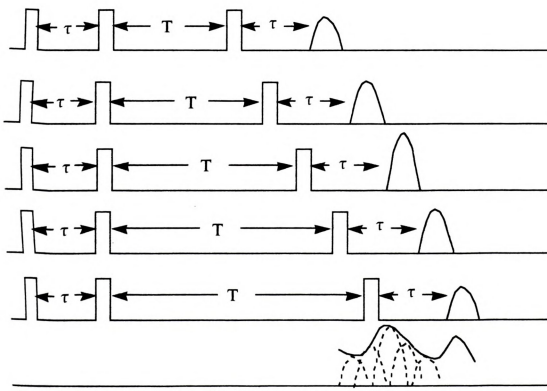

Figure II-7. Three-pulse ESEEM experiment scheme.

first and second pulses. Because of this τ-suppression effect, the linesh
of three-pulse ESEEM peaks can be distorted. When $\tau=2n\pi/\omega_\alpha$,
amplitude of the ω_β modulation component completely disappears or
versa. Even though the τ-suppression effect can prevent observation of
entire lineshape for a modulation component, it can be used to rem
unwanted peaks from complicated spectra or to identify correlati
between peaks.

During the time T in three pulse ESEEM experiments, the nuc
spin coherence decays with the transverse nuclear relaxation time, T_{2n}
Hence, the decay of the echo amplitude depends on T_{2n} or T_{1e} in the
of $T_{1e}<T_{2n}$. Because T_{2n} and T_{1e} are usually much longer than T_M,
resolution of three-pulse ESEEM spectra is much better than that of t
pulse ESEEM spectra. In the case of randomly oriented samp
destructive interference between different frequencies can cause a fa
decay of the modulation. For these samples, the decay of d.c amplitud
much longer than that of a.c amplitude.

The three-pulse spin echo sequence generates several two-p
echoes. These two-pulse echoes overlap with the three-pulse echo posi
when $T=\tau$ or 2τ to create pronounced distortions in the ESEEM patt
To remove the influence of these unwanted two-pulse echoes, the phas
the MW pulses is cycled to produce alteranate negative and positive
pulse echoes while the three-pulse echoes always remain posit
Summation of the echoes from an even numbers of phase cycles ext
the pure three-pulse echo amplitude free from distortions caused by
pulse echoes.[25]

2-3. Four-Pulse ESEEM

The four-pulse ESEEM experiment is performed by varying th time interval, T, between the second and fourth pulses with a fixed τ [Fig II-8]. The third pulse is always centered between the second and fourt pulses. The formula for an S=1/2, I=1/2 spin system is given by[26]

$$E(\tau,T)= 1-\frac{k}{4}[C_o+C_\alpha\cos(\frac{\omega_\alpha T}{2}+\frac{\omega_\alpha\tau}{2}) + C_\beta\cos(\frac{\omega_\beta T}{2}+\frac{\omega_\beta\tau}{2}) + C_+\cos(\frac{\omega_+ T}{2}+\frac{\omega_+\tau}{2}) + C_-\cos(\frac{\omega_- T}{2}+\frac{\omega_-\tau}{2})] \qquad [II\text{-}8]$$

where

$$C_o = 3-\cos(\omega_\alpha\tau)-\cos(\omega_\beta\tau)-s^2\cos(\omega_+\tau)-c^2\cos(\omega_-\tau),$$

$$C_\alpha = 2[c^2\cos(\omega_\beta\tau-\frac{\omega_\alpha\tau}{2})+s^2\cos(\omega_\beta\tau+\frac{\omega_\alpha\tau}{2})-\cos(\frac{\omega_\alpha\tau}{2})],$$

$$C_\beta = 2[c^2\cos(\omega_\alpha\tau-\frac{\omega_\beta\tau}{2})+s^2\cos(\omega_\alpha\tau+\frac{\omega_\beta\tau}{2})-\cos(\frac{\omega_\beta\tau}{2})],$$

$$C_+ = -4c^2\sin(\frac{\omega_\alpha\tau}{2})\sin(\frac{\omega_\beta\tau}{2}),$$

$$C_- = -4s^2\sin(\frac{\omega_\alpha\tau}{2})\sin(\frac{\omega_\beta\tau}{2}),$$

$$s^2 = \frac{|\omega_I^2-\frac{1}{4}(\omega_\alpha+\omega_\beta)^2|}{\omega_\alpha\omega_\beta} = |I_f|^2,$$

$$c^2 = \frac{|\omega_I^2-\frac{1}{4}(\omega_\alpha-\omega_\beta)^2|}{\omega_\alpha\omega_\beta} = |I_a|^2, \text{ and}$$

$$k = 4s^2c^2. \qquad [II\text{-}9]$$

As seen in Eq. II-8, the four-pulse echo is modulated with frequencies o $\omega_\alpha/2$, $\omega_\beta/2$, $(\omega_\alpha+\omega_\beta)/2$, and $(\omega_\alpha-\omega_\beta)/2$. An advantage of the four-puls

experiment is that the combination bands are detected with high frequency resolution. Even though the combination bands are detected in the two- pulse experiment, the echo amplitude decay broadens the linewidth. In four-pulse measurements, the decay of the echo amplitude follows T_{2n} or T_{1e} as in the three-pulse experiment. Therefore, the four-pulse experiment provides a more accurate method for measuring the frequency and lineshape of the sum combination peak. This case will be described in chapter V. Four-pulse ESEEM experiments are also subject to T suppression effects.

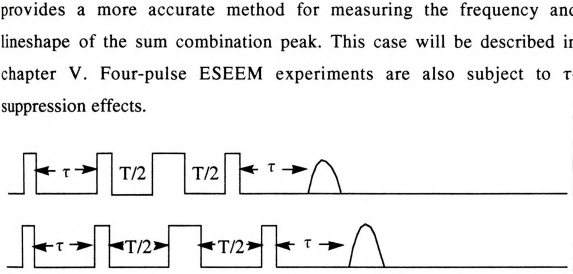

Figure II-8. Four-pulse ESEEM experiment scheme.

The four-pulse ESEEM experiment suffers from interference due to the unwanted two- and three- pulse echoes. All of These unwanted echoes can be removed by a phase cycling except for the three-pulse echo derived

from the first, second and third pulses.[26] This echo can not be removed by phase cycling because the phases of this echo and the four-pulse echo are always the same. The phase cycle suggested by ref. 26 results in the alteration of the signs of the four-pulse echo. This scheme was somewhat inconvenient for our data collection system and a new four-step phase cycle of +(0,0,0,0), +(π,π,0,0), +(0,0,π,0), +(π,π,π,0) was developed. Here, the sign of the four-pulse echo is unaltered [Table II-1].

Table II-1. Four step phase cycle for four-pulse ESEEM

Pulses				Echo										
Phase				2-Pulse						3-Pulse				4-Pulse
p1	p2	p3	p4	12	13	14	23	24	34	123	124	134	234	1234
0	0	0	0	+	+	+	+	+	+	+	+	+	+	+
π	π	0	0	-	-	-	-	-	+	+	+	-	-	+
0	0	π	0	+	+	+	+	+	-	-	+	-	-	+
π	π	π	0	-	-	-	-	-	-	-	+	+	+	+
Sum				0	0	0	0	0	0	0	4+	0	0	4+

References

1. E. L. Hahn, *Phys. Rev.*, **80**, 580 (1950).
2. H. Y. Carr, and E. M. Purcell, *Phys. Rev.*, **94**, 630 (1954).
3. L.G. Rowan, E. L. Hahn, and W. B, Mims, *Phys. Rev.*, **A137**, 61 (1965).
4. W. B. Mims, *Phys. Rev.*, **B5**, 2409 (1972).
5. W. B. Mims, and J. Peisach, *J. Chem. Phys.*, **69**, 4921 (1978).
6. A. A. Shubin, and S. A. Dikanov, *J. Magn. Reson.*, **52**, 1 (1983).
7. M. Romanelli, D. Goldfarb, and L. Kevan, *Magn. Reson. Rev.*, **13**, 179 (1988).
8. W. B. Mims, and J. Peisach, in *Biological Magnetic Resonance*, L. J. Berliner, and J. Reuben, Ed., Plenum, New York, 213 (1981).
9. L. Kevan, in *Time Domain Electron Spin Resonace*, L. Kevan, and R. N. Schwartz, Ed., Wiley-Interscience, New York, 279 (1979).

10. W. B. Mims, and J. Peisach, in *Advanced EPR*, A. J. Hoff, Ed., Elsevier, Amsterdam, 1 (1989).
11. S. A. Dikanov, and A. V. Astashkin, in *Advanced EPR*, A. J. Hoff, Ed., Elsevier, Amsterdam, 59 (1989).
12. A. Schweiger, in *Advanced EPR*, A. J. Hoff, Ed., Elsevier, Amsterdam, 243 (1989).
13. A. Schweiger, in *Modern Pulsed and Continuous-Wave Electron Spin Resonance*, L. Kevan, and M. Bowman, Ed., John Wiley & Sons, New York, 43 (1990).
14. E. J. Reijerse, N. A. J. M. Van Aerle, and C. P. Keijers, *J. Magn. Reson.*, **67**, 114 (1986).
15. J. L. Davis, and W. B. Mims, *Rev. Sci. Instrum.*, **52**, 131 (1981).
16. P. A. Narayana, R. J. Massoth, and L. Kevan, *Rev. Sci. Instrum.*, **53**, 624 (1981).
17. W. Barendswaard, J. A. J. M. Disselhorst, and J. Schmidt, *J. Magn. Reson.*, **58**,477 (1984).
18. D. Van Ormondt, and K. Nederveen, *Chem. Phys. Lett.*, **82**, 443 (1981).
19. W. B. Mims, *J. Magn Reson.*, **59**,291 (1984).
20. R. de Beer, and D. Ormondt, in *Advanced EPR*, A. J. Hoff, Ed., Elsevier, Amsterdam, 135 (1989).
21. H. Cho, S. Pfenninger, C. Gemperle, A. Schweiger, and R. R. Ernst, *Chem. Phys. Lett.*, **160**, 391 (1989).
22. C. Gemperle, A. Schweiger, and R. R. Ernst, *Chem. Phys. Lett.*, **178**, 565 (1991).
23. A. Schweiger, and R. R. Ernst, *J. Magn. Reson.*, **77**,512 (1988).
24. J. -M. Fauth, A. Schweiger, and R. R. Ernst, *J. Magn. Reson.*, **81**,262 (1989).
25. J. -M. Fauth, A. Schweiger, L. Braunschweiler, J. Forrer, and R. R. Ernst, *J. Magn. Reson.*, **66**, 74 (1986).
26. C. Gemperle, G. Abeli, A. Schweiger, and R. R. Ernst, *J. Magn. Reson.*, **88**, 241 (1990).

III. FORMALISM OF ESEEM

If a system evolves with time, the density matrix form especially useful to describe the time dependence of the physical p of the system.[1,2] In ESEEM experiments, the echo modulation res the time evolution of the coupled spin system in response to microwave pulses and free precession. This chapter will explain th matrix or density operator and derive the formulas of ESEEM.

1. Density Matrix

Consider a system which consists of a time dependent cc $c_n(t)$ and a complete set of orthonormal functions, $\{|\phi_n\rangle\}$.

$$|\Psi(t)\rangle = \sum_n c_n(t)|\phi_n\rangle \qquad [1$$

where $|\Psi(t)\rangle$, is normalized so that

$$\sum_n |c_n(t)|^2 = 1. \qquad [1$$

The expectation value of an observable **A** is given by

$$\langle \mathbf{A} \rangle(t) = \langle \Psi(t)|\mathbf{A}|\Psi(t)\rangle \qquad [1$$

$$= \sum_{nm} c_n^*(t) c_m(t) \langle \phi_n | \mathbf{A} | \phi_m \rangle$$
$$\equiv \sum_{nm} c_n^*(t) c_m(t) \langle n | \mathbf{A} | m \rangle.$$

Now, define density operator, ρ, as

$$\rho(t) = |\Psi(t)\rangle\langle\Psi(t)|. \qquad \text{[III-4}$$

The density operator is represented in the $\{\phi_n\rangle\}$ basis set by a d matrix whose elements, $\rho_{nm}(t)$, are expressed as

$$\rho_{nm}(t) = \langle n|\rho(t)|m\rangle = c_m^*(t) c_n(t). \qquad \text{[III-5}$$

Therefore, from Eq. III-2 and III-5,

$$\sum_n |c_n(t)|^2 = \sum_n \rho_{nn}(t) = \mathrm{Tr}\{\rho(t)\} = 1, \qquad \text{[III-6}$$

the sum of the diagonal elements of the density matrix is equal t Substitution of Eq. III-5 into Eq. III-3 shows that the expectation valu be expressed by

$$\langle \mathbf{A} \rangle(t) = \sum_{nm} \rho_{mn}(t) \langle n|\mathbf{A}|m\rangle = \sum_{nm} \langle m|\rho(t)|n\rangle\langle n|\mathbf{A}|m\rangle. \qquad \text{[III-}$$

Since the set, $\{|\phi_n\rangle\}$, is orthonormal ($|n\rangle\langle n| = \mathbf{I}$, $\mathbf{I}$ is an identity ma

$$\langle \mathbf{A} \rangle(t) = \sum_m \langle m|\rho(t)\mathbf{A}|m\rangle = \mathrm{Tr}\{\rho(t)\mathbf{A}\}. \quad \text{[III-8]}$$

Since the evolution of $|\Psi(t)\rangle$ is described by the time-depend Schrödinger equation,

$$i\hbar\frac{d}{dt}|\Psi(t)\rangle = \mathbf{H}(t)|\Psi(t)\rangle, \quad \text{[III-9]}$$

where $\mathbf{H}(t)$ is the Hamiltonian of the system, the time evolution of density operator $\rho(t)$ is derived from Eq. III-4 as

$$\begin{aligned}\frac{d}{dt}\rho(t) &= \left(\frac{d}{dt}|\Psi(t)\rangle\right)\langle\Psi(t)| + |\Psi(t)\rangle\left(\frac{d}{dt}\langle\Psi(t)|\right) \quad \text{[III-10]}\\ &= \frac{1}{i\hbar}\mathbf{H}(t)|\Psi(t)\rangle\langle\Psi(t)| + \frac{1}{-i\hbar}|\Psi(t)\rangle\langle\Psi(t)|\mathbf{H}(t)\\ &= \frac{1}{i\hbar}\mathbf{H}(t)\rho(t) - \frac{1}{i\hbar}\rho(t)\mathbf{H}(t)\\ &= \frac{1}{i\hbar}[\mathbf{H}(t),\rho(t)].\end{aligned}$$

In summary, the expectation value of a physical observable A obtained by using the density operator,

$$\langle \mathbf{A} \rangle(t) = \mathrm{Tr}\{\rho(t)\mathbf{A}\}, \quad \text{[III-11]}$$

and the time evolution of the density operator $\rho(t)$ can be derived by equation of motion,

$$\frac{d}{dt}\rho(t) = \frac{i}{\hbar}[\mathbf{H}(t),\rho(t)]. \quad \text{[III-12]}$$

$\rho(0)$ is the thermal equilibrium density matrix or operator prio application of $\mathbf{H}(t)$

2. The Density Matrix Formalism of ESEEM

2-1. Two-Pulse ESEEM

In two-pulse ESEEM experiments, the transverse electron magnetization is observed along the -y-direction of a rotating fra Hence, the normalized expectation value of the echo magnetization whic generated at time 2τ after the first pulse is expressed from Eq. III-8 by

$$E(\tau) = \frac{Tr\{\rho(2\tau)S_y\}}{Tr\{\rho(0)S_y\}} \qquad \text{[III-13}$$

where $\rho(2\tau)$ is the density matrix at time 2τ and $\mathbf{S}_y$ is the electron angular momentum operator along the y-axis in the rotating frame. Hamiltonian for ESE experiments consists of time independent and dependent parts,

$$\mathbf{H}_{tot} = \mathbf{H}_o + \mathbf{H}_t, \qquad \text{[III-14}$$

where $\mathbf{H}_o$ and $\mathbf{H}_t$ describe interactions between an electron spin sy including coupling nuclear spins and a static external magnetic field, interactions between the spin system and a MW pulse which is ap perpendicular to the external field, respectively. For simplicity, ass

that the Hamiltonian is already expressed in the rotating frame abou external field direction with the carrier frequency of the MW p During the free precession period, $\mathbf{H}_{tot} = \mathbf{H}_o$. Assuming that interactions between the electron spin and the MW field are much la than $\mathbf{H}_o$, $\mathbf{H}_{tot} = \mathbf{H}_t$ when the spin system is subject to MW pulse excitati

From Eq. III-12, the density matrix $\rho(t)$ is obtained by

$$\rho(t) = \exp[-i\mathbf{H}t/\hbar]\rho(0)\exp[i\mathbf{H}t/\hbar]. \qquad \text{[III-15}$$

If we let the exponential operators for the precession time (pulse off) the nutation time (pulse on) be as

$$\mathbf{R}_t = \exp[-i\mathbf{H}_o t/\hbar], \text{ and} \qquad \text{[III-16}$$

$$\mathbf{R}_{ip} = \exp[-i\mathbf{H}_t t_{ip}/\hbar], \qquad \text{[III-17}$$

then, the density matrix, $\rho(2\tau)$, at the time of two-pulse echo is given b

$$\rho(2\tau) = \mathbf{R}\rho(0)\mathbf{R}^+ \qquad \text{[III-18}$$

where

$$\mathbf{R} = \mathbf{R}_\tau\mathbf{R}_{2p}\mathbf{R}_\tau\mathbf{R}_{1p} \qquad \text{[III-19}$$

Assuming that there is no mixing between α and β electron states, and letting the eigenvalues and eigenvectors of the time indepe Hamiltonian, $\boldsymbol{H_o}$, be given by

$$\boldsymbol{H_o}\psi_{\alpha,i} = \omega_{\alpha,i}\psi_{\alpha,i}\,, \qquad \text{[III-13]}$$

$$\boldsymbol{H_o}\psi_{\beta,k} = \omega_{\beta,k}\psi_{\beta,k}\,,$$

$$\psi_\alpha = M_\alpha|\alpha,m_I>, \text{ and}$$

$$\psi_\beta = M_\beta|\beta,m_I>,$$

where

$$\boldsymbol{H_o} = \begin{bmatrix} M_\alpha & 0 \\ 0 & M_\beta \end{bmatrix}\boldsymbol{H_o}\begin{bmatrix} M^+_\alpha & 0 \\ 0 & M^+_\beta \end{bmatrix}, \qquad \text{[III-14]}$$

then M_α and M_β represent the eigenvectors, ψ_α and ψ_β, which span the complete sets of "high-field" spin functions, $|\alpha,m_I>$ and $|\beta,m_I>$, respectively. The dimension of M_α and M_β are 2I+1 where I is a nuclear spin number. The eigenvectors, ψ_α and ψ_β, are the linear combinations of $\psi_{\alpha,i}$'s and $\psi_{\beta,k}$'s, respectively while $\boldsymbol{H_o}$ is diagonalized by the unitary transformation of Eq. III-4. Now $\boldsymbol{R_t}$, $\boldsymbol{R_{ip}}$, $\rho(0)$ and $\boldsymbol{S_y}$ can be obtained in terms of the diagonalized $\boldsymbol{H_o}$ by the unitary transformations,

$$\boldsymbol{R_t} = \begin{bmatrix} M_\alpha & 0 \\ 0 & M_\beta \end{bmatrix}\exp[-i\boldsymbol{H_o}t/\hbar]\begin{bmatrix} M^+_\alpha & 0 \\ 0 & M^+_\beta \end{bmatrix} \equiv \begin{bmatrix} P_t^+ & 0 \\ 0 & Q_t^+ \end{bmatrix}, \qquad \text{[III-15]}$$

$$\begin{aligned} \boldsymbol{R_{1p}} &= \begin{bmatrix} M_\alpha & 0 \\ 0 & M_\beta \end{bmatrix}\exp[-i\boldsymbol{H}_t t_{1p}/\hbar]\begin{bmatrix} M^+_\alpha & 0 \\ 0 & M^+_\beta \end{bmatrix} \qquad \text{[III-16]} \\ &= \begin{bmatrix} M_\alpha & 0 \\ 0 & M_\beta \end{bmatrix}\exp[-i\boldsymbol{S}_x\pi/2]\begin{bmatrix} M^+_\alpha & 0 \\ 0 & M^+_\beta \end{bmatrix} \\ &= \begin{bmatrix} M_\alpha & 0 \\ 0 & M_\beta \end{bmatrix}\begin{bmatrix} I\cos\pi/2 & -iI\sin\pi/2 \\ -iI\sin\pi/2 & I\cos\pi/2 \end{bmatrix}\begin{bmatrix} M^+_\alpha & 0 \\ 0 & M^+_\beta \end{bmatrix} \\ &= \sqrt{2}/2\begin{bmatrix} I & -iM \\ -iM^+ & I \end{bmatrix}, \end{aligned}$$

$$\boldsymbol{R}_{2p} = \begin{bmatrix} M_\alpha & 0 \\ 0 & M_\beta \end{bmatrix} \exp[-i\mathbf{H}_{t2p}/\hbar] \begin{bmatrix} M^+_\alpha & 0 \\ 0 & M^+_\beta \end{bmatrix} \quad \text{[III-17]}$$

$$= \begin{bmatrix} M_\alpha & 0 \\ 0 & M_\beta \end{bmatrix} \exp[-i\mathbf{S}_x\pi] \begin{bmatrix} M^+_\alpha & 0 \\ 0 & M^+_\beta \end{bmatrix}$$

$$= \begin{bmatrix} 0 & -iM \\ -iM^+ & 0 \end{bmatrix},$$

$$\boldsymbol{S}_y = \begin{bmatrix} M_\alpha & 0 \\ 0 & M_\beta \end{bmatrix} \mathbf{S}_y \begin{bmatrix} M^+_\alpha & 0 \\ 0 & M^+_\beta \end{bmatrix} \quad \text{[III-18]}$$

$$= \begin{bmatrix} M_\alpha & 0 \\ 0 & M_\beta \end{bmatrix} \begin{bmatrix} 0 & -i\mathbf{I}/2 \\ i\mathbf{I}/2 & 0 \end{bmatrix} \begin{bmatrix} M^+_\alpha & 0 \\ 0 & M^+_\beta \end{bmatrix}$$

$$= \begin{bmatrix} 0 & -iM/2 \\ iM^+/2 & 0 \end{bmatrix}, \text{ and}$$

$$\rho(0) = \begin{bmatrix} M_\alpha & 0 \\ 0 & M_\beta \end{bmatrix} \rho(0) \begin{bmatrix} M^+_\alpha & 0 \\ 0 & M^+_\beta \end{bmatrix} \quad \text{[III-19]}$$

$$= \begin{bmatrix} a\mathbf{I} & 0 \\ 0 & b\mathbf{I} \end{bmatrix}$$

where

$$P^+ = \begin{bmatrix} \exp[-i\omega_{\alpha 1}t] & 0 & 0 \\ 0 & : & 0 \\ 0 & 0 & \exp[-i\omega_{\alpha(2I+1)}t] \end{bmatrix}, \quad \text{[III-20]}$$

$$Q^+ = \begin{bmatrix} \exp[-i\omega_{\beta 1}t] & 0 & 0 \\ 0 & : & 0 \\ 0 & 0 & \exp[-i\omega_{\beta(2I+1)}t] \end{bmatrix}, \quad \text{[III-21]}$$

$M=M_\alpha M_\beta^+$, and $\mathbf{I}$ is an identity matrix. a and b represent the populati of α and β spin states in the external magnetic field.

Now the density matrix at time 2τ is

$$\rho(2\tau) = \boldsymbol{R}\rho(0)\boldsymbol{R}^+ \quad \text{[III-22}$$

where

$$\boldsymbol{R} = \boldsymbol{R}_{\tau}\boldsymbol{R}_{2p}\boldsymbol{R}_{\tau}\boldsymbol{R}_{1p} \; . \qquad \text{[III-23]}$$

Therefore, the normalized two-pulse echo amplitude is given by[3]

$$\begin{aligned} E(\tau) &= \frac{Tr\{\rho(2\tau)S_y\}}{Tr\{\rho(0)S_y\}} \\ &= \frac{1}{2I+1}Re[Tr\{Q_{\tau}^{+}M^{+}P_{\tau}^{+}MQ_{\tau}M^{+}P_{\tau}M\}]. \end{aligned} \qquad \text{[III-24]}$$

If more than one nuclear spin is coupled to the electron spin, total echo amplitude is given by product rule.[3]

$$E(\tau) = \prod_{i}^{n} E_i(\tau). \qquad \text{[III-25]}$$

2-2. Three-Pulse ESEEM

The three-pulse spin echo is produced at time $2\tau+T$ after the pulse. Here, τ and T are the time intervals between the first and sec and the second and third MW pulses, respectively. Since all three pulses $\pi/2$ pulses, the density matrix at time, $2\tau+T$ is expressed by

$$\rho(2\tau+T) = \boldsymbol{R}_3\rho(0)\boldsymbol{R}_3^{+} \qquad \text{[III-26}$$

where

$$\boldsymbol{R}_3 = \boldsymbol{R}_\tau \boldsymbol{R}_{3p} \boldsymbol{R}_T \boldsymbol{R}_{2p} \boldsymbol{R}_\tau \boldsymbol{R}_{1p} \,. \qquad \text{[III-2}$$

Here, $\boldsymbol{R}_{1p}$, $\boldsymbol{R}_{2p}$, and $\boldsymbol{R}_{3p}$ are identical to $\boldsymbol{R}_{1p}$ of Eq. III-16. The amplitude can be described by[3]

$$\begin{aligned} E(\tau,T) &= \frac{\mathrm{Tr}\{\rho(2\tau+T)\, S_y\}}{\mathrm{Tr}\{\rho(0) S_y\}} \\ &= \frac{1}{2(2I+1)} \mathrm{Re}[\mathrm{Tr}\{Q_\tau{}^+ M^+ P_\tau{}^+ P_T{}^+ M Q_\tau M^+ P_T P_\tau M \\ &\quad + Q_\tau{}^+ Q_T{}^+ M^+ P_\tau{}^+ M Q_T Q_\tau M^+ P_\tau M\}]. \end{aligned} \qquad \text{[III-2}$$

For the cases where several nuclei are involved, the product rule is ap only within the same electron spin states.[4]

$$E(\tau,T) = \frac{1}{2}[\prod_i^n E_{\alpha,i}(\tau,T) + \prod_j^n E_{\beta,j}(\tau,T)]. \qquad \text{[III-2}$$

2-3. Four-Pulse ESEEM

The four-pulse echo amplitude can be obtained using the formalism. Let the time intervals between first and second, second third, and third and forth pulses be τ, t_1, and t_2, respectively. The amplitude is expressed as

$$\begin{aligned} E(\tau,t_1,t_2) = \frac{1}{4(2I+1)} \mathrm{Re}[\mathrm{Tr}\{ & \qquad \text{[III-3} \\ & M Q^+{}_\tau Q^+{}_{t2} M^+ P^+{}_{t1} P^+{}_\tau M Q_\tau M^+ P_{t1} M Q_{t2} M^+ P_\tau \\ & - M Q^+{}_\tau Q^+{}_{t2} M^+ P^+{}_{t1} P^+{}_\tau M Q_\tau Q_{t1} M^+ P_{t2} P_\tau \\ & + M Q^+{}_\tau Q^+{}_{t2} M^+ P^+{}_{t1} M Q^+{}_\tau M^+ P_\tau P_{t1} M Q_{t2} M^+ P_\tau \end{aligned}$$

$$+ MQ^{+}_{\tau}Q^{+}_{t2}M^{+}P^{+}_{t1}MQ^{+}_{\tau}M^{+}P_{\tau}MQ_{t1}M^{+}P_{t2}P_{\tau}$$
$$+ MQ^{+}_{\tau}M^{+}P^{+}_{t2}MQ^{+}_{t1}Q^{+}_{\tau}M^{+}P_{\tau}P_{t1}MQ_{t2}M^{+}P_{\tau}$$
$$+ MQ^{+}_{\tau}M^{+}P^{+}_{t2}MQ^{+}_{t1}Q^{+}_{\tau}M^{+}P_{\tau}MQ_{t1}M^{+}P_{t2}Pt$$
$$- MQ^{+}_{\tau}M^{+}P^{+}_{t2}MQ^{+}_{t1}M^{+}P^{+}_{\tau}MQ_{\tau}M^{+}P_{t1}MQ_{t2}M^{+}P_{\tau}$$
$$+ MQ^{+}_{\tau}M^{+}P^{+}_{t2}MQ^{+}_{t1}M^{+}P^{+}_{\tau}MQ_{\tau}Q_{t1}M^{+}P_{t2}P_{\tau}\}]$$

or

$$E(\tau,t_1,t_2) = 2Re[\sum_{ijklmn} M_{il}M_{lj}{}^{+}M_{jm}M_{mk}{}^{+}M_{kn}M_{ni}{}^{+} \quad \text{[III-31]}$$

$$X \exp\{-i(\omega_{ij}\tau+\omega_{ik}t_2+\omega_{ln}\tau+\omega_{lm}t_1)\}$$

$$+ \sum_{ijklmn} M_{il}M_{lj}{}^{+}M_{jm}M_{mk}{}^{+}M_{kn}M_{ni}{}^{+}$$

$$X \exp\{-i(\omega_{ik}\tau+\omega_{jk}t_2+\omega_{ln}\tau+\omega_{mn}t_1)\}].$$

For four-pulse ESEEM experiments, the echo modulation function obtained by inserting $t_1=t_2=T/2$. If an electron spin is coupled to sev nuclear spins and $t_1=t_2$, the echo modulation is obtained using the form derived for two-pulse ESEEM.[6]

$$E(\tau,T/2) = \prod_{i}^{n} E_i(\tau,T/2). \quad \text{[III-32]}$$

If t_1 and t_2 are independently varied as they are in HYSCORE experime the echo amplitude is given the by three-pulse formulation of the proc rule[6] because this experiment is basically a three-pulse experiment[7]

$$E(\tau,t_1,t_2) = \frac{1}{2}[\prod_{i}^{n} E_{\alpha,i}(\tau,t_1,t_2) + \prod_{j}^{n} E_{\beta,j}(\tau,t_1,t_2)]. \quad \text{[III-33]}$$

3. Formulas of ESEEM

General formulas for two- and three-pulse ESEEM were deri from Eq.'s III-24 and III-28 by Mims.[8] They are

$$E(\tau) = \frac{1}{2I+1}[X_o + 2\sum_i \sum_{i<j} X^{(\alpha)}_{ij} \cos\omega\alpha_{ij}\tau \qquad \text{[III-34}$$
$$+2\sum_k \sum_{k<n} X^{(\beta)}_{kn} \cos\omega\beta_{kn}\tau$$
$$+2\sum_i \sum_{i<j} \sum_k \sum_{k<n} X^{(\alpha,\beta)}_{ijkn}\{\cos(\omega\alpha_{ij}+\omega\beta_{kn})\tau + \cos(\omega\alpha_{ij}-\omega\beta_{kn})\tau\}$$

and

$$E(\tau,T) = \frac{1}{2I+1}[X_o \qquad \text{[III-35]}$$
$$+\sum_i \sum_{i<j} X^{(\alpha)}_{ij}\{\cos\omega\alpha_{ij}\tau + \cos\omega\alpha_{ij}(\tau+T)\}$$
$$+\sum_k \sum_{k<n} X^{(\beta)}_{kn}\{\cos\omega\beta_{kn}\tau + \cos\omega\beta_{kn}(\tau+T)\}$$
$$+2\sum_i \sum_{i<j} \sum_k \sum_{k<n} X^{(\alpha,\beta)}_{ijkn}\{\cos\omega\alpha_{ij}(\tau+T)\cos\omega\beta_{kn}\tau$$
$$+\cos\omega\beta_{kn}(\tau+T)\cos\omega\alpha_{ij}\tau\}]$$

where $\omega^{(\alpha)}_{ij} = \omega^{(\alpha)}_i - \omega^{(\alpha)}_j$, $\omega^{(\beta)}_{kn} = \omega^{(\beta)}_k - \omega^{(\beta)}_n$, and

$$X_o = \sum_i \sum_k |M_{ik}|^4, \qquad \text{[III-36}$$
$$X^{(\alpha)}_{ij} = \sum_k |M_{ik}|^2 |M_{jk}|^2,$$
$$X^{(\beta)}_{kn} = \sum_i |M_{ik}|^2 |M_{in}|^2,$$
$$X^{(a,\beta)}_{ijkn} = \mathrm{Re}[M^*_{ik} M_{in} M^*_{jn} M_{jk}].$$

3-1. Formulas for S=1/2 and I=1/2

The spin Hamiltonian for electron spin, S=1/2, is weakly coupled
nuclear spin, I=1/2, consists of electronic Zeeman, electron-nuc
hyperfine (HFI) and nuclear Zeeman interactions and is given by

$$\mathbf{H_o} = \beta \mathbf{S}\cdot\mathbf{g}\cdot\mathbf{B_o} + \mathbf{S}\cdot\mathbf{A}\cdot\mathbf{I} - g_n\beta_n\mathbf{B_o}\cdot\mathbf{I}. \qquad \text{[III-37}$$

β, in Eq. III-37, is the Bohr magneton, **S** is the electron spin angu
momentum operator, **g** is the electron g-tensor, $\mathbf{B_o}$ is the external magn
field vector, **A** is the hyperfine interaction tensor, **I** is the nuclear s
angular momentum operator, g_n is nuclear g-value, and β_n is the nuc
magneton. Assuming that the electron g-tensor is isotropic, the elect
spin is quantized along the field direction. In the rotating frame with
angular velocity of ω_o, the Hamiltonian can be rewritten in the form of

$$\mathbf{H_o} = \hbar[(\omega_S-\omega_o)\mathbf{S_Z} + A\mathbf{S_Z}\mathbf{I_Z} + B\mathbf{S_Z}\mathbf{I_X} - \omega_I\mathbf{I_Z}] \qquad \text{[III-38}$$

where ω_s is the electron Larmor frequency, A and B are the secular
off-diagonal components of the electron-nuclear hyperfine field, and ω
the nuclear Larmor frequency. The hyperfine eigenvalues and eigenvec
of α and β electron spin states of the operator,

$$\mathbf{K}_{\alpha,\beta}/\hbar = -\omega_I\mathbf{I_Z} \pm (1/2)[A\mathbf{I_Z} + B\mathbf{I_X}], \qquad \text{[III-39}$$

along the field can be obtained as

$$E_{\alpha,\beta} = \hbar\omega_{\alpha,\beta} = \hbar[(\pm A/2-\omega_I)^2+B^2/4]^{1/2} \quad \text{[III-40}$$

$$M_\alpha = \exp[-i\varphi \mathbf{I}_y] \quad \text{[III-42}$$

$$M_\beta = \exp[-i\xi \mathbf{I}_y] \quad \text{[III-43}$$

where

$$\tan\varphi = \frac{B/2}{A/2-\omega_I} \text{ and } \tan\xi = \frac{B/2}{A/2+\omega_I}. \quad \text{[III-44}$$

Because the quantidization axes for α and β states are obtained by rota of the $\mathbf{I}_z$ axis by φ and ξ about $\mathbf{I}_y$, respectively, the eigenvectors ca expressed as the rotation operators (Eq.'s III-42 and III-43). Then eigenvalues and eigenvectors for the Hamiltonian, Eq. III-38, are

$$E(m_s,m_I) = \hbar(\omega-\omega_o)m_s + \hbar[(m_I A/-\omega_I)^2+B^2/4]^{1/2} \quad \text{[III-45}$$

$$\psi(1/2,m_I) = M_\alpha|1/2,m_I> \quad \text{[III-46}$$

$$\psi(-1/2,m_I) = M_\beta|-1/2,mI> \quad \text{[III-47}$$

where

$$M_\alpha = \exp[-i\varphi \mathbf{I}_y] = \begin{bmatrix} \cos\frac{\varphi}{2} & -\sin\frac{\varphi}{2} \\ \sin\frac{\varphi}{2} & \cos\frac{\varphi}{2} \end{bmatrix} \text{ and} \quad \text{[III-48}$$

$$M_\beta = \exp[-i\xi \mathbf{I}_y] = \begin{bmatrix} \cos\frac{\xi}{2} & -\sin\frac{\xi}{2} \\ \sin\frac{\xi}{2} & \cos\frac{\xi}{2} \end{bmatrix}. \quad \text{[III-49}$$

Hence, $M = M_\alpha M^+_\beta = \exp[-i(\varphi-\xi)\mathbf{I}_y] = \begin{bmatrix} \cos\frac{\varphi-\xi}{2} & -\sin\frac{\varphi-\xi}{2} \\ \sin\frac{\varphi-\xi}{2} & \cos\frac{\varphi-\xi}{2} \end{bmatrix}$. [III-50]

Now, we have all elements for Eq.'s III-34, III-35, and III-36. For S=1/2, I=1/2 spin system, the following results are obtained

$$X_o = 2\text{-}\sin^2(\varphi\text{-}\xi), \qquad \text{[III-51]}$$

$$X^{(\alpha)}{}_{12} = X^{(\beta)}{}_{12} = (1/2)\sin^2(\varphi\text{-}\xi), \text{ and}$$

$$X^{(\alpha,\beta)}{}_{1212} = -(1/4)\sin^2(\varphi\text{-}\xi)$$

where

$$\sin^2(\varphi\text{-}\xi) = \left(\frac{\omega_I B}{\omega_\alpha \omega_\beta}\right)^2 \equiv k. \qquad \text{[III-52]}$$

Inserting Eq.'s III-51 and III-52 into Eq's, III-34 and III-35, the two-p and three-pulse echo amplitude functions for an S=1/2, I=1/2 spin sys are given by

$$E(\tau)=1\text{-}k/4\{2\text{-}2\cos(\omega_\alpha\tau)\text{-}2\cos(\omega_\beta\tau)+\cos(\omega_-\tau)+\cos(\omega_+\tau)\} \qquad \text{[III-53]}$$

and

$$E(\tau,T)=1\text{-}k/4[\{1\text{-}\cos(\omega_\alpha\tau)\}\{1\text{-}\cos(\omega_\beta(\tau+T))\} + \{1\text{-}\cos(\omega_\beta\tau)\}\{1\text{-}\cos(\omega_\alpha(\tau+T))\}], \qquad \text{[III-54]}$$

respectively. Here, $\omega_+=\omega_\alpha+\omega_\beta$, $\omega_-=\omega_\alpha-\omega_\beta$. For the four-pulse ESEEM, the echo amplitude is expressed by,[9]

$$E(\tau,T) = 1-\frac{k}{4}[C_o+C_\alpha\cos(\frac{\omega_\alpha T}{2}+\frac{\omega_\alpha\tau}{2}) + C_\beta\cos(\frac{\omega_\beta T}{2}+\frac{\omega_\beta\tau}{2}) + C_+\cos(\frac{\omega_+ T}{2}+\frac{\omega_+\tau}{2}) + C_-\cos(\frac{\omega_- T}{2}+\frac{\omega_-\tau}{2})] \quad \text{[III-55]}$$

where

$$C_o = 3-\cos(\omega_\alpha\tau)-\cos(\omega_\beta\tau)-s^2\cos(\omega_+\tau)-c^2\cos(\omega_-\tau),$$

$$C_\alpha = 2[c^2\cos(\omega_\beta\tau-\frac{\omega_\alpha\tau}{2})+s^2\cos(\omega_\beta\tau+\frac{\omega_\alpha\tau}{2})-\cos(\frac{\omega_\alpha\tau}{2})],$$

$$C_\beta = 2[c^2\cos(\omega_\alpha\tau-\frac{\omega_\beta\tau}{2})+s^2\cos(\omega_\alpha\tau+\frac{\omega_\beta\tau}{2})-\cos(\frac{\omega_\beta\tau}{2})],$$

$$C_+ = -4c^2\sin(\frac{\omega_\alpha\tau}{2})\sin(\frac{\omega_\beta\tau}{2}),$$

$$C_- = -4s^2\sin(\frac{\omega_\alpha\tau}{2})\sin(\frac{\omega_\beta\tau}{2}),$$

$$s^2 = \frac{|\omega_I^2-\frac{1}{4}(\omega_\alpha+\omega_\beta)^2|}{\omega_\alpha\omega_\beta},$$

$$c^2 = \frac{|\omega_I^2-\frac{1}{4}(\omega_\alpha-\omega_\beta)^2|}{\omega_\alpha\omega_\beta}, \text{ and}$$

$$k = 4s^2c^2. \quad \text{[III-56]}$$

3-2. Formulas for S=1/2 and I≥1

For a spin system of I≥1 nuclei, the spin Hamiltonian includes the nuclear quadrupole interaction (NQI). Hence, the total Hamiltonian is given by

$$\mathbf{H}_o = \beta \mathbf{S}\cdot\mathbf{g}\cdot\mathbf{B}_o + \mathbf{S}\cdot\mathbf{A}\cdot\mathbf{I} - g_n\beta_n\mathbf{B}_o\cdot\mathbf{I} + \mathbf{I}\cdot\mathbf{Q}\cdot\mathbf{I} \qquad \text{[III-57}$$

where **Q** is nuclear quadrupole interaction tensor. Approximate analyt expressions of the echo modulation function where electron-nuc hyperfine and nuclear quadrupole interactions can be treated us pertubation theory have been derived.[4,10-13] Completely gen expressions for this case must be obtained numerically.

In the case of an isotropic electron g-tensor, the eigenvalues eigenvectors of the Hamiltonian without the electron Zeeman interac can be used for calculation of the echo modulation. Hence, we need c consider the nuclear spin Hamiltonian,

$$\mathbf{H}_N = \mathbf{S}\cdot\mathbf{A}\cdot\mathbf{I} - g_n\beta_n\mathbf{B}_o\cdot\mathbf{I} + \mathbf{I}\cdot\mathbf{Q}\cdot\mathbf{I}. \qquad \text{[III-58}$$

If only HFI and nuclear Zeeman interactions are involved, the Hamilto is

$$\mathbf{H}_{HFI} = \mathbf{S}\cdot\mathbf{A}\cdot\mathbf{I} - g_n\beta_n\mathbf{B}_o\cdot\mathbf{I}. \qquad \text{[III-59}$$

For spin systems where the electron g-tensor is isotropic the electron s operator can be replaced by a ficticious spin operator, where $\mathbf{S} = \mathbf{S}'_z$ I_y, I_z), and

$$\mathbf{H}_{HFI}/\hbar = (\mathbf{S}'_z A_{xx}-\omega_I)I_x\mathbf{I}_x + (\mathbf{S}'_z A_{yy}-\omega_I)I_y\mathbf{I}_y + (\mathbf{S}'_z A_{zz}-\omega_I)I_z\mathbf{I}_z. \qquad \text{[III-60]}$$

$l_x=\sin\theta\cos\phi$, $l_y=\sin\theta\sin\phi$, and $l_z=\cos\theta$ are direction cosines that desc
the orientation of B_o with respect to the HFI principal axis system (
PAS) [Fig. III-1]. A_{xx}, A_{yy}, and A_{zz} are the principle values of
hyperfine tensor. The matrix elements, $\langle m_s,m_I|H_{HFI}|m_s,m_I\rangle$, of
Hamiltonian, Eq. III-60, for I=1, 3/2, 5/2, and 7/2 spin systems are liste
Appendix, A1. The matrices of A1-1, 2, 3, and 4 are readily diagonali
and the

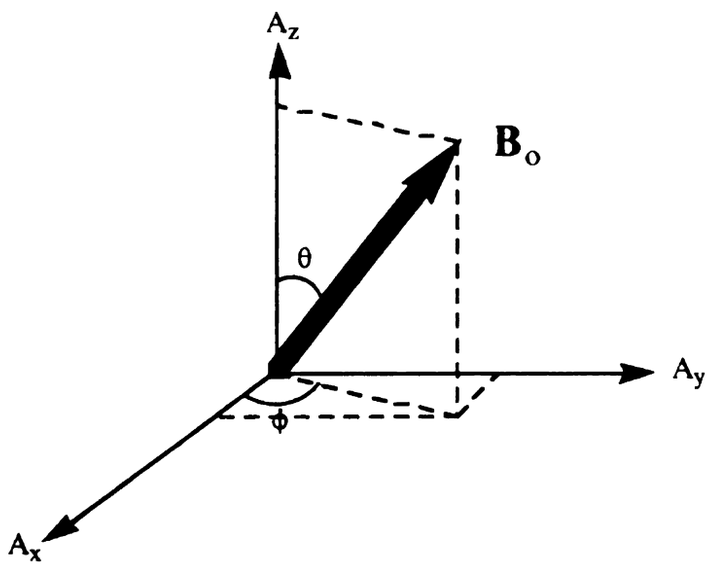

Figure III-1. Relative orientation of the external magnetic field with re
to the principle hyperfine axes.

diagonalized matrix elements are $m_I\sqrt{X^2+Y^2+Z^2}$. Here, $X=(hm_sA$
$g_n\beta_nB_o)\sin\theta\cos\phi$, $Y=(hm_sA_{yy}-g_n\beta_nB_o)\sin\theta\sin\phi$, and $Z=(hm_sA$
$g_n\beta_nB_o)\cos\theta$. The eigenvectors of the Hamiltonian can be taken as
rotational operator matrices whose elements are given by[14]

$$d^j_{mn}(\gamma)=\Sigma_t(-1)^t\frac{[(j+m)!(j-m)!(j+n)!(j-n)!]^{1/2}}{(j+m-t)!(j-n-t)!t!(t+n-m)!}(\cos\frac{\gamma}{2})^{2j+m-n-2t}(\sin\frac{\gamma}{2})^{2t+n-m} \qquad \text{[III-61]}$$

where i=I, m and n = m_I's, t=-m_I -> m_I, and γ is the rotation angle. For t
M matrices of our calculation, $\gamma=\varphi-\xi$ where $\tan\varphi=Z_\alpha/\sqrt{X^2_\alpha+Y^2_\alpha}$ a
$\tan\xi=Z_\beta/\sqrt{X^2_\beta+Y^2_\beta}$. The M matrices obtained from Eq. III-61 are list
in Appendix, A2. The echo modulation can be obtained by inserting t
eigenvalues of $m_I\sqrt{X^2+Y^2+Z^2}$ and the M matrices of Table A2-1, 2, 3, a
4 into the Eq.'s, III-34 and III-35 for two-pulse and three-pulse ESEE
and the Eq. III-31 for four-pulse ESEEM.

If NQI are involved in the spin Hamiltonian, the above eigenvalu
and the M matrices are no longer valid. The NQI Hamiltonian is given by

$$\mathbf{H}_{NQI} = \mathbf{I}'\cdot\mathbf{Q}\cdot\mathbf{I}' = \frac{\hbar e^2qQ}{4I(2I-1)}[3I'_z{}^2-I'^2+\eta(I'_x{}^2-I'_y{}^2)] \qquad \text{[III-62]}$$

where e^2qQ and η are the quadrupole coupling constant and asymme
parameter, respectively. The prime notation means that the spin operat
refer to the NQI principal axis system (NQI PAS). If the HFI PAS is t
standard coordinate system for our calculation, the NQI PAS must
rotated into the HFI PAS by an Euler rotation. The NQI Hamiltoni
matrices for I=1, 3/2, 5/2, and 7/2 in the HFI PAS are listed in Append
A3. The eigenvalues and eigenvectors of the total Hamiltonian, $\mathbf{H}_{HFI}$
$\mathbf{H}_{NQI}$, can be numerically obtained from the Tables in Appendix, A1 a
A3. From the results, the echo modulation can be calculated.

When the molecules are randomly distributed with respect to t
external magnetic field, the modulation functions must be orientational
averaged over all possible orientations of the spin system with respect
the lab axis system.

$$\langle E\rangle_\theta = \frac{1}{4\pi}\int_0^{2\pi}\int_0^{\pi} E(\theta)\sin\theta\, d\theta\, d\phi. \qquad \text{[III-63}$$

Appendix, A4 shows the computer programs for two-pulse three-pulse echo modulation functions in the time domain for the case o isotropic electron g-tensor. The programs are written in the C comp language (Symantec, v.4.0). The diagonalization subroutines are ta from the NuTools numerical package (Metaphor, v.1.02).

References

1. C. Cohen-Tannoudji, B. Diu, and F. Laloë, *Quantum Mechanics*, John Wiley & Sons, New York, 295 (1977).
2. C. P. Slichter, *Principles of Magnetic Resonance*, 3rd Ed., Springer-Verlag, Berlin, 157 (1989).
3. W. B. Mims, *Phys. Rev.*, **B5**, 2409 (1972).
4. S. A. Dikanov, A. A. Shubin, and V. N. Parmon, *J. Magn. Reson* **42**, 474 (1981).
5. E. J. Reijerse, and S. A. Dikanov, *Pure & Appl. Chem.*, **64**, 789 (1992).
6. A. M. Tyryshkin, S. A. Dikanov, and D. Goldfarb, *J. Magn. Reso* **A105**, 271 (1993).
7. P. Höfer, A. Grupp, H. Nebenführ, and M. Mehring, *Chem. Phys Lett.*, **132**, 279 (1986).
8. W. B. Mims, *Phys. Rev.*, **B6**, 3543 (1972).
9. C. Gemperle, G. Abeli, A. Schweiger, and R. R. Ernst, *J. Magn. Reson.*, **88**, 241 (1990).
10. A. A. Shubin, and S. A. Dikanov, *J. Magn. Reson.*, **52**, 1 (1983).
11. M. Heming, M. Narayana, and L. Kevan, *J. Chem. Phys.*, **83**, 14 (1985).
12. M. Romanelli, M. Narayana, and L. Kevan, *J. Chem. Phys.*, **83**, 4395 (1985).
13. K. Matar, and D. Goldfarb, *J. Chem. Phys.*, **96**, 6464 (1992).
14. D. M. Brink, and G. R. Satchler, *Angular Momemtum*, Clarendo Press, Oxford University, London, 22 (1968).

IV. INSTRUMENTATION

The pulsed-EPR spectrometer used for the research in this thesis was built by Professor J. McCracken at Michigan State University in 1990. The details of its design have been described elsewhere.[1] As part of this thesis work, several modifications have been made to the pulse programming portion of the spectrometer to provide a more open structure for the incorporation of new pulsed-EPR methods. Currently, the instrument can perform 2-, 3-, and 4-pulse ESEEM,[2-4] HYSCORE (hyperfine sublevel correlation spectroscopy),[5] Mims pulsed-ENDOR,[6] Davis pulsed-ENDOR,[7] ESE-EPR (electron spin echo detected EPR),[8] "2+1" ESE,[9] and DEER (double electron electron resonance) ESE.[10] A schematic diagram of the spectrometer is shown in Fig. IV-1.

The spectrometer was constructed with wideband frequency components and covers a frequency range from 6 to 18 GHz. A microwave synthesizer (Gigatronics, Model 610) serves as the microwave source. The synthesizer output is divided by a directional coupler (Omni Spectra, Model PN2025-6018-10) so that 90 % of the MW power goes to a reference arm and 10 % is directed to two microwave pulse-forming arms. The reference arm has an adjustable phase shifter (ARRA, Model 9828A) and makes detection of the magnetization in the rotating frame possible by phase sensitive detection. A power divider (Omni Spectra, Model PN2089-6209-00) splits the remaining source power into two

independent pulse channels through an isolator (Innowave, Model 1119IR). Each pulse channel consists of a low-power, high-speed PIN diode switch

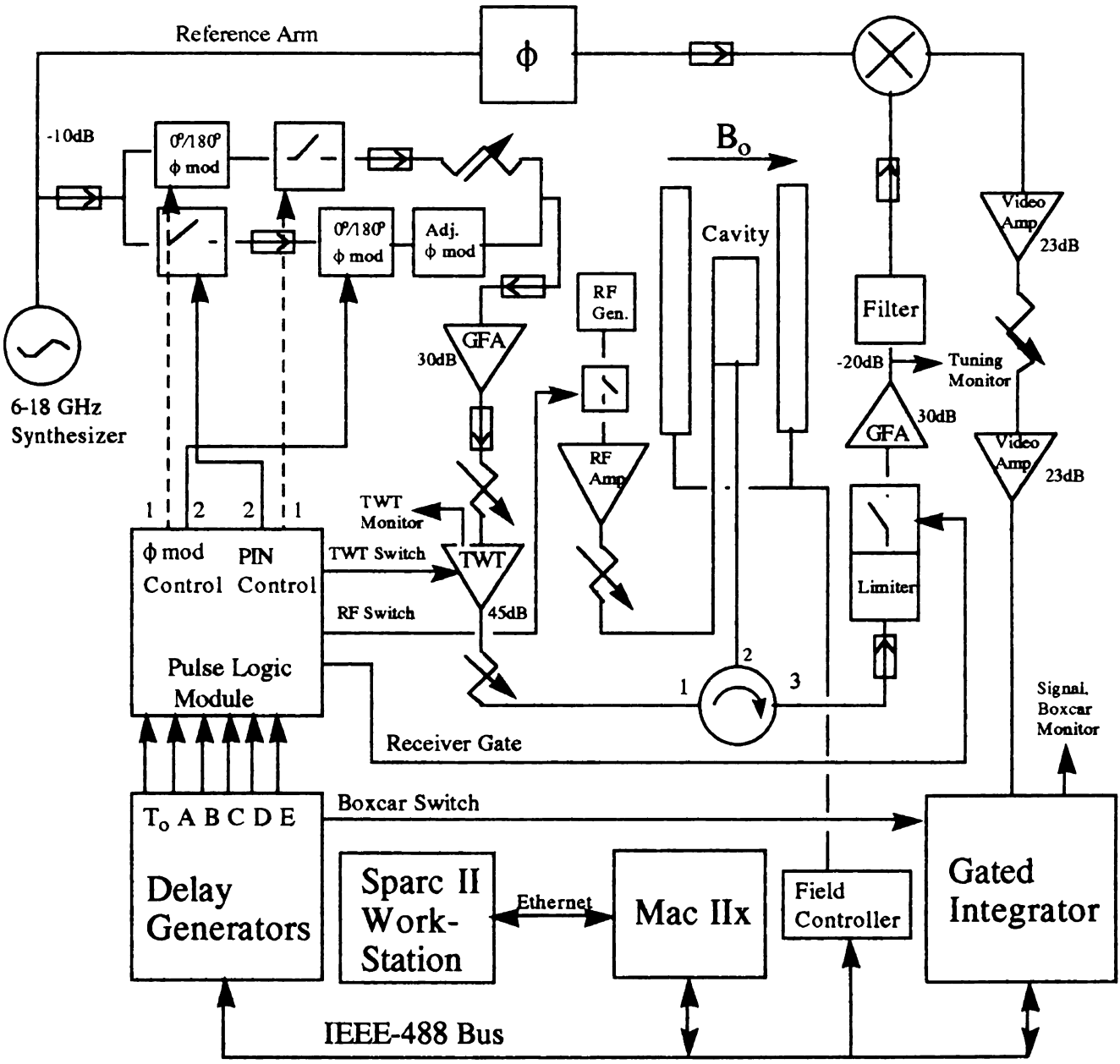

Figure IV-1. Schematic diagram of pulsed-EPR spectrometer built in Michigan State University

(General Microwave, Model FM864-BH), a high-speed 0°/180° wideband digital phase modulator (General Microwave, Model F1938) and an isolator. The pulse widths and phases of each channel are controlled by a home-built pulse logic circuit whose circuit drawings and timing diagrams

are in Appendix, A5. One of the pulse channels has an attenuator (ARR/
Model P9804-20) and the other has an adjustable phase shifter. By th
adaptation of the two MW pulse channels, the phases and the amplitude
the MW pulses are controlled independently to do phase-cycling ar
"pulse-swapping".[11] The MW pulses of each channel are combined at
power divider and fed into a medium power GaAs FET amplifi
(Avantek, Model SWL-89-0437) which amplifies the low power M
pulses to the required minimum input power of the travelling wave tub
amplifier. The MW pulse power is fed into a 1kW pulsed travelling wa
tube (TWT) amplifier (Applied Systems Engineering, Model 117) via a
attenuator. The high power MW pulses from the TWT are passed throug
a rotary vane attenuator (Hewlett Packard, Model X382A) and fed into
reflection type resonator through a circulator (MACOM, Model MA
8K269). The cavity used for the experiments described in this thes
employs a folded half-wave resonator[12] and an X-band Gordon coupler.
Signals from the resonator are fed to a low-noise GaAs FET amplifi
(Avantek, Model AWT-18635). This amplifier is protected from the hig
power excitation pulses by a medium-power, high-speed PIN diode limit
(Innowave, Model VPL-6018) and a fast PIN diode switch (Gener
Microwave, Model F9114) which is controlled by the pulse-logic circuit.
% of the amplified signal is fed into an oscilloscope (Hewlett Packar
Model 54520A) for spectrometer tuning via a directional coupler. Tl
signal is fed into a double balanced mixer (RHG, Model DM2-18 Al
through a bandpass filter (K & L Microwave, Model 3H10-2000/1800
0/0) which serves to remove radio frequency noise introduced by the PI
swithches. The mixing scheme is a conventional homodyne arrangemer
At the mixer, the signals from the reference arm and the receiver a

combined to generate signals at the sum and difference of the two inp frequencies. The amplitude of the signal is proportional to the two inp amplitudes and their relative phases. In our instrument, the amplitude the difference frequency is chosen to be amplified and adjusted by sever video amplifiers (Comlinear, Model E220) and a variable attenuator (JFW Model 50DR-003). The amplified signal is fed into a gated integrat (Stanford Research, Model 250) which is triggered by a signal from delay generator (Stanford Research, Model DG535).

The spectrometer is controlled by a Macintosh IIx microcomput (Apple Computer) via an IEEE-488 interface (National Instruments) to th delay generator, the gated integrator and a computer interface modu (Stanford Research, Model SR245). The delay generator is used to genera the accurate timing signals which are transferred to the pulse logic circu to control microwave pulse generation and spacing, trigger the gate integrator, and control the overall repetition rate of the experiment. Th computer interface module serves to digitize the output of the gate integrator, to count the number of pulse sequences repeated at a given MW pulse spacing, and to clear the gated integrator after its analog output ha been read. Data collection and analysis software are written using the computer language (Symantec). In Appendix, A6, computer programs fo performing four-pulse ESEEM and HYSCORE are listed. The Macintos microcomputer is connected via ethernet to a SPARCstation 2 workstatio (Sun Microsystems) where more sophisticated analysis programs ar written in the MATLAB computer language (The Mathworks, Inc).

ESE-ENDOR experiments can be performed using an RF generat (Hewlett Packard, Model 8656B). The low power RF signal is pulsed by RF GaAs switch (Mini Circuits, Model YSW-50DR) which can b

controlled by another home-built pulse logic circuit. The RF pulse powe amplified by a RF amplifier (ENI, Model 3200L) and fed into resonator via a variable attenuator (JFW, Model 50DR-003).

The magnetic field strength is provided by an electro-mag (Walker Scientific, Model HF-12H) and controlled over a range from 5 to 15000 G by a Hall-effect field controller (Bruker, Model B-H15). field controller is interfaced to the spectrometer computer via the IE 488 interface to perform ESE-EPR experiments.

References

1. J. McCracken, D. -H. Shin, and J. L. Dye, *Appl. Magn. Reson.*, **3** 305 (1992).
2. W. B. Mims, *Phys. Rev.* , **B5**, 2409 (1972).
3. W. B. Mims, *Phys. Rev.* , **B6**, 3543 (1972).
4. C. Gemperle, G. Abeli, A. Schweiger, and R. R. Ernst, *J. Magn. Reson.*, **88**, 241 (1990).
5. P. Höfer, A. Grupp, H. Nebenführ, and M. Mehring, *Chem. Phys Lett.*, **132**, 279 (1986).
6. W. B. Mims, *Proc. Roy. Soc.*, **A283**, 452 (1965).
7. E. R. Davis, *Phys. Lett.*, **A47**, 1 (1974).
8. R. T. Weber, J. A. J. M. Disselhorst, L. J. Prevo, J. Schmidt, and Th. Wenckebach, *J. Magn. Reson.*, **81**, 129 (1989).
9. V. V. Kurshev, A. M. Raitsimring, and Yu. D. Tsvetkov, *J. Magn Reson.*, **81**, 441 (1989).
10. A. D. Milov, K. M. Salikhov, and M. D. Shchirov, *Sov. Phys. Sol State*, **23**, 565 (1981)
11. J. -M. Fauth, A. Schweiger, L. Braunschweiler, J. Forrer, and R. Ernst, *J. Magn. Reson.*, **66**, 74 (1986).
12. C. P. Lin, M. K. Bowman, Norris, J. R., *J. Magn. Reson.*, **65**, 36 (1985).
13. R. D. Britt, M. K. Klein, *J. Magn. Reson.*, **74**, 535 (1987).

V. FOUR-PULSE ELECTRON SPIN ECHO ENVELOPE MODULATION STUDIES OF AXIAL WATER LIGATION TO BIS-AQUO TETRACYANONICKELATE(III)

1. Abstract

Four-pulse electron spin echo envelope modulation (ESEEM) studies aimed at enhancing our previous characterization of the hyperfine interactions between protons of axially bound water molecules and nickel ion in $Ni(III)(CN)_4(H_2O)_2^-$ were carried out. Because the ligand hyperfine coupling of the strongly bound water protons to Ni(III) is characterized by a large anisotropic interaction, an ESEEM feature at the sum combination band, $\nu_\alpha+\nu_\beta$, that shows pronounced shifts from twice the proton Larmor frequency is observed. In contrast to our previous study where a two-pulse ($\pi/2$-τ-π) microwave pulse sequence was used, four-pulse data show deep modulation with reduced damping for the sum combination feature that results in a 10-fold increase in spectral resolution. The corresponding ESEEM spectra provide lineshape and frequency constraints that allow for a more accurate and complete characterization of the bound water proton hyperfine coupling tensor. Theoretical simulation of the magnetic field profile dependence of the $\nu_\alpha+\nu_\beta$ lineshapes and frequency shifts from the twice the Larmor frequency gave an effective Ni-H dipole-dipole distance of 2.33±0.03 Å and a θ_n, the orientation for the principal axis system of

the ^1H hyperfine coupling tensor with respect to the g_3 axis of the Ni(g-tensor, of 18±3°. The τ-suppression behavior of the $\nu_\alpha+\nu_\beta$ lineshape a fixed magnetic field position was used to place more exact constraints the isotropic hyperfine coupling constant than possible with a simple tv pulse approach. An isotropic hyperfine coupling constant of 2.5±0.5 M was found for the bound axial water protons.

2. Introduction

The electron spin echo envelope modulation (ESEEM) technique pulsed EPR spectroscopy is a useful tool for characterizing weak hyperf interactions (HFI) that are not resolved in conventional continuous wa (CW) EPR due to inhomogeneous line broadening.[1-3] When the hyperf interaction is largely anisotropic, the fundamental hyperfine frequenc (ν_α and ν_β) are broadened and marked by lineshape singularities t provide for the accurate determination of hyperfine couplings in orientationally disordered system. Unfortunately in ESEEM spectrosco the anisotropy in the modulation amplitudes obscures these singularities a often prevents or hampers the determination of hyperfine ten components.[4] In two-pulse ESEEM spectra, fundamental, sum ($\nu_\alpha+\nu_\beta$) a difference ($\nu_\alpha-\nu_\beta$) combination frequencies are observed for coup nuclei.[5,6] Of these spectral features, the sum combination peak has recei much attention in recent studies because of the sensitivity of its freque position to the anisotropic portion of the hyperfine interaction.[7-9] T advantages of using the proton sum combination peak in ESEEM spec for characterizing large anisotropic hyperfine couplings are that spectral lines are narrow and occur at frequencies where there is

relatively clean spectral window,[10] and for spin systems where g- o hyperfine anisotropy dominate the EPR absorption spectrum, the variatio in the sum combination frequency shift from twice the nuclear Larmo frequency as a function of magnetic field strength allows accurat determination of the orientation of the ligand hyperfine tensor principa axes.[11-13] However, the spectral resolution of a two-pulse ESEE experiment is limited by relatively short electron spin phase memory time (T_M). To overcome these problems, a four-pulse ESEEM experiment ($\pi/2$ τ-$\pi/2$-T/2-π-T/2-$\pi/2$) has been suggested.[14-16] In these experiments, a π pulse is applied in the middle of the free precession period between th second and third pulses of a stimulated echo ESEEM sequence. The tim domain ESEEM data are collected as a function of T, the time interva between the second and fourth pulses of the sequence. The sun combination band can also be detected using this sequence, but with spectral resolution that is dependent on T_1.

The lineshape properties of the sum combination band have bee derived for systems with an isotropic electron g-tensor and an axia electron nuclear hyperfine tensor.[9] When the hyperfine coupling is smal so that $|T+2a| << 2\nu_I$ (where the dipolar part of the hyperfine tensor i represented by principal values (-T, -T, 2T), "a" is the isotropic couplin and ν_I is the nuclear Larmor frequency), the position of the lineshap singularity is expressed by $\nu_\alpha+\nu_\beta = 2\nu_I+(9/16)T^2/\nu_I$.[9,17] For systems wit axial g-tensors, analytical expressions for the sum combination pea positions at magnetic field positions corresponding to $g_\parallel$ and $g_\perp$ extrema c an EPR spectrum have also been developed.[12,18]

Recently, two-pulse ESEEM studies have been used to characteriz the proton hyperfine couplings of the axially bound water ligand o

$Ni(III)(CN)_4(H_2O)_2^-$.[13] Because the proton hyperfine interaction for the strongly-bound water ligands was mostly anisotropic, the sum combinati band provided a useful tool for the study. Field profiles constructed by t plotting the frequency shifts of the sum combination peaks from twice t Larmor frequency as a function of magnetic field strength across the EF absorption spectrum were used as a foundation for a more comple analysis of the anisotropic portion of hyperfine tensor and the orientati of the hyperfine tensor principal axes with respect to the g-tensor. Fro the analysis of the field profile, an effective Ni-H dipole-dipole distance 2.4 ± 0.1 Å, a scalar or isotropic hyperfine coupling of ≤ 4 MHz, and relative orientation of principal hyperfine axis with respect to g_3 axis (θ of 12 ± 3^o were determined.[13] The chief shortcomings of this field profi analysis are that the frequency shifts are only marginally sensitive to t isotropic portion of the hyperfine coupling,[9,11,12] and the reduction of t sum combination peak to a single frequency shift value precludes recove of the information contained in the lineshape.

Recently, four-pulse ESEEM studies of ^{15}N, ^1H, and ^2H have be reported. In these experiments, more accurate hyperfine and/or nucle quadrupole interaction (NQI) coupling parameters could be determin using an analysis based on sum combination peaks and their improv spectral resolution.[18,19] In this paper, our previous characterization of t ^1H-ligand hyperfine coupling for the axially bound water ligands $Ni(III)(CN)_4(H_2O)_2^-$ is refined using the four-pulse ESEEM technique a an enhanced sum combination peak analysis. Our analysis extends the fie profile strategy introduced in the previous study to include the behavior the sum combination peak lineshape singularities for a randomly orient sample. This method is developed for a spin system described by axial

and ligand hyperfine tensors, but can be easily extended to conside rhombic interactions. The selection of τ, the time interval between the firs and second pulses, can be used to tailor the amplitudes of the ESEEM components in an analogous way to that frequently used in conventiona three-pulse ESEEM studies. For the sum combination band, the suppressio effect is a function of the fundamental modulation frequencies which are in turn, sensitive to the isotropic hyperfine coupling.[14,16,18] The isotropi hyperfine coupling for the axially bound water protons was determine using the τ suppression behavior of the sum combination peak lineshape The results reveal a more refined hyperfine coupling tensor for thes protons.

3. Experimental

Bis-aquo tetracyanonickelate(III), $Ni(III)(CN)_4(H_2O)_2^-$, wa prepared according to the literature procedures.[20,21] Samples for CW-EPI and ESEEM experiments were mixed with an equal volume of ethylen glycol prior to freezing in liquid nitrogen.

CW-EPR spectra were obtained on a Varian E-4 X-band EPI spectrometer at 77K. ESEEM experiments were executed on a home-bui pulsed-EPR spectrometer which has been described in detail elsewhere.[2] An EIP model 25B frequency counter and a Micro-Now model 515B NMI gaussmeter were used to calibrate the microwave frequency and magneti field strength of the pulsed-EPR spectrometer. The ESEEM data wer collected at X-band using a reflection cavity that employed a folde stripline resonant element and a Gordon coupling arrangement suitable fc studies in a cryogenic immersion dewar.[23,24]

A four-pulse ($\pi/2$-τ-$\pi/2$-T/2-π-T/2-$\pi/2$) microwave pulse sequence was used to collect the ESEEM data. A second microwave pulse channel was employed for the π-pulse so that its width and amplitude could be controlled independently. The length (full-width at half maximum) of all four microwave pulses was 16 ns with the peak power of the π-pulse being the twice that of the $\pi/2$-pulses.[18] A four step phase cycle, +(0,0,0,0), +(π,π,0,0), +(0,0,π,0), +(π,π,π,0), was used to eliminate unwanted echo modulations. Four-pulse ESEEM data were collected as a function of T, the time interval between second and fourth pulses. Fourier transformation of the time domain ESEEM data were done without dead-time reconstruction. The fourier transformation and computer simulations were performed on a SPARCstation 2 workstation (Sun Microsystems) using software written in MATLAB v 4.2 (The Mathworks, Inc.).

4. Theory

The intensity of the sum combination peak derived from two-pulse ESEEM experiments on an orientationally disordered, S=1/2, I=1/2 spin system described by isotropic g- and axial hyperfine tensors is given by[9]

$$\mathbf{I}_{\nu\alpha+\nu\beta}(\theta) = \frac{1}{8}k(\theta)\sin\theta\left|\frac{\partial\theta}{\partial(\nu_\alpha+\nu_\beta)}\right| \qquad \text{[V-1]}$$

where

$$\mathbf{k} = \left(\frac{\nu_I B}{\nu_\alpha \nu_\beta}\right)^2,$$

$$\boldsymbol{\nu}_{\boldsymbol{\alpha}(\beta)} = [(\nu^2_{\|\alpha(\beta)} - \nu^2_{\perp\alpha(\beta)})\cos^2\theta + \nu^2_{\perp\alpha(\beta)}]^{1/2},$$

$$\nu_{\|\alpha(\beta)} = -\nu_I \pm \frac{a+2T}{2},$$

$$\nu_{\perp\alpha(\beta)} = -\nu_I \pm \frac{a-T}{2},$$

$B = 3T\sin\theta\cos\theta,$

$T = g_e g_n \beta_e \beta_n / hr^3$, and

$\nu_I = g_n \beta_n B_o / h.$ [V-2]

The terms in the above equations are: ν_I, the Larmor frequency of th coupled nucleus; $\nu_{\alpha(\beta)}$, the fundamental hyperfine frequencies in α and electron spin manifolds; a, the isotropic hyperfine coupling; θ, the angl between the external magnetic field and the principal hyperfine axis; g_e, th electron g-value; g_n, the nuclear g-value; β_e, the Bohr magneton; β_n, th nuclear magneton; r, the electron-nuclear distance; h, Planck's constan and B_o, the external magnetic field strength. The lineshape features ar governed by turning points of the sum combination frequency determine by calculating the conditions for which $\frac{\partial(\nu_\alpha+\nu_\beta)}{\partial\theta}=0$. For turning poin that occur at $\theta = 0$ and $\pi/2$, the modulation depth parameter, k, is equal t zero, so that no intensity singularities are observed. A third turning poi condition, for which an intensity singularity does exist, was derived b Reijerse and Dikanov,[9] and occurs when

$$\cos^2\theta = \frac{1}{2} + \frac{\frac{3}{2}T(T+2a)}{16\nu_I^2 - (T+2a)^2}, \qquad [V-3]$$

for $0 \le \cos^2\theta \le 1$ and $|T + 2a| < 4\nu_I$. These authors also derived th expression for the sum frequency of this turning point, $\nu_\alpha+\nu_\beta = 2\nu_I$

$(9/16)T^2/\nu_I$, allowing for direct determination of the dipolar hyperf coupling for isotropic electron spin systems.

For systems with an anisotropic g-tensor, the fundamental ESEE or ENDOR frequencies of an S=1/2 and I=1/2 spin system are giv by[25,26,27]

$$\nu_{\alpha(\beta)} = [(m_s A_1 - \nu_I l_1)^2 + (m_s A_2 - \nu_I l_2)^2 + (m_s A_3 - \nu_I l_3)^2]^{1/2} \qquad [V\text{-}4]$$

where m_s=1/2 or -1/2 for the α and β spin manifolds, respectively. T other terms in Eq. V-4 are

$$l_1 = \sin\theta\cos\phi,$$
$$l_2 = \sin\theta\sin\phi,$$
$$l_3 = \cos\theta,$$
$$A_1 = [g_1 l_1 (g_1 D(3n_1^2-1)+a) + 3g_2^2 l_2 D n_1 n_2 + 3g_3^2 l_3 D n_1 n_3]/g_e,$$
$$A_2 = [3g_1^2 l_1 D n_1 n_2 + g_2 l_2 (g_2 D(3n_2^2-1)+a) + 3g_3^2 l_3 D n_2 n_3]/g_e,$$
$$A_3 = [3g_1^2 l_1 D n_1 n_3 + 3g_2^2 l_2 D n_2 n_3 + g_3 l_3 (g_3 D(3n_3^2-1)+a)]/g_e,$$
$$n_1 = \sin\theta_n\cos\phi_n,$$
$$n_2 = \sin\theta_n\sin\phi_n,$$
$$n_3 = \cos\theta_n, \text{ and}$$
$$D = -g_n\beta_e\beta_n/hr^3. \qquad [V\text{-}5]$$

l_1,l_2,and l_3 are direction cosines that define the orientation of the exter magnetic field with respect to the g-tensor axes. n_1, n_2, and n_3 are direction cosines of the principal hyperfine tensor axis with respect to g-tensor. g_1, g_2, and g_3 are the principal values of the electron g-tensor. is the effective electron g-value for a discrete measurement with

$g_e = [(g_1l_1)^2 + (g_2l_2)^2 + (g_3l_3)^2]^{1/2}$.

In orientation selective ESEEM experiments with axial g-
hyperfine tensors, the angle between the external magnetic field and th
axis, θ, is fixed by the external magnetic field strength and the microv
pulse frequency. The hyperfine frequencies are also independent of ϕ_n
azimuthal angle used to describe the orientation of the hyperfine princ
axis system with respect to the g-tensor. Because θ_n, the angle betwee
principal hyperfine axis and the g_3 axis, is constant for a given li
geometry, the lineshape functions of the hyperfine frequencies will
function of ϕ, the azimuthal angle that describes the external magnetic
direction with respect to the g-tensor axes.

For an S=1/2, I=1/2 spin system, the echo modulation function
results from a four-pulse ESEEM experiment was derived by Gemp
et. al.,[14,16,18] and is given by

$$E_{mod}(\tau,T) = 1-\frac{k}{4}[C_o+C_\alpha\cos(\frac{\omega_\alpha T}{2}+\frac{\omega_\alpha \tau}{2}) + C_\beta\cos(\frac{\omega_\beta T}{2}+\frac{\omega_\beta \tau}{2}) + C_+\cos(\frac{\omega_+ T}{2}+\frac{\omega_+ \tau}{2}) + C_-\cos(\frac{\omega_- T}{2}+\frac{\omega_- \tau}{2})] \quad [V\text{-}6]$$

where

$$C_o = 3-\cos(\omega_\alpha\tau)-\cos(\omega_\beta\tau)-s^2\cos(\omega_+\tau)-c^2\cos(\omega_-\tau),$$

$$C_\alpha = 2[c^2\cos(\omega_\beta\tau-\frac{\omega_\alpha\tau}{2})+s^2\cos(\omega_\beta\tau+\frac{\omega_\alpha\tau}{2})-\cos(\frac{\omega_\alpha\tau}{2})],$$

$$C_\beta = 2[c^2\cos(\omega_\alpha\tau-\frac{\omega_\beta\tau}{2})+s^2\cos(\omega_\alpha\tau+\frac{\omega_\beta\tau}{2})-\cos(\frac{\omega_\beta\tau}{2})],$$

$$C_+ = -4c^2\sin(\frac{\omega_\alpha\tau}{2})\sin(\frac{\omega_\beta\tau}{2}),$$

$$C_- = -4s^2\sin(\frac{\omega_\alpha\tau}{2})\sin(\frac{\omega_\beta\tau}{2}),$$

$$s^2 = \frac{|\omega_I^2 - \frac{1}{4}(\omega_\alpha+\omega_\beta)^2|}{\omega_\alpha\omega_\beta},$$

$$c^2 = \frac{|\omega_I^2 - \frac{1}{4}(\omega_\alpha-\omega_\beta)^2|}{\omega_\alpha\omega_\beta}, \text{ and}$$

$$k = 4s^2c^2. \qquad [V\text{-}7]$$

$\omega_{\alpha(\beta)}$ are the angular frequencies of $\nu_{\alpha(\beta)}$ which are given in Eq. V-4 a
$\omega_\pm = \omega_\alpha \pm \omega_\beta$. c^2 and s^2 are the EPR transition probabilities. Hence, t
lineshape function of the four-pulse sum combination band is determin
by the depth parameter, $k(\phi)$, the τ-dependent coefficient, C_+ in Eq. V-
and the line integral weighting factor, $[(\partial\theta/\partial\phi)^2+\sin^2\theta]^{1/2}d\phi$.[28] F
systems described by axial g and ligand hyperfine tensors, θ is constant f
a given measurement and the lineshape function of the sum combinati
band detected in four-pulse ESEEM experiments can be expressed as

$$I_{\nu\alpha+\nu\beta}(\phi) = k(\phi)c^2\sin(\frac{\omega_\alpha\tau}{2})\sin(\frac{\omega_\beta\tau}{2})\sin\theta\left|\frac{\partial\phi}{\partial(\nu_\alpha+\nu_\beta)}\right|. \qquad [V\text{-}8]$$

The frequency distribution range of the sum combination band
determined by the turning points of the sum frequencies where t
condition, $\frac{\partial(\nu_\alpha+\nu_\beta)}{\partial\phi}=0$, is satisfied. For the case where both g- and liga
hyperfine tensors are axial, ϕ_n can be set to be zero and the derivative,

$$\frac{\partial\nu_{\alpha(\beta)}}{\partial\phi} = \frac{3m_sDl_2n_1}{g_e\nu_{\alpha(\beta)}}[g_1^2n_1l_1\{2\nu_I - \frac{m_s}{g_e}g_1(g_1D+2a)\}] \qquad [V\text{-}9]$$

$$+ n_3 l_3\{(g_1^2+g_3^2)\nu_I - \frac{m_s}{g_e} g_1 g_3 (g_1 g_3 D + (g_1+g_3)a)\}]$$

is obtained. When $l_2 = \sin\theta\sin\phi = 0$ and $\sin\theta \neq 0$, there are the tur
points for the sum frequency when $\phi = 0$ and π. The other turning p
can not be derived analytically, but can be obtained numerically for a g
θ by calculation of ϕ values for which $\frac{\partial(\nu_\alpha+\nu_\beta)}{\partial\phi} = 0$. At these tur
points, the intensities of the sum frequencies show singularities exce
$\nu_\alpha+\nu_\beta=2\nu_I$ where branching of the EPR transitions ceases (s^2 and k
zero in Eq. V-7 and V-8).

These turning points can also be estimated using Eq. V-2 in
strong field limit. For axial g- and ligand hyperfine tensors,
fundamental frequencies are given by

$$\nu_{\alpha(\beta)} = [(\nu^2_{\parallel\alpha(\beta)} - \nu^2_{\perp\alpha(\beta)})\cos^2\kappa + \nu^2_{\perp\alpha(\beta)}]^{1/2} \qquad \text{[V-10}$$

where κ defines the angle between the external magnetic field direction
the principal axis of the hyperfine tensor with

$$\cos\kappa = \sin\theta\sin\theta_n\cos\phi + \cos\theta\cos\theta_n \qquad \text{[V-11}$$

and $\phi_n=0$. The turning points of the sum combination peak obtained
Eq. V-10 occur when $\phi=0, \pi$, $\cos\phi = -\frac{\cos\theta\cos\theta_n}{\sin\theta\sin\theta_n}$ (for $\sin\theta\sin\theta_n \neq 0$ a
$\leq \cos\phi \leq 1$), and when $\cos^2\kappa = \frac{1}{2} + \frac{\frac{3}{2}T(T+2a)}{16\nu_I^2 - (T+2a)^2}$ (for $\cos(\theta+\theta$
$\cos\kappa \leq \cos(\theta-\theta n)$ and $|T+2a| < 4\nu_I$). The latter condition is identical to

of Eq. V-3, but the limits have changed because of the relative orientatio between the magnetic field and the hyperfine principal axis system. Th turning point for $\cos\phi = -\frac{\cos\theta\cos\theta_n}{\sin\theta\sin\theta_n}$ is also obtained when $g_1=g_3$ in Ec V-9. At this turning point, an intensity singularity is not observed becaus the sum frequency is equal to twice the Larmor frequency. Tyryshkin e al.[12,18] have derived analytical expressions for the sum frequencies of th singularity points at the $g_{\|}$ and $g_{\perp}$ extremes of the EPR absorptio spectrum utilizing Eq. V-10. These expressions are useful fc determination of the dipolar hyperfine coupling and the relative orientatio of the hyperfine principal axis with respect to the g-tensor, but are les sensitive to the isotropic hyperfine couplings.

Fig. V-1 shows plots of the simulated sum frequency shi $[\Delta\nu=(\nu_\alpha+\nu_\beta)-2\nu_I]$ profiles of the turning or lineshape singularity points a a function of magnetic field strength across the EPR absorption line as function of θ_n for a spin system described by axial g- and ligand hyperfin tensors. The sum frequencies of the turning points were calculated usin Eq. V-4 and V-5, principal g values of 2.198, 2.198, and 2.007, and microwave frequency of 8.789 GHz. The solid line represents th singularity point for which $\phi=0$ and the dashed line shows the field profil of the $\phi=\pi$ singularity. The curves plotted using "+++" or "***" pattern represent singularities that were determined numerically. The dipole-dipol distance and the isotropic hyperfine coupling were fixed at 2.4 Å and MHz, respectively.

The field profile patterns of Fig. V-1 show a strong dependence o the angle between the principal axis of the hyperfine coupling tensor an the g_3 axis, θ_n. For $\theta_n=0$ (Fig. V-1 (a)), the hyperfine tensor principal axi

Figure V-1. Simulated field profiles of the frequency shifts, $(\nu_\alpha+\nu_\beta)-2\nu_I$, for the turning points of the proton sum combination bands across the EPR absorption spectrum as a function of θ_n. Parameters common to all simulations were $g_\perp$, 2.198; $g_\parallel$, 2.007; microwave frequency, 8.789 GHz; effective dipole-dipole distance, 2.4 Å; and isotropic hyperfine coupling, 0 MHz. For (a) θ_n=0°; (b) θ_n=30°; (c) θ_n=45°; (d) θ_n=60°; and (e) θ_n=90°. The solid and dashed curves represent singularities calculated for ϕ=0 and π, respectively, while "++++" and "****" patterns are for numerically calculated features. The frequency shifts were calculated at 46 magnetic field positions across the EPR absorption spectrum. The arrows in (b) indicate the field positions where the lineshapes are computed in Fig. V-2.

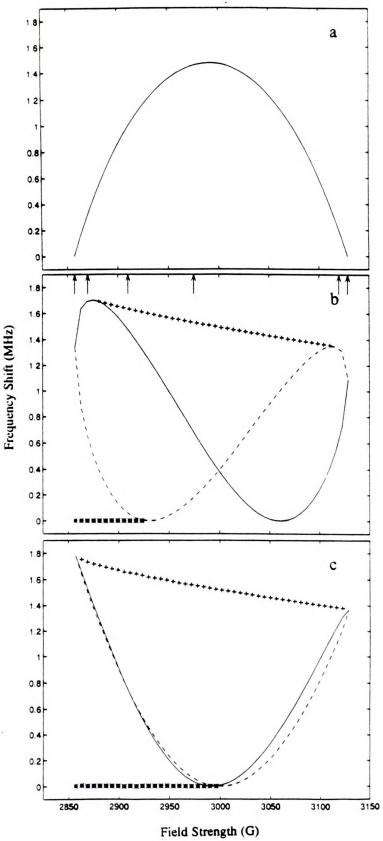
a
b
c
Frequency Shift (MHz)
Field Strength (G)
2850
2900
2950
3000
3050
3100
3150

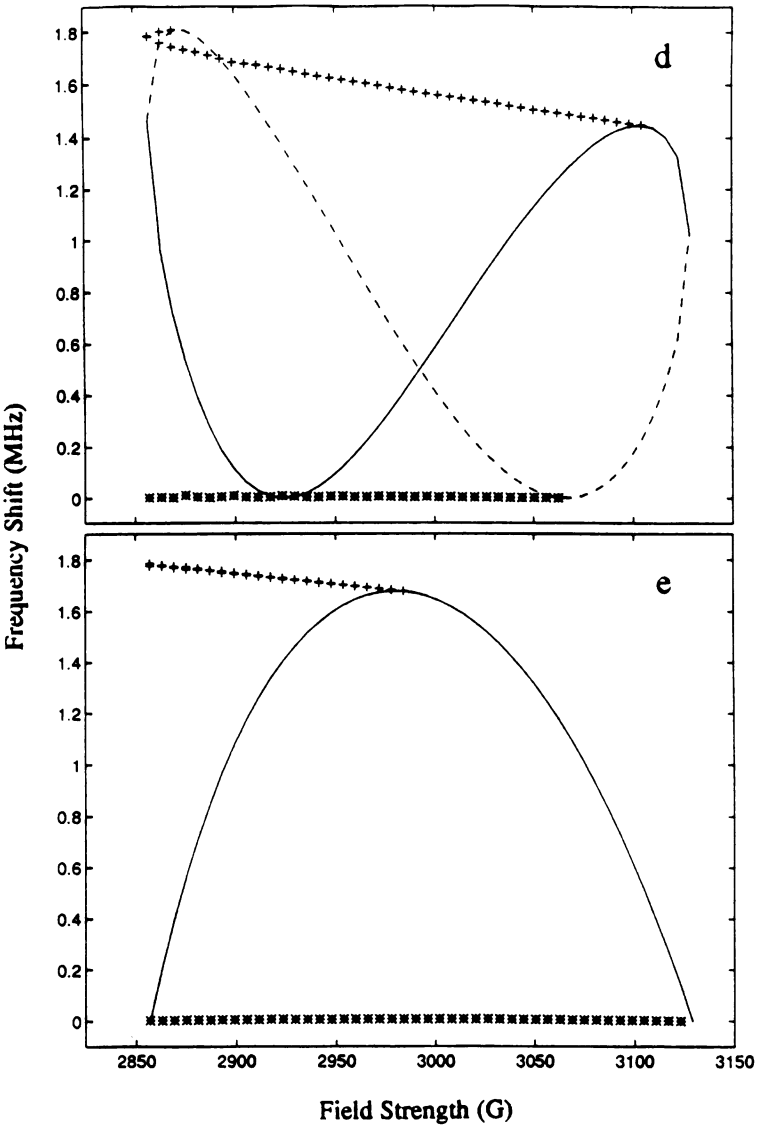
d
e
Frequency Shift (MHz)
Field Strength (G)
1.8
1.6
1.4
1.2
1
0.8
0.6
0.4
0.2
0
2850
2900
2950
3000
3050
3100
3150

is along g_3, so that the angle, κ, is equal to θ which varies from 90^o to 0^o across EPR absorption envelope. Hence, the ϕ dependence of the sum combination band (Eq. V-4 and V-5) is removed and the lineshape maxima occur at a single frequency for each magnetic field value. At $g_{\|}$ and $g_{\perp}$ extremes in Fig. V-1 (a), the angles, κ, are 0^o or 90^o, and the sum frequency shifts are zero. The resulting field profile is identical to that obtained using two-pulse ESEEM methods.[13]

At the high field extreme for each orientation shown in Fig. V-1, the magnetic field direction is aligned with g_3 axis. For this orientation, κ is determined by θ_n and the ϕ dependence of sum combination band is removed. Hence, the sum frequencies have only one singularity, or turning point, and show shifts from $2\nu_I$ that vary from 0 MHz when $\theta_n=0^o$ or 90^o to a maximum when $\theta_n=45^o$. At the $g_{\perp}$ extreme, $\theta=90^o$ and the angle, κ, will range from $\theta-\theta_n$ to $\theta+\theta_n$ with the sum frequency lineshape showing features determined by θ_n. The sum combination peak lineshape will cover frequencies from $2\nu_I$ to singularity points described by $\phi=0$, π or numerical solution of $\frac{\partial(\nu_\alpha+\nu_\beta)}{\partial\theta}=0$.

As θ_n is increased in Fig. V-1 (b)-(e), κ ranges from $\theta-\theta_n$ to $\theta+\theta_n$ and the sum frequency peak can show more than one singularity or turning point at a single magnetic field position. The field profiles marked with asterisks were numerically determined, and correspond to turning points that can be estimated from the relationship $\cos\phi = -\frac{\cos\theta\cos\theta_n}{\sin\theta\sin\theta_n}$, as derived from Eq. V-10. For this feature the sum frequency shift is zero. These turning points become intensity singularity points with non-zero frequency shifts from $2\nu_I$ when isotropic ligand hyperfine couplings are large and Eq. V-10 is no longer valid. With an electron-nuclear distance of 2.4 Å,

Figure V-2. Lineshapes of proton sum combination bands at field positions across the EPR absorption spectrum indicated by the arrows in Fig. V-1 (b). The magnetic field strengths represented are (a) 2857.0 G ($g_{\perp}$), (b) 2870.0 G, (c) 2910.0 G, (d) 2975.0 G, (e) 3120.0 G, and (f) 3128.8 G ($g_{||}$). An intrinsic linewidth (FWHM) of 0.03 MHz was used in the calculation to reveal all of the discrete lineshape features.

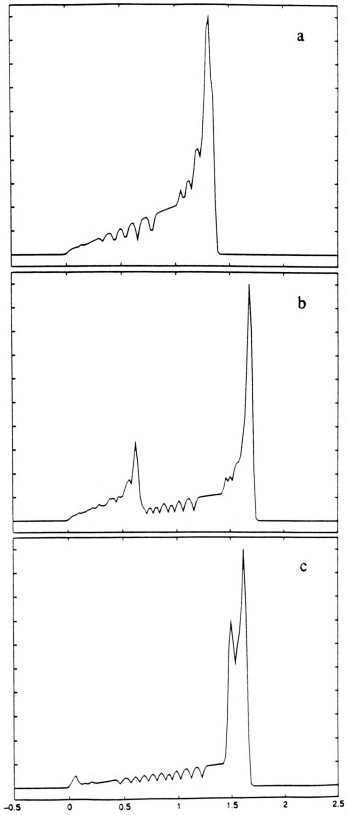
a
b
c
-0.5
0
0.5
1
1.5
2
2.5
Frequency Shift (MHz)

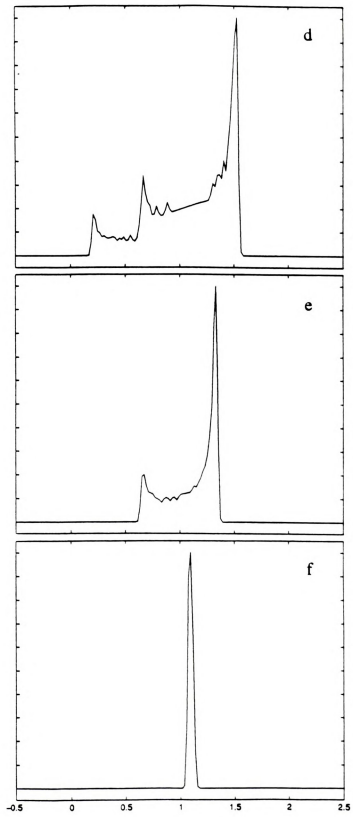
d
e
f
-0.5
0
0.5
1
1.5
2
2.5
Frequency Shift (MHz)

these turning points show intensity singularities when $a \geq 18$ MHz. The turning or singularity points marked with plus signs in Fig. V-1 can be estimated using the expression, $\cos^2\kappa = \frac{1}{2} + \frac{\frac{3}{2}T(T+2a)}{16\nu_I^2 - (T+2a)^2}$ from Eq. V-10. One interesting feature is shown in Fig.V-1 (d) (θ_n=60°) where a foldover of this turning point is observed at low magnetic field.

The predicted sum combination peak lineshapes that correspond to the various field values indicated by arrows on Fig. V-1 (b) (θ_n=30) are shown in Fig. V-2. The frequency shift, $(\nu_\alpha+\nu_\beta)-2\nu_I$, is displayed on the x-axis. At 2857.0 G ($g_\perp$), there are two turning points (Fig. V-1 (b)). One is an intensity singularity corresponding to ϕ=0 and π, and the other is numerically determined and occurs at zero frequency shift. Hence, the sum frequencies are spread from twice the Larmor frequency where the intensity is zero to the singularity point (Fig. V-2 (a)). At 2870G, the predicted sum frequency peak lineshape singularities occur at frequency shifts of 0.6 MHz and 1.7 MHz (Fig. V-2 (b)). The lineshapes shown in Fig. V-2 (c)-(f) mirror the changing pattern of singularity points across the EPR spectrum (Fig. V-1 (b)) in an analogous fashion. At the $g_\parallel$ extreme (3128.8 G), all singularity points occur at the same frequency position and only a single peak is predicted (Fig. V-1 (b) and Fig. V-2 (f)).

5. Results and Discussion

The CW-EPR spectrum of $Ni(III)(CN)_4(H_2O)_2^-$ showed $g_\parallel$ and $g_\perp$ features at 2.198 and 2.007, respectively, in agreement with previous findings.[13,21] Four-pulse ESEEM time domain data and the corresponding magnitude FT-ESEEM spectrum obtained at g=2.107 with τ=197 ns are

Figure V-3. Four-pulse ESEEM (a) time domain data and (b) corresponding magnitude FT spectrum. The experimental conditions were magnetic field strength, 2981 G; microwave frequency, 8.789 GHz; microwave pulse powers of $\pi/2$ and π pulses, 31.5 W and 63 W; pulse width, 16 ns (FWHM); sample temperature, 4.2 K; pulse sequence repetition rate, 10 Hz; events averaged/pt, 12; and τ, 197 ns.

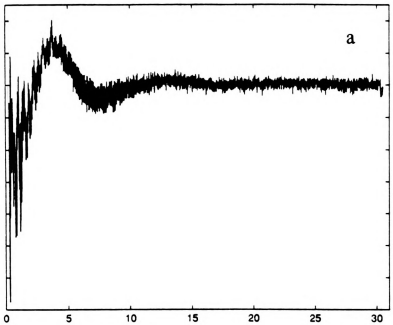

$\tau + T$ (μsec)

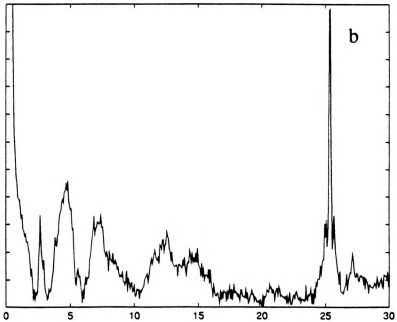

Frequency (MHz)

shown in Fig. V-3. Low frequency peaks are observed at 2.66, 2.8, and 5 MHz and are assigned to ^{14}N of the equatorially bound cyanide group The broad peaks that extend from 10 to 16 MHz are the fundament frequency bands of the axially bound water protons. The sharp, inten peak at 25.38 MHz, twice the proton Larmor frequency ($2\nu_I$) at 2981G, the second harmonic frequency of the matrix water protons. The su combination peak for the axially bound water protons is observed at 27.1 MHz, shifted 1.76 MHz from $2\nu_I$. Two well resolved, sharp peaks centere about $2\nu_I$ at 25.68 and 25.06 MHz can be assigned to combinatic frequencies that arise from the product of ESEEM contributions at 0.2 MHz due to ^{14}N and the matrix proton sum combination line[18,29-31] Th 0.26 MHz ^{14}N ESEEM component is not shown in Fig. V-3 (b) but can b seen in expanded spectra as a dominant feature.

Four-pulse ESEEM spectra collected at several magnetic fiel positions across the EPR absorption band showed that the sum frequenc peak positions of the axial water protons are shifted 0.8-1.9 MHz abov twice the Larmor frequency. The field profile constructed by plotting th measured frequency shifts of the sum frequencies *vs.* magnetic fiel strength is shown in Fig. V-4. The data were collected using a microwav frequency of 8.789 GHz and various τ values. The analysis of th experimental field profile was achieved using the singularity concept a explained in the above theory section. The frequency shifts in Fig. V-4 wi be on one of the singularity points at the experimental field strength. Fig V-5 shows a comparison of the experimental frequency shifts and th simulated singularity curves across the EPR absorption spectrum fo different dipole-dipole distances and fixed values of θ_n=18° and a=0 MH As expected the frequency shifts are strongly dependent on the dipole-

Figure V-4. A plot of the four-pulse ESEEM experimental proton sum frequency shifts (circles) from twice the proton Larmor frequency, $(\nu_\alpha+\nu_\beta)-2\nu_I$, *vs.* magnetic field strength for $Ni(III)(CN)_4(H_2O)_2^-$. Experimental conditions were same as in Fig. V-3 except magnetic field strengths and τ values which were 3131 G, 186 ns; 3041 G, 193 ns; 3011 G, 195 ns; 2981 G, 197 ns; 2951G, 199 ns; 2921 G, 201 ns; 2891 G, 203 ns; 2869 G, 205 ns; and 2844 G, 206 ns. Error bars represent the intrinsic uncertainty in measuring frequencies from four-pulse ESEEM spectra.

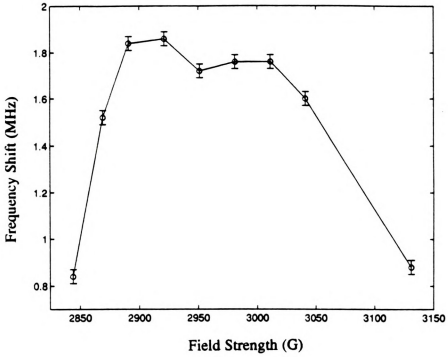
Frequency Shift (MHz)
2
1.8
1.6
1.4
1.2
1
0.8
2850
2900
2950
3000
3050
3100
3150
Field Strength (G)

Figure V-5. A comparison of the field profile of the axial water proton sum frequencies (circles) with simulated field profiles of the turning points of the proton sum combination peak lineshape for different effective dipole-dipole distances. The simulation parameters were $g_{\perp}$, 2.198; $g_{||}$, 2.007; microwave frequency, 8.789 GHz; a, 0 MHz, θ_n, 18°; r_{eff}, (a) 2.28 Å, (b) 2.33 Å, (c) 2.38 Å. The frequency shifts were calculated at 46 magnetic field positions across the EPR absorption spectrum.

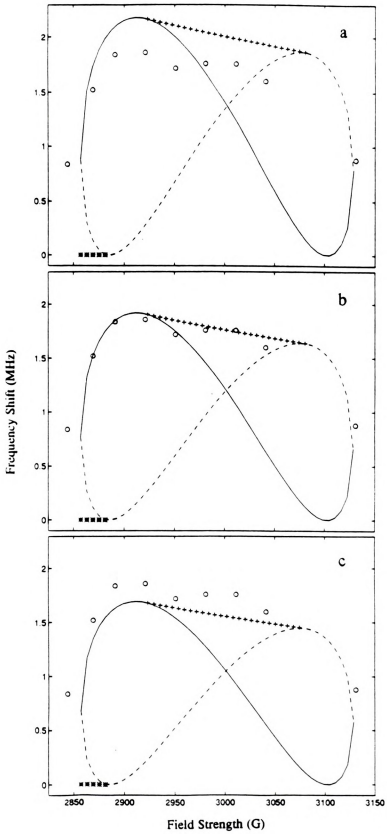
a
b
c
Frequency Shift (MHz)
Field Strength (G)
0
0.5
1
1.5
2
2850
2900
2950
3000
3050
3100
3150

dipole distance. Within the experimental resolution limit, the effective Ni-H dipole-dipole distance was found to be 2.33±0.03 Å. In Fig. V-6, the experimental field profile is compared to the calculated profiles for θ_n values of 13°, 18° and 23° holding r_{eff}=2.33 Å and a=0 MHz. The calculated field profiles show that the singularity curve for the ϕ=0 feature (solid line) rises more steeply in the low field region as θ_n increases within a reasonable range of values. A θ_n range of 18±3° is satisfactory for characterization of the axially bound water protons. The profile patterns and the frequency shifts were relatively insensitive to isotropic hyperfine couplings as expected.

For orientation selective ESEEM experiments on spin systems such as Ni(III)$(CN)_4(H_2O)_2^-$, where axial g- and ligand hyperfine tensors apply multiple lineshape singularities can be observed for the sum combination band. The nature of these singularities depend on the relative orientations of the tensors and are best observed in studies of the τ dependence of four-pulse ESEEM spectra. Fig. V-7 shows the sum combination peak regions of two four-pulse FT-ESEEM spectra obtained at g=2.109 with (a) τ=239 ns and (b) τ=260 ns. In the spectra, the sharp second harmonic peaks of the matrix protons are observed at 25.06 MHz, twice the proton Larmor frequency at 2944 G. The sum combination peaks are shown at (a) 26.66 MHz (τ=239 ns) and (b) 26.94 MHz (τ=260 ns) shifted 1.60 MHz and 1.88 MHz from twice the proton Larmor frequency, respectively. These lineshapes are broadened toward higher frequency because of the overlap of the sum combination band with a combination peak near 27.70 MHz resulting from the product of the matrix proton second harmonic ESEEM frequency with an ^{14}N fundamental peak at 2.6 MHz. The sum combination peak positions obtained using two different τ values at

Figure V-6. A comparison of the field profile of the axial water proton sum combination frequencies (circles) with the simulated field profile of the turning points of the proton sum combination peak lineshape for θ_n of (a) 13°, (b) 18° and (c) 23°. Other simulation parameters were identical to those of Fig. V-5 except r_{eff}, 2.33 Å; and a, 0 MHz.

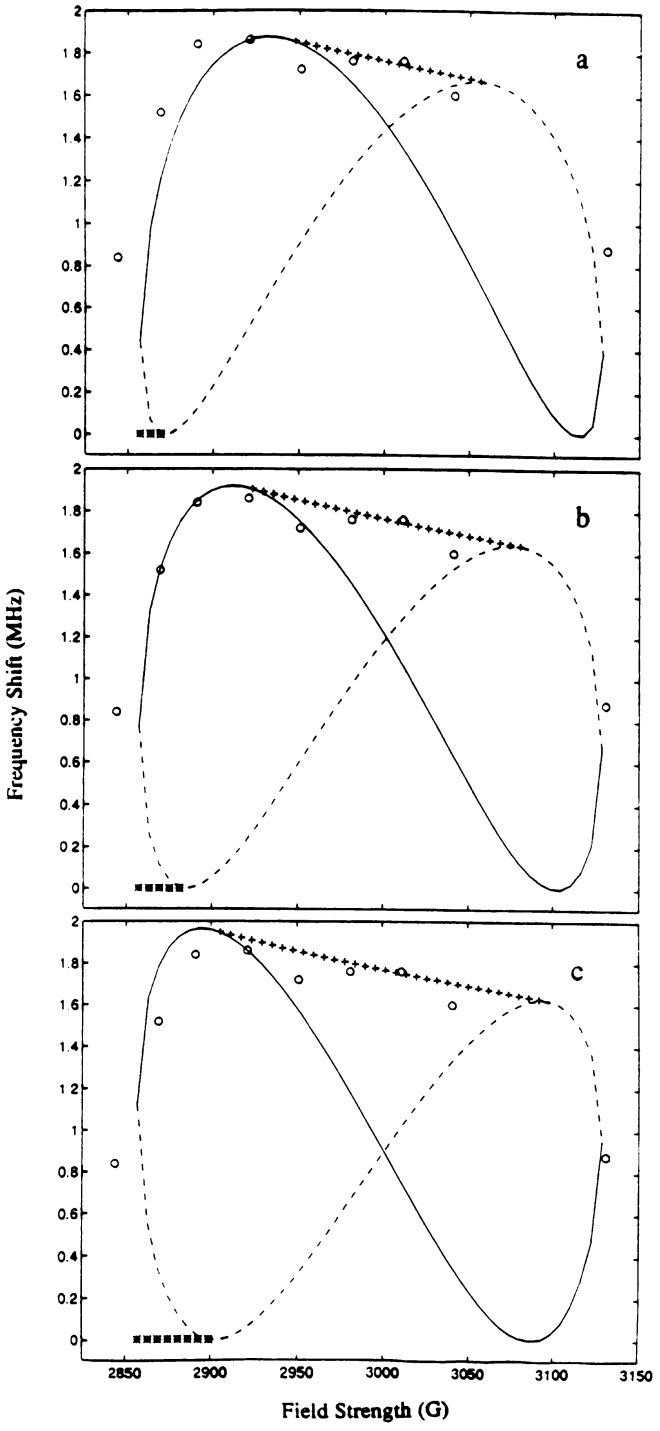
a
b
c
Frequency Shift (MHz)
Field Strength (G)
2850
2900
2950
3000
3050
3100
3150

Figure V-7. Proton sum combination peak lineshapes obtained from four-pulse magnitude FT-ESEEM spectra of $Ni(III)(CN)_4(H_2O)_2^-$. Experimental conditions were same as in Fig. V-3 except magnetic field strength, 2944G; microwave frequency, 8.691 GHz; τ, (a) 239 ns and (b) 260 ns.

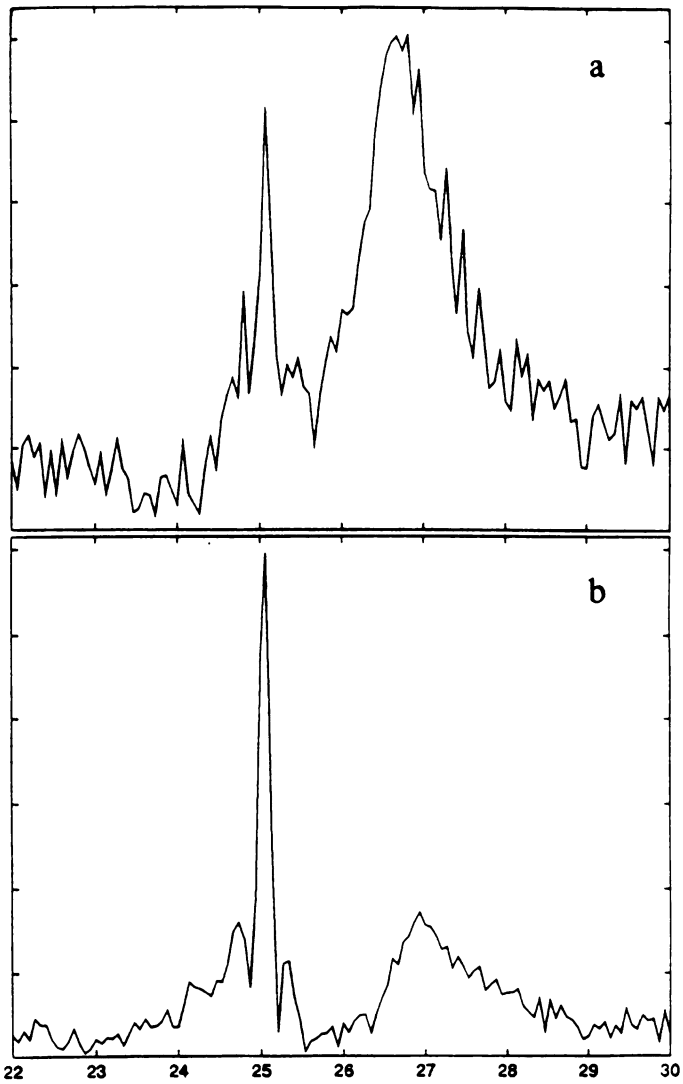
a
b
22
23
24
25
26
27
28
29
30
Frequency (MHz)

g=2.109 are plotted in Fig. V-8 along with the simulated singularity curves for r_{eff}=2.31 Å, θ_n=18°, (a) a=0 MHz, and (b) a=4 MHz. Fig. V-8 shows that both measured frequency shifts of sum combination peaks are accounted for by predicted lineshape singularities.

A major shortcoming of this field profile strategy as implemented using two-pulse ESEEM measurements was the lack of sensitivity of the method to the isotropic hyperfine coupling.[13] A comparison of the profiles shown in Fig. V-8 (a) and (b) show this same problem because they are calculated from Eq. V-4 and V-5 without the inclusion of ESEEM intensity weightings or the predicted singularity amplitudes. Because the τ suppression behavior of the sum combination peak amplitude depends on the isotropic hyperfine coupling, it is possible to use four-pulse ESEEM studies to refine its determination. In Fig. V-9, two sum combination peak lineshapes calculated with different intrinsic linewidths of (a) 0.03 MHz and (b) 0.4 MHz along with common hyperfine coupling parameters of r_{eff}=2.31 Å, θ_n=18°, and a=0 MHz are compared. The spectra in Fig. V-9 were calculated using Eq. V-8 with $\sin(\frac{\omega_\alpha \tau}{2})\sin(\frac{\omega_\beta \tau}{2})=1$. As a result, they show the entire lineshape without distortion from τ-suppression effects. In Fig. V-9 (a), all three singularity points at 26.06, 26.68, and 26.98 MHz are observed. To facilitate comparison between experiment and theory, a proper gauge of the intrinsic linewidth must be utilized. Fig. V-8 (a) shows that at the $g_{||}$ extreme, the sum frequency lineshape features collapse to a single frequency. Using the ESEEM spectrum collected at that magnetic field strength, we estimated the intrinsic linewidth to be 0.4 MHz. As shown in Fig. V-9 (b), when this intrinsic linewidth is used to calculate the

Figure V-8. A comparison of the measured proton sum frequency shifts (circles) from twice the proton Larmor frequency in Fig. V-7 with the simulated field profile of the turning points of proton sum combination band. The parameters for simulation were microwave frequency, 8.691 GHz; r_{eff}, 2.31 Å, θ_n, 18°; a, (a) 0 MHz, and (b) 4 MHz.

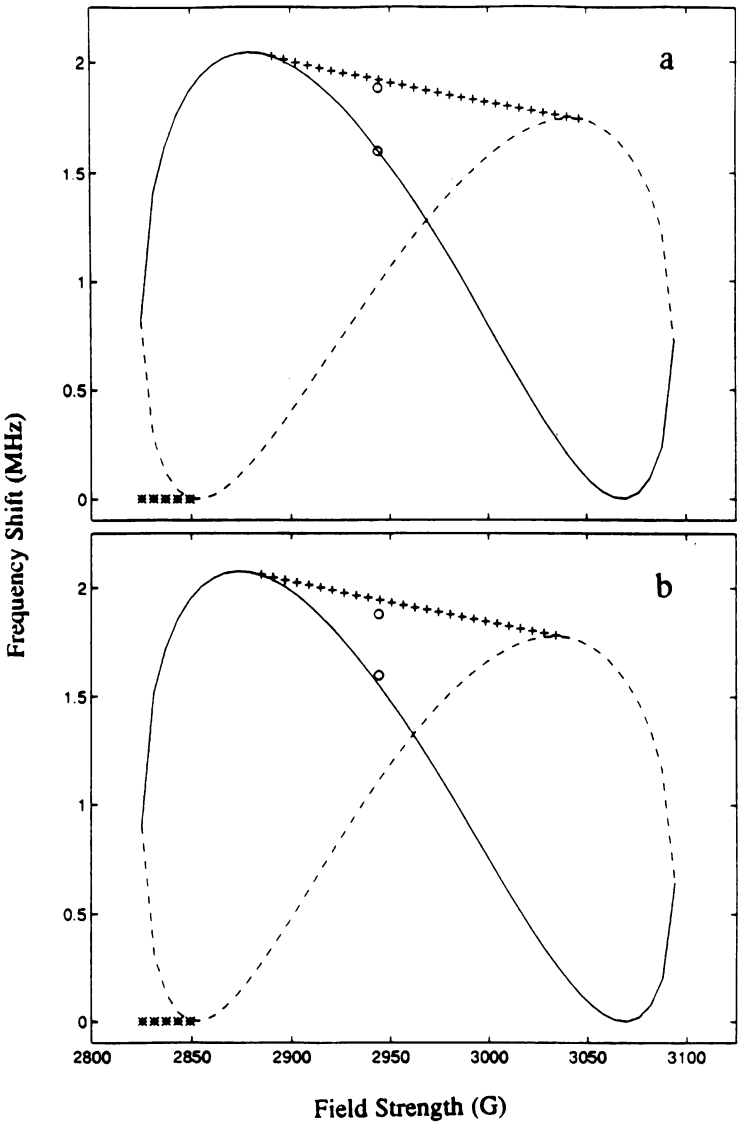
a
b
Frequency Shift (MHz)
Field Strength (G)
2
1.5
1
0.5
0
2800
2850
2900
2950
3000
3050
3100

Figure V-9. Simulations of the proton sum combination peak lineshapes the in frequency domain without the τ dependent coefficient of Eq. V-8. The simulation parameters were magnetic field strength, 2944 G, microwave frequency, 8.691 GHz, r_{eff}, 2.31 Å, θ_n, 18° and a, 0 MHz. Intrinsic gaussian linewidths (FWHM) were (a) 0.03 MHz, and (b) 0.4 MHz.

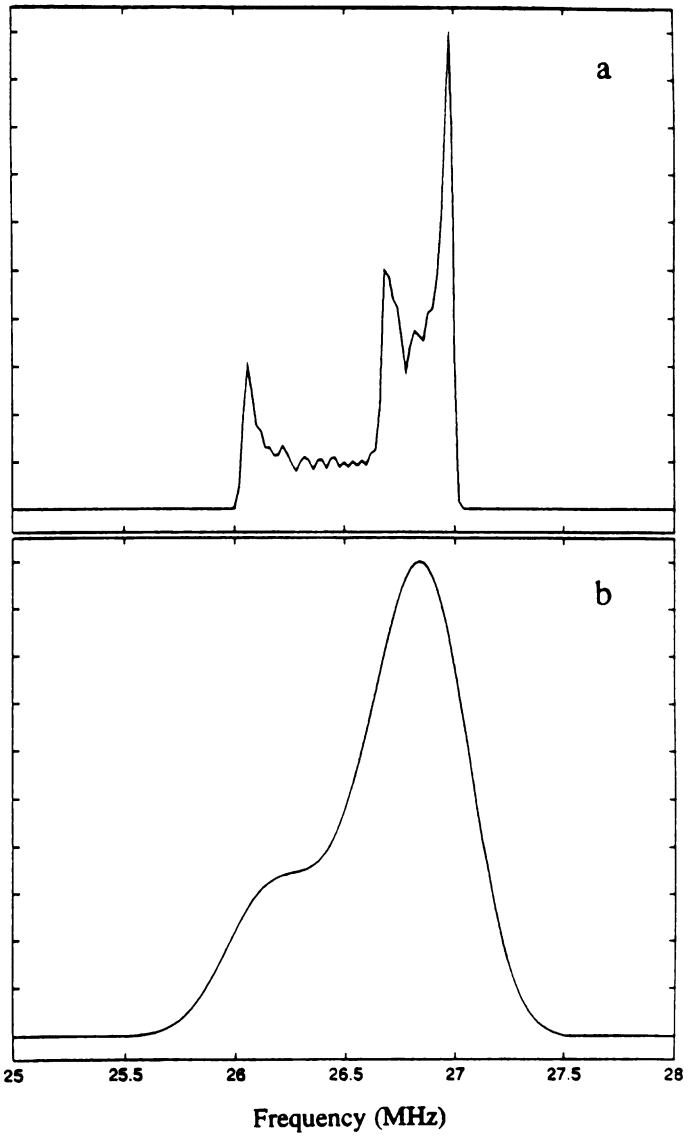
a
b
25
25.5
26
26.5
27
27.5
28
Frequency (MHz)

sum combination peak lineshape, the two higher frequency singularit points are not resolved.

Predicted sum combination peak lineshapes at g=2.109 using τ value of 239 and 260 ns are shown for different values of the scalar hyperfin coupling in Fig. V-10. For a=0 MHz with τ=239 ns (Fig. V-10 (a), botto trace), two peaks are predicted at 26.14 MHz and 26.90 MHz. When τ i increased to 260 ns leaving a=0 MHz (Fig. V-10 (b), bottom trace), only single peak at 26.76 MHz is found. As the isotropic hyperfine coupling i increased while holding θ_n and r_{eff} constant, pronounced changes in th number and frequency positions of the lineshape extrema are predicted fo the two τ values considered. In Fig. V-10 (a), with τ=239 ns, the peak du to the ϕ=0 singularity point appears when a ≥ 2 MHz, and for τ=260 n the feature that arises from the singularity point corresponding to $\cos^2\kappa$ = $\frac{1}{2} + \frac{\frac{3}{2}T(T+2a)}{16\nu_I^2 - (T+2a)^2}$ of Eq. V-10 is seen when a ≥ 1.5 MHz. Th lineshape feature corresponding to the $\phi=\pi$ singularity point is resolve when a ≥ 3 MHz. A comparison of these simulations with the data of Fig V-7 allow an isotropic hyperfine coupling of 2.5±0.5 MHz for the axiall bound water protons to be determined.

The results reported in this work are more refined than those of th previous two-pulse ESEEM studies where r_{eff}=2.4±0.1Å, a ≤ 4 MHz an θ_n=12±5° were obtained from a field profile analysis.[13] The improvemer arises from the higher resolution of the four-pulse ESEEM measuremen extension of the field profile analysis to include the details of the sur combination peak lineshape, and analysis of the τ-dependence of th lineshape. Since the hyperfine coupling mechanism of the axial wate protons to $Ni(III)(CN)_4(H_2O)_2^-$ is similar to that of the equatorially

Figure V-10. Simulated proton sum combination peak lineshapes including the τ dependent coefficient of Eq. V-8 and different isotropic hyperfine coupling constants. The simulation parameters were identical to those of Fig. V-9 except that the isotropic hyperfine coupling constants shown in figure were varied from 0 to 4.0 MHz, and intrinsic gaussian linewidths (FWHM) of 0.4 MHz were utilized. For the simulated lineshapes of Fig. V-10 (a), τ=239 ns, while for Fig. V-10 (b), τ=260 ns.

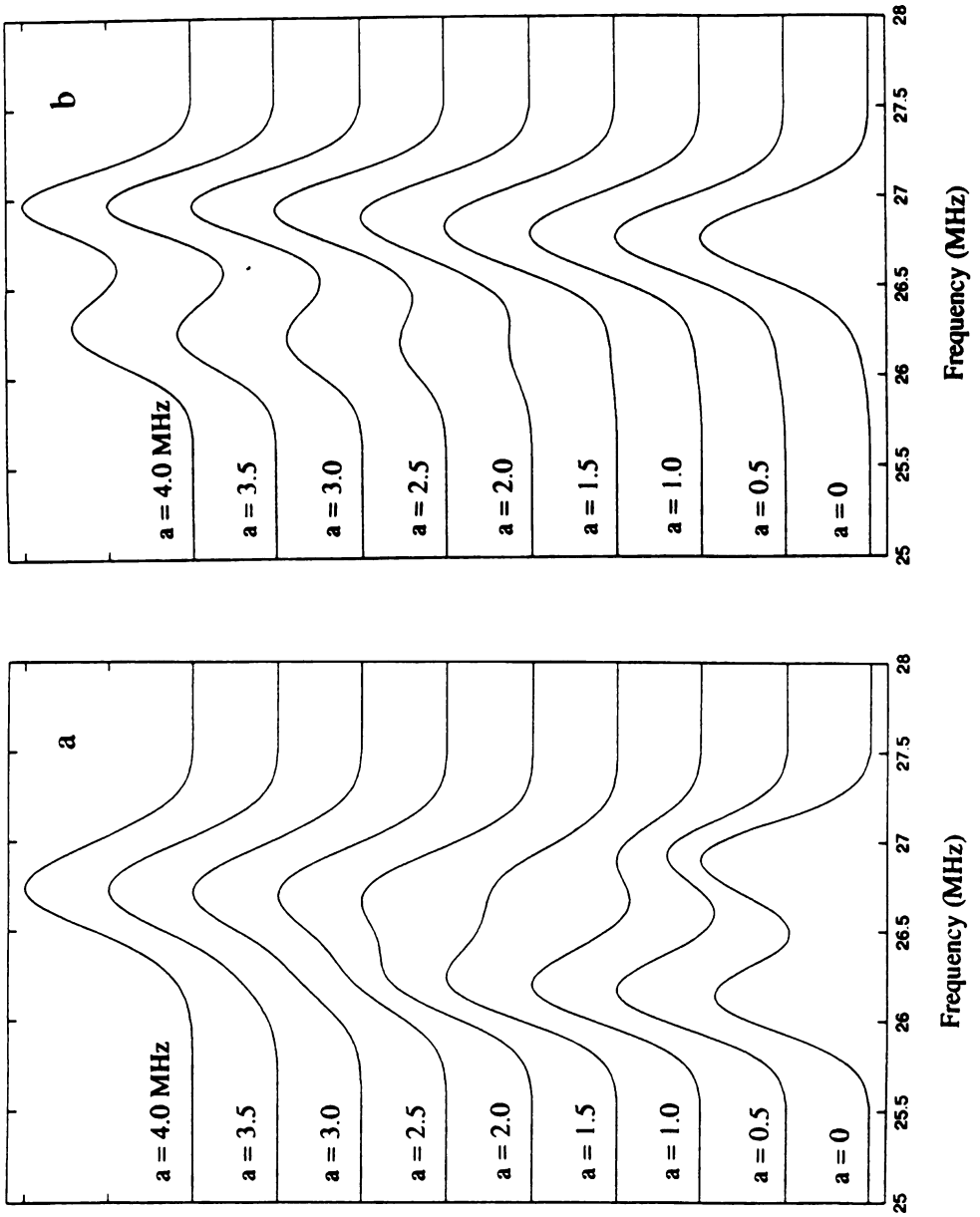
a
a = 4.0 MHz
a = 3.5
a = 3.0
a = 2.5
a = 2.0
a = 1.5
a = 1.0
a = 0.5
a = 0
25
25.5
26
26.5
27
27.5
28
Frequency (MHz)
b
a = 4.0 MHz
a = 3.5
a = 3.0
a = 2.5
a = 2.0
a = 1.5
a = 1.0
a = 0.5
a = 0
25
25.5
26
26.5
27
27.5
28
Frequency (MHz)

bound water protons of $Cu(II)(H_2O)_6^{2+}$, their ligand hyperfine couplings are expected to be comparable. Both scalar and dipolar portions of the proton hyperfine couplings found for $Ni(III)(CN)_4(H_2O)_2^-$ in this study are slightly larger than those reported previously for the equatorial protons of $Cu(II)(H_2O)_6^{2+}$ where isotropic ligand hyperfine couplings of $\leq$ 1.2 MHz and dipolar couplings of approximately 5 MHz were measured in single crystal ENDOR experiments.[32] The difference in isotropic hyperfine coupling is consistent with the larger crystal field splittings expected for CN^- *vs.* H_2O ligation.[21]

EPR methods have played an important role in characterizing the structure and biological function of the nickel cofactor of Ni-Fe hydrogenases which catalyze the reversible oxidation of dihydrogen.[33-35] Two oxidized and inactive forms (Ni-A and Ni-B) of the enzyme give distinct EPR signals.[36,37] The dominant species, Ni-A, has principle g-values of 2.31, 2.26, and 2.02, and the second species, Ni-B, has principle g-values of 2.33, 2.16, and 2.02. When the enzyme is activated under a H_2 atmosphere, only a third Ni EPR signal, Ni-C, characterized by a rhombic g-tensor with principle values of 2.19, 2.15 and 2.02 is observed.[36] Previous Q-band ENDOR studies of the Ni-C form of *D. Gigas* Ni-Fe hydrogenase at g_1=2.19 revealed that two kinds of exchangeable protons are bound to the Ni-C site with the hyperfine couplings of 4.4 MHz and 16.8 MHz assigned to bound H_2O or OH^- ligands and a proton directly coordinated to Ni, respectively.[38] Q-band ENDOR simulation with the results obtained from the present studies showed that the 4.4 MHz hyperfine coupling is in good agreement with the HFI couplings of the axial water proton of $Ni(III)(CN)(H_2O)_2^-$.[13] Recent Q-band studies of the Ni-C sites of the hydrogenase from *T. Roseopersicina* resolved a 20 MHz

hyperfine coupling from solvent exchangeable protons that originated from dihydrogen.[39] This extent of proton hyperfine coupling could not be realized using the hyperfine coupling parameters of $Ni(III)(CN)_4(H_2O)_2$.[13]

The Ni-C EPR signal from a Ni-Fe hydrogenase isolated from *T. Roseopersicina* showed a clean, rhombic EPR signal while that from *D. Gigas* was overlapped with spectral contributions from a reduced 4Fe-4S center at high field.[38,39] In the case of *T. Roseopersicina,* four-pulse ESEEM studies of the field profile of the proton sum combination bands will be helpful to identify more detailed structural information than available from the previous ENDOR and XAS studies of the enzyme.[39] Fig. V-11 shows numerically calculated field profiles of the turning points of the proton sum frequencies with g_1=2.19, g_2=2.15, and g_3=2.02 as observed for the Ni-C form of the enzyme and with r_{eff}=2.33 Å, a=2.5 MHz, (a) θ_n=18° and (b) θ_n=30°. The frequency shifts are $(\nu_\alpha+\nu_\beta)-2\nu_I$ as in the above field profiles. To determine the frequencies of the turning points, the magnetic field strength and microwave frequency were first used to calculate continuous angle sets (θ, ϕ) that were selected[25-28] and then the sum frequencies were calculated as a function of these angle sets using the ligand hyperfine couplings based on Eq. V-4 and numerically determined $d(\nu_\alpha+\nu_\beta)=0$ points. As shown in Fig. V-11, the overall field profile patterns are mainly determined by θ_n. In the calculated field profiles, there are ϕ_n-sensitive regions around g_2, so it should be possible to determine θ_n and ϕ_n separately. The effective dipole-dipole distances did not affect the profile shape, but frequency shifts were strongly dependent on r_{eff} as in the axial g-tensor case. The frequency shifts and field profile pattern were weakly sensitive to the isotropic HFI coupling, as expected. If

Figure V-11. Computed field profiles of the frequency shifts of the turning points of the proton sum combination bands from twice the proton Larmor frequencies in rhombic g-tensor system. The parameters for the simulations were g_1=2.19; g_2=2.15; g_3=2.02; microwave frequency, 9.0 GHz; r_{eff}, 2.33 Å; a, 2.5 MHz; (a) θ_n, 18°; ϕ_n, 0°; (b) θ_n, 18°; ϕ_n, 45°; (c) θ_n, 18°; ϕ_n, 90°; (d) θ_n, 30°; ϕ_n, 0°; (e) θ_n, 30°; ϕ_n, 45°; and (f) θ_n, 30°; ϕ_n, 90°.

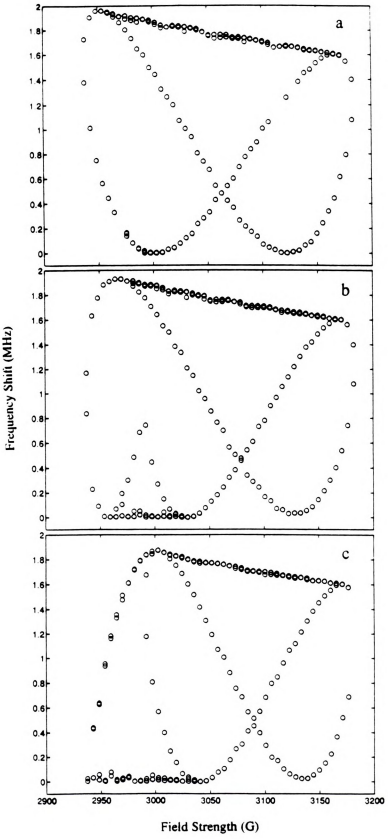
a
b
c
Frequency Shift (MHz)
Field Strength (G)
2900
2950
3000
3050
3100
3150
3200

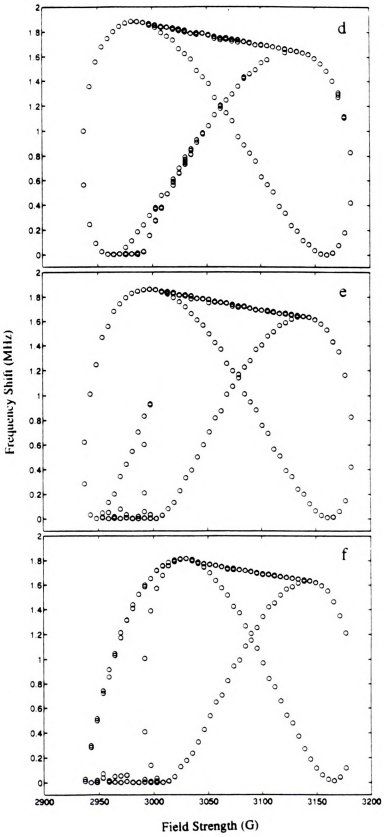
d
e
f
Frequency Shift (MHz)
Field Strength (G)
2900
2950
3000
3050
3100
3150
3200

more than one singularity point is found at a single magnetic field position, the τ-suppression behavior of the sum combination band lineshapes will provide a means for measuring the isotropic HFI couplings. Therefore, four-pulse ESEEM field profile studies of the proton sum combination band of the Ni-C species of *T. Roseopersicina* should allow for a more complete characterization of the strong proton couplings reported from ENDOR studies.

References

1. L. Kevan, in *Time Domain Electron Spin Resonance*, L. Kevan, and R. N. Schwartz, Ed., Wiley-Interscience, New York, Chapter 8 (1979).
2. A. J. Hoff, Ed., in *Advanced EPR. Applications in Biology and Biochemistry*, Elsevier, New York, Chapters 1, 2, 3 and 6. (1989).
3. L. Kevan, in *Modern Pulsed and Continuous -Wave Electron Spin Resonance*, L. Kevan, and M. K. Bowman, Ed., John Wiley & Sons, New York, Chapter 5 (1990).
4. A. de Groot, R. Evelo, and A. J. Hoff, *J. Magn. Reson.*, **66**, 331 (1986).
5. W. B. Mims, *Phys. Rev.*, **B5**, 2409 (1972).
6. W. B. Mims, *Phys. Rev.*, **B6**, 3543 (1972).
7. A. V. Astashkin, S. A. Dikanov, and Yu. D. Tsvetkov, *Chem. Phys. Lett.*, **136**, 204 (1987).
8. S. A. Dikanov, A. V. Astashkin, and Yu. D. Tsvetkov, *Chem. Phys. Lett.*, **144**, 251 (1988).
9. E. J. Reijerse, and S. A. Dikanov, *J. Chem. Phys.*, **95**, 836 (1991).
10. W. B. Mims, J. Peisach, and J. L. Davis, *J. Chem. Phys.*, **66**, 5536 (1977).
11. G. J. Gerfen, P. M. Hanna, N. D. Chasteen, and D. J. Singel, *J. Am. Chem. Soc.*, **113**, 9513 (1991).
12. A. M. Tyryshkin, S. A. Dikanov, R. G. Evelo, and A. J. Hoff, *J. Chem. Phys.*, **97**, 42 (1992).
13. J. McCracken and S. Friedenberg, *J. Phys. Chem.*, **98**, 467 (1994).

14. C. Gemperle, G. Abeli, A. Schweiger, and R. R. Ernst, *J. Magn. Reson.*, **88**, 241 (1990).
15. A. Schweiger, *Angew. Chem. Int. Ed. Engl.*, **30**, 265 (1991).
16. A. Schweiger, in *Modern Pulsed and Continuous -Wave Electron Spin Resonance*, L. Kevan, and M. K. Bowman, Ed., John Wiley & Sons, New York, Chapter 2 (1990).
17. E. J. Reijerse, and S. A. Dikanov, *Pure & Appl. Chem.*, **64**, 789 (1992).
18. A. M. Tyryshkin, S. A. Dikanov, and D. Goldfarb, *J. Magn. Reson.*, **A105**, 271 (1993).
19. S. A. Dikanov, C. Burgard, and J. Hutterman, *Chem. Phys. Lett.*, **212**, 493 (1993).
20. T. L. Pappenhagen, and D. W. Margerum, *J. Am. Chem. Soc.*, **107**, 4576 (1985).
21. Y. L. Wang, M. W. Beach, T. L. Pappenhagen, and D. W. Margerum, *Inorg. Chem.*, **27**, 27, 4464 (1988).
22. J. McCracken, D. H. Shin, and J. L. Dye, *Appl. Magn. Reson.*, **3**, 205 (1992).
23. C. P. Lin, M. K. Bowman, and J. L. Norris, *J. Magn. Reson.*, **65**, 369 (1985).
24. R. D. Britt and M. P. Klein, *J. Magn. Reson.*, **74**, 535 (1987).
25. C. A. Hutchison and D. B. McKay, *J. Chem. Phys.*, **66**, 3311 (1977).
26. G. C. Hurst, T. A. Henderson, and R. W. Kreilick, *J. Am. Chem. Soc.*, **107**, 7294 (1985).
27. T. A. Henderson, G. C. Hurst, and R. W. Kreilick, *J. Am. Chem. Soc.*, **107**, 7299(1985).
28. B. M. Hoffman, J. Martinsen, and R. A. Venters, *J. Magn. Reson.*, **59**, 110 (1984).
29. L. G. Rowan, E. L. Hahn, and W. B. Mims, *Phys. Rev.*, **A137**, 61 (1965).
30. D. J. Kosman, J. Peisach, and W. B. Mims, *Biochemistry*,**19**, 1306 (1980).
31. C. P. Lin, M. K. Bowman, and J. R. Norris, *J. Chem. Phys.*, **85**, 56 (1986)
32. N. M. Atherton and A. J. Horsewill, *J. Molec. Phys.*, **37**, 1349 (1979).
33. J. C. Salerno, in *The Bioinorganic Chemistry of Nickel*, J. R. Lancaster Jr., Ed., VCH Publication, New York, Chapters 3, 8 (1988).
34. M. W. W. Adams, *Biochim. Biophys. Acta*, **1020**, 115 (1990).
35. A. E. Przybyla, J. Robbins, N. Menon, and H. D. J. Peck, *FEMS Microbiol. Rev.*, **88**, 109 (1992).

36. M. Teixeira, I. Moura, A. V. Xevier, B. H. Hyunh, D. V. Der Vartanian, H. D. Peck, J. LeGall, and J. J. G. Moura, *J. Biol Chem.*, **260**, 8942 (1985).
37. V. M. Fernadez, C. E. Hatchikian, D. S. Patil, and R. Cammack, Biochim. Biophys. Acta, **883**, 145 (1986).
38. C. Fan, M. Teixeira, J. J. G. Moura, B. H. Hyunh, J. LeGall, H. D. Peck, and B. M. Hoffman, *J. Am. Chem. Soc.*, **113**, 20 (1991).
39. J. P. Whitehead, R. J. Gurbiel, C. Bagyinka, B. M. Hoffman, and M. J. Maroney, *J. Am. Chem. Soc.*, **115**, 5629 (1993).

VI. FOUR-PULSE ELECTRON SPIN ECHO ENVELOPE MODULATION STUDIES OF $Cu(II)(H_2O)_6^{2+}$

1. Abstract

Four-pulse electron spin echo envelope modulation (ESEEM) studies aimed at characterizing hyperfine interactions between protons of equatorially and axially bound water molecules and the copper ion in $Cu(II)(H_2O)_6^{2+}$ were carried out. Four-pulse ESEEM experiments showed that these hyperfine couplings are characterized by large anisotropic interactions resulting in the shifts of the proton sum combination peaks, $\nu_\alpha+\nu_\beta$, from twice the Larmor frequency, $2\nu_I$. For the equatorially bound water protons, a distribution of sum combination peak frequency shifts that spanned the range from twice the Larmor frequency to 1.4-1.7 MHz above twice the Larmor frequency at each magnetic field strength was found. At a given magnetic field strength the sum combination frequency shift from these strongly bound water protons varied with the τ value used in the measurement so that a discrete field profile pattern was not found. These features result from the rotational distribution of the equatorially bound water molecules about Cu-O bonds at 4.2 K in frozen solution. Theoretical simulation of the field profile of the turning points of the proton sum combination lineshape revealed an effective Cu-H distance of 2.49 Å, an angle between the principal axis of the ligand hyperfine tensor and the g_3

axis (θ_N), that was distributed between 71° and 90°, and an isotrop hyperfine coupling constant of ≤ 4 MHz for the equatorially bound wat protons. Attempts were made to distinguish the sum combination peaks the axially bound water protons by using the τ-suppression behavior of t four-pulse ESEEM. It was found that the intensities and lineshapes of t sum combination peaks for these protons were relatively well develope and distinguished from the sum combination peaks of the equatori protons when τ was set to values near n/ν_I (n=integer). Simulation of t frequency shifts of the axial proton sum combination peaks *vs.* magneti field yielded an effective Cu-H distance of 3.05 Å, θ_N=11° and an isotropi hyperfine coupling of ≤ 4 MHz.

2. Introduction

Copper ions are found to play important roles in sever metalloenzymes.[1] Native copper proteins may contain Cu(I) and/or Cu(I forms. Cu(II) forms are paramagnetic and give rise to electro paramagnetic resonance (EPR) signals. In electronic spectra of copp complexes, weak copper d-d transitions are often masked by strong ligand electronic transitions. For this reason, EPR has played an importa role in characterizing the structure and biological function of copper i copper proteins. In these proteins, copper ligands may consist of grou supplied by the protein backbone, amino acid side chains, enzymati cofactors, or solvent molecules.

Although EPR studies of copper sites give useful information, mo detailed ligand structural information is not easily obtained since the ligan hyperfine interactions are generally much weaker than the hyperfi

interaction between the copper nucleus and the unpaired electron. Electr
spin echo envelope modulation (ESEEM)[2-4] is especially sensitive
Cu(II)-ligand interactions because the weak hyperfine interactions that a
hidden by the broad Cu-EPR lineshape can be detected. Many ESEE
studies of copper containing proteins have demonstrated the capabilities
this method for the identification of Cu(II) ligands and their coordinati
geometries.[5-9] In ESEEM studies of copper proteins, the binding
histidine side chains as equatorial copper ligands has been we
characterized because at X-band microwave frequencies, the hyperfi
interaction of the remote nitrogen of the equatorially bound imidazole ri
is most distinctive. This characteristic ^{14}N-ESEEM pattern results from
coupling regime known as "exact cancellation" where characteristic ^{14}
nuclear quadrupole resonance lines are well resolved.[10,11] ^{14}N-ESEE
studies of copper model complexes that support the assignment of
characteristic Cu-His interaction have been reported.[12,13]

Several studies have also shown that the copper sites of ma
proteins are accessible to solvent water molecules thought to have critic
functions in catalytic processes. ESEEM studies of the accessibility
solvent H_2O molecules to copper sites and the direct measurement of wat
ligand hyperfine couplings have been most often done with D_2O exchan
experiments.[7,9] The hyperfine interactions between Cu(II) and the proto
or deuterons of coordinated H_2O or D_2O are characterized as large
anisotropic by CW-ENDOR studies on single crystals. Even at X-ba
frequencies, the nuclear Larmor frequencies of protons and deuterons a
larger than the isotropic hyperfine couplings. As a result, these stro
anisotropic hyperfine interactions prevent the fundamental frequencies (ν
$\nu\beta$) from splitting and cause only broadened lineshapes centered about t

Larmor frequencies. This lack of resolution gives rise to difficulties characterizing the ligand hyperfine interactions of bound wa molecules.[14] Previous attempts at ESEEM characterization of bound wa molecules involved the use of data ratioing methods[15,16] to remove large background provided by matrix protons or deuterons. Often, contribution from the matrix deuterons could not be separated fr ESEEM due to bound D_2O so that the accurate measurement of deuteron hyperfine interaction and water geometry were difficult. For t reason, the sum combination frequency ($\nu_\alpha+\nu_\beta$), where pronounc differences have been observed between axial and equatorially bound D in two-pulse ESEEM, was studied.[7,9]

The properties of ESEEM sum combination peaks have been w characterized in the recent literature.[17-22] The advantage in using the s combination band is that the sum combination peak positions are sensit to the anisotropic portion of the ligand hyperfine interaction and that spectral line is narrow enough to be easily resolved. Sum combinat peaks are characterized by frequency shifts from twice the nuclear Lar frequency. For a spin system described by an isotropic electron g-ten and an axial ligand hyperfine tensor, the sum combination peak freque shift is given by $\Delta\nu=\nu_\alpha+\nu_\beta-2\nu_I=(9/16)T^2/\nu_I$ where ν_α and ν_β are fundamental hyperfine frequencies of α and β electron spin manifolds is the Larmor frequency of the coupled nucleus; and T is the anisotrc portion of the perpendicular component of the ligand hyperfine tenso For this simple spin system, the frequency shifts are dependent on relative orientation between external magnetic field and principal lig hyperfine axis.[17-19] The sum combination frequency shifts found for nuclei are approximately 6.5 times less than those observed for identic

coupled protons due to the difference in their gyromagnetic ratios. Hen
anisotropic hyperfine couplings are better resolved using the proton su
combination peak. Also, the proton sum combination band is found in
region where there is a relatively clean spectral window.[23]

We have recently introduced sum frequency field profiles obtain
by plotting the frequency shifts of the sum combination peaks from tw
the Larmor frequencies as a function of magnetic field strength across t
EPR absorption spectrum to serve as a foundation for a more systema
analysis of the ligand hyperfine tensor in anisotropic electron sp
systems.[21] This method was applied to the $Ni(III)(CN)_4(H_2O)_2^-$ system
characterize the ligand proton hyperfine couplings of the axially bou
water molecules by using two-pulse ESEEM experiments.[21] More recent
we have extended this field profile analysis to include the behavior of t
sum combination peak lineshape singularities.[22] This enhanced field prof
analysis strategy was applied to the same $Ni(III)(CN)_4(H_2O)_2^-$ sample
using four-pulse ESEEM[24,25] where the sum combination band lineshape
better resolved.[22] The τ-suppression behavior[24,25] of the sum combinati
lineshape of four-pulse ESEEM was used to place more exact constrai
on the isotropic hyperfine coupling constant than possible using two-pu
methods.[22]

In the present chapter, the enhanced sum frequency field prof
analysis of the proton sum combination peak is applied to $Cu(II)(H_2O)_6$
in frozen solution to distinguish the ligand hyperfine interactions of axia
and equatorially bound water protons using four-pulse ESEE
experiments. Our goals in undertaking this work were to address t
usefulness of four-pulse ESEEM experiments for studies of mo
complicated spin systems, and to test the analysis procedures developed

the $Ni(III)(CN)_4(H_2O)_2^-$ system on a compound where single crystal EPI and ENDOR results are available. For Cu(II) in a tetragonally distorte octahedral ligand field, the unpaired electron is mostly distributed in d_{x^2-y} orbital. Hence, the ligand hyperfine interaction in the equatorial plane i expected to be stronger and give rise to larger sum frequency shifts fro $2\nu_I$ than interactions placed along the axial direction. However, a portio of the lineshape of the equatorial proton sum combination band wi overlap the lineshape of the axial protons making the analysis mor difficult.[22] Attempts at distinguishing the the sum combination peaks an the ligand hyperfine interactions of these two different populations o protons were made using the τ-suppression behavior of the four-puls ESEEM lineshapes. Four-pulse ESEEM spectra of axial water ligand bound to Cu(II)-tetraphenylporphyrin [Cu(II)TPP] were also obtained t compare with those of $Cu(II)(H_2O)_6^{2+}$.

3. Experimental

The $Cu(II)(H_2O)_6^{2+}$ sample was prepared by dissolvin $Cu(II)(NO_3)_2$ [Aldrich] salt in distilled water. The sample for electron spi echo experiments was mixed with an equal volume of ethylene glycol pri to freezing in liquid nitrogen. The resulting concentration $Cu(II)(H_2O)_6^{2+}$ was 6 mM. Cu(II)-tetraphenylporphyrin [Cu(II)TPI complexes with axially bound water ligands were prepared by dissolvin Cu(II)TPP [Aldrich] into dehydrated CH_2Cl_2. The resulting solution wa mixed with excess amount of water and vigorously shaken. The CH_2C layer where Cu(II)TPP is dissolved was separated and frozen in liqui

nitrogen. The final concentration of the Cu(II)TPP was 0.45 mM to avoi aggregation or dimerization.[26]

Electron Spin Echo detected-EPR (ESE-EPR) and ESEEM experiments were executed on a home-built pulsed-EPR spectrometer which has been explained in detail elsewhere[27] and in chapter IV. A stimulated echo microwave pulse sequence ($\pi/2$-τ-$\pi/2$-T-$\pi/2$) was used t collect ESE-EPR data by varying external field strength at fixed τ and T values. A four-pulse sequence ($\pi/2$-τ-$\pi/2$-T/2-π-T/2-$\pi/2$) was used t produce the ESEEM data. The length (full-width at half maximum) of a four microwave pulses was 16 ns. The peak power of the π-pulse was twic that of $\pi/2$-pulse.[22,25] A four step phase cycle, +(0,0,0,0), +(0,0,π,π) +(0,0,π,0), +(π,π,π,0), was used to eliminate unwanted echo modulation.[2] The ESEEM data were collected as a function of T, the time interva between the second and fourth pulses. Fourier transformation of the tim domain ESEEM data were done without dead-time reconstruction. Th fourier transformation and computer simulations were performed o SPARCstation 2 workstation (Sun Microsystems) using software written i MATLAB v.4.2 (The Mathworks, Inc.).

4. Theoretical Aspects

4-1. Angle Selection

For CW-EPR spectra dominated by large anisotropic g- and/or meta hyperfine tensors such as in Cu(II)$(H_2O)_6^{2+}$, each portion of the EP absorption spectrum of randomly oriented samples represents EP transitions from complexes which have specific orientations with respect t

the external magnetic field direction. Specific orientations that contrib to the EPR absorption are determined by the microwave frequen magnetic field strength, and the nature of the anisotropic magn interactions. To interpret ESEEM spectra of randomly oriented samp obtained at a fixed external field strength and microwave frequency, orientation or angle selection analysis is needed.

The angle selection analysis portion of this study made use of approach of Hurst, Henderson, and Kreilick for the interpretation ENDOR spectra of a bis(2,4-pentanedionato)copper(II) powder.[28,29] $Cu(II)(H_2O)_6^{2+}$, the metal quadrupole and ligand hyperfine interacti were not included because these interactions are small enough to be trea by the ESEEM lineshape function or background decay. Also, differen resulting from the natural abundance of ^{63}Cu (69%) and ^{65}Cu (31%) too small to be distinguished in ESEEM studies. The Hamiltonian for Cu(II) EPR transition is then expressed as

$$H = \beta_e \mathbf{S}\cdot\mathbf{g}\cdot\mathbf{H} + \mathbf{S}\cdot\mathbf{A}\cdot\mathbf{I} \qquad [VI\text{-}1]$$

where β_e is the electron Bohr magneton, **S** is electronic spin ang momentum operator, **g** is the electron g-tensor, **H** is the external f vector, **A** is the metal hyperfine tensor, and **I** is the nuclear spin ang momentum operator. From Eq. VI-1, the resonance field position o EPR transition is given by

$$H_r = \frac{h\nu - M_I A(\theta,\phi)}{\beta_e g(\theta,\phi)} \qquad [VI\text{-}2]$$

where h is Planck's constant, v is the microwave frequency, M_I is the
nuclear spin quantum number,

$$g(\theta,\phi) = [\sum_{i=1}^{3}(g_i l_i)^2]^{1/2}, \text{ and} \qquad \text{[VI-3}$$

$$A(\theta,\phi) = \frac{[\sum_{i=1}^{3}(\sum_{j=1}^{3}A_{ji}g_j l_j)^2]^{1/2}}{g(\theta,\phi)}.$$

Here, $l_1=\sin\theta\cos\phi$, $l_2=\sin\theta\sin\phi$, $l_3=\cos\theta$, g_1, g_2, g_3 are the princip
tensor values, θ is the angle between the external field and g_3 axis, ϕ
azimuthal angle of the field with respect to g-tensor axes, and the A
the metal hyperfine tensor matrix elements. The orientations (θ,ϕ)
satisfy the resonace condition at a fixed field strength and micro
frequency can be obtained analytically in the case where the both g
metal hyperfine tensors are axial and coincident.[28] For other general
the angle set can be obtained numerically. Appendix, A7 lists com
programs written for this purpose. The program calculates Eq. VI-2
around the roots of Eq. VI-2 so that the calculation time can be re
when compared to parabolic search algorithms commonly used by
researchers in the field.

4-2. Lineshape Properties of Four-Pulse ESEEM Sum Combination Ba

For systems with an anisotropic g-tensor, the fundamental ES
or ENDOR frequencies of an S=1/2, I=1/2 spin system are given by[28]

$$\nu_{\alpha(\beta)} = [\sum_{i=1}^{3}[\frac{m_s}{g(\theta,\phi)}(\sum_{j=1}^{3} g_j l_j A_{ji}) - l_i \nu_I]^2]^{1/2} \qquad \text{[VI-4]}$$

where

$$A_{ji} = \frac{-\beta_e g_N \beta_N}{hr^3} g_i(3n_i n_j - \delta_{ij}) + a\delta_{ij}, \qquad \text{[VI-5]}$$

m_s is the electron spin quantum number, g_N is the nuclear g value, β_N i Bohr magneton, r is the electron-nuclear dipole-dipole distance $n_1=\sin\theta_N\cos\phi_N$, $n_2=\sin\theta_N\sin\phi_N$, $n_3=\cos\theta_N$, θ_N is the angle between th ligand hyperfine principal axis and g_3 axis, ϕ_N is the azimuthal angle of th ligand hyperfine principal axis with respect to g-tensor axes and "a" is th isotropic ligand hyperfine coupling constant. (Note: A_{ji} of Eq. VI-5 i different from A_{ji} of Eq. VI-3 which is the metal hyperfine tenso component.)

For the system where both g- and metal hyperfine tensors are axia and coincident, the angle θ is determined by the microwave frequency an external field strength (Eq. VI-2). If the ligand hyperfine interaction i axial, the hyperfine frequencies are independent of ϕ_N. Because θ_N i constant for a given ligand geometry, the lineshape of an orientatio selective ESEEM peak is a function of ϕ for the above spin system and th lineshape function of the sum combination band as obtained by four-puls ESEEM is given by[22]

$$I_{\nu\alpha+\nu\beta}(\phi) = k(\phi)c^2\sin(\frac{\omega_\alpha\tau}{2})\sin(\frac{\omega_\beta\tau}{2})\sin\theta\left|\frac{\partial\phi}{\partial(\nu_\alpha+\nu_\beta)}\right| \qquad \text{[VI-6]}$$

where

$$s^2 = \frac{|\omega_I^2 - \frac{1}{4}(\omega_\alpha+\omega_\beta)^2|}{\omega_\alpha\omega_\beta}, \qquad [VI\text{-}7]$$

$$c^2 = \frac{|\omega_I^2 - \frac{1}{4}(\omega_\alpha-\omega_\beta)^2|}{\omega_\alpha\omega_\beta},$$

$k = 4s^2c^2$, and

ω_α and ω_β are the angular frequencies of ν_α and ν_β, respectively. Th frequency distribution range of the sum combination band is determined b the turning points of the sum frequencies where the condition $\frac{d(\nu_\alpha+\nu_\beta)}{d\phi}=0$, is satisfied.[19,22] Provided $\phi_N=0$, the turning points occur a $\phi=0$, π and values determined numerically by solution of the abov relationship.[22] At these turning points, the intensities of the sur frequencies show singularities except at $\nu_\alpha+\nu_\beta=2\nu_I$ where branching of th EPR transition ceases (k and s^2 are zero.).

The frequency shift [$\Delta\nu=\nu_\alpha+\nu_\beta-2\nu_I$] field profile[21,22] of the turnin points of the sum combination band is sensitive to the effective electron nuclear distance and θ_N, but less sensitive to isotropic ligand hyperfin coupling. The τ-suppression effect on the lineshape of the sum combinatio band of four-pulse ESEEM shows the sensitivity to the isotropic hyperfin coupling.[22] The τ-suppression behavior of the sum combination lineshap of four-pulse ESEEM requires a more complete theoretical treatmen Appendix, A8, shows the computer program to calculate orientatio selective four-pulse ESEEM spectra for S=1/2, I=1/2 spin system.

5. Results and Discussion

The electron spin echo-detected EPR (ESE-EPR) spectrum (so curve) of $Cu(II)(H_2O)_6^{2+}$ is shown along with the simulated E absorption spectrum (dashed curve) in Fig. VI-1. The simulation revea that electron g- and copper hyperfine tensor components of $g_\perp$=2.0 $g_\parallel$=2.411, $A_\perp$=10 MHz and $A_\parallel$=418 MHz are well fit to the experimen result. The low-field region, where the only EPR transition arises from copper M_I=3/2 spin manifold, is most suitable for Cu(II) ESEE orientation selection experiments because only a single value of θ, the an between the external field and g_3 axis, is selected. At higher field strengt more than one copper hyperfine spin manifold is involved in the E absorption so that more than one value of θ is selected. ESEEM spec collected in the higher-field region may become too complicated to analyzed.

Fig. VI-2 (a) and (b) show the proton sum combination peak regi of four-pulse FT-ESEEM spectra obtained at g=2.563 with (a) τ=239 and (b) τ=287 ns. In the spectra, sharp peaks shown at 20.88 MHz are second harmonic frequency of matrix protons at 2452G. For τ=239 [Fig. VI-2 (a)], a peak was resolved at 21.20 MHz, shifted 0.32 MHz fr $2\nu_I$ and one broad feature was found at higher frequency with maxim intensity position of 22.27 MHz. These peaks are assigned to the s combination peaks of axially and/or equatorially bound water protons. T four-pulse ESEEM spectrum obtained with τ=287 ns [Fig. VI-2 (b)] sho

Figure VI-1. Electron spin echo detected-EPR (solid) and simula
(dashed) absorption spectra of $Cu(II)(H_2O)_6^{2+}$. The stimulated ech
$\pi/2$-T-$\pi/2$) microwave pulse sequence was used to generate elect
echo signal with τ=250 ns and T=2000 ns. Other experimental c
were microwave frequency, 8.820 GHz; microwave pulse power,
microwave pulse width (FNHM), 16 ns; averaging number, 1
repetition rate, 12 Hz, and temperature, 4.2 K. The simulated spec
obtained with EPR parameters of $g_\perp$=2.083, $g_\parallel$=2.411, $A_\perp$=10 M
$A_\parallel$=418 MHz.

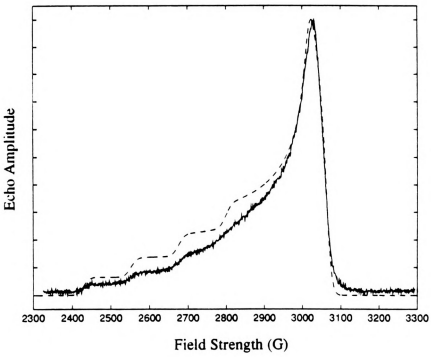
Echo Amplitude
2300
2400
2500
2600
2700
2800
2900
3000
3100
3200
3300
Field Strength (G)

Figure VI-2. Four-pulse magnitude FT-ESEEM spectra of $Cu(II)(H_2O)_6^{2+}$ at proton sum combination frequency region. Experimental conditions were magnetic field strength, 2452G; microwave frequency, 8.795 GHz; microwave pulse powers of π-pulse, 141 W and $\pi/2$-pulse, 71 W; averaging number, 30; pulse repetition rate, 30. τ values are (a) 239 ns and (b) 287 ns.

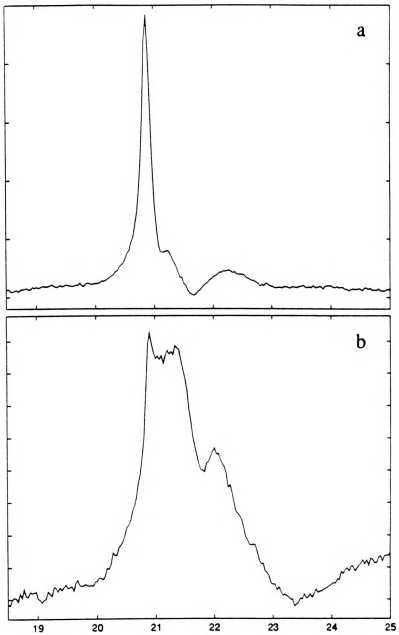
a
b
19
20
21
22
23
24
25
Frequency (MHz)

different features from that with τ=239 ns. In Fig. VI-2 (b), the second harmonic frequency peak of the matrix proton is partially suppressed because the τ value is set to $3/\nu_I$.[18,31] The sum combination peaks of the coordinated water protons are resolved at 21.34 and 22.00 MHz shifted 0.46 and 1.12 MHz from $2\nu_I$, respectively. The frequency shift $[\Delta\nu=\nu_\alpha+\nu_\beta-2\nu_I]$ of the proton sum combination peak positions obtained for several τ values at six different field positions, where only EPR transitions of copper M_I=3/2 spin manifold occur, are plotted as a function of magnetic field strength in Fig. VI-3. As shown in Fig. VI-3, the proton sum frequency shifts are almost continuously distributed at each magnetic field strength. Previously, we have utilized this field profile approach to study the proton ligand hyperfine interactions of axially bound water protons in $Ni(III)(CN)_4(H_2O)_2^-$.[21,22] In those experiments, the sum combination peaks were placed on one of the turning points of the sum combination lineshape. The same field profile approach should be applicable to the results of this study.

Fig. VI-4 shows comparisons of the experimental proton sum frequency shifts (circles) with the simulated field profiles of the turning points of the sum combination bands across the EPR spectrum for an effective Cu-H distance (r_{eff}) of 2.49 Å, an isotropic hyperfine coupling constant ("a") of 0 MHz, and θ_N, the angle between the principal axis of the proton ligand hyperfine interaction and g_3 axis, of (a) 90°, (b) 80°, and (c) 71°. As shown in Fig. VI-4, there are always experimental proton sum combination peaks that correspond to the simulated turning point curves.

The features found in the studies of $Cu(II)(H_2O)_6^{2+}$ can be explained by the rotation of coordinated water molecules about Cu-O bond axis. At room temperature, the coordinated water molecules freely rotate about

Figure VI-3. Proton sum combination frequency shifts (circles) [$\Delta\nu=\nu_\alpha+\nu_\beta-2\nu_I$] of four-pulse ESEEM spectra obtained at magnetic field strengths, 2431 G, 2452 G, 2473 G, 2494 G, 2515 G, and 2536 G. Other experimental conditions were same as in Fig. VI-2 except τ value. At each field strength, τ values are were changes between $2.5/\nu_I$ and $3/\nu_I$ with 10 ns or 8 ns step.

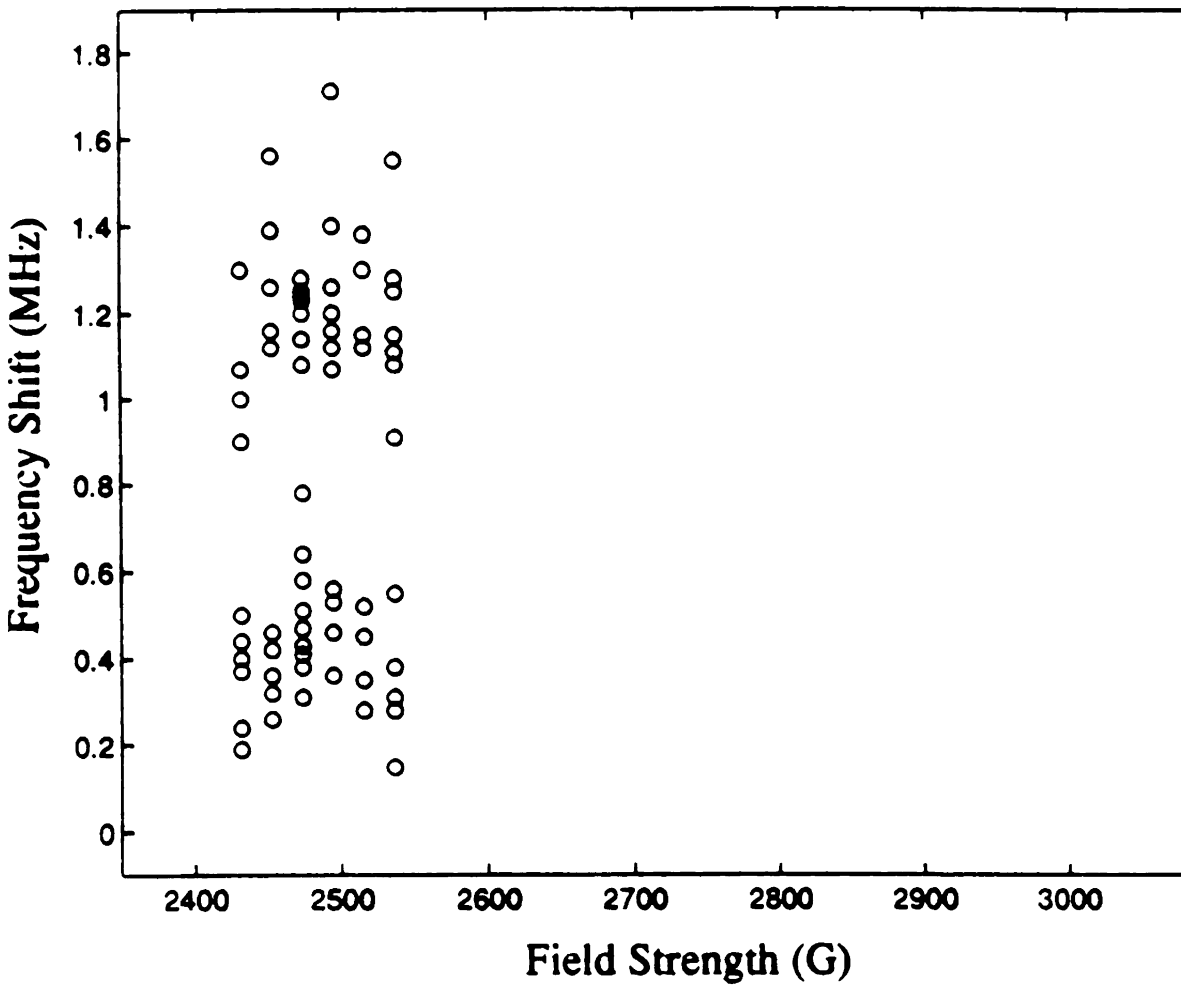
Frequency Shift (MHz)
1.8
1.6
1.4
1.2
1
0.8
0.6
0.4
0.2
0
2400
2500
2600
2700
2800
2900
3000
Field Strength (G)

Figure VI-4. A comparison of the measured proton sum combinati
frequency shifts (circles) with simulated field profile of the turning poi
of proton sum combination peak lineshape. The EPR parameters for an
selection were $g_{\perp}$, 2.083; $g_{||}$, 2.411; $A_{\perp}$, 10 MHz; $A_{||}$, 418 MHz; copp
M_I,3/2; and microwave frequency, 8.795 GHz. The ESEEM simulati
(ligand hyperfine) parameters were r_{eff}, 2.49 Å; a, 0 MHz; θ_N, (a) 90°,
80°, and (c) 71°. The sum frequency shifts were calculated with 46 θ,
angle between the external magnetic field and g_3 axis, values (0° ~ 9
which cover the EPR absorption spectrum. In the simulated field profi
solid and dashed curves correspond to the turning points occurring at ϕ=
and π, respectively. The turning points of plus signs were numerica
determined.

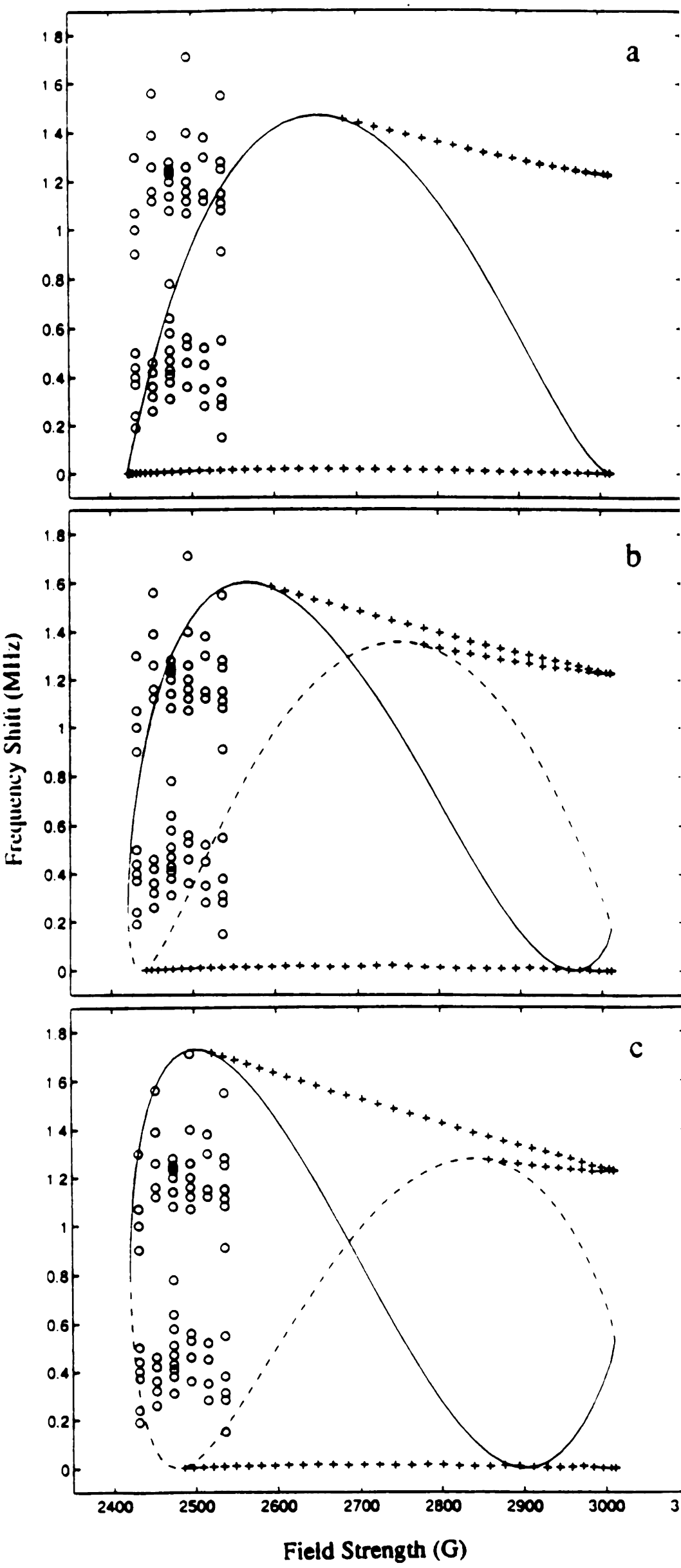
a
b
c
Frequency Shift (MHz)
Field Strength (G)
2400
2500
2600
2700
2800
2900
3000

corresponding Cu-O bonds. But at the ESEEM experimental temperat
4.2K, the rotation of the water molecules is restricted and the geomet
of the water molecules take on thermodynamically stable orientations.
equatorially bound water molecules, the rotation of the ligand brings ab
a change of θ_N and ϕ_N, the polar and azimuthal angles that describe
orientation of the principal axis of the proton ligand hyperfine tensor v
respect to g-tensor axes. In case of a randomly oriented Cu(II)(H_2O)
sample where both the g- and metal hyperfine tensors are axial
coincident and the ligand hyperfine interaction is also axial, the variatio
ϕ_N has no effect on ESEEM spectra, but the variation of θ_N gives ris
changes in the lineshapes and the field profiles of the sum combinat
peak.[21,22] Because rotation of the axially bound water molecules aff
only ϕ_N, a specific pattern or field profile of the sum combination pea
expected as in the Ni(III)$(CN)_4(H_2O)_2^-$ case.[21,22] Hence, the four-p
ESEEM data of Cu(II)$(H_2O)_6^{2+}$ and the simulated field profiles of
turning points of the proton sum combination band show that θ_N values
the equatorially bound water protons are distributed from 90° to
Considering the structure of Cu(II)$(H_2O)_6^{2+}$,[32] the above feature indic
that the dihedral angles between the g_3 axis and H-O bonds of
equatorially bound waters are distributed from 0° to 360° at 4.
However, these four-pulse ESEEM experiments are not sufficient to
conclusive information about this distribution of the dihedral angles.

Considering the intrinsic uncertainty in the determination of the
frequency peak positions by four-pulse ESEEM experiments, an r_{e}
2.49±0.04 Å can be assigned to the equatorial protons. Because the
profile is not sensitive to the isotropic hyperfine coupling, th
suppression behavior of the sum combination peak lineshape has

previously used to determine the isotropic ligand proton hyperfine coupling in $Ni(III)(CN)_4(H_2O)_2^-$.[22] For equatorially bound water protons of $Cu(II)(H_2O)_6^{2+}$, determination of the isotropic ligand hyperfine coupling constant is not possible due to the rotational distribution of the equatorial ligands. However, based on simulations with r_{eff}=2.49 Å and θ_N=71° for most of the shifted peaks, an isotropic hyperfine coupling constant of less than 4 MHz can be estimated.

Another problem of our field profile approach for analyzing the ligand hyperfine interactions of protons in $Cu(II)(H_2O)_6^{2+}$ is that the sum combination peaks arising from axially bound water protons, of which the ligand hyperfine interactions are expected to be weaker than that of the equatorial protons, are not resolved because of the rotational distribution of the equatorial water molecules about the Cu-O bonds. Attempts to extract the sum combination peaks of the axial water protons were made using the τ-suppression behavior of four-pulse ESEEM spectra. The proton sum combination frequency regions of four-pulse ESEEM spectra collected with τ values of n/ν_I (n=integer value), like in Fig. VI-2 (b), generally showed three peaks. One of these peaks is the second harmonic frequency of the matrix protons and the other two are the sum combination peaks of the coordinated water protons. The field profile obtained by plotting the frequency shift of the lower-frequency component of the sum combination peaks against magnetic field strength showed a trend where the frequency shift was found to increase with increasing field strength (Fig. VI-5). The simulated field profile of the turning points of the proton sum combination frequency for the ligand hyperfine coupling parameters of r_{eff}=3.05 Å θ_N=11°, and a=0 MHz are best fit to the experimental frequency shifts of Fig. VI-5 (Fig. VI-6). The simulation, considering the errors in measuring

Figure VI-5. Experimental proton sum frequency shifts (circles) of lower-frequency peak of the two sum frequency peaks obtained with τ values of around $3/\nu_I$ (See text). Experimental conditions were same as in Fig. VI-2 except τ values of 282 ns, 290 ns at 2431 G; 279 ns, 287 ns at 2451 G; 277 ns at 2473 G; 282 ns at 2494 G; 280 ns at 2515 G; and 271 ns at 2536 G.

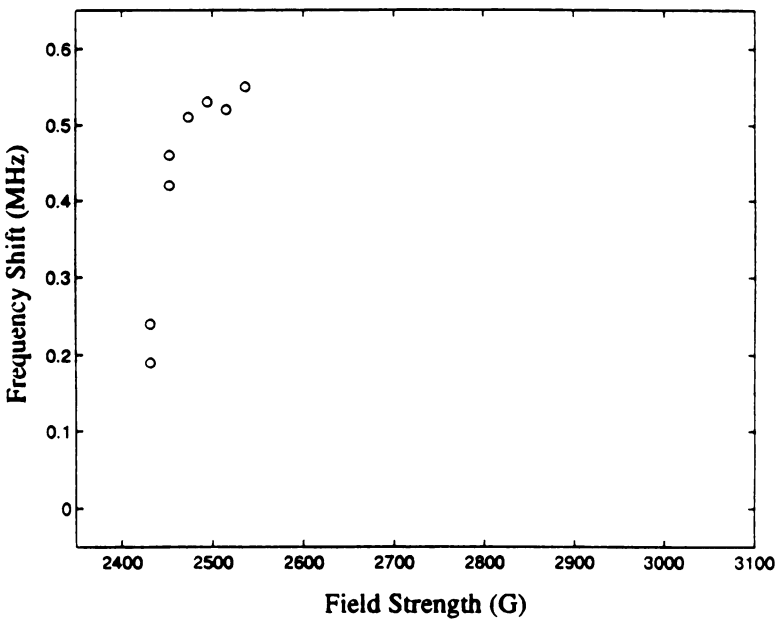
Frequency Shift (MHz)
0.6
0.5
0.4
0.3
0.2
0.1
0
2400
2500
2600
2700
2800
2900
3000
3100
Field Strength (G)

Figure VI-6. A comparison of the measured proton sum frequency shifts (circles) of Fig. VI-5 with the simulated filed profile of the turning points of the proton sum combination peak lineshape. The ligand hyperfine parameters for the simulation were r_{eff}=3.05 Å, a=0 MHz, and θ_N=11°. The other parameters were same as in Fig. VI-4.

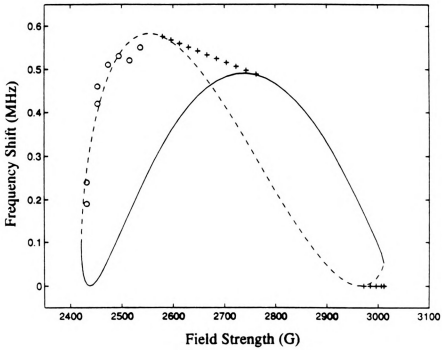
Frequency Shift (MHz)
0.6
0.5
0.4
0.3
0.2
0.1
0
2400
2500
2600
2700
2800
2900
3000
3100
Field Strength (G)

the sum combination frequencies, revealed that the components of the ligand hyperfine tensor showing the trend of Fig. VI-5 are expected to be r_{eff}=3.05±0.1 Å, θ_N=11±6°, and a ≤ 4 MHz.

Fig. VI-7 shows a comparison of the relative intensities of the sum combination bands simulated with the ligand hyperfine parameters obtained for the equatorial protons and Fig. VI-5 at six field positions where the four-pulse ESEEM experiments were performed. In the calculation of Fig. VI-7, the lineshapes and intensities were calculated from Eq. VI- 4 and Eq. VI-6, and τ values are fixed to $3/\nu_I$. Solid curves are calculated with the parameters of Fig. VI-6 and the other curves are calculated with parameters for the equatorially bound water protons. Fig. VI-7 shows that for low-frequency shift regions, the intensities of the lineshapes represented by solid curve dominate the spectra. Even though there are contributions from the simulated sum combination bands for the equatorially bound water protons (non-solid curves) in the low-frequency shift regions, the intensities are much less than those represented by solid curve. Considering the intensities and peak positions of the experimental sum combination bands obtained with τ values near $3/\nu_I$ (Fig. VI-2 (b) and other spectra at different field positions), the low-frequency shift peaks could not result from ligand hyperfine interactions of the equatorially bound water protons. The only possible assignment for the low frequency lineshapes used to construct the field profile of figures VI-5 and VI-6 is to the sum combination peaks arising from the axially bound water protons.

Fig. VI-8 shows the lineshapes and relative intensities of the sum combination bands predicted with $\tau=2.5/\nu_I$ and the ligand hyperfine parameters of axial (solid curves) and equatorial (other curves) protons at (a) 2431G and (b) 2515G. Large intensity contributions for the equatorial

Figure VI-7. Simulated Lineshapes and relative intensities of proton sum combination band for data of Fig. VI-5 (solid curves) and the equatorially bound water protons (the other curves) with $\tau=3/\nu_I$. Parameters for the angle selection were same as in Fig. VI-4. Ligand hyperfine parameters for the simulation of the solid curves were same as in Fig. VI-6. Ligand hyperfine parameters for the other curves were r_{eff}=2.49 Å, a=1 MHz and θ_N values are in the figures. τ values and magnetic field strengths were (a) 290 ns, 2431 G; (b) 287 ns, 2452 G; (c) 285 ns, 2473 G; (d) 282 ns, 2494 G; (e) 280 ns, 2515 G; and (f) 278 ns, 2536 G. The arrows indicate the frequency of $2\nu_I$. Intrinsic gaussian linewidth (FWHM) of 0.2 MHz were used in the calculation.

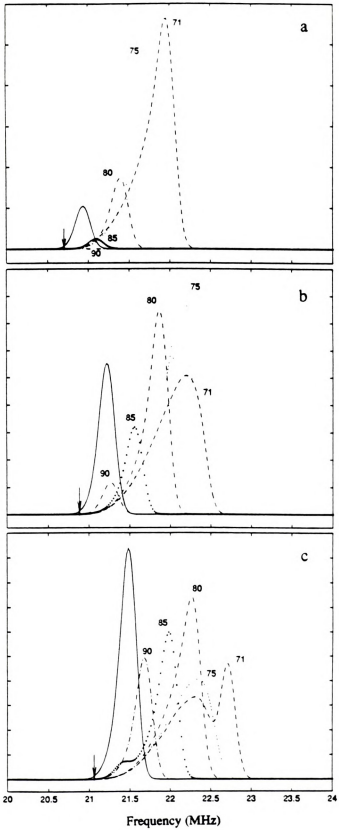
a
71
75
80
85
90
b
75
80
71
85
90
c
80
85
90
75
71
20
20.5
21
21.5
22
22.5
23
23.5
24
Frequency (MHz)

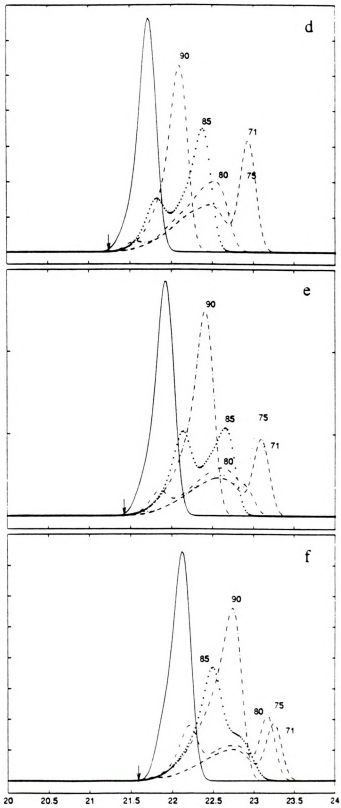
d
90
85
71
80
75
e
90
85
75
71
80
f
90
85
80
75
71
20
20.5
21
21.5
22
22.5
23
23.5
24
Frequency (MHz)

Figure VI-8. Simulated Lineshapes and relative intensities of proton sum combination band for the axially bound water protons (solid curves) and the equatorially bound water protons (the other curves) with $\tau=2.5/\nu_I$. Parameters for the simulations were same as in Fig. VI-7 except τ values and magnetic field strengths of (a) 242 ns and 2431 G; (b) 233 ns and 2515 G. The arrows indicate the frequency of $2\nu_I$. Intrinsic gaussian linewidth (FWHM) of 0.2 MHz were used in the calculation.

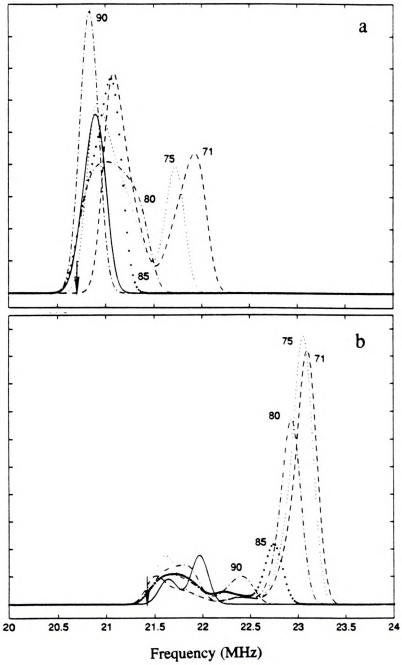
a
90
75
71
80
85
b
75
71
80
85
90
20
20.5
21
21.5
22
22.5
23
23.5
24
Frequency (MHz)

proton sum combination frequencies are expected to overlap the axial proton sum frequency. Therefore, extraction of the sum combination peaks of the axial water protons may be difficult in the four-pulse ESEEM experiments. Simulations with different τ values between $2.5/\nu_I$ and $3/\nu_I$ showed that the relative contribution of the equatorial proton sum combination band in the axial proton sum combination band region decreases as τ values increase.

The hyperfine interactions for equatorially bound water protons obtained in this study (r_{eff}=2.49 Å and $a \leq 4$ MHz) are slightly larger than those previously reported from single crystal ENDOR study of $Cu(II)(H_2O)_6^{2+}$ where the isotropic hyperfine coupling of ≤ 1.2 MHz and the dipolar couplings of approximately 5.6 MHz were measured.[33] The discrepancy arises from the difficulty of the sum frequency field profile approach due to the rotational distribution of the equatorial water molecules at 4.2 K. But the hyperfine couplings of the axially bound water protons from this study (r_{eff}=3.05 Å, $a \leq 4$ MHz) are in good agreement with those from the ENDOR study where the dipolar couplings of approximately 3.6 MHz and the isotropic couplings of ≤ 0.5 MHz were reported.[33] The inaccuracy of the isotropic coupling constant of the axial protons from this study comes from the weak sensitivity of the sum frequency field profile to the isotropic hyperfine interaction. When four-pulse ESEEM experiments are performed in the higher field regions of the Cu(II) EPR spectrum where more than one θ value is selected, more constraints on the isotropic hyperfine coupling are expected by using the τ-suppression effect.

To compare the ligand hyperfine couplings of the axial water protons obtained from the four-pulse ESEEM experiments of

Figure VI-9. Electron spin echo detected-EPR spectrum of axial-H_2O ligand-containing Cu(II)TPP. The stimulated echo sequence was used with τ=220 ns and T=2000 ns. Other experimental conditions were microwave frequency, 8.978 GHz; microwave pulse power, 29.5 W; microwave pulse width (FWHM), 16 ns; averaging number, 30; pulse repetition rate, 10 Hz; and temperature, 4.2 K. The arrow indicates the field position where four-pulse ESEEM experiments were performed.

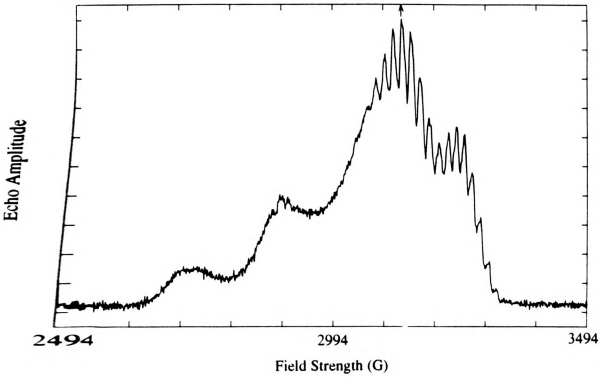
Echo Amplitude
2494
2994
3494
Field Strength (G)

Figure VI-10. Proton sum combination peak region of four-pulse magnitude FT-ESEEM spectrum of axial-H_2O ligand-containing Cu(II)TPP. Experimental conditions were microwave frequency, 8.798 GHz; magnetic field strength, 3131 G; τ, 225 ns; microwave pulse powers of π-pulse, 178 W and $\pi/2$-pulse, 89 W; averaging number, 30; and pulse repetition rate, 10 Hz.

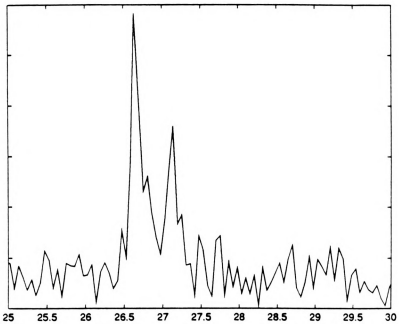
25
25.5
26
26.5
27
27.5
28
28.5
29
29.5
30
Frequency (MHz)

$Cu(II)(H_2O)_6^{2+}$ with results from a more discrete system, four-pulse ESEEM experiments of axial H_2O ligation to Cu(II)TPP were carried out. Fig. VI-9 shows the ESE-EPR spectrum of $Cu(II)TPP(H_2O)_2$. The spectrum shows strong copper hyperfine couplings along $g_{\|}$ and hyperfine splittings of equatorially coordinated nitrogen nuclei at $g_{\perp}$.[34,35] The proton sum combination frequency region of the four-pulse ESEEM spectrum of the $Cu(II)TPP(H_2O)_2$ obtained at $g_{\perp}$ is shown in Fig. VI-10. In the spectrum, the second harmonic frequency peak of the matrix protons is found at 26.66 MHz and the sum combination peak of the axial water protons appears at 27.11 MHz, shifted 0.45 MHz from $2\nu_I$. The ESEEM spectra obtained at $g_{\perp}$ will give rise to a lineshape that approximates that expected for an isotropic electron g-tensor spin system because of the distribution of θ values that are selected due to the hyperfine interactions of the copper and the coordinated nitrogen and because spin packets at several different magnetic field positions around the external field value will be effectively excited due to the microwave pulse bandwidth. Using the well known equation of the sum frequency shift [$\Delta\nu=\nu_\alpha+\nu_\beta-2\nu_I$] drived for isotropic g- and axial ligand hyperfine tensor spin systems,[19] $\Delta\nu=(9/16)T^2/\nu_I$, T=3.3 MHz and r_{eff}=2.9 Å for the axially bound water protons. This value is in good agreement with the dipolar hyperfine couplings of the axial water protons obtained from the four-pulse ESEEM presented above and previous ENDOR[33] studies of $Cu(II)(H_2O)_6^{2+}$.

References

1. R. Lontie, Ed., in *Copper Proteins and Copper Enzymes*, Vol. I. II. III., CRC Press, Boca Roton (1984).

2. L. Kevan, in *Time Domain Electron Spin Resonance*, L. Kevan and R. N. Schwartz, Ed., Wiley-Interscience, New York, Chpter 8 (1979).
3. A. J. Hoff, Ed., in *Advanced EPR. Applications in Biology and Biochemistry*, Elsevier, New York, Chapters 1, 2, 3, and 6 (1989).
4. L. Kevan, in *Modern Pulsed and Continuous -Wave Electron Spin Resonance*, L. Kevan and M. K. Bowman, Ed., John Wiley & Sons, New York, Chapter 5 (1990).
5. W. B. Mims, and J. Peisach, in *Biological Magnetic Resonace*, L. J. Berliner, J. Reuben, Ed., Plenum, New York, Vol. 3, 213 (1981).
6. J. L. Zweier, J. Peisach, and W. B. Mims, *J. Biol. Chem.*, **257**, 10314 (1982)
7. J. McCracken, J. Peisach, and D. M. Dooley, *J. Am. Chem. Soc.*, **109**, 4046 (1987).
8. J. McCracken, S. Pember, S. J. Benkovic, J. J. Villafranca, R. J. Miller, and J. Peisach, *J. Am. Chem. Soc.*, **110**, 1069 (1988).
9. F. Jiang, J. Peisach, L. -J. Ming, L. Que, Jr., and V. J. Chen, *Biochemistry*, **30**, 11437 (1991).
10. W. B. Mims, and J. Peisach, *J. Chem. Phys.*, **19**, 4921 (1978).
11. K. L. Flagan, and D. J. Singel, *J. Chem. Phys.*, **87**, 5606 (1987).
12. J. B. Cornelius, J. McCracken, R. B. Clarkson, R. B. Belford, and J. Peisach, *J. Phys. Chem.*, **94**, 6977 (1990).
13. D. Goldfarb, J. -M. Fauth, Y. Tor, and A. Shanzer, *J. Am. Chem. Soc.*, **113**, 1941 (1991).
14. A. De Groot, R. Evelo, and A. J. Hoff, *J. Magn. Reson.*, **66**, 331 (1986).
15. W. B. Mims, J. L. Davis, and J. Peisach, *Biophys. J.*, **45**, 755 (1984).
16. J. Peisach, W. B. Mims, and J. L. Davis, *J. Biol. Chem.*, **259**, 2704 (1984).
17. A. V. Astashkin, S. A. Dikanov, and Yu. D. Tsvetkov, *Chem. Phys. Lett.*, **136**,204 (1987).
18. S. A. Dikanov, A. V. Astashkin, and Yu. D. Tsvetkov, *Chem. Phys. Lett.*, **144**, 251 (1988).
19. E. J. Reijerse, and S. A. Dikanov, *J. Chem. Phys.*, **95**, 836 (1991).
20. A. M. Tyryshkin, S. A. Dikanov, R. G. Evelo, and A. J. Hoff, *J. Chem. Phys.*, **97**, 42 (1992).
21. J. McCracken and S. Friedenberg, *J. Phys. Chem.*, **98**, 467 (1994).
22. H. -I. Lee, and J. McCracken, submitted to *J. Phys.Chem.*
23. W. B. Mims, J. Peisach, and J. L. Davis, *J. Chem. Phys.*, **66**, 5536 (1977).
24. C. Gemperle, G. Abeli, A. Schweiger, and R. R. Ernst, *J. Magn. Reson.*, **88**, 241 (1990).

25. A. M. Tyryshkin, S. A. Dikanov, and D. Goldfarb, *J. Magn. Reson.*, **A105**, 271 (1993).
26. W. J. White, in *The Porphins*, D. Dolphin, Ed., Academic Press, New York, Vol. V, Chapter 7 (1978).
27. J. McCracken, D. -H. Shin, and J. L. Dye, *Appl. Magn. Reson.*, **3**, 205 (1992).
28. G. C. Hurst, T. A. Henderson, and R. W. Kreilick, *J. Am. Chem. Soc.*, **107**, 7294 (1985).
29. T. A. Henderson, G. C. Hurst, and R. W. Kreilick, *J. Am. Chem. Soc.*, **107**, 7299(1985).
30. C. A. Hutchison, and D. B. McKay, *J. Chem. Phys.*, **66**, 3311 (1977).
31. C. Germperle, G. Abeli, A. Schweiger, and R. R. Ernst, *J. Magn. Reson.*, **88**, 241 (1990).
32. G. M. Brown, and R. Chidambaram, *Acta. Cryst.*, **B25**, 676 (1969).
33. N. M. Atherton, and A. J. Horsewill, *J. Molec. Phys.*, **37**, 1349 (1979).
34. W. C. Lin, in *The Porphyrins*, D. Dolphin, Ed., Academic Press, New York, Vol. IV, Chapter 7 (1978).
35. J. Subramanian, in *Porphyrins and Metalloporphyrins*, K. M. Smith, Ed., Elsevier, Amsterdam, Chapter 13 (1975).

VII. ELECTRON SPIN ECHO ENVELOPE MODULATION STUDIES OF COPPER(II)-PTERIN MODEL COMPLEXES

1. Abstract

The Electron Spin Echo Envelope Modulation (ESEEM) technique of pulsed EPR spectroscopy has been used to characterize the ligation of pteridine ligands to Cu(II) in a variety of complexes prepared in aqueous and non-aqueous solvents. These studies were aimed at understanding the structural relationship between the Cu(II) and pterin cofactors in Phenylalanine Hydroxylase (PAH) from *Chromobacterium Violaceum* where previous continuous wave EPR results have provided evidence for equatorial binding of 6,7-dimethyltetrahydropterin to the metal through N-5. ESEEM studies of the protein show deep ^{14}N modulations originating from two equatorially bound histidyl imidazole groups strongly bound to Cu(II), but provided no evidence for coordinated pterin. For the model compound, $Cu(II)(ethp)_2(H_2O)_2$ (ethp = 2-ethylthio-4-hydroxypterin), X-ray crystallographic studies showed bidentate coordination of ethp through O-4 and N-5. ESEEM spectra obtained for this compound show intense, sharp peaks at 0.6, 2.4, 3.0 MHz and a broad peak at 5.4 MHz. The spectrum is indicative of two identically coupled ^{14}N nuclei and is assigned to N-3 of the coordinated ethp ligands. Similar spectra were obtained for a Cu(II)-folic acid (FA) complex at pH=9.5 in aqueous media. ESEEM

studies of compounds where mixed equatorial-axial ligation of the pterin moiety has been found by X-ray analysis, show little or no ^{14}N contributions in their ESEEM spectra. This complex includes Cu(II)(bpy)(PC) where N-5 is equatorially bound while O-4 is axially coordinated (PC = 6-carboxy pterin). Because the ^{14}N ESEEM response from equatorially coordinated pterin is intense and the peaks occur in a spectral region where there would be little interference from the protein, the experimental results are most consistent with a mixed equatorial-axial ligation of this cofactor at the Cu(II) site of PAH.

2. Introduction

Phenylalanine hydroxylase (PAH)[1,2] catalyzes the hydroxylation of phenylalnine to tyrosine in the presence of molecular oxygen and a reduced pterin cofactor. One atom of the oxygen molecule is in corporated into tyrosine and the other forms water. In the reaction, four electrons are transfered to molecular oxygen, two electrons are from breaking of the C-H bond of phenylalanine and the other from a reduced pterin cofactor. The overall reaction is depicted in Scheme I. Mammalian PAH contains a single iron per monomer[1] while PAH isolated from *Chromobacterium Violaceum* has copper.[2] The iron is required for the enzymatic activity in all mammalian pterin-dependent monooygenases such as PAH, tyrosine hydroxylase, and tryptophan hydroxylase.[3-5] In both mammalian and bacterial enzymes, the metal ions must be reduced to lower oxidation states (Fe(II), Cu(I)) to show activity.[2,6,7] It has been thought that in both the enzymes the transition metal ions play a critical role in the overall catalytic reaction. However, recent studies have shown that copper is not required

for bacterial PAH enzymatic activity.[8] In addition, evidence that Cu(II) inhibits or regulates catalysis was presented. The overall mechanism including the redox chemistry and ligation structure of the copper is not clear for bacterial PAH.

Scheme I.

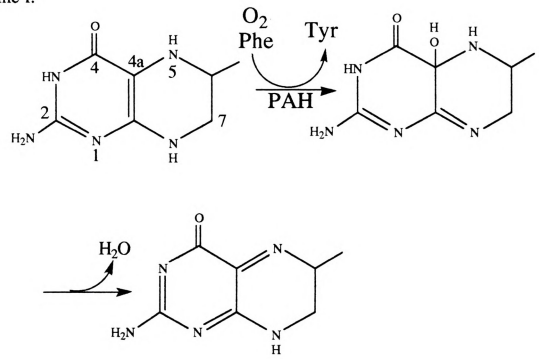

The study of the coordination of Cu(II) is important for understanding the mechanism of inhibition and the redox chemistry of bacterial PAH. S-band continuous wave (CW) EPR studies of 5-^{14}N and 5-^{15}N-labeled 6,7-dimethyltetrahydropterin bound to PAH have revealed that the pterin cofator is coordinated to Cu(II) via N-5 of the pterin.[9] Electron spin echo envelope modulation (ESEEM)[11-13] studies of the enzyme have shown two equatorially bound histidyl imidazole groups strongly bound to Cu(II), but provided no evidence for coordinated pterin.[10] EXAFS studies

of the enzyme has also suggested a Cu(II) coordination of two histidines and two additional O/N-donor groups.[14a]

In this investigation, we undertake ESEEM studies of a variety of Cu(II)-pterin model complexes prepared in aqueous and non-aqueous solvents to provide a better understanding of the ligation of pteridine ligands to Cu(II).

3. Experimental

$Cu(II)(ethp)_2(H_2O)_2$ [ethp = 2-ethylthio-4-hydroxypterin (Fig. VII-1 (c))] was prepared as described by Perkinson et al.[14b] Other complexes were synthesized in water. $Cu(II)(FA)_2(H_2O)_2$ [FA=folic acid (Fig. VII-1 (d))] was made by adding 10-fold excess of FA into 2.9 mM $Cu(II)(NO_3)_2$. The final pH of the solution was adjusted to 9.5 with NaOH. Cu(II)(bpy) [bpy=2,2'-bipyridine] complexes were made by adding a 1:1 stoichiometric ratio of bpy to an aqueous solution of $Cu(II)(NO_3)_2$. Cu(II)(bpy)(PC)$(H_2O)_2$ [PC=6-carboxy pterin (Fig. VII-1 (b))] was made by adding an 1.1:1 molar ratio of PC to the Cu(II)(bpy) solution and adjusting the pH to 7.5. Cu(II)(bpy)(PC)(im) [im=imidazole] was prepared by adding a stoichiometric amount of imidazole to an aqueous solution of Cu(II)(bpy)(PC)(H_2O). The pH of the resulting solution was adjusted to 8. $Cu(II)(ethp)_2(H_2O)_2$ powder samples were dissolved in a DMF [dimethylformamide]/Toluene (50/50) mixture prior to freezing in liquid nitrogen for ESEEM experiments. The presence of an equal volume of toluene promoted formation of a glass upon freezing. The other aqueous compounds were mixed with an equal volume of ethylene glycol prior to freezing in liquid nitrogen. The CW-EPR spectrum of $Cu(II)(ethp)_2(H_2O)_2$

showed a clean axially symmetric electronic g-tensor dominated by a single species.[14b] The CW-EPR spectrum of $Cu(II)(FA)_2(H_2O)_2$ showed also a clean spetrum dominated by a single species ($g_{\perp}$=2.114, $g_{||}$=2.373, and $A_{||}$=111G) . About 70% and 50% of populations of Cu(II)(byp)(PC)(H_2O) and Cu(II)(byp)(PC)(im) were judged by Odani et al. in their aqueous solutions, respectively.[14b,25]

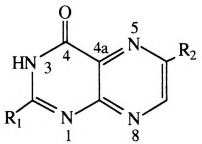

(a) pterin (R_1=NH_2, R_2=H)
(b) PC = 6-carboxy pterin (R_1=NH_2, R_2=COOH)
(c) ethp = 2-ethylthio-4-hydroxypterin (R_1=SCH_2CH_3, R_2=H)
(d) FA = folic acid (R_1=NH_2, R_2=CH_2NH-C_6H_4-CONH-CH(COOH)CH_2CH_2-COOH)

Figure VII-1. Pterin derivatives.

ESEEM experiments were executed on a home-built pulsed-EPR spectrometer which has been described in detail elsewhere[15] and in chapter IV. A three-pulse ($\pi/2$-τ-$\pi/2$-T-$\pi/2$) microwave pulse sequence was used to collect the ESEEM data. The length (full-width at half maximum) of all three microwave pulses was 16 ns. A two step phase cycle, +(0,0,0), +(π,π,0), was used to eliminate unwanted echo modulations. Three-pulse ESEEM data were collected as a function of T, the time interval between second and third pulses. Fourier transformation of the time domain ESEEM data was done using a modified dead-time reconstruction method

developed by Mims.[16] Simulation programs were written in C (Symantec) using a density matrix formalism[17,18] and executed on a Macintosh IIcx microcomputer (Apple Computer Co.).

4. Results and Discussion

Fig. VII-2 shows the time-domain ESEEM and FT-ESEEM spectrum of Cu(II)(ethp)$_2$(H_2O)$_2$ in DMF/Toluene as obtained in the $g_\perp$ region. The spectrum shows four major frequency components, three narrow lines at 0.6, 2.4, and 3.0 MHz and a broad peak at 5.4 MHz as well as weaker lines at 1.2, 1.8, 3.6 and 6.0 MHz. These ESEEM features are similar to those reported for Cu(II)-2-methylimidazole where deep ^{14}N modulations were assigned to the remote ^{14}N of the equatorially coordinated 2-methylimidazole ligand[10]. ^{14}N ESEEM spectra of this type that show three strong sharp lines, where the two lower frequencies add to give the third, and one broad line positioned near $2\nu_I+A_{iso}$, where ν_I is the nuclear Larmor frequency and A_{iso} is the isotropic hyperfine coupling constant, are characteristic of a coupling regime known as "exact cancellation".[19,20] Exact cancellation occurs when the isotropic hyperfine coupling is approximately equal to twice the nuclear Zeeman interaction and the electron-nuclear dipolar interaction is weak.[20] As a result, for one of the electron spin manifolds the hyperfine and nuclear Zeeman interactions cancel each other so that the energy level splittings are determined by the ^{14}N nuclear quadrupole interaction (NQI) as in Fig. VII-3. Because the NQI is independent of the magnetic field, this spin manifold gives rise to three sharp lines at low frequency. For the other electron spin manifold, the hyperfine and nuclear Zeeman interactions are additive and give rise to

Figure VII-2. (a) Three-pulse ESEEM data and (b) cosine fourier transformation spectrum of $Cu(II)(ethp)_2(H_2O)_2$. Experimental conditions are magnetic field strength, 3265 G; microwave frequency, 9.406 GHz, microwave power, 63 W; scanning number, 30; pulse repetition rate, 80 Hz; τ, 140 ns; and temperature, 4.2 K.

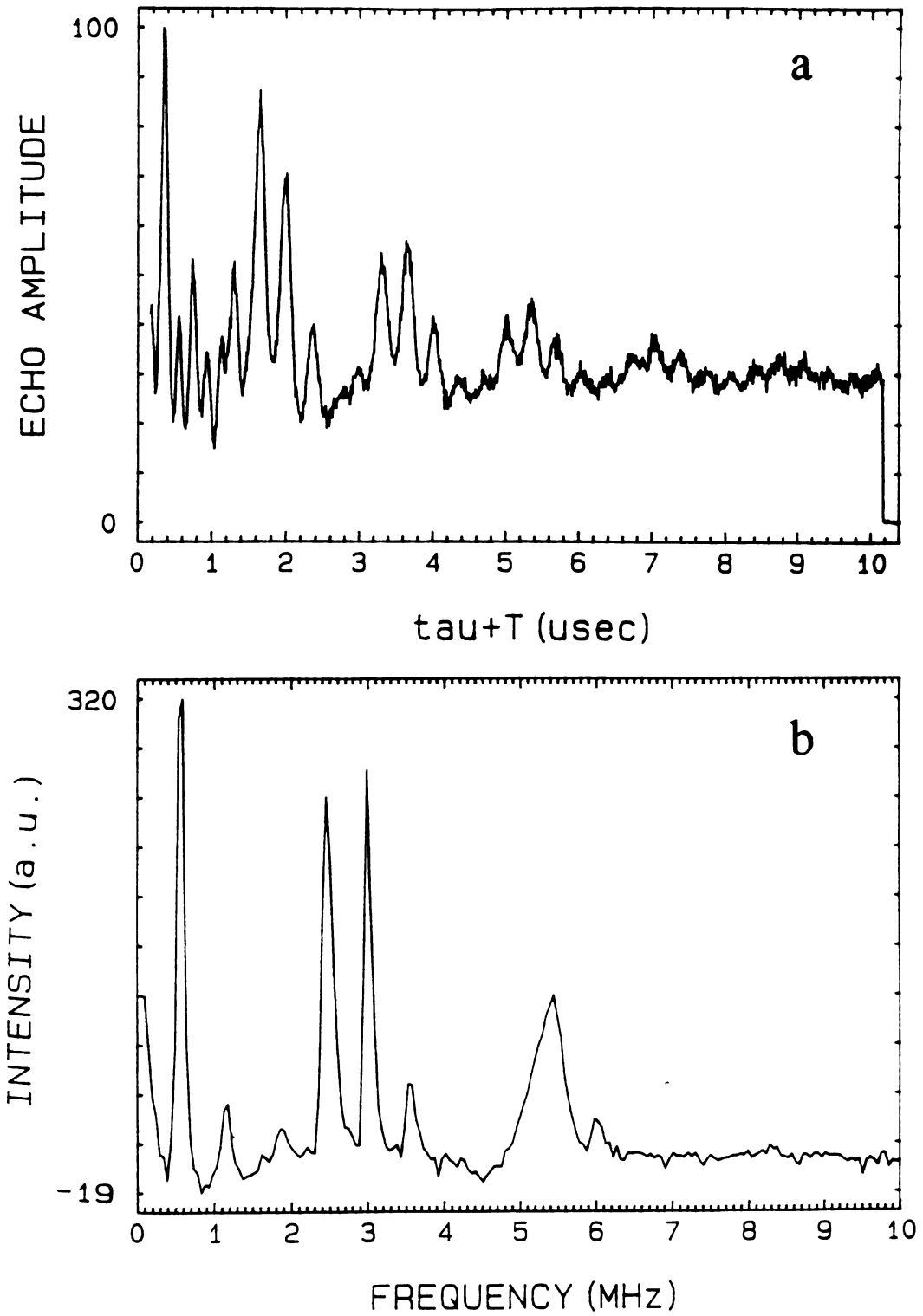
a
100
0
ECHO AMPLITUDE
0 1 2 3 4 5 6 7 8 9 10
tau+T (usec)
b
320
-19
INTENSITY (a.u.)
0 1 2 3 4 5 6 7 8 9 10
FREQUENCY (MHz)

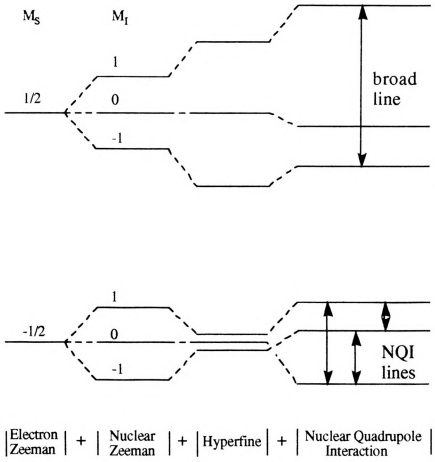

Figure VII-3. Electron spin enegy level diagram for ^{14}N near eaxct cancellation regime.

broad peaks for a randomly oriented sample. (Fig. VII-3). Another feature in spectrum of Fig. VII-2 is the appearance of four narrow and weak lines at 1.2, 1.8, 3.6 and 6.0 MHz. These peaks are combination bands of the three strong peaks at 0.6, 2.4, and 3.0 MHz that result from the product rule when more than one nucleus, with electron-nuclear couplings that result in strong ESEEM, is coupled to the same electron spin.[10,21]

The crystal structure of $Cu(II)(ethp)_2(H_2O)_2$ has been determined and is shown in Fig. VII-4. The ethp ligand is bidentate and coordinated to

Cu(II) through equatorial N-5 and O-4.[14] For ESEEM spectra of $Cu(II)(ethp)_2(H_2O)_2$, the hyperfine coupling of the directly coordinated

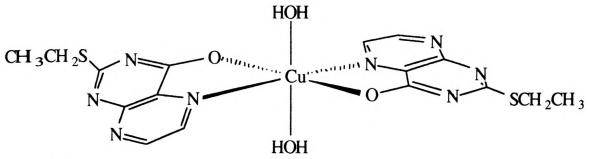

Figure VII-4. Crystal structure of $Cu(II)(ethp)_2(H_2O)_2$.

N-5 nucleus is expected to be too large to give rise to envelope modulation as found for Cu(II)-imidazole. There are three possible nitrogens of the equatorially-bound ethp ligand that could give rise to the modulation of Fig. VII-2. The ESEEM pattern of Fig. VII-2 is dominated by hyperfine coupling from N-3. The reasons for this assignment will be explained later with a comparison of the ESEEM features of $Cu(II)(ethp)_2(H_2O)_2$ with those of $Cu(II)(FA)_2(H_2O)_2$. Quantitative analysis of the ESEEM data from $Cu(II)(ethp)_2(H_2O)_2$ was carried out with computer simulations based on the density matrix formalism.[17,18] The spin Hamiltonian used to describe electron-nuclear coupling for ^{14}N-ESEEM is given by

$$\boldsymbol{H} = - g_n\beta_n\mathbf{B}_o\cdot\mathbf{I} + \mathbf{S}\cdot\underline{\mathbf{A}}\cdot\mathbf{I} + \mathbf{I}\cdot\underline{\mathbf{Q}}\cdot\mathbf{I} \qquad \text{[VII-1]}$$

where $\mathbf{S}$ is the electron spin angular momentum operator, $\mathbf{B}_o$ is the external magnetic field vector, $\underline{\mathbf{A}}$ is the hyperfine interaction tensor, $\mathbf{I}$ is the nuclear spin angular momentum operator, g_n is nuclear g-value, and β_n is the nuclear magneton, and $\underline{\mathbf{Q}}$ is nuclear quadrupole interaction tensor.

When ^{14}N ESEEM shows near-cancellation character, the isotrop hyperfine coupling constant can be estimated as $A_{iso} \simeq 2\nu_I$ and the NQ parameters can be estimated from the frequencies of the three sha nuclear quadrupole resonance lines[19] using Eq. VII-2.

$$\nu_{\pm} = (3/4)e^2qQ\ (1 \pm \eta/3) \qquad [VII\text{-}2]$$
$$\nu_o = (1/2)e^2qQ\eta$$

q, in Eq. VII-2, is the principle value of electric field gradient tensor[22], is the nuclear quadrupole moment, and η is the asymmetry paramete Simulations for the ESEEM of $Cu(II)(ethp)_2(H_2O)_2$ were started usir estimated hyperfine and NQI parameters of A_{iso}=2.0 MHz, e^2qQ=3.6 MH and η=0.30 and the simulation parameters were refined until a best fit the experimental result was obtained. Fig. VII-5 shows the time doma and FT spectra simulated with the parameters which are given in tl caption of Fig. VII-5. In the simulation, it was assumed that tw magnetically equivalent nitrogens are coupled to Cu(II). The simulatic results indicated that the crystal structure of $Cu(II)(ethp)_2(H_2O)_2$ was st valid in DMF/Toluene media.

To study the ligation of pterin derivatives of Cu(II) in aqueo solution, ESEEM experiments on $Cu(II)(FA)_x(H_2O)_{[6-x \text{ or } 6-2x]}$. Sampl were made as described in the experimental section. A typical time-doma ESEEM pattern and FT spectrum collected in the $g_\perp$ region of the Cu(EPR spectrum are shown in Fig. VII-6. The spectrum shows very simil features to those obtained from $Cu(II)(ethp)_2(H_2O)_2$. Three strong sha peaks were found at 0.9, 1.9, and 2.8 MHz along with smaller bands at 3 , 4.7, 5.2, and 5.6 MHz. ESEEM data obtained at a second magnetic fie

Figure VII-5. (a) Time domain ^{14}N-ESEEM simulation and (b) Fourier transformation. Hamiltonian parameters for the simulations are A_{xx}=2.12; A_{yy}=2.12 MHz; A_{zz}=2.60 MHz; e^2qQ=3.63 MHz; η=0.30; Euler angles, α=81o, β=90o, γ=0o; magnetic field strength, 3265 G; and τ=140 ns. Two ^{14}N nitrogen contribution to ESEEM was assumed.

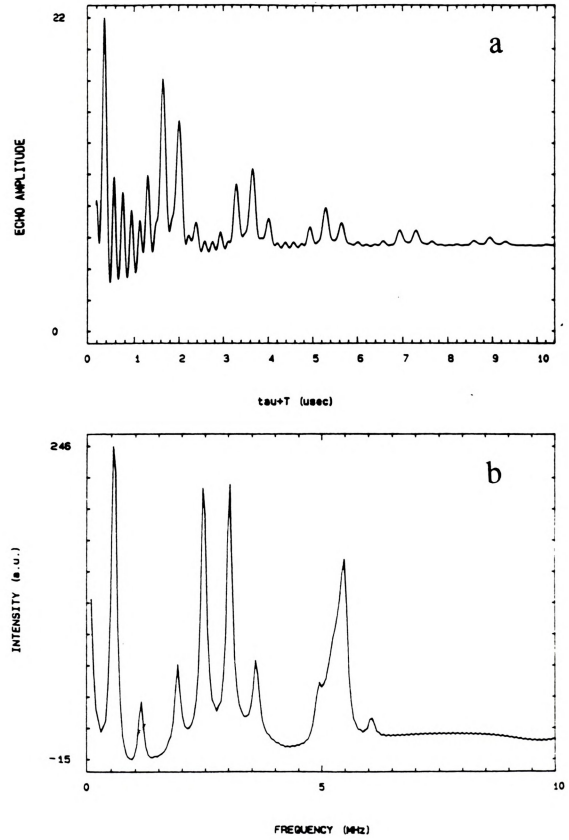
a
22
0
ECHO AMPLITUDE
0
1
2
3
4
5
6
7
8
9
10
tau+T (usec)
b
246
-15
INTENSITY (a.u.)
0
5
10
FREQUENCY (MHz)

Figure VII-6. (a) Three-pulse ESEEM data and (b) cosine fourier transformation spectrum of $Cu(II)(FA)_2(H_2O)_2$. Experimental conditions are magnetic field strength, 3100 G; microwave frequency, 8.926 GHz, microwave power, 63 W; scanning number, 30; pulse repetition rate, 30 Hz; τ, 152 ns; and temperature, 4.2 K.

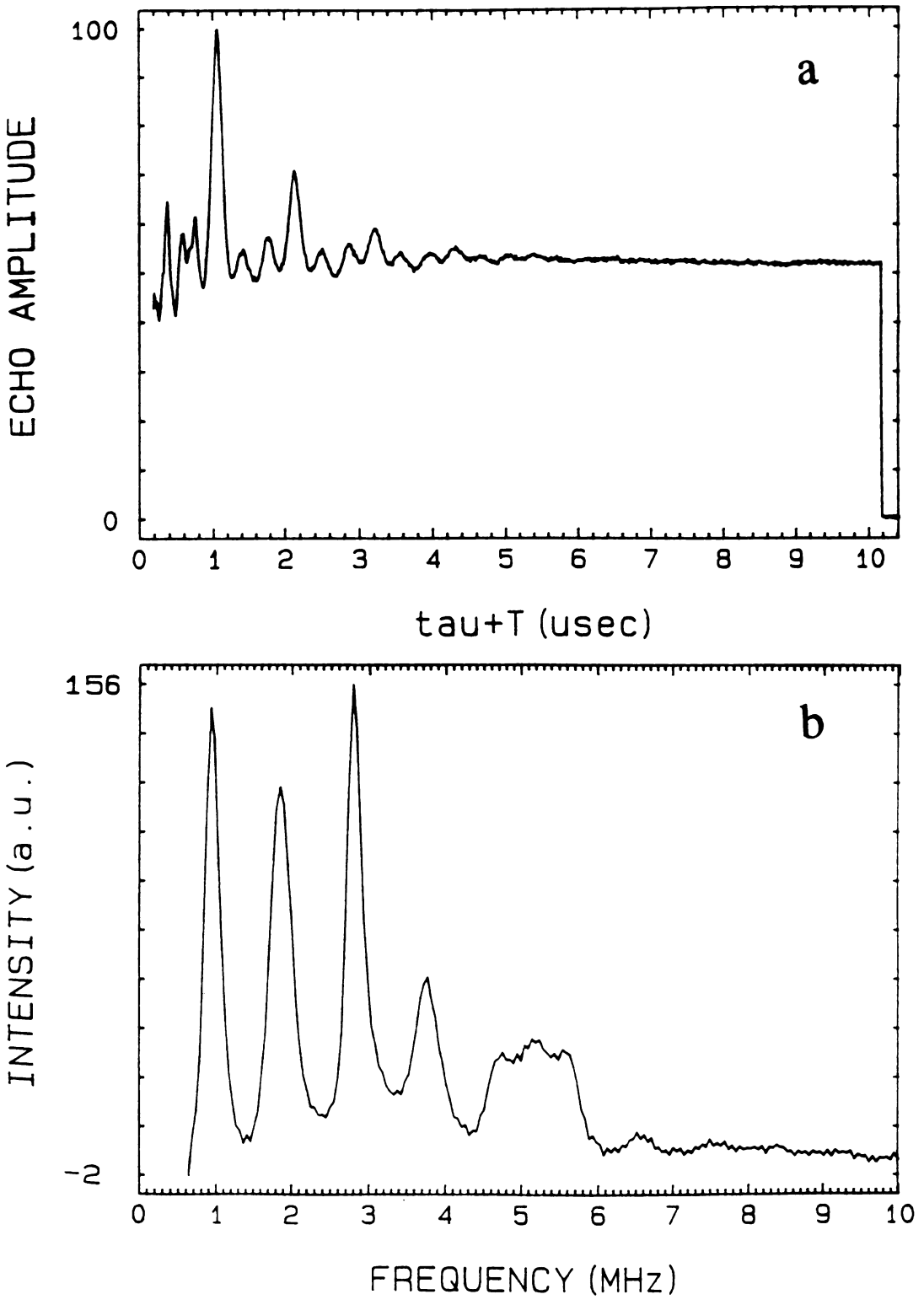
100
a
ECHO AMPLITUDE
0
0 1 2 3 4 5 6 7 8 9 10
tau+T (usec)
156
b
INTENSITY (a.u.)
-2
0 1 2 3 4 5 6 7 8 9 10
FREQUENCY (MHz)

strength showed that the 5.2 MHz peak was shifted by approximately $2\Delta\nu_I$, twice the change in the nitrogen Larmor frequency. The frequencies of the other ESEEM lines remained the same. These observations are characteristic of the "exact cancellation" regime of ^{14}N hyperfine coupling. Simulations using parameters of A_{iso}=2.45 MHz, A_{dip}=0.12 MHz, e^2qQ=3.05 MHz, and η=0.57 adequately described the three strong sharp lines at 0.9, 1.9, and 2.8 MHz and the broad peak at 5.2 MHz. When two equivalent nitrogens were assumed to be coupled to Cu(II), the experimental modulation depth and the other combination bands were properly predicted. These hyperfine parameters are close to those obtained from our analysis of Cu(II)(ethp)$_2$(H$_2$O)$_2$ where an A_{iso} of 2.28 MHz and A_{dip} of 0.16 MHz were found. Hence, it can be concluded that two FA ligands are coordinated to Cu(II) through equatorial N-5 and O-4 as in the Cu(II)(ethp)$_2$(H$_2$O)$_2$ case. The differences in the NQI parameters are due to the different groups substituted at the C-2 position.[23] Because the electronic environments of N-1 and N-8 are similar for ethp and FA, if the modulations arose from hyperfine couplings to these nuclei, the ESEEM results would show similar NQI parameters for Cu(II)(ethp)$_2$(H$_2$O)$_2$ and Cu(II)(FA)$_2$(H$_2$O)$_2$. Because our experimental results show completely different spectra for two samples, the modulations must be dominated by hyperfine coupling to N-3.

Time-domain ESEEM data of Cu(II)(bpy)(PC)(H$_2$O), where X-ray crystalograpic analysis has shown that the N-5 nitrogen, O-4 oxygen, and carboxylate oxygen are bound to Cu(II) as shown in Fig. VII-7,[14,24] is shown in Fig. VII-8. For this compound only shallow modualtions are observed. The large change in the ^{14}N-ESEEM observed for this compound shows that N-8 can not be the source of the deep modulations

observed for the folic acid and ethp complexes and strenghens our above assignment to N-3. The equatorially bound water molecule of Cu(II)(bpy)(PC)(H_2O) can be replaced by imidazole under slightly basic

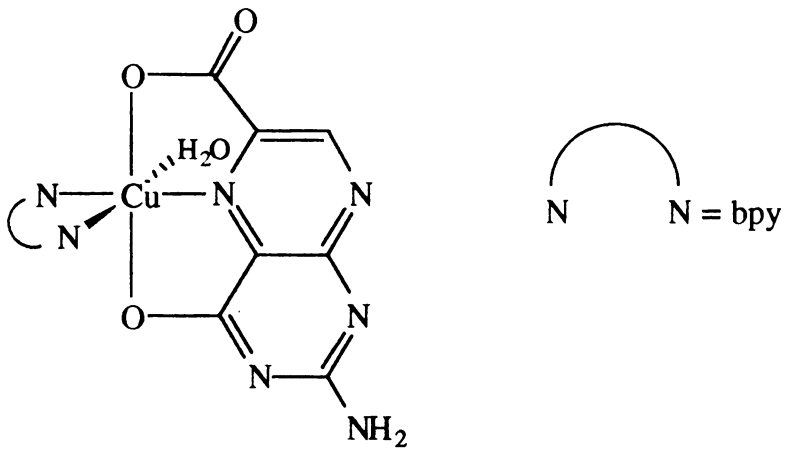

Figure VII-7. Crystal structure of Cu(II)(bpy)(PC)(H_2O).

conditions.[25] Time and frequency domain ESEEM results obtained for Cu(II)(bpy)(PC)(im) are shown in Fig. VII-9. These ESEEM features are identical to those of Cu(II)(dien)(im) [dien = diethylenetriamine] where imidazole is equatorially bound to Cu(II).[19,25] The modulation arises from hyperfine couplings between the remote nitrogen of equatorially bound imidazole and Cu(II).[19] Fig. VII-9 shows that the magnetic couplings of the remote nitrogen of equatorially bound imidazole are not perturbed by the coordination of PC. ESEEM patterns obtained from Cu(II)(dien)(FA)(H_2O) and Cu(II)(bpy)(pterin)$(H_2O)_2$ were the same as those found for Cu(II)(bpy)(PC)(H_2O). ^{14}N-ESEEM spectra of Cu(II)(bpy)(pterin)(im)(H_2O) were also identical to those of Cu(II)(bpy)(PC)(im) and Cu(II)(dien)(im). Therefore, FA and pterin ligands seem to be coordinated to Cu(II) equatorially through N-5 and

Figure VII-8. Three-pulse ESEEM data of Cu(II)(bpy)(PC)(H_2O). Experimental conditions are magnetic field strength, 3050 G; microwave frequency, 8.774 GHz; microwave power, 36 W; scanning number, 100; pulse repetition rate, 30 Hz; τ, 155 ns; and temperature, 4.2 K.

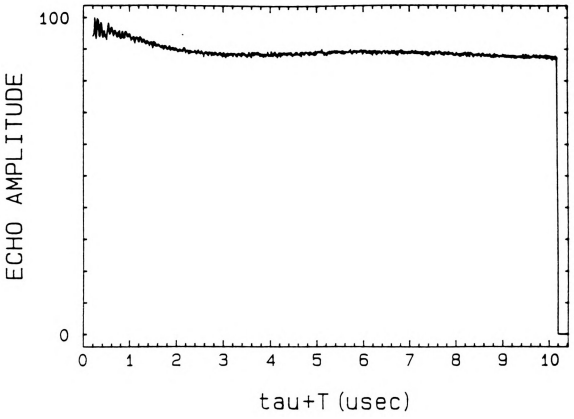
100
0
ECHO AMPLITUDE
0
1
2
3
4
5
6
7
8
9
10
tau+T (usec)

Figure VII-9. (a) Three-pulse ESEEM data and (b) cosine fourier transformation spectrum of Cu(II)(bpy)(PC)(im). Experimental conditions are magnetic field strength, 3050 G; microwave frequency, 8.897 GHz, microwave power, 45 W; scanning number, 30; pulse repetition rate, 30 Hz; τ, 155 ns; and temperature, 4.2 K.

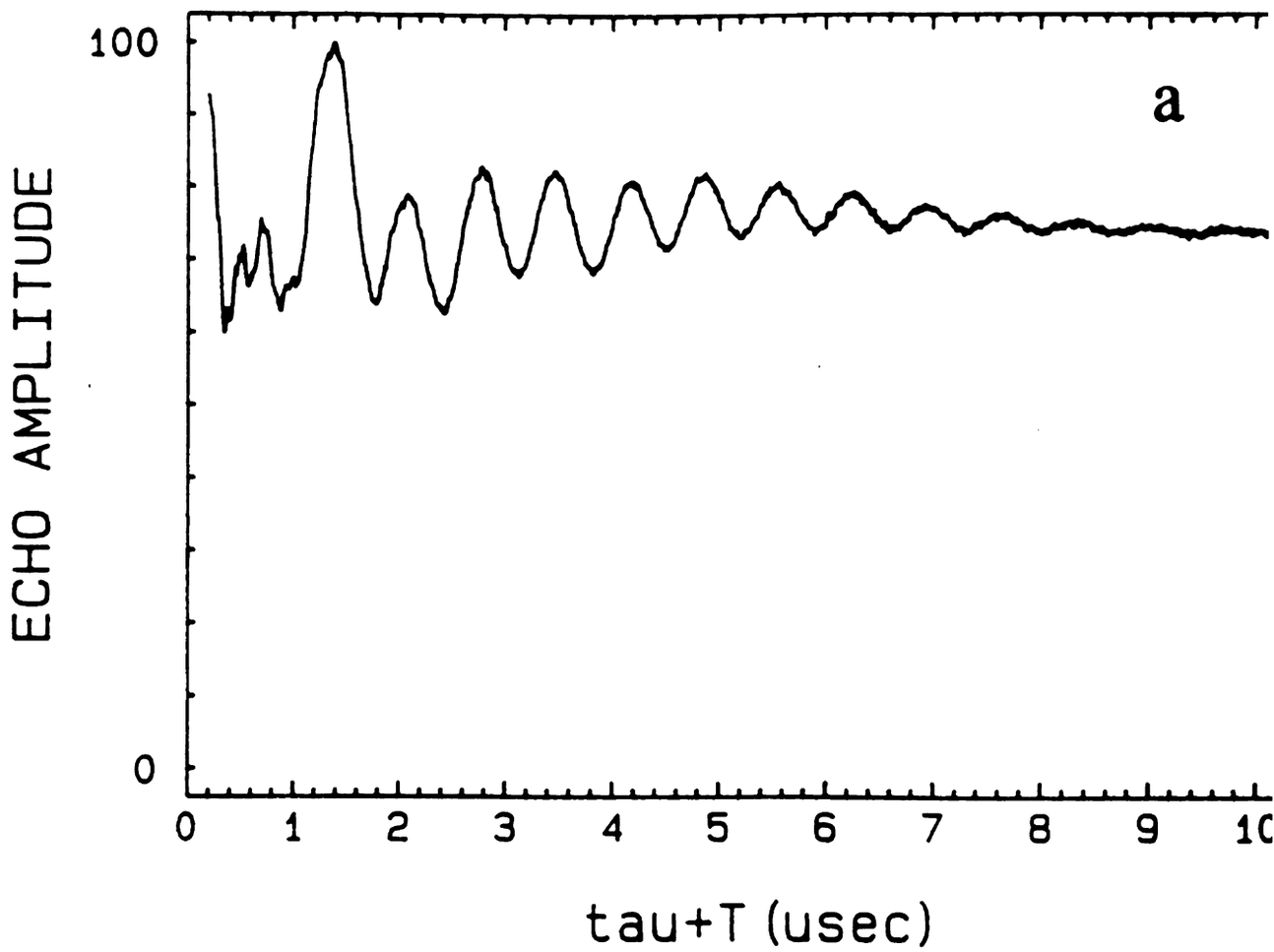
100
a
ECHO AMPLITUDE
0
0 1 2 3 4 5 6 7 8 9 10
tau+T (usec)

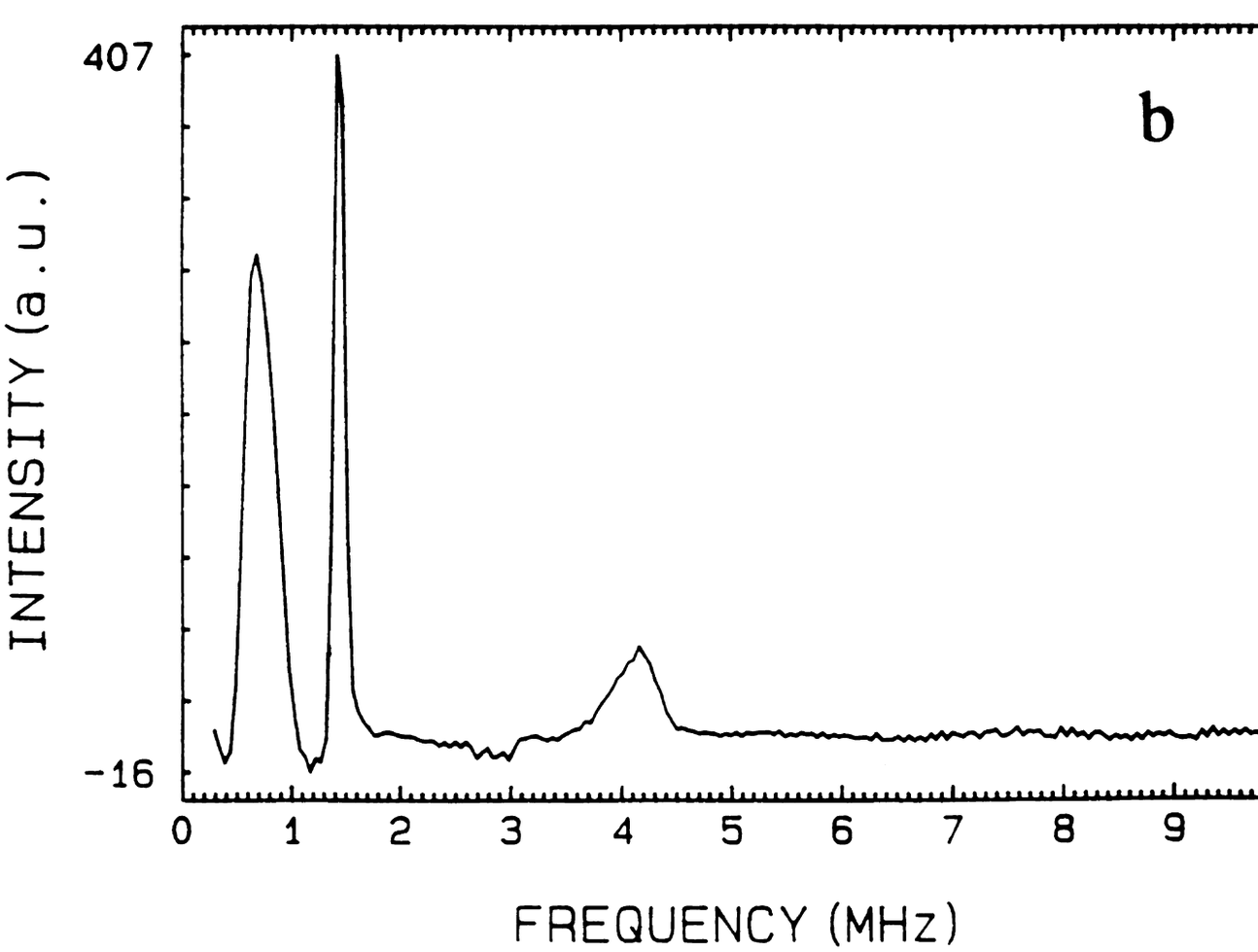
407
b
INTENSITY (a.u.)
-16
0 1 2 3 4 5 6 7 8 9
FREQUENCY (MHz)

axially through O-4 in a similar fashion to PC in crystallin Cu(II)(bpy)(PC)(H_2O).

Previous ESEEM studies of PAH have revealed that the Cu(II) i coordinated to two histidine ligands in an equatorial fashion, but hav provided no evidence for the coordination of the pterin cofactor.[10] CW EPR studies of identical samples showed equatorial coordination of N-5 c 6,7-dimethyltetrahydropterin cofactor. Hence, the present ESEEM studie of our Cu(II)-pterin model complexes are consistent with the equatoria coordination of N-5 and axial coordination O-4 of the pterin cofactor t Cu(II) at the active site of the enzyme. This study shows that the ligation c oxidized pterin derivatives to Cu(II) prefers axial O-4 and equatorial N- coordination when two nitrogen donors are present. This bidentat coordination of the pterin cofactor may prevent the formation of a 4a hydroxypterin intermediate and bear some reponsibility for the role c Cu(II) as an inhibitor of PAH.

References

1. D. Gottschall, R. F. Dietrich, S. J. Benkovic, and R. Shiman, *J. Bio Chem.*, **257**, 845 (1982).
2. S. O. Pember, J. J. Villafranca, and S. J. Benkovic, *Biochemistry*, **25**, 6611 (1986).
3. D. B. Fischer, R. Kirkwood, and S. Kaufman, *J. Biol. Chem.*, **247**, 5161 (1972).
4. T. A. Dix, and S. J. Benkovic, *Biochemistry*, **24**, 5839 (1985).
5. D. M. Kuhn, W. Lovenberg, in *Folates and Pterins*, R. L. Blakely, J. Benkovic, Ed., Vol.2, Wiley-Interscience, New York, 363 (1985)
6. D. E. Wallick, L. M. Bloom, B. J. Gaffney, and S. J. Benkovic, *Biochemistry*, **23**, 1295 (1984).
7. J. J. A. Marota, and R. Shiman, *Biochemistry*, **23**, 1304 (1984).

8. R. T. Carr, and S. J. Benkovic, Biochemistry, **32**, 14132 (1993).
9. S. O. Pember, S. J. Benkovic, J. J. Villafranca, M. Pasenkiewicz-Gierula, and W. E. Antholine, *Biochemistry*, 26, 4477 (1987).
10. J. McCracken, S.Pember, S.J. Benkovic, J.J. Villafranca, R.J. Miller, and J. Peisach, *J. Am. Chem. Soc.* **110**, 1069 (1988).
11. L. Kevan, in *Time Domain Electron Spin Resonance*, L. Kevan, and R. N. Schwartz, Ed., Wiley-Interscience, New York, Chapter 8 (1979).
12. A. J. Hoff, Ed., in *Advanced EPR. Applications in Biology and Biochemistry*, Elsevier, New York, Chapters 1, 2, 3 and 6. (1989).
13. L. Kevan, in *Modern Pulsed and Continuous -Wave Electron Spin Resonance*, L. Kevan, and M. K. Bowman, Ed., John Wiley & Sons, New York, Chapter 5 (1990).
14a. N. J. Blackburn, R. W. Strange, R.T. Carr, and S. J. Benkovic, *Biochemistry*, **31**, 5298 (1992).
14b. J. Perkinson, S. Brodie, K. Yoon, K. Mosny, P. J. Caroll, T. V. Morgan, and S. J. N. Burgmayer, *Inorg. Chem.*, **30**, 719 (1991).
15. J. McCracken, D. H. Shin, and J. L. Dye, *Appl. Magn. Reson.*, **3**, 205 (1992).
16. W. B. Mims, *J. Magn Reson.*, **59**,291 (1984).
17. W. B. Mims, *Phys. Rev.*, **B5**, 2409 (1972).
18. W. B. Mims, *Phys. Rev.*, **B6**, 3543 (1972).
19. W. B. Mims, and J. Peisach, *J. Chem. Phys.*, **69**, 4921 (1978).
20. K. L. Flagan, and D. J. Singel, *J. Chem. Phys.*, **87**, 5606 (1987).
21. S. A. Dikanov, A. A. Shubin, and V. N. Parmon, *J. Magn. Reson.*, **42**, 474 (1981).
22. E. A. C. Lucken, Ed., in *Nuclear Quadrupole Coupling Constants*, Academic Press, New York, 156 (1966).
23. F. Jiang, J. McCracken, and J. Peisach, *J. Am. Chem. Soc.*, **112**, 9035 (1990).
24. T. Kohzuma, H. Masuda, and O. Yamauchi, *J. Am. Chem. Soc.*, **111**, 3431 (1989).
25. A. Odani, H. Masuda, K. Inukai, and O. Yamauchi, *J. Am. Chem. Soc.*, **114**, 6294 (1992).

APPENDIX

A1. Hamitonian Matrices for Hyperfine (HFI) and Nuclear Zeeman Interactions (NZI)

Table A1-1. Matrix elements of HFI and NZI of I=1*

m_I	1	0	-1
1	Z	$\frac{\sqrt{2}}{2}(X-iY)$	0
0	$\frac{\sqrt{2}}{2}(X+iY)$	0	$\frac{\sqrt{2}}{2}(X-iY)$
-1	0	$\frac{\sqrt{2}}{2}(X+iY)$	-Z

* $X=(hm_sA_{xx}-g_n\beta_nB_o)\sin\theta\cos\phi$

$Y=(hm_sA_{yy}-g_n\beta_nB_o)\sin\theta\sin\phi$

$Z=(hm_sA_{zz}-g_n\beta_nB_o)\cos\theta$

Table A1-2. Matrix elements of HFI and NZI of I=3/2

m_I	3/2	1/2	-1/2	-3/2
3/2	$\frac{3}{2}Z$	$\frac{\sqrt{3}}{2}(X-iY)$	0	0
1/2	$\frac{\sqrt{3}}{2}(X+iY)$	$\frac{1}{2}Z$	X-iY	0
-1/2	0	X+iY	$-\frac{1}{2}Z$	$\frac{\sqrt{3}}{2}(X-iY)$
-3/2	0	0	$\frac{\sqrt{3}}{2}(X+iY)$	$-\frac{3}{2}Z$

Table A1-3. Matrix elements of HFI and NZI of I=5/2

m_I	5/2	3/2	1/2	-1/2	-3/2	-5/2
5/2	$\frac{5}{2}Z$	$\frac{\sqrt{5}}{2}(X-iY)$	0	0	0	0
3/2	$\frac{\sqrt{5}}{2}(X+iY)$	$\frac{3}{2}Z$	$\sqrt{2}(X-iY)$	0	0	0
1/2	0	$\sqrt{2}(X+iY)$	$\frac{1}{2}Z$	$\frac{3}{2}(X-iY)$	0	0
-1/2	0	0	$\frac{3}{2}(X+iY)$	$-\frac{1}{2}Z$	$\sqrt{2}(X-iY)$	0
-3/2	0	0	0	$\sqrt{2}(X+iY)$	$-\frac{3}{2}Z$	$\frac{\sqrt{5}}{2}(X-iY)$
-5/2	0	0	0	0	$\frac{\sqrt{5}}{2}(X+iY)$	$-\frac{5}{2}Z$

Table A1-4. Matrix elements of HFI and NZI of I=7/2

m_I	7/2	5/2	3/2	1/2	-1/2	-3/2	-5/2	-7/2
7/2	$\frac{7}{2}Z$	$\frac{\sqrt{7}}{2}(X-iY)$	0	0	0	0	0	0
5/2	$\frac{\sqrt{7}}{2}(X+iY)$	$\frac{5}{2}Z$	$\sqrt{3}(X-iY)$	0	0	0	0	0
3/2	0	$\sqrt{3}(X+iY)$	$\frac{3}{2}Z$	$\frac{\sqrt{15}}{2}(X-iY)$	0	0	0	0
1/2	0	0	$\frac{\sqrt{15}}{2}(X+iY)$	$\frac{1}{2}Z$	$2(X-iY)$	0	0	0
-1/2	0	0	0	$2(X+iY)$	$-\frac{1}{2}Z$	$\frac{\sqrt{15}}{2}(X-iY)$	0	0
-3/2	0	0	0	0	$\frac{\sqrt{15}}{2}(X+iY)$	$-\frac{3}{2}Z$	$\sqrt{3}(X-iY)$	0
-5/2	0	0	0	0	0	$\sqrt{3}(X+iY)$	$-\frac{5}{2}Z$	$\frac{\sqrt{7}}{2}(X-iY)$
-7/2	0	0	0	0	0	0	$\frac{\sqrt{7}}{2}(X+iY)$	$-\frac{7}{2}Z$

A2. M Matrices for the Hamiltonian containing only Hyperfine and Nucle
Zeeman Interactions

Table A2-1. M matrix elements for I=1*

m_I	1	0	-1
1	$\frac{1}{2}(\cos\gamma+1)$	$-\frac{1}{\sqrt{2}}\sin\gamma$	$\frac{1}{2}(-\cos\gamma+1)$
0	$\frac{1}{\sqrt{2}}\sin\gamma$	$\cos\gamma$	$-\frac{1}{\sqrt{2}}\sin\gamma$
-1	$\frac{1}{2}(-\cos\gamma+1)$	$\frac{1}{\sqrt{2}}\sin\gamma$	$\frac{1}{2}(\cos\gamma+1)$

* See Eq. III-61 and Text.

Table A2-2. M matrix elements for I=3/2

m_I	3/2	1/2	-1/2	-3/2
3/2	$\cos^3(\frac{\gamma}{2})$	$-\sqrt{3}\cos^2(\frac{\gamma}{2})$ x $\sin(\frac{\gamma}{2})$	$\sqrt{3}\cos(\frac{\gamma}{2})$ x $\sin^2(\frac{\gamma}{2})$	$-\sin^3(\frac{\gamma}{2})$
1/2	$\sqrt{3}\cos^2(\frac{\gamma}{2})$ x $\sin(\frac{\gamma}{2})$	$\cos(\frac{\gamma}{2})[3\cos3(\frac{\gamma}{2})$ -2]	$\sin(\frac{\gamma}{2})[3\sin^2(\frac{\gamma}{2})$ -2]	$\sqrt{3}\cos(\frac{\gamma}{2})$ x $\sin^2(\frac{\gamma}{2})$
-1/2	$\sqrt{3}\cos(\frac{\gamma}{2})$ x $\sin^2(\frac{\gamma}{2})$	$\sin(\frac{\gamma}{2})[3\sin^2(\frac{\gamma}{2})$ -2]	$\cos(\frac{\gamma}{2})[3\cos^3(\frac{\gamma}{2})$ -2]	$-\sqrt{3}\cos^2(\frac{\gamma}{2})$ x $\sin(\frac{\gamma}{2})$
-3/2	$\sin^3(\frac{\gamma}{2})$	$\sqrt{3}\cos(\frac{\gamma}{2})$ x $\sin^2(\frac{\gamma}{2})$	$-\sqrt{3}\cos^2(\frac{\gamma}{2})$ x $\sin(\frac{\gamma}{2})$	$\cos^3(\frac{\gamma}{2})$

Table A2-3. M matrix elements for I=5/2

mI	5/2	3/2	1/2	-1/2	-3/2	-5/2
5/2	$\cos^5(\frac{\gamma}{2})$	$-\sqrt{5}\cos^4(\frac{\gamma}{2})$ X $\sin(\frac{\gamma}{2})$	$\sqrt{10}\cos^3(\frac{\gamma}{2})$ X $\sin^2(\frac{\gamma}{2})$	$-\sqrt{10}\cos^2(\frac{\gamma}{2})$ X $\sin^3(\frac{\gamma}{2})$	$\sqrt{5}\cos(\frac{\gamma}{2})$ X $\sin^4(\frac{\gamma}{2})$	$-\sin^5(\frac{\gamma}{2})$
3/2	$\sqrt{5}\cos^4(\frac{\gamma}{2})$ X $\sin(\frac{\gamma}{2})$	$\cos^3(\frac{\gamma}{2})[5\cos^2(\frac{\gamma}{2})-4]$	$\sqrt{2}\cos^2(\frac{\gamma}{2})$ x $\sin(\frac{\gamma}{2})[5\sin^2(\frac{\gamma}{2})-2]$	$\sqrt{2}\cos(\frac{\gamma}{2})$ x $\sin^2(\frac{\gamma}{2})[5\cos^2(\frac{\gamma}{2})-2]$	$\sin^3(\frac{\gamma}{2})[5\sin^2(\frac{\gamma}{2})-4]$	$\sqrt{5}\cos(\frac{\gamma}{2})$ X $\sin^4(\frac{\gamma}{2})$
1/2	$\sqrt{10}\cos^3(\frac{\gamma}{2})$ X $\sin^2(\frac{\gamma}{2})$	$-\sqrt{2}\cos^2(\frac{\gamma}{2})$ x $\sin(\frac{\gamma}{2})[5\sin^2(\frac{\gamma}{2})-2]$	$\cos(\frac{\gamma}{2})[10\cos^4(\frac{\gamma}{2})-12\cos^2(\frac{\gamma}{2})+3]$	$-\sin(\frac{\gamma}{2})[10\sin^4(\frac{\gamma}{2})-12\sin^2(\frac{\gamma}{2})+3]$	$\sqrt{2}\cos(\frac{\gamma}{2})$ x $\sin^2(\frac{\gamma}{2})[5\cos^2(\frac{\gamma}{2})-2]$	$-\sqrt{10}\cos^2(\frac{\gamma}{2})$ X $\sin^3(\frac{\gamma}{2})$
-1/2	$\sqrt{10}\cos^2(\frac{\gamma}{2})$ X $\sin^3(\frac{\gamma}{2})$	$\sqrt{2}\cos(\frac{\gamma}{2})$ x $\sin^2(\frac{\gamma}{2})[5\cos^2(\frac{\gamma}{2})-2]$	$\sin(\frac{\gamma}{2})[10\sin^4(\frac{\gamma}{2})-12\sin^2(\frac{\gamma}{2})+3]$	$\cos(\frac{\gamma}{2})[10\cos^4(\frac{\gamma}{2})-12\cos^2(\frac{\gamma}{2})+3]$	$\sqrt{2}\cos^2(\frac{\gamma}{2})$ x $\sin(\frac{\gamma}{2})[5\sin^2(\frac{\gamma}{2})-2]$	$\sqrt{10}\cos^3(\frac{\gamma}{2})$ X $\sin^2(\frac{\gamma}{2})$
-3/2	$\sqrt{5}\cos(\frac{\gamma}{2})$ X $\sin^4(\frac{\gamma}{2})$	$-\sin^3(\frac{\gamma}{2})[5\sin^2(\frac{\gamma}{2})-4]$	$\sqrt{2}\cos(\frac{\gamma}{2})$ x $\sin^2(\frac{\gamma}{2})[5\cos^2(\frac{\gamma}{2})-2]$	$-\sqrt{2}\cos^2(\frac{\gamma}{2})$ x $\sin(\frac{\gamma}{2})[5\sin^2(\frac{\gamma}{2})-2]$	$\cos^3(\frac{\gamma}{2})[5\cos^2(\frac{\gamma}{2})-4]$	$-\sqrt{5}\cos^4(\frac{\gamma}{2})$ X $\sin(\frac{\gamma}{2})$
-5/2	$\sin^5(\frac{\gamma}{2})$	$\sqrt{5}\cos(\frac{\gamma}{2})$ X $\sin^4(\frac{\gamma}{2})$	$\sqrt{10}\cos^2(\frac{\gamma}{2})$ X $\sin^3(\frac{\gamma}{2})$	$\sqrt{10}\cos^3(\frac{\gamma}{2})$ X $\sin^2(\frac{\gamma}{2})$	$\sqrt{5}\cos^4(\frac{\gamma}{2})$ X $\sin(\frac{\gamma}{2})$	$\cos^5(\frac{\gamma}{2})$

Table A2-4. M matrix elements for I=7/2

m_I	7/2	5/2	3/2	1/2	-1/2	-3/2	-5/2	-7/2
7/2	$\cos^7(\frac{\gamma}{2})$	$-\sqrt{7}\cos^6(\frac{\gamma}{2})$ x $\sin(\frac{\gamma}{2})$	$\sqrt{21}\cos^5(\frac{\gamma}{2})$ x $\sin^2(\frac{\gamma}{2})$	$-\sqrt{35}\cos^4(\frac{\gamma}{2})$ x $\sin^3(\frac{\gamma}{2})$	$\sqrt{35}\cos^3(\frac{\gamma}{2})$ x $\sin^4(\frac{\gamma}{2})$	$-\sqrt{21}\cos^2(\frac{\gamma}{2})$ x $\sin^5(\frac{\gamma}{2})$	$\sqrt{7}\cos(\frac{\gamma}{2})$ x $\sin^6(\frac{\gamma}{2})$	$-\sin^7(\frac{\gamma}{2})$
5/2	$\sqrt{7}\cos^6(\frac{\gamma}{2})$ x $\sin(\frac{\gamma}{2})$	$\cos^5(\frac{\gamma}{2})[6\cos^2(\frac{\gamma}{2})-5]$	$\sqrt{3}\cos^4(\frac{\gamma}{2})$ x $\sin(\frac{\gamma}{2})$ $[7\sin^2(\frac{\gamma}{2})-2]$	$\sqrt{5}\cos^3(\frac{\gamma}{2})$ x $\sin^2(\frac{\gamma}{2})$ $[7\cos^2(\frac{\gamma}{2})-4]$	$\sqrt{5}\cos^2(\frac{\gamma}{2})$ x $\sin^3(\frac{\gamma}{2})$ $[7\sin^2(\frac{\gamma}{2})-4]$	$\sqrt{3}\cos(\frac{\gamma}{2})$ x $\sin^4(\frac{\gamma}{2})$ $[7\cos^2(\frac{\gamma}{2})-2]$	$\sin^5(\frac{\gamma}{2})[6\sin^2(\frac{\gamma}{2})-5]$	$\sqrt{7}\cos(\frac{\gamma}{2})$ x $\sin^6(\frac{\gamma}{2})$
3/2	$\sqrt{21}\cos^5(\frac{\gamma}{2})$ x $\sin^2(\frac{\gamma}{2})$	$-\sqrt{3}\cos^4(\frac{\gamma}{2})$ x $\sin(\frac{\gamma}{2})$ $[7\sin^2(\frac{\gamma}{2})-2]$	$\cos^3(\frac{\gamma}{2})[21\cos^4(\frac{\gamma}{2})-30\cos^2(\frac{\gamma}{2})+10]$	$-\sqrt{15}\cos^2(\frac{\gamma}{2})$ x $\sin(\frac{\gamma}{2})$ $[3\cos^4(\frac{\gamma}{2})-2]$	$\sqrt{15}\cos(\frac{\gamma}{2})$ x $\sin^2(\frac{\gamma}{2})$ $[3\sin^4(\frac{\gamma}{2})-2]$	$-\sin^3(\frac{\gamma}{2})[21\sin^4(\frac{\gamma}{2})-30\sin^2(\frac{\gamma}{2})+10]$	$\sqrt{3}\cos(\frac{\gamma}{2})$ x $\sin^4(\frac{\gamma}{2})$ $[7\cos^2(\frac{\gamma}{2})-2]$	$-\sqrt{21}\cos^2($ x $\sin^5(\frac{\gamma}{2})$
1/2	$\sqrt{35}\cos^4(\frac{\gamma}{2})$ x $\sin^3(\frac{\gamma}{2})$	$\sqrt{5}\cos^3(\frac{\gamma}{2})$ x $\sin^2(\frac{\gamma}{2})$ $[7\cos^2(\frac{\gamma}{2})-4]$	$\sqrt{15}\cos^2(\frac{\gamma}{2})$ x $\sin(\frac{\gamma}{2})$ $[3\cos^4(\frac{\gamma}{2})-2]$	$\cos(\frac{\gamma}{2})[55\cos^6(\frac{\gamma}{2})-60\cos^4(\frac{\gamma}{2})+30\cos^4(\frac{\gamma}{2})-4]$	$\sin(\frac{\gamma}{2})[55\sin^6(\frac{\gamma}{2})-60\sin^4(\frac{\gamma}{2})+30\sin^4(\frac{\gamma}{2})-4]$	$\sqrt{15}\cos(\frac{\gamma}{2})$ x $\sin^2(\frac{\gamma}{2})$ $[3\sin^4(\frac{\gamma}{2})-2]$	$\sqrt{5}\cos^2(\frac{\gamma}{2})$ x $\sin^3(\frac{\gamma}{2})$ $[7\sin^2(\frac{\gamma}{2})-4]$	$\sqrt{35}\cos^3($ x $\sin^4(\frac{\gamma}{2})$
-1/2	$\sqrt{35}\cos^3(\frac{\gamma}{2})$ x $\sin^4(\frac{\gamma}{2})$	$-\sqrt{5}\cos^2(\frac{\gamma}{2})$ x $\sin^3(\frac{\gamma}{2})$ $[7\sin^2(\frac{\gamma}{2})-4]$	$\sqrt{15}\cos(\frac{\gamma}{2})$ x $\sin^2(\frac{\gamma}{2})$ $[3\sin^4(\frac{\gamma}{2})-2]$	$-\sin(\frac{\gamma}{2})[55\sin^6(\frac{\gamma}{2})-60\sin^4(\frac{\gamma}{2})+30\sin^4(\frac{\gamma}{2})-4]$	$\cos(\frac{\gamma}{2})[55\cos^6(\frac{\gamma}{2})-60\cos^4(\frac{\gamma}{2})+30\cos^4(\frac{\gamma}{2})-4]$	$-\sqrt{15}\cos^2(\frac{\gamma}{2})$ x $\sin(\frac{\gamma}{2})$ $[3\cos^4(\frac{\gamma}{2})-2]$	$\sqrt{5}\cos^3(\frac{\gamma}{2})$ x $\sin^2(\frac{\gamma}{2})$ $[7\cos^2(\frac{\gamma}{2})-4]$	$-\sqrt{35}\cos^4$ x $\sin^3($
-3/2	$\sqrt{21}\cos^2(\frac{\gamma}{2})$ x $\sin^5(\frac{\gamma}{2})$	$\sqrt{3}\cos(\frac{\gamma}{2})$ x $\sin^4(\frac{\gamma}{2})$ $[7\cos^2(\frac{\gamma}{2})-2]$	$\sin^3(\frac{\gamma}{2})[21\sin^4(\frac{\gamma}{2})-30\sin^2(\frac{\gamma}{2})+10]$	$\sqrt{15}\cos(\frac{\gamma}{2})$ x $\sin^2(\frac{\gamma}{2})$ $[3\sin^4(\frac{\gamma}{2})-2]$	$\sqrt{15}\cos^2(\frac{\gamma}{2})$ x $\sin(\frac{\gamma}{2})$ $[3\cos^4(\frac{\gamma}{2})-2]$	$\cos^3(\frac{\gamma}{2})[21\cos^4(\frac{\gamma}{2})-30\cos^2(\frac{\gamma}{2})+10]$	$\sqrt{3}\cos^4(\frac{\gamma}{2})$ x $\sin(\frac{\gamma}{2})$ $[7\sin^2(\frac{\gamma}{2})-2]$	$\sqrt{21}\cos^5$ x $\sin^2($
-5/2	$\sqrt{7}\cos^6(\frac{\gamma}{2})$ x$\sin(\frac{\gamma}{2})$	$-\sin^5(\frac{\gamma}{2})[6\sin^2(\frac{\gamma}{2})-5]$	$\sqrt{3}\cos(\frac{\gamma}{2})$ x $\sin^4(\frac{\gamma}{2})$ $[7\cos^2(\frac{\gamma}{2})-2]$	$-\sqrt{5}\cos^2(\frac{\gamma}{2})$ x $\sin^3(\frac{\gamma}{2})$ $[7\sin^2(\frac{\gamma}{2})-4]$	$\sqrt{5}\cos^3(\frac{\gamma}{2})$ x$\sin^2(\frac{\gamma}{2})$ $[7\cos^2(\frac{\gamma}{2})-4]$	$-\sqrt{3}\cos^4(\frac{\gamma}{2})$ x $\sin(\frac{\gamma}{2})$ $[7\sin^2(\frac{\gamma}{2})-2]$	$\cos^5(\frac{\gamma}{2})[6\cos^2(\frac{\gamma}{2})-5]$	$-\sqrt{7}\cos^6($ x $\sin(\frac{\gamma}{2})$
-7/2	$\sin^7(\frac{\gamma}{2})$	$\sqrt{7}\cos^6(\frac{\gamma}{2})$ x $\sin(\frac{\gamma}{2})$	$\sqrt{21}\cos^2(\frac{\gamma}{2})$ x $\sin^5(\frac{\gamma}{2})$	$\sqrt{35}\cos^3(\frac{\gamma}{2})$ x $\sin^4(\frac{\gamma}{2})$	$\sqrt{35}\cos^4(\frac{\gamma}{2})$ x $\sin^3(\frac{\gamma}{2})$	$\sqrt{21}\cos^5(\frac{\gamma}{2})$ x $\sin^2(\frac{\gamma}{2})$	$\sqrt{7}\cos^6(\frac{\gamma}{2})$ x $\sin(\frac{\gamma}{2})$	$\cos^7(\frac{\gamma}{2})$

A3. Hamiltonian Matrices for Nuclear Quadrupole Interaction (NQI) alon
Hyperfine Interaction Principle Axis System (HFI PAS)

Table A3-1. Matrix elements of NQI of I=1*

m_I	1	0	-1
1	$\frac{1}{2}(Q_{11}+Q_{22})$ $+Q_{33}$	$\frac{\sqrt{2}}{2}(Q_{13}-iQ_{23})$	$\frac{1}{2}(Q_{11}-Q_{22})$ $-iQ_{12}$
0	$\frac{\sqrt{2}}{2}(Q_{13}+iQ_{23})$	$Q_{11}+Q_{22}$	$\frac{\sqrt{2}}{2}(-Q_{13}+iQ_{23})$
-1	$\frac{1}{2}(Q_{11}-Q_{22})$ $+iQ_{12}$	$\frac{\sqrt{2}}{2}(-Q_{13}-iQ_{23})$	$\frac{1}{2}(Q_{11}+Q_{22})$ $+Q_{33}$

* Qij values are listed in Section A3-1.

Table A3-2. Matrix elements of NQI of I=3/2

m_I	3/2	1/2	-1/2	-3/2
3/2	$\frac{3}{4}(Q_{11}+Q_{22})$ $+\frac{9}{4}Q_{33}$	$\sqrt{3}(Q_{13}-iQ_{23})$	$\frac{\sqrt{3}}{2}(Q_{11}-Q_{22})$ $-i\sqrt{3}Q_{12}$	0
1/2	$\sqrt{3}(Q_{13}+iQ_{23})$	$\frac{7}{4}(Q_{11}+Q_{22})$ $+\frac{1}{4}Q_{33}$	0	$\frac{\sqrt{3}}{2}(Q_{11}-Q_{22})$ $-i\sqrt{3}Q_{12}$
-1/2	$\frac{\sqrt{3}}{2}(Q_{11}-Q_{22})$ $+i\sqrt{3}Q_{12}$	0	$\frac{7}{4}(Q_{11}+Q_{22})$ $+\frac{1}{4}Q_{33}$	$\sqrt{3}(-Q_{13}+iQ_{23})$
-3/2	0	$\frac{\sqrt{3}}{2}(Q_{11}-Q_{22})$ $+i\sqrt{3}Q_{12}$	$\sqrt{3}(-Q_{13}-iQ_{23})$	$\frac{3}{4}(Q_{11}+Q_{22})$ $+\frac{9}{4}Q_{33}$

Table A3-3. Matrix elements of NQI of I=5/2

m_I	5/2	3/2	1/2	-1/2	-3/2	-5/2
5/2	$\frac{5}{4}(Q_{11}+Q_{22})$ $+\frac{25}{4}Q_{33}$	$2\sqrt{5}(Q_{13}$ $-iQ_{23})$	$\frac{\sqrt{10}}{2}(Q_{11}-Q_{22})$ $-i\sqrt{10}Q_{12}$	0	0	0
3/2	$2\sqrt{5}(Q_{13}+$ $iQ_{23})$	$\frac{13}{4}(Q_{11}+Q_{22})$ $+\frac{9}{4}Q_{33}$	$2\sqrt{2}(Q_{13}$ $-iQ_{23})$	$\frac{3\sqrt{2}}{2}(Q_{11}$ $-Q_{22})$ $-i3\sqrt{2}Q_{12}$	0	0
1/2	$\frac{\sqrt{10}}{2}(Q_{11}-$ $Q_{22})$ $+i\sqrt{10}Q_{12}$	$2\sqrt{2}(Q_{13}$ $-iQ_{23})$	$\frac{17}{4}(Q_{11}$ $+Q_{22})+\frac{1}{4}Q_{33}$	0	$\frac{3\sqrt{2}}{2}(Q_{11}$ $-Q_{22})$ $-i3\sqrt{2}Q_{12}$	0
-1/2	0	$\frac{3\sqrt{2}}{2}(Q_{11}$ $-Q_{22})$ $+i3\sqrt{2}Q_{12}$	0	$\frac{17}{4}(Q_{11}$ $+Q_{22})+\frac{1}{4}Q_{33}$	$2\sqrt{2}(-Q_{13}$ $+iQ_{23})$	$\frac{\sqrt{10}}{2}(Q_{11}-Q_{22})$ $-i\sqrt{10}Q_{12}$
-3/2	0	0	$\frac{3\sqrt{2}}{2}(Q_{11}$ $-Q_{22})$ $+i3\sqrt{2}Q_{12}$	$2\sqrt{2}(-Q_{13}$ $-iQ_{23})$	$\frac{13}{4}(Q_{11}+Q_{22})$ $+\frac{9}{4}Q_{33}$	$2\sqrt{5}(-Q_{13}$ $+iQ_{23})$
-5/2	0	0	0	$\frac{\sqrt{10}}{2}(Q_{11}-Q_{22})$ $+i\sqrt{10}Q_{12}$	$2\sqrt{5}(-Q_{13}$ $-iQ_{23})$	$\frac{5}{4}(Q_{11}+Q_{22})$ $+\frac{25}{4}Q_{33}$

Table A3-4. Matrix elements of NQI of I=7/2

m_I	7/2	5/2	3/2	1/2	-1/2	-3/2	-5/2	-7/2
7/2	$\frac{7}{4}(Q_{11}+Q_{22})+\frac{9}{4}Q_{33}$	$3\sqrt{7}(Q_{13}-iQ_{23})$	$\frac{\sqrt{21}}{2}(Q_{11}-Q_{22})-i\sqrt{21}Q_{12}$	0	0	0	0	0
5/2	$3\sqrt{7}(Q_{13}+iQ_{23})$	$\frac{19}{4}(Q_{11}+Q_{22})+\frac{25}{4}Q_{33}$	$4\sqrt{3}(Q_{13}-iQ_{23})$	$\frac{3\sqrt{5}}{2}(Q_{11}-Q_{22})-i3\sqrt{5}Q_{12}$	0	0	0	0
3/2	$\frac{\sqrt{21}}{2}(Q_{11}-Q_{22})+i\sqrt{21}Q_{12}$	$4\sqrt{3}(Q_{13}+iQ_{23})$	$\frac{27}{4}(Q_{11}+Q_{22})+\frac{9}{4}Q_{33}$	$\sqrt{15}(Q_{13}-iQ_{23})$	$\sqrt{15}(Q_{11}-Q_{22})-i2\sqrt{15}Q_{12}$	0	0	0
1/2	0	$\frac{3\sqrt{5}}{2}(Q_{11}-Q_{22})+i3\sqrt{5}Q_{12}$	$\sqrt{15}(Q_{13}+iQ_{23})$	$\frac{31}{4}(Q_{11}+Q_{22})+1/4Q_{33}$	0	$\sqrt{15}(Q_{11}-Q_{22})-i2\sqrt{15}Q_{12}$	0	0
-1/2	0	0	$\sqrt{15}(Q_{11}-Q_{22})+i2\sqrt{15}Q_{12}$	0	$\frac{31}{4}(Q_{11}+Q_{22})+1/4Q_{33}$	$\sqrt{15}(-Q_{13}+iQ_{23})$	$\frac{3\sqrt{5}}{2}(Q_{11}-Q_{22})-i3\sqrt{5}Q_{12}$	0
-3/2	0	0	0	$\sqrt{15}(Q_{11}-Q_{22})+i2\sqrt{15}Q_{12}$	$\sqrt{15}(-Q_{13}-iQ_{23})$	$\frac{27}{4}(Q_{11}+Q_{22})+\frac{9}{4}Q_{33}$	$4\sqrt{3}(-Q_{13}+iQ_{23})$	$\frac{\sqrt{21}}{2}(Q_{11}-Q_{22})-i\sqrt{21}Q_{12}$
-5/2	0	0	0	0	$\frac{3\sqrt{5}}{2}(Q_{11}-Q_{22})+i3\sqrt{5}Q_{12}$	$4\sqrt{3}(-Q_{13}-iQ_{23})$	$\frac{19}{4}(Q_{11}+Q_{22})+\frac{25}{4}Q_{33}$	$3\sqrt{7}(-Q_{13}+iQ_{23})$
-7/2	0	0	0	0	0	$\frac{\sqrt{21}}{2}(Q_{11}-Q_{22})+i\sqrt{21}Q_{12}$	$3\sqrt{7}(-Q_{13}-iQ_{23})$	$\frac{7}{4}(Q_{11}+Q_{22})+\frac{49}{4}Q_{33}$

A3-1. Q elements in Tables A3-1, 2, 3, and 4

$$Q_{ij} = Q_1 A_{1i} A_{1j} + Q_2 A_{2i} A_{2j} + Q_2 A_{3i} A_{3j}$$

where

$$Q_1 = \frac{he^2qQ}{4I(2I-1)}(\eta-1)$$

$$Q_2 = \frac{he^2qQ}{4I(2I-1)}(\eta+1)$$

$$Q_3 = \frac{he^2qQ}{2I(2I-1)}$$

$A_{11} = \cos\gamma\cos\beta\cos\alpha - \sin\gamma\sin\alpha$

$A_{12} = \cos\gamma\cos\beta\sin\alpha + \sin\gamma\cos\alpha$

$A_{13} = -\cos\gamma\sin\beta$

$A_{21} = -\sin\gamma\cos\beta\cos\alpha - \cos\gamma\sin\alpha$

$A_{22} = -\sin\gamma\cos\beta\sin\alpha + \cos\gamma\cos\alpha$

$A_{23} = \sin\gamma\sin\beta$

$A_{31} = \sin\beta\cos\alpha$

$A_{32} = \sin\beta\sin\alpha$

$A_{33} = \cos\beta$

A4. Computer Programs for Two-Pulse and Three-Pulse ESEEM Time Domain Simulations for I=1, 3/2, 5/2, and 7/2

These Programs are written in the C computer language (Symantec v.4.0). The diagonalization routine for Hermitian matrices was taken from a numerical package called "NuTools:Numerical Methods in C" (Metaphor, v.1.02).

A4-1. Main Program for Two-Pulse ESEEM

```
/**
 *
 *  2pulsesim.c = 2-pulse ESEEM simulation (I=1, 3/2, 5/2, and 7/2 ,g=isotropic) in time domain
 *
 **/

 #include <console.h>
 #include <NuToolsNumerical.h>
 #include <nu_test.h>

 main()
 {
    int i,parai[6],err[1];
    float paraf[10];
     vector sinthe,costhe,sinphi,cosphi;
    float qr[M+1][M+1],qi[M+1][M+1]; /* M=2I+1, I=nuclear spin number */
    float emod[1024],oremod[1024];

    /** parametersetting
    *
          *  Floating Parametersetting
          *
          *      paraf[0]=nuclear g-value
          *      paraf[1]=field strength (G)
          *      paraf[2]=Axx (MHz)
          *      paraf[3]=Ayy (MHz)
          *      paraf[4]=Azz (MHz)
          *      paraf[5]=eeqQ (MHz)
          *      paraf[6]=eta (asymmetry parameter)
          *      paraf[7]=alpha (radian)
          *      paraf[8]=beta  (radian)
          *      paraf[9]=gamma (radian)
          *
          *  Integer parameter setting
          *
          *      parai[0]=tau (ns)
          *      parai[1]=starting T (ns) set to zero
          *      parai[2]=time increment (ns)
          *      parai[3]=number of data points desired
          *      parai[4]=number of theta increments (# of theta between 0 and π)
```

```
        *       parai[5]=number of phi increments (# of phi between 0 and π)
        *
        **/

   paraset(paraf,parai);

   /* sine and cosine table */

   sinthe = costhe = sinphi = cosphi = InitV();

     sincostable(parai,&sinthe,&costhe,&sinphi,&cosphi);

   /* quadrupole energy */

   quadrupole2hlf(paraf,qr,qi); /* I=1 */
   quadrupole3hlf(paraf,qr,qi); /* I=3/2 */
   quadrupole5hlf(paraf,qr,qi); /* I=5/2 */
   quadrupole7hlf(paraf,qr,qi); /* I=7/2 */

   /* hyperfine energy + quadrupole energy */

     emodulation(paraf,parai,&sinthe,&costhe,&sinphi,&cosphi,qr,qi,emod);

   /* save simulation data */

   savesimdata(oremod,parai,paraf);
}
```

A4-2. Main Program for Three-Pulse ESEEM

```
/**
 *
 *  3pulsesim.c = 3-pulse ESEEM simulation (I=1,3/2,5/2,7/2,g=isotropic)
 *
 **/

#include <console.h>
#include <NuToolsNumerical.h>
#include <nu_test.h>

main()
{
   int i,parai[6];
   float paraf[10];
     vector sinthe,costhe,sinphi,cosphi;
   float qr[M+1][M+1],qi[M+1][M+1]; /* M=2I+1, I=nuclear spin number */
   float emod[2][1024],emodsum[1024];

   /* parametersetting */

   parasetSE(paraf,parai);

   /* sine and cosine table */

   sinthe = costhe = sinphi = cosphi = InitV();

     sincostable(parai,&sinthe,&costhe,&sinphi,&cosphi);

   /* quadrupole energy */
```

```
  quadrupole2hlf(paraf,qr,qi); /* I=1 */
  quadrupole3hlf(paraf,qr,qi); /* I=3/2 */
  quadrupole5hlf(paraf,qr,qi); /* I=5/2 */
  quadrupole7hlf(paraf,qr,qi); /* I=7/2 */

  /* hyperfine energy + quadrupole energy */

    emodulationSE(paraf,parai,&sinthe,&costhe,&sinphi,&cosphi,qr,qi,emod);

  /* Save the simulation data */

    savesimdataSE(emod,parai,paraf);

}
```

A4-3. Subprograms

```
/**
 *
 *  echoamp.c = echo amplitude at a certain theta and phi and
 *              integration of the amplitude overall orientation of phi for 2-pulse
 *
 **/

echoamp(nu,parai,da,db,x0,xa,xb,xab,echamp,sphi,delphi)

  int nu,parai[];
   float  x0[],xa[],xb[],xab[],echamp[],sphi,delphi;
  vector *da,*db;
{
   int ii,jj,kk;
   int i,j,k,n;
  int ind,inda;
   float wa[9][9],wb[9][9],tau,temp,echo;
   float temp1,temp2,temp3,temp4;
  float fnu;

  fnu=nu;

   for(jj=2;jj<=nu;jj++)
  {
    temp1=da->base[jj-1];
    temp3=db->base[jj-1];

     for(ii=1;ii<=jj-1;ii++)
    {
      temp2=da->base[ii-1];
      temp4=db->base[ii-1];

       wa[ii][jj]=temp2-temp1;
       wb[ii][jj]=temp4-temp3;
    }
  }

   for(kk=0;kk<=parai[3]-1;kk++)
  {

     tau=(parai[0]+parai[2]*kk)*0.001;  /* unit correction (*0.001) */
    echo=0.0;
    inda=0;
```

```
    ind=0;

    for(j=2;j<=nu;j++)
    {
      for(i=1;i<=j-1;i++)
      {
        for(n=2;n<=nu;n++)
        {
          for(k=1;k<=n-1;k++)
          {
            temp=cos((wa[i][j]+wb[k][n])*tau)+cos((wa[i][j]-wb[k][n])*tau);
            echo+=temp*xab[ind];
            ind++;
          }
        }
        echo+=xa[inda]*cos(tau*wa[i][j])+xb[inda]*cos(tau*wb[i][j]);
        inda++;
      }
    }
    echo=(x0[0]+2*echo)/fnu;

    /* integration of Modulation amplitude overall orientation of phi */

    echamp[kk]+=echo*sphi*delphi;
  }
  return;
}

/**
 *
 *  echoampSE.c = echo amplitude at a certain theta and phi and
 *                integration of the amplitude overall orientation of phi
 *
 *          for 3-pulse ESEEM
 **/

#include <NuToolsNumerical.h>
#include <math.h>

echoampSE(nu,parai,da,db,x0,xa,xb,xab,echamp,sphi,delphi)

  int nu,parai[];
   float x0[],xa[],xb[],xab[],echamp[2][1024],sphi,delphi;
  vector *da,*db;
{
  int ii,jj,kk;
  int i,j,k,n;
  int ind,inda;
   float wa[9][9],wb[9][9],tau,tauplusT,echo0,echo1;
   float cosAtau[9][9],cosBtau[9][9],cosAtauT[9][9],cosBtauT[9][9];
  float fnu;

  tau=parai[0]*0.001;                    /* unit correction (*0.001) */
  fnu=nu;

   for(jj=2;jj<=nu;jj++)
  {
     for(ii=1;ii<=jj-1;ii++)
     {
       wa[ii][jj]=da->base[ii-1]-da->base[jj-1];
       wb[ii][jj]=db->base[ii-1]-db->base[jj-1];

       cosAtau[ii][jj]=cos(wa[ii][jj]*tau);
       cosBtau[ii][jj]=cos(wb[ii][jj]*tau);
```

```
  }
 }

  for(kk=0;kk<=parai[3]-1;kk++)
 {

    tauplusT=(parai[0]+parai[1]+parai[2]*kk)*0.001;
   echo0=0.0;
   echo1=0.0;
   inda=0;
   ind=0;

   for(jj=2;jj<=nu;jj++)
  {
     for(ii=1;ii<=jj-1;ii++)
    {
       cosAtauT[ii][jj]=cos(wa[ii][jj]*tauplusT);
       cosBtauT[ii][jj]=cos(wb[ii][jj]*tauplusT);
    }
  }

   for(j=2;j<=nu;j++)
  {
     for(i=1;i<=j-1;i++)
    {
      for(n=2;n<=nu;n++)
      {
        for(k=1;k<=n-1;k++)
        {
           echo0+=2.0*cosBtau[k][n]*cosAtauT[i][j]*xab[ind];
           echo1+=2.0*cosAtau[i][j]*cosBtauT[k][n]*xab[ind];
          ind++;
        }
       }
        echo0+=cosBtau[i][j]*xb[inda]+cosAtauT[i][j]*xa[inda];
        echo1+=cosAtau[i][j]*xa[inda]+cosBtauT[i][j]*xb[inda];
       inda++;
     }
  }
    echo0=(x0[0]*0.5+echo0)/fnu;
    echo1=(x0[0]*0.5+echo1)/fnu;

    /* integration of Modulation amplitude overall orientation of phi */

    echamp[0][kk]+=echo0*sphi*delphi;
    echamp[1][kk]+=echo1*sphi*delphi;
 }
 return;
}
/**
 *
 *  emodulation.c = caculation of Emodulation for 2-pulse
 *
 **/

#include <math.h>
#include <NuToolsNumerical.h>

emodulation(paraf,parai,sinthe,costhe,sinphi,cosphi,qr,qi,emod)

  int parai[];
  float paraf[],qr[M+1][M+1],qi[M+1][M+1],emod[]; /* M=2I+1, I=nuclear spin number */
   vector *sinthe,*costhe,*sinphi,*cosphi;
```

```
{
   int i,j,k,n,kk,ii,m,mm,p;
  float gn,h0,Axx,Ayy,Azz;
  float r2,vn;
   float xaa,yaa,zaa,xbb,ybb,zbb;
  float x,y,z;
  cmatrix ha,hb,ma,mb,mc;
 vector da,db;
   float x0[1],xa[28],xb[28],xab[784];
   float sthe,sphi,delthe,delphi,eamp[1024];
   float st,ct,sp,cp;

 gn=paraf[0];                    /* nuclear g-value */
 h0=paraf[1];                    /* field strength (G) */
 Axx=paraf[2];                   /* Axx (MHz) */
 Ayy=paraf[3];                   /* Ayy (MHz) */
 Azz=paraf[4];                   /* Azz (MHz) */

 r2=1.414213562;                 /* square root 2 */
   vn=gn*5.0507866*h0*0.001/6.6260755;

 /***** Hyperfine + Quadrupole energy in MHz unit *****/

   xaa=(0.5*Axx-vn)*6.283185306;
   yaa=(0.5*Ayy-vn)*6.283185306;
   zaa=(0.5*Azz-vn)*6.283185306;

   xbb=(-0.5*Axx-vn)*6.283185306;
   ybb=(-0.5*Ayy-vn)*6.283185306;
   zbb=(-0.5*Azz-vn)*6.283185306;

  delthe=(3.14159265358979/parai[4])/3.0;   /* for simpson's integration */
  delphi=(3.14159265358979/parai[5])/3.0;   /* for simpson's integration */

  for(kk=0;kk<=parai[3]-1;kk++) emod[kk]=0.0;

 ha = hb = ma = mb = mc = InitCGM();
 da = db = InitV();

 for(i=0;i<=parai[4];i++)                /* theta range */
 {
    if(i==0 || i==parai[4]) sthe=1.0;        /* for simpson's integration */
     else if((kk=fmod(i,2))==1) sthe=2.0;
    else sthe=4.0;

    st=sinthe->base[i];
    ct=costhe->base[i];

     for(kk=0;kk<=parai[3]-1;kk++) eamp[kk]=0.0;

   for(j=0;j<=parai[5];j++)              /* phi range */
   {
      if(j==0 || j==parai[5]) sphi=1.0;      /* for simpson's integration */
      else if((kk=fmod(j,2))==1) sphi=2.0;
     else sphi=4.0;

     /* Ms=1/2 */

      sp=sinphi->base[j];
      cp=cosphi->base[j];

     x=xaa*st*cp;
      y=yaa*st*sp;
     z=zaa*ct;
```

```
      HF2hlf(&ha,qr,qi,x,y,z); /* I=1 */
      HF3hlf(&ha,qr,qi,x,y,z); /* I=3/2 */
      HF5hlf(&ha,qr,qi,x,y,z); /* I=5/2 */
      HF7hlf(&ha,qr,qi,x,y,z); /* I=7/2 */

     EigCHM(&da,&ha,NU_ALL_VECTORS,&ma); /* eigenvaule and eigen vector for alpha state */

     TransposeCGM(&ma);

     ConjCGM(&ma); /* Ma+ */

     /* Ms=-1/2 */

     x=xbb*st*cp;
     y=ybb*st*sp;
     z=zbb*ct;

      HF2hlf(&ha,qr,qi,x,y,z); /* I=1 */
      HF3hlf(&ha,qr,qi,x,y,z); /* I=3/2 */
      HF5hlf(&ha,qr,qi,x,y,z); /* I=5/2 */
      HF7hlf(&ha,qr,qi,x,y,z); /* I=7/2 */

     EigCHM(&db,&hb,NU_ALL_VECTORS,&mb); /* eigenvaule and eigen vector for beta state */

     MulCGM(&mc,&ma,&mb); /* M matrix */

      xmatrix(M,x0,xa,xb,xab,&mc); /* M=2I+1, I=nuclear spin number */

     /* echo amplitude at a certain phi and theta */

       echoamp(M,parai,&da,&db,x0,xa,xb,xab,eamp,sphi,delphi); /* M=2I+1, I=nuclear spin number */
   }

    /* integration Modulation amplitude overall orientation of theta */

   for(p=0;p<=parai[3]-1;p++)
   {
     emod[p]=emod[p]+eamp[p]*st*sthe*delthe;
   }
 }

 /* normalization of the integration */

  for(ii=0;ii<=parai[3]-1;ii++)
 {
     emod[ii]=emod[ii]/(2.0*3.14159265358979);
 }

 return;
}

/**
 *
 *  emodulationSE.c = caculation of Emodulation for 3-pulse
 *
 **/

#include <math.h>
#include <NuToolsNumerical.h>

emodulationSE(paraf,parai,sinthe,costhe,sinphi,cosphi,qr,qi,emod)

  int parai[];
```

```
 float para[],qr[M+1][M+1],qi[M+1][M+1],emod[2][1024]; /* M=2I+1, I=nuclear spin number */
  vector *sinthe,*costhe,*sinphi,*cosphi;

{
  int i,j,k,n,kk,ii,m,mm,p;
  float gn,h0,Axx,Ayy,Azz;
  float r2,vn;
  float xaa,yaa,zaa,xbb,ybb,zbb;
  float x,y,z;
  ematrix ha,hb,ma,mb,mc;
  vector da,db;
  float x0[1],xa[28],xb[28],xab[784];
  float sthe,sphi,delthe,delphi,eamp[2][1024];
  float st,ct,sp,cp;

gn=para[0];                    /* nuclear g-value */
h0=para[1];                    /* field strength (G) */
Axx=para[2];                   /* Axx (MHz) */
Ayy=para[3];                   /* Ayy (MHz) */
Azz=para[4];                   /* Azz (MHz) */

r2=1.414213562;                /* square root 2 */
  vn=gn*5.0507866*h0*0.001/6.6260755;

/***** Hyperfine + Quadrupole energy in MHz unit *****/

  xaa=(0.5*Axx-vn)*6.283185306;
  yaa=(0.5*Ayy-vn)*6.283185306;
  zaa=(0.5*Azz-vn)*6.283185306;

  xbb=(-0.5*Axx-vn)*6.283185306;
  ybb=(-0.5*Ayy-vn)*6.283185306;
  zbb=(-0.5*Azz-vn)*6.283185306;

 delthe=(3.14159265358979/para[4])/3.0;      /* for simpson's integration */
 delphi=(3.14159265358979/para[5])/3.0;   /* for simpson's integration */

 for(kk=0;kk<=para[3]-1;kk++)
{
  emod[0][kk]=0.0;
  emod[1][kk]=0.0;
}

ha = hb = ma = mb = mc = InitCGM();
da = db = InitV();

for(i=0;i<=para[4];i++)                 /* theta range */
{
  if(i==0 || i==para[4]) sthe=1.0;          /* for simpson's integration */
   else if((kk=fmod(i,2))==1) sthe=2.0;
   else sthe=4.0;

   st=sinthe->base[i];
   ct=costhe->base[i];

   for(kk=0;kk<=para[3]-1;kk++)
  {
    eamp[0][kk]=0.0;
    eamp[1][kk]=0.0;
  }

   for(j=0;j<=para[5];j++)              /* phi range */
   {
     if(j==0 || j==para[5]) sphi=1.0;       /* for simpson's integration */
```

```
    else if((kk=fmod(j,2))==1) sphi=2.0;
    else sphi=4.0;

    /* Ms=1/2 */

    sp=sinphi->base[j];
    cp=cosphi->base[j];

    x=xaa*st*cp;
    y=yaa*st*sp;
    z=zaa*ct;

     HF2hlf(&ha,qr,qi,x,y,z); /* I=1 */
     HF3hlf(&ha,qr,qi,x,y,z); /* I=3/2 */
     HF5hlf(&ha,qr,qi,x,y,z); /* I=5/2 */
     HF7hlf(&ha,qr,qi,x,y,z); /* I=7/2 */

    EigCHM(&da,&ha,NU_ALL_VECTORS,&ma);

    TransposeCGM(&ma);

    ConjCGM(&ma);

    /* Ms=-1/2 */

    x=xbb*st*cp;
    y=ybb*st*sp;
    z=zbb*ct;

     HF2hlf(&ha,qr,qi,x,y,z); /* I=1 */
     HF3hlf(&ha,qr,qi,x,y,z); /* I=3/2 */
     HF5hlf(&ha,qr,qi,x,y,z); /* I=5/2 */
     HF7hlf(&ha,qr,qi,x,y,z); /* I=7/2 */

    EigCHM(&db,&hb,NU_ALL_VECTORS,&mb);

    MulCGM(&mc,&ma,&mb);

     xmatrix(M,x0,xa,xb,xab,&mc); /* M=2I+1, I=nuclear spin number */

    /* echo amplitude at a certain phi and theta */

      echoampSE(M,parai,&da,&db,x0,xa,xb,xab,eamp,sphi,delphi); /* M=2I+1, I=nuclear spin number */
  }

   /* integration Modulation amplitude overall orientation of theta */

   for(p=0;p<=parai[3]-1;p++)
  {
     emod[0][p]+=eamp[0][p]*st*sthe*delthe;
     emod[1][p]+=eamp[1][p]*st*sthe*delthe;
  }
 }

 /* normalization of the integration */

  for(ii=0;ii<=parai[3]-1;ii++)
 {
     emod[0][ii]/=(2.0*3.14159265358979);
     emod[1][ii]/=(2.0*3.14159265358979);
 }

 return;
}
```

```
/****
 *
 *   euler.c = Euler Angle Rotation ==> Change Quadrupole Principle Axis to Hyperfine PAS
 *
 ****/

 #include <console.h>
 #include <math.h>

 euler(para,q)

   float para[],q[4][4];

{
   int i,j;
    float eta,alpha,beta,gamma;
     float csa,csb,csg,sna,snb,sng;
   float matr[4][4];

   eta=para[6];
   alpha=para[7];
   beta=para[8];
   gamma=para[9];

   csa=cos(alpha);
   csb=cos(beta);
   csg=cos(gamma);

   sna=sin(alpha);
   snb=sin(beta);
   sng=sin(gamma);

    matr[1][1]=csa*csb*csg-sna*sng;
    matr[1][2]=sna*csb*csg+csa*sng;
    matr[1][3]=-snb*csg;
    matr[2][1]=-csa*csb*sng-sna*csg;
    matr[2][2]=-sna*csb*sng+csa*csg;
    matr[2][3]=snb*sng;
   matr[3][1]=csa*snb;
   matr[3][2]=sna*snb;
   matr[3][3]=csb;

   /* q[][] = Q matrix in Hyperfine Principle Axis System */

    for(j=1;j<=3;j++)
  {
     for(i=1;i<=3;i++)
    {
        q[i][j]=(eta-1.0)*matr[1][i]*matr[1][j]-(eta+1.0)*matr[2][i]*matr[2][j];
       q[i][j]+=2.0*matr[3][i]*matr[3][j];
    }
  }

   return;

}

/**
 *
 *  HF2hlf.c = Hyperfine & Quadrupole Energy (I=1)
 *
 **/
```

```
#include <NuToolsNumerical.h>
#include <math.h>

HF2hlf(a,qr,qi,x,y,z)

  cmatrix *a;
   float qr[4][4],qi[4][4],x,y,z;

{
    int i,j,DIM;
    float r2;

   DIM=3;
   r2=sqrt(2);

    AllocateCGM(a,DIM,DIM);
    if(nu_error) return;
    else{
     for(i=0;i<DIM;i++)
    {
       for(j=0;j<DIM;j++)
      {
         a->mat[i][j].re=qr[i+1][j+1];
         a->mat[i][j].im=qi[i+1][j+1];
      }
    }

    a->mat[0][0].re+=z;
    a->mat[0][1].re+=x/r2;
    a->mat[1][0].re+=x/r2;
    a->mat[1][2].re+=x/r2;
    a->mat[2][1].re+=x/r2;
    a->mat[2][2].re-=z;

     a->mat[0][1].im-=y/r2;
     a->mat[1][0].im+=y/r2;
     a->mat[1][2].im-=y/r2;
     a->mat[2][1].im+=y/r2;
   }
return;
}

/**
*
*  HF3hlf.c = Hyperfine & Quadrupole Energy (I=3/2)
*
**/

#include <NuToolsNumerical.h>
#include <math.h>

 HF3hlf(a,qr,qi,x,y,z)

  cmatrix *a;
   float qr[5][5],qi[5][5],x,y,z;

{
     int i,j,DIM;
     float r3;

    DIM=4;
    r3=sqrt(3);

     AllocateCGM(a,DIM,DIM);
```

```
    if(nu_error) return;
    else{
     for(i=0;i<DIM;i++)
    {
       for(j=0;j<DIM;j++)
      {
          a->mat[i][j].re=qr[i+1][j+1];
          a->mat[i][j].im=qi[i+1][j+1];
      }
    }

      a->mat[0][0].re+=1.5*z;
      a->mat[0][1].re+=r3*0.5*x;
      a->mat[1][0].re=a->mat[0][1].re;
      a->mat[1][1].re+=0.5*z;
     a->mat[1][2].re+=x;
      a->mat[2][1].re=a->mat[1][2].re;
      a->mat[2][2].re-=0.5*z;
      a->mat[2][3].re+=0.5*r3*x;
      a->mat[3][2].re=a->mat[2][3].re;
      a->mat[3][3].re-=1.5*z;

      a->mat[0][1].im-=0.5*r3*y;
      a->mat[1][0].im=-a->mat[0][1].im;
     a->mat[1][2].im-=y;
      a->mat[2][1].im=-a->mat[1][2].im;
      a->mat[2][3].im-=0.5*r3*y;
      a->mat[3][2].im=-a->mat[2][3].im;
   }
return;
}

/**
 *
 *  HF5hlf.c = Hyperfine & Quadrupole Energy (I=5/2)
 *
 **/

#include <NuToolsNumerical.h>
#include <math.h>

HF5hlf(a,qr,qi,x,y,z)

  cmatrix *a;
   float qr[7][7],qi[7][7],x,y,z;

{
    int i,j,DIM;
    float r2,r5;

    DIM=6;

    r2=sqrt(2);
    r5=sqrt(5);

    AllocateCGM(a,DIM,DIM);
    if(nu_error) return;
    else{
     for(i=0;i<DIM;i++)
    {
       for(j=0;j<DIM;j++)
      {
          a->mat[i][j].re=qr[i+1][j+1];
          a->mat[i][j].im=qi[i+1][j+1];
```

```
    }
   }

    a->mat[0][0].re+=2.5*z;
    a->mat[0][1].re+=r5*0.5*x;
    a->mat[1][0].re=a->mat[0][1].re;
    a->mat[1][1].re+=1.5*z;
    a->mat[1][2].re+=r2*x;
    a->mat[2][1].re=a->mat[1][2].re;
    a->mat[2][2].re+=0.5*z;
    a->mat[2][3].re+=1.5*x;
    a->mat[3][2].re=a->mat[2][3].re;
    a->mat[3][3].re-=0.5*z;
    a->mat[3][4].re+=r2*x;
    a->mat[4][3].re=a->mat[3][4].re;
    a->mat[4][4].re-=1.5*z;
    a->mat[4][5].re+=0.5*r5*x;
    a->mat[5][4].re=a->mat[4][5].re;
    a->mat[5][5].re-=2.5*z;

    a->mat[0][1].im-=0.5*r5*y;
    a->mat[1][0].im=-a->mat[0][1].im;
    a->mat[1][2].im-=r2*y;
    a->mat[2][1].im=-a->mat[1][2].im;
    a->mat[2][3].im-=1.5*y;
    a->mat[3][2].im=-a->mat[2][3].im;
    a->mat[3][4].im-=r2*y;
    a->mat[4][3].im=-a->mat[3][4].im;
    a->mat[4][5].im-=0.5*r5*y;
    a->mat[5][4].im=-a->mat[4][5].im;
  }
return;
}

/**
*
* HF7hlf.c = Hyperfine & Quadrupole Energy (I=7/2)
*
**/

#include <NuToolsNumerical.h>
#include <math.h>

HF7hlf(a,qr,qi,x,y,z)

 cmatrix *a;
  float qr[9][9],qi[9][9],x,y,z;

{
   int i,j,DIM;
   float r3,r7,r15;

  DIM=8;

   r3=1.732050808;
   r7=2.645751311;
   r15=3.872983346;

  AllocateCGM(a,DIM,DIM);
  if(nu_error) return;
  else{
  for(i=0;i<DIM;i++)
 {
    for(j=0;j<DIM;j++)
```

```
    {
        a->mat[i][j].re=qr[i+1][j+1];
        a->mat[i][j].im=qi[i+1][j+1];
    }
  }

    a->mat[0][0].re+=3.5*z;
    a->mat[0][1].re+=r7*0.5*x;
    a->mat[1][0].re=a->mat[0][1].re;
    a->mat[1][1].re+=2.5*z;
    a->mat[1][2].re+=r3*x;
    a->mat[2][1].re=a->mat[1][2].re;
    a->mat[2][2].re+=1.5*z;
    a->mat[2][3].re+=0.5*r15*x;
    a->mat[3][2].re=a->mat[2][3].re;
    a->mat[3][3].re+=0.5*z;
    a->mat[3][4].re+=2.0*x;
    a->mat[4][3].re=a->mat[3][4].re;
    a->mat[4][4].re-=0.5*z;
    a->mat[4][5].re+=0.5*r15*x;
    a->mat[5][4].re=a->mat[4][5].re;
    a->mat[5][5].re-=1.5*z;
    a->mat[5][6].re+=r3*x;
    a->mat[6][5].re=a->mat[5][6].re;
    a->mat[6][6].re-=2.5*z;
    a->mat[6][7].re+=0.5*r7*x;
    a->mat[7][6].re=a->mat[6][7].re;
    a->mat[7][7].re-=3.5*z;

    a->mat[0][1].im-=0.5*r7*y;
    a->mat[1][0].im=-a->mat[0][1].im;
    a->mat[1][2].im-=r3*y;
    a->mat[2][1].im=-a->mat[1][2].im;
    a->mat[2][3].im-=0.5*r15*y;
    a->mat[3][2].im=-a->mat[2][3].im;
    a->mat[3][4].im-=2.0*y;
    a->mat[4][3].im=-a->mat[3][4].im;
    a->mat[4][5].im-=0.5*r15*y;
    a->mat[5][4].im=-a->mat[4][5].im;
    a->mat[5][6].im-=r3*y;
    a->mat[6][5].im=-a->mat[5][6].im;
    a->mat[6][7].im-=0.5*r7*y;
    a->mat[7][6].im=-a->mat[6][7].im;
  }
return;
}

/**
*
* quadrupole2hlf.c = Nuclear Quadrupole Energy in Hyperfine Axis (I=1, MHz unit)
*
*  qr[][] = Re (quadrupole energy)
*  qi[][] = Im(quadrupole energy) in Hyperfine PAS (MHz unit)
*
**/

#include <math.h>

quadrupole2hlf(paraf,qr,qi)

  float paraf[],qr[4][4],qi[4][4];

{
  int i,j;
```

```
 float eeqQ,q[4][4];

 euler(paraf,q);

 eeqQ=paraf[5];

 /* q matrix in MHz unit */

  for(i=1;i<=3;i++)
 {
     for(j=1;j<=3;j++) q[i][j]=0.25*eeqQ*q[i][j]*6.283185306;
 }

 /* qr[][] = Re (quadrupole energy) qi[][] = Im(quadrupole energy) in Hyperfine PAS */

  qr[1][1]=0.5*(q[1][1]+q[2][2])+q[3][3];
  qr[1][2]=0.707106781*q[1][3];
  qr[1][3]=0.5*(q[1][1]-q[2][2]);
 qr[2][1]=qr[1][2];
 qr[2][2]=q[1][1]+q[2][2];
  qr[2][3]=-0.707106781*q[1][3];
 qr[3][1]=qr[1][3];
 qr[3][2]=qr[2][3];
 qr[3][3]=qr[1][1];

  qi[1][1]=0.0;
   qi[1][2]=-0.707106781*q[2][3];
 qi[1][3]=-q[1][2];
 qi[2][1]=-qi[1][2];
 qi[2][2]=0.0;
  qi[2][3]=0.707106781*q[2][3];
 qi[3][1]=-qi[1][3];
 qi[3][2]=-qi[2][3];
 qi[3][3]=0.0;

 return;
}

/**
 *
 * quadrupole3hlf.c = Nuclear Quadrupole Energy in Hyperfine Axis (I=3/2, MHz unit)
 *
 *   qr[][] = Re (quadrupole energy)
 *   qi[][] = Im(quadrupole energy) in Hyperfine PAS (MHz unit)
 *
 **/

#include <math.h>

quadrupole3hlf(paraf,qr,qi)

   float paraf[],qr[5][5],qi[5][5];

{
  int i,j;
  float eeqQ,q[4][4],r3;

  euler(paraf,q);

  r3=sqrt(3.0);
 eeqQ=paraf[5];

  /* q matrix in MHz unit */
```

```
 for(i=1;i<=3;i++)
{
     for(j=1;j<=3;j++) q[i][j]=eeqQ*q[i][j]*6.283185306/12.0;
}

/* qr[][] = Re (quadrupole energy) qi[][] = Im(quadrupole energy) in Hyperfine PAS */

  qr[1][1]=0.75*(q[1][1]+q[2][2])+2.25*q[3][3];
  qr[1][2]=r3*q[1][3];
  qr[1][3]=(r3/2.0)*(q[1][1]-q[2][2]);
  qr[1][4]=0.0;
  qr[2][1]=qr[1][2];
  qr[2][2]=1.75*(q[1][1]+q[2][2])+0.25*q[3][3];
  qr[2][3]=0.0;
  qr[2][4]=0.5*r3*(q[1][1]-q[2][2]);
  qr[3][1]=qr[1][3];
  qr[3][2]=0.0;
  qr[3][3]=qr[2][2];
  qr[3][4]=-r3*q[1][3];
  qr[4][1]=0.0;
  qr[4][2]=qr[2][4];
  qr[4][3]=qr[3][4];
  qr[4][4]=qr[1][1];

  qi[1][1]=0.0;
  qi[1][2]=-r3*q[2][3];
  qi[1][3]=-r3*q[1][2];
  qi[1][4]=0.0;
  qi[2][1]=-qi[1][2];
  qi[2][2]=0.0;
  qi[2][3]=0.0;
  qi[2][4]=-r3*q[1][2];
  qi[3][1]=-qi[1][3];
  qi[3][2]=0.0;
  qi[3][3]=0.0;
  qi[3][4]=r3*q[2][3];
  qi[4][1]=0.0;
  qi[4][2]=-qi[2][4];
  qi[4][3]=-qi[3][4];
  qi[4][4]=0.0;

 return;
}

/**
 *
 * quadrupole5hlf.c = Nuclear Quadrupole Energy in Hyperfine Axis (I=5/2, MHz unit)
 *
 *  qr[][] = Re (quadrupole energy)
 *  qi[][] = Im(quadrupole energy) in Hyperfine PAS (MHz unit)
 *
 **/

#include <math.h>

quadrupole5hlf(paraf,qr,qi)

  float paraf[],qr[7][7],qi[7][7];

{
  int i,j;
  float eeqQ,q[4][4],r2,r5,r10;

  euler(paraf,q);
```

```
r2=sqrt(2);
r5=sqrt(5);
r10=sqrt(10);
eeqQ=para[5];

/* q matrix in MHz unit */

 for(i=1;i<=3;i++)
{
     for(j=1;j<=3;j++) q[i][j]=eeqQ*q[i][j]*6.283185306/40.0;
}

 for(i=1;i<=6;i++)
{
   for(j=1;j<=6;j++)
  {
     qr[i][j]=0.0;
     qi[i][j]=0.0;
  }
}

/* qr[][] = Re (quadrupole energy) qi[][] = Im(quadrupole energy) in Hyperfine PAS */

  qr[1][1]=1.25*(q[1][1]+q[2][2])+6.25*q[3][3];
  qr[1][2]=2.0*r5*q[1][3];
  qr[1][3]=0.5*r10*(q[1][1]-q[2][2]);
qr[2][1]=qr[1][2];
  qr[2][2]=3.25*(q[1][1]+q[2][2])+2.25*q[3][3];
  qr[2][3]=2.0*r2*q[1][3];
  qr[2][4]=1.5*r2*(q[1][1]-q[2][2]);
qr[3][1]=qr[1][3];
qr[3][2]=qr[2][3];
  qr[3][3]=4.25*(q[1][1]+q[2][2])+0.25*q[3][3];
  qr[3][5]=1.5*r2*(q[1][1]-q[2][2]);
qr[4][2]=qr[2][4];
qr[4][4]=qr[3][3];
  qr[4][5]=-2.0*r2*q[1][3];
  qr[4][6]=0.5*r10*(q[1][1]-q[2][2]);
qr[5][3]=qr[3][5];
qr[5][4]=qr[4][5];
qr[5][5]=qr[2][2];
  qr[5][6]=-2.0*r5*q[1][3];
qr[6][4]=qr[4][6];
qr[6][5]=qr[5][6];
qr[6][6]=qr[1][1];

  qi[1][2]=-2.0*r5*q[2][3];
  qi[1][3]=-r10*q[1][2];
  qi[2][1]=-qi[1][2];
  qi[2][3]=-2.0*r2*q[2][3];
  qi[2][4]=-3.0*r2*q[1][2];
  qi[3][1]=-qi[1][3];
  qi[3][2]=-qi[2][3];
  qi[3][5]=-3.0*r2*q[1][2];
  qi[4][2]=-qi[2][4];
  qi[4][5]=2.0*r2*q[2][3];
  qi[4][6]=-r10*q[1][2];
  qi[5][3]=-qi[3][5];
  qi[5][4]=-qi[4][5];
  qi[5][6]=2.0*r5*q[2][3];
  qi[6][4]=-qi[4][6];
  qi[6][5]=-qi[5][6];
```

```
  return;
}

/**
 *
 * quadrupole7hlf.c = Nuclear Quadrupole Energy in Hyperfine Axis (I=7/2, MHz unit)
 *
 *  qr[][] = Re (quadrupole energy)
 *  qi[][] = Im(quadrupole energy) in Hyperfine PAS (MHz unit)
 *
 **/

#include <math.h>

quadrupole7hlf(paraf,qr,qi)

   float paraf[],qr[9][9],qi[9][9];

{
  int i,j;
   float ecqQ,q[4][4],r3,r5,r7,r15,r21;

  euler(paraf,q);

  r3=sqrt(3);
  r5=sqrt(5);
  r7=sqrt(7);
  r15=sqrt(15);
  r21=sqrt(21);

  ecqQ=paraf[5];

  /* q matrix in MHz unit */

  for(i=1;i<=3;i++)
  {
     for(j=1;j<=3;j++) q[i][j]=ecqQ*q[i][j]*6.283185306/84.0;
  }

  for(i=1;i<=8;i++)
  {
    for(j=1;j<=8;j++)
   {
     qr[i][j]=0.0;
     qi[i][j]=0.0;
   }
  }

  /* qr[][] = Re (quadrupole energy) qi[][] = Im(quadrupole energy) in Hyperfine PAS */

   qr[1][1]=1.75*(q[1][1]+q[2][2])+12.25*q[3][3];
   qr[1][2]=3.0*r7*q[1][3];
   qr[1][3]=0.5*r21*(q[1][1]-q[2][2]);
  qr[2][1]=qr[1][2];
   qr[2][2]=4.75*(q[1][1]+q[2][2])+6.25*q[3][3];
   qr[2][3]=4.0*r3*q[1][3];
   qr[2][4]=1.5*r5*(q[1][1]-q[2][2]);
  qr[3][1]=qr[1][3];
  qr[3][2]=qr[2][3];
   qr[3][3]=6.75*(q[1][1]+q[2][2])+2.25*q[3][3];
  qr[3][4]=r15*q[1][3];
   qr[3][5]=r15*(q[1][1]-q[2][2]);
  qr[4][2]=qr[2][4];
  qr[4][3]=qr[3][4];
```

```
    qr[4][4]=7.75*(q[1][1]+q[2][2])+0.25*q[3][3];
    qr[4][6]=r15*(q[1][1]-q[2][2]);
    qr[5][3]=qr[3][5];
    qr[5][5]=qr[4][4];
    qr[5][6]=-r15*q[1][3];
    qr[5][7]=1.5*r5*(q[1][1]-q[2][2]);
    qr[6][4]=qr[4][6];
    qr[6][5]=qr[5][6];
    qr[6][6]=qr[3][3];
    qr[6][7]=-4.0*r3*q[1][3];
    qr[6][8]=0.5*r21*(q[1][1]-q[2][2]);
    qr[7][5]=qr[5][7];
    qr[7][6]=qr[6][7];
    qr[7][7]=qr[2][2];
    qr[7][8]=-3.0*r7*q[1][3];
    qr[8][6]=qr[6][8];
    qr[8][7]=qr[7][8];
    qr[8][8]=qr[1][1];

    qi[1][2]=-3.0*r7*q[2][3];
    qi[1][3]=-r21*q[1][2];
    qi[2][1]=-qi[1][2];
    qi[2][3]=-4.0*r3*q[2][3];
    qi[2][4]=-3.0*r5*q[1][2];
    qi[3][1]=-qi[1][3];
    qi[3][2]=-qi[2][3];
    qi[3][4]=-r15*q[2][3];
    qi[3][5]=-2.0*r15*q[1][2];
    qi[4][2]=-qi[2][4];
    qi[4][3]=-qi[3][4];
    qi[4][6]=-2.0*r15*q[1][2];
    qi[5][3]=-qi[3][5];
    qi[5][6]=r15*q[2][3];
    qi[5][7]=-3.0*r5*q[1][2];
    qi[6][4]=-qi[4][6];
    qi[6][5]=-qi[5][6];
    qi[6][7]=4.0*r3*q[2][3];
    qi[6][8]=-r21*q[1][2];
    qi[7][5]=-qi[5][7];
    qi[7][6]=-qi[6][7];
    qi[7][8]=3.0*r7*q[2][3];
    qi[8][6]=-qi[6][8];
    qi[8][7]=-qi[7][8];

  return;
}

/***
*
*  sincostable.c = generating SIN and COS table
*
*
***/

#include <NuToolsNumerical.h>
#include <math.h>

 sincostable(parai,sint,cost,sinp,cosp)

   int parai[];
    vector *sint,*cost,*sinp,*cosp;

{
   int i,SIZE;
```

```
  float theta,phi,pi;

  pi=3.14159265358979;          /* constant π */

  /* caculation of theta and phi increments */

  theta=parai[4];
  phi=parai[5];

  theta=pi/theta;
  phi=pi/phi;

  SIZE=parai[4]+1;

  AllocateV(sint,SIZE);
  if(nu_error) return;
  AllocateV(cost,SIZE);
  if(nu_error) return;

  /* making tables (theta) */

  for(i=0;i<=parai[4];i++)
  {
     sint->base[i]=sin(i*theta);
     cost->base[i]=cos(i*theta);
  }

  /* making tables (phi) */

  SIZE=parai[5]+1;

  AllocateV(sinp,SIZE);
  if(nu_error) return;
  AllocateV(cosp,SIZE);
  if(nu_error) return;

  for(i=0;i<=parai[5];i++)
  {
     sinp->base[i]=sin(i*phi);
     cosp->base[i]=cos(i*phi);
  }

  return;
}


/**
*
*   xmatrix.c = xmatrix(nu,x0,xa,xab,mr,mi)
*
*    calculate the X coefficients
*
**/

xmatrix(nu,x0,xa,xb,xab,m)

  int nu;
  float x0[],xa[],xb[],xab[];
  cmatrix *m;
{
  int i,j,k,n;
  int inda,indb,indab;
    float x,temp1,temp2,temp3,temp4,temp5,temp6,temp7,temp8,temp;
```

```
/* Xo */

 x0[0]=0.0;

 for(i=1;i<=nu;i++)
{
   for(k=1;k<=nu;k++)
  {
     temp1=m->mat[i-1][k-1].re;
     temp2=m->mat[i-1][k-1].im;
     temp=temp1*temp1+temp2*temp2;
    x0[0]+=temp*temp;
  }
}

/* Xij */

inda=0;

 for(j=2;j<=nu;j++)
{
   for(i=1;i<=j-1;i++)
  {
    x=0.0;

     for(k=1;k<=nu;k++)
    {
      temp1=m->mat[i-1][k-1].re;
      temp2=m->mat[i-1][k-1].im;
      temp3=m->mat[j-1][k-1].re;
      temp4=m->mat[j-1][k-1].im;
       x+=(temp1*temp1+temp2*temp2)*(temp3*temp3+temp4*temp4);
    }

    xa[inda]=x;
    inda++;
  }
}

indb=0;

 for(n=2;n<=nu;n++)
{
  for(k=1;k<=n-1;k++)
  {
    x=0.0;

     for(i=1;i<=nu;i++)
    {
      temp1=m->mat[i-1][k-1].re;
      temp2=m->mat[i-1][k-1].im;
      temp3=m->mat[i-1][n-1].re;
      temp4=m->mat[i-1][n-1].im;
       x+=(temp1*temp1+temp2*temp2)*(temp3*temp3+temp4*temp4);
    }

    xb[indb]=x;
    indb++;
  }
}


/* Xijkn */
```

```
indab=0;

for(j=2;j<=nu;j++)
{
   for(i=1;i<=j-1;i++)
  {
     for(n=2;n<=nu;n++)
    {
       for(k=1;k<=n-1;k++)
      {
         temp1=m->mat[i-1][k-1].re;
         temp2=m->mat[i-1][k-1].im;
         temp3=m->mat[i-1][n-1].re;
         temp4=m->mat[i-1][n-1].im;
         temp5=m->mat[j-1][k-1].re;
         temp6=m->mat[j-1][k-1].im;
         temp7=m->mat[j-1][n-1].re;
         temp8=m->mat[j-1][n-1].im;

           temp=(temp1*temp3+temp2*temp4)*(temp5*temp7+temp6*temp8);
           temp-=(temp1*temp4-temp2*temp3)*(temp7*temp6-temp8*temp5);

        xab[indab]=temp;
        indab++;
      }
    }
  }
}

 return;
}
```

A5. Pulse Logic Circuits

The following drawings are of the pulse logic circuits which are installed in the pulsed-EPR spectrometer at Michigan State University. The ideas for the logic circuits were given by Professor J. McCracken. The original circuits were designed by Mr. Marty Rabb in the electronics shop of the Chemistry department and modified by Prof. McCracken and myself.

In the figures, the IC's are numbered in bold type. The IC's used in these circuits are 7400 (**1**, **34**, **205**, Quad 2-input positive NAND gate), 7404 (**2**, **209**, Hex inverter), 74123 (**3**, **4***, **6**, **11**, **15**, **17**, **19**, **20**, **36**, **203**, Dual retriggerable monostable mutivibrators with clear), 7430 (**4**, 8-input positive-NAND gate), 74121 (**16**, **18**, Monostable multivibrator), 7405 (**7**, **21**, Hex inverter with open-collector output), 7402 (**8**, Quad 2-input positive NOR gate), 74128 (**9**, **31**, 50Ω Line driver; NOR gate), 74140 (**9***, **207**, Dual 4-input positive-NAND 50Ω Line Driver), 7432 (**10**, **208**, Quad 2-input positive-OR gate), 74373 (**21**, **22**, **23**, **24**, **25**, **26**, **27**, **28** in phase module, Octal D-type latches), 7454 (**29**, **30**, 4-wide AND-OR-Invert Ggate), 7493 (**32**, 4-Bit binary counter), 74138 (**33**, 3 to 8-Line decorder), 7474 (**35**, **206**, Dual-D-type positive-edge-triggered flip-flops with preset and clear), 7408 (**205**, Quad 2-input positive-AND gate), PPG-33F-5 (**12**, **13**, **14**, Programmable pulse generator), and ECG 8520 (**201**, **202**, Modulo-n divider).

The logic circuits shown on the next four pages are Figure A5-1, PIN 1 Circuit; Figure A5-2, PIN 2 Circuit; Figure A5-3, Phase Control Circuit; and Figure A5-4, Receiver Control Circuit.

Figure A5-1. PIN 1 Circuit

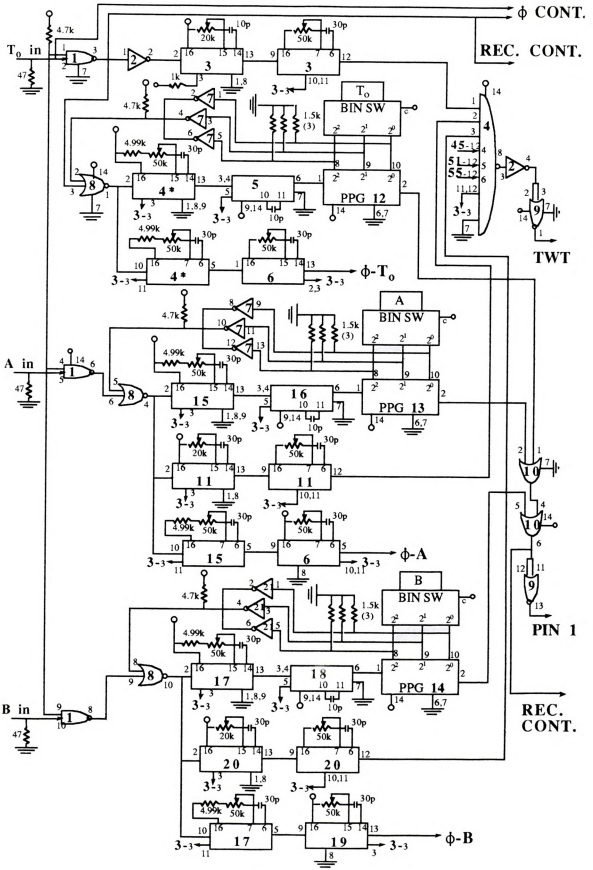
φ CONT.
REC. CONT.
T0 in
A in
B in
BIN SW
PPG 12
PPG 13
PPG 14
TWT
PIN 1
REC. CONT.
φ-T0
φ-A
φ-B
4.7k
20k
50k
4.99k
30p
10p
1.5k (3)

Figure A5-2. PIN 2 Circuit

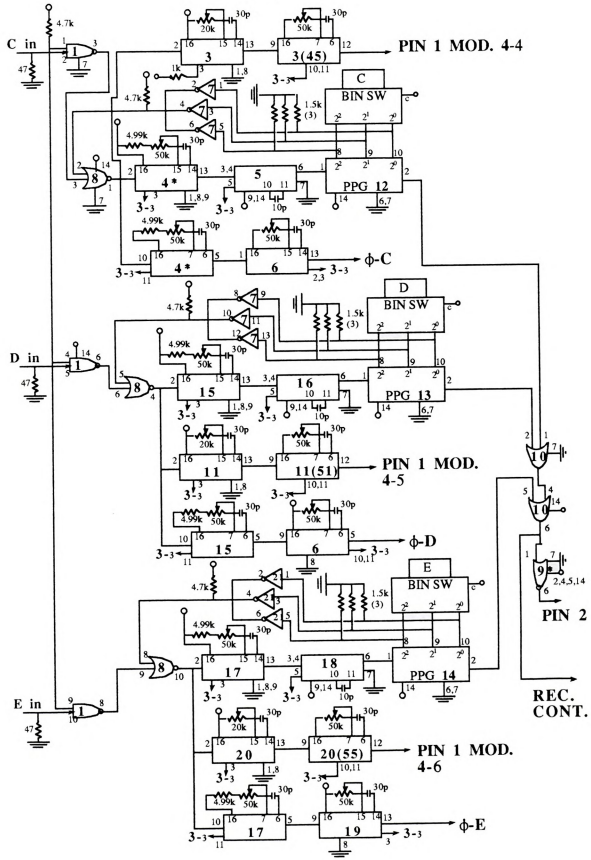
C in
D in
E in
4.7k
47
30p
20k
50k
4.99k
1k
1.5k (3)
BIN SW
C
D
E
PPG 12
PPG 13
PPG 14
PIN 1 MOD. 4-4
PIN 1 MOD. 4-5
PIN 1 MOD. 4-6
PIN 2
REC. CONT.
ϕ-C
ϕ-D
ϕ-E
3(45)
11(51)
20(55)
4 *
3-3
10p

Figure A5-3. Phase Control Circuit

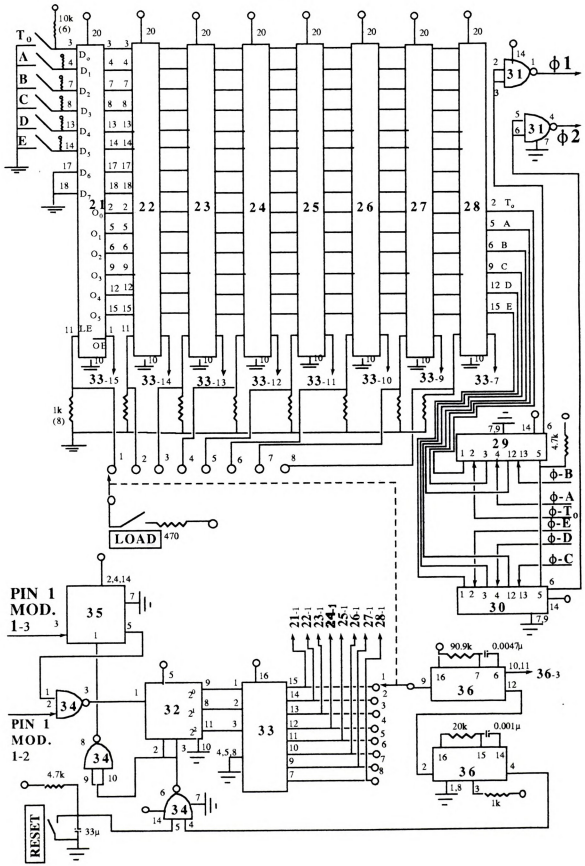
T0
A
B
C
D
E
10k (6)
D0
D1
D2
D3
D4
D5
D6
D7
21
22
23
24
25
26
27
28
O0
O1
O2
O3
O4
O5
O6
O7
T0
A
B
C
D
E
O.E
33-15
33-14
33-13
33-12
33-11
33-10
33-9
33-7
1k (8)
LOAD 470
φ1
φ2
φ-B
φ-A
φ-T0
φ-E
φ-D
φ-C
29
30
PIN 1 MOD. 1-3
PIN 1 MOD. 1-2
35
34
32
33
36
36-3
90.9k
0.0047μ
20k
0.001μ
4.7k
33μ
RESET
1k

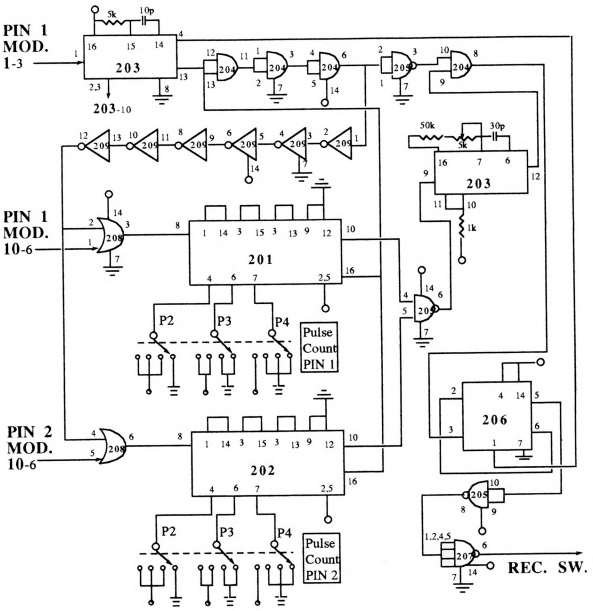

Figure A5-4. Receiver Control Circuit

The timing diagrames of the above circuits are depicted as followings.

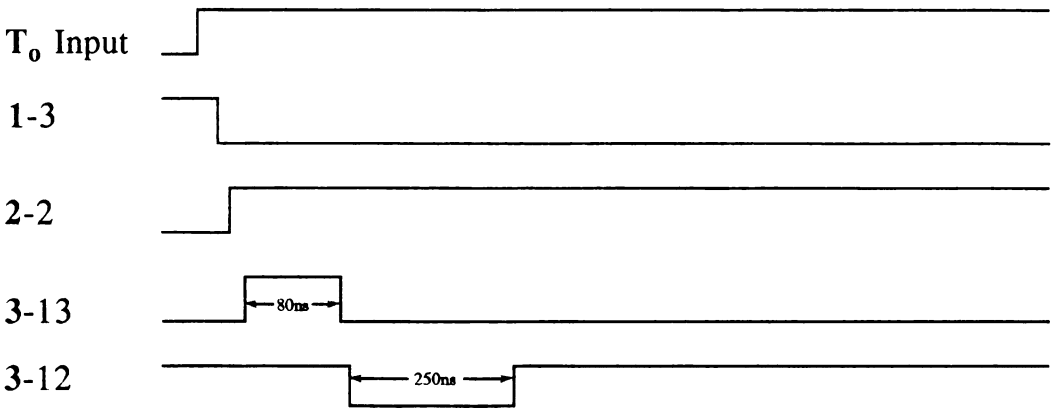

Figure A5-5. Timing diagram of from T_0 delay input to **4** input (8-NAND gate) in PIN 1

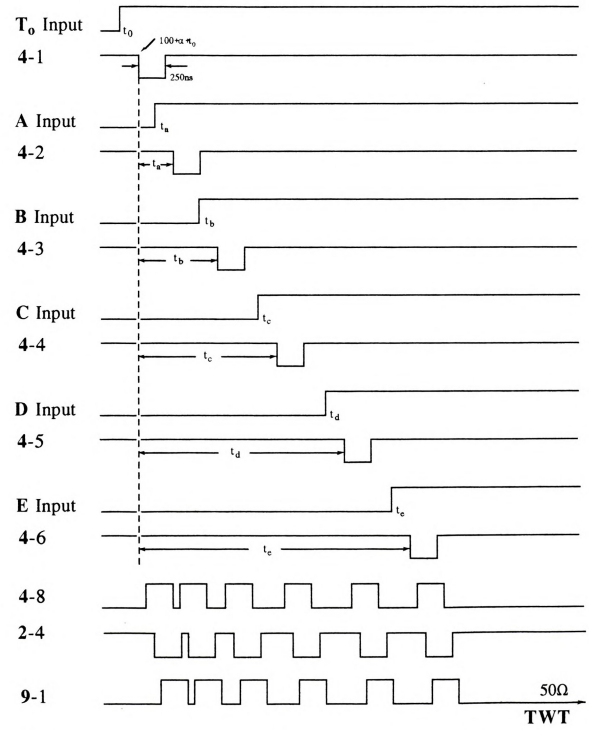

Figure A5-6. Timing diagram of from delay inputs to TWT input

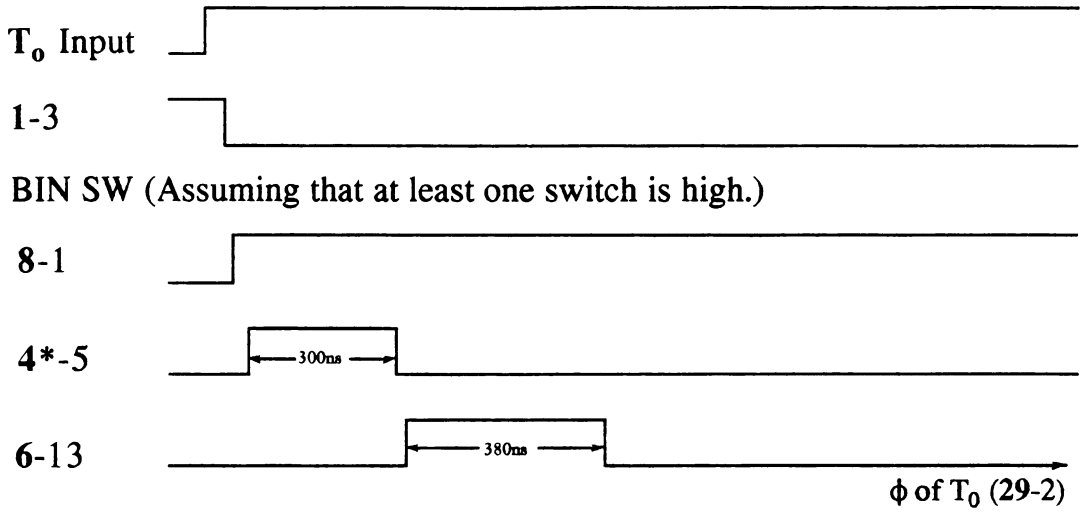

Figure A5-7. Timing diagram of from T_0 delay input to phase circuit input.

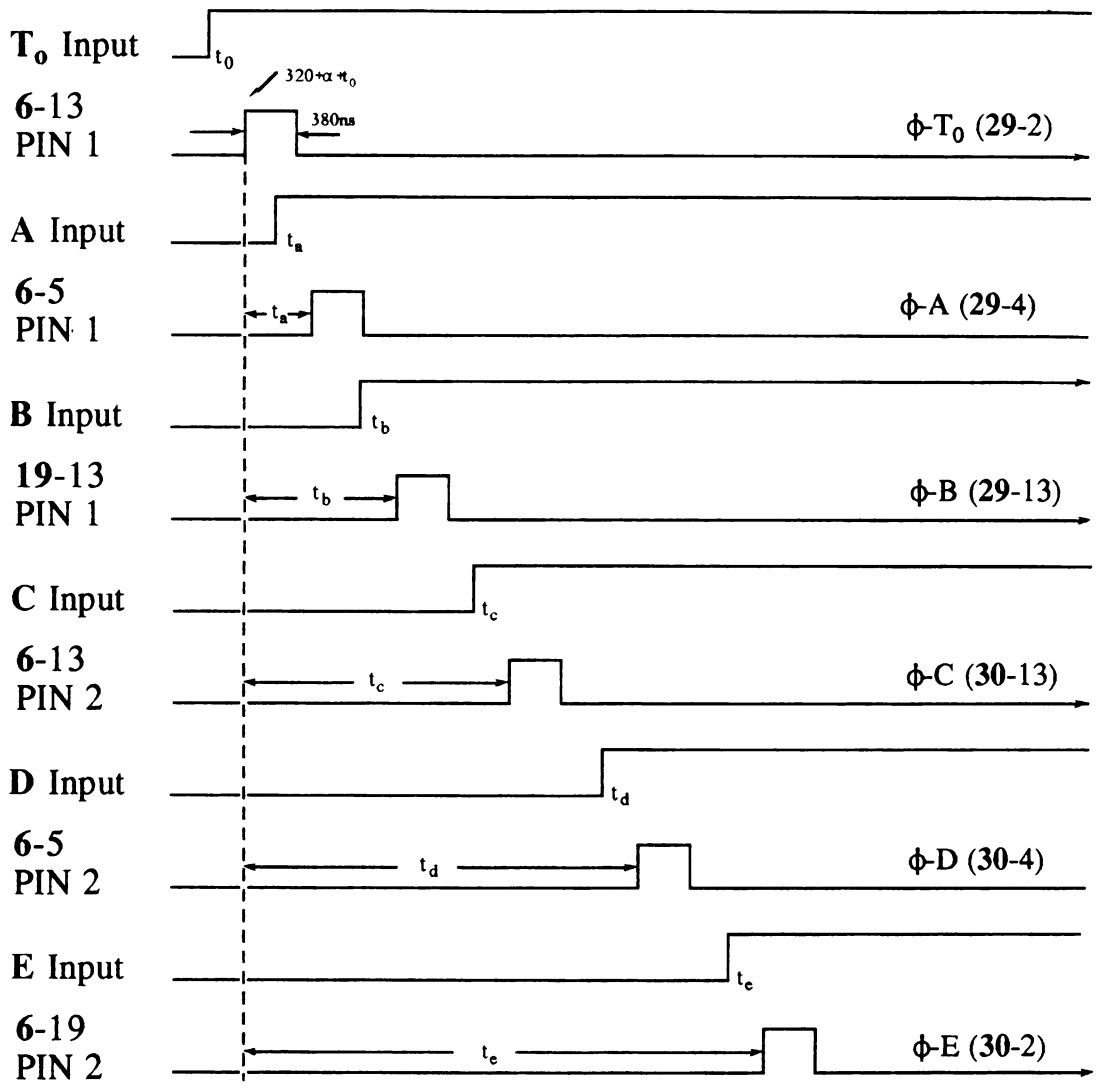

Figure A5-8. Timing diagram of from delay inputs to phase circuit inputs.

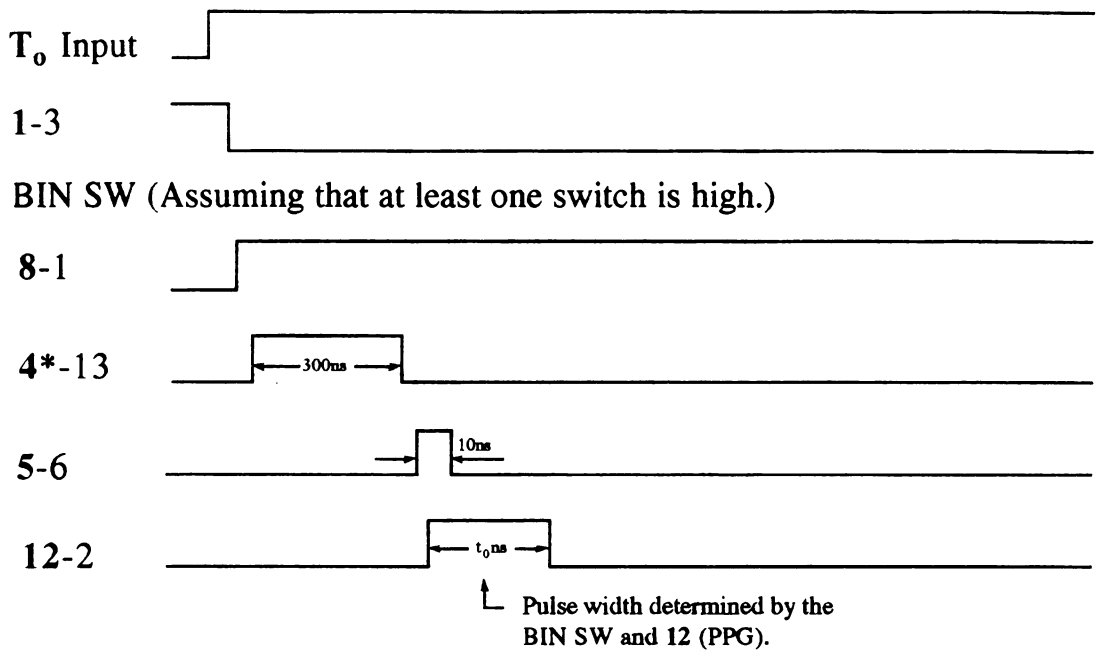

Figure A5-9. Timing diagram of from T_0 delay input to **10** input

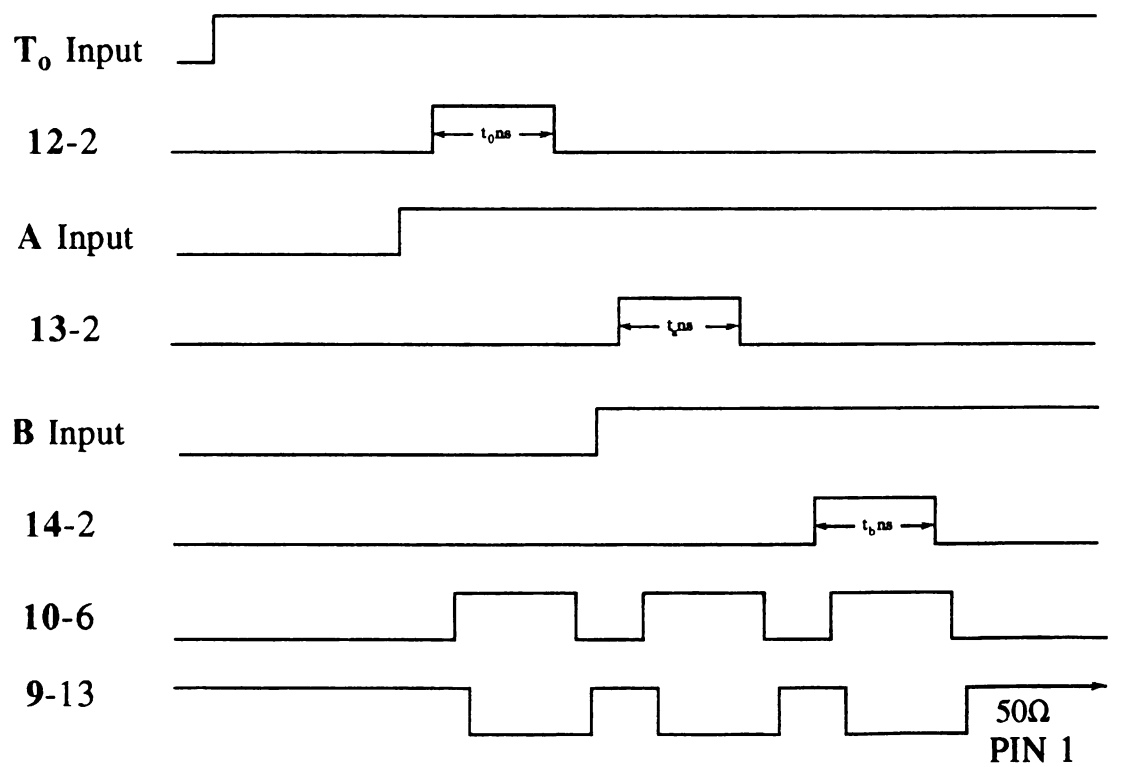

Figure A5-10. Timing diagram of from T_0, A, B delay input to PIN 1 input

Assuming 4-step phse cylcle (T_o, A, B - 000, 011, 110, 101)

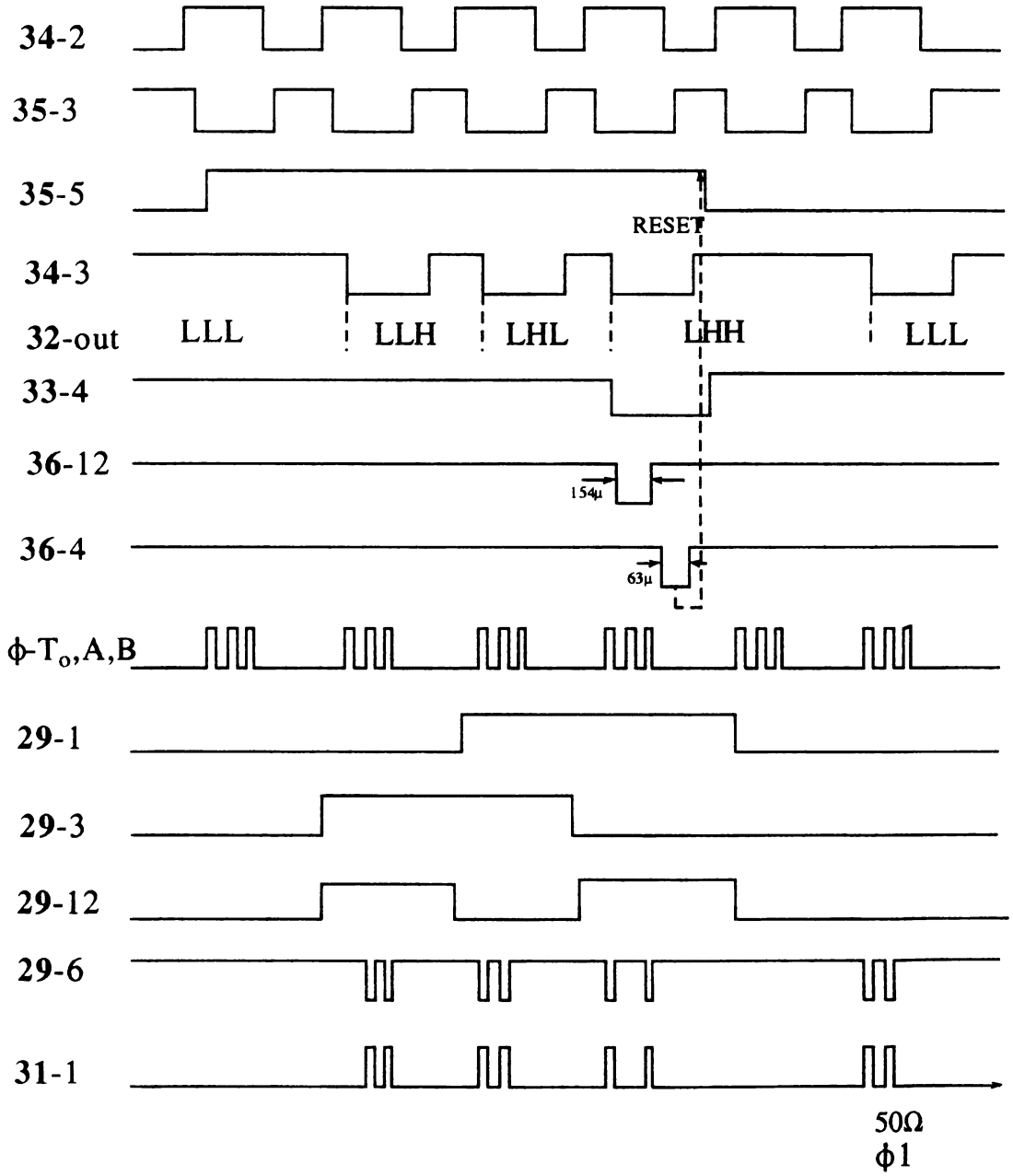

Figure A5-11. Timing diagram of phase control circuit

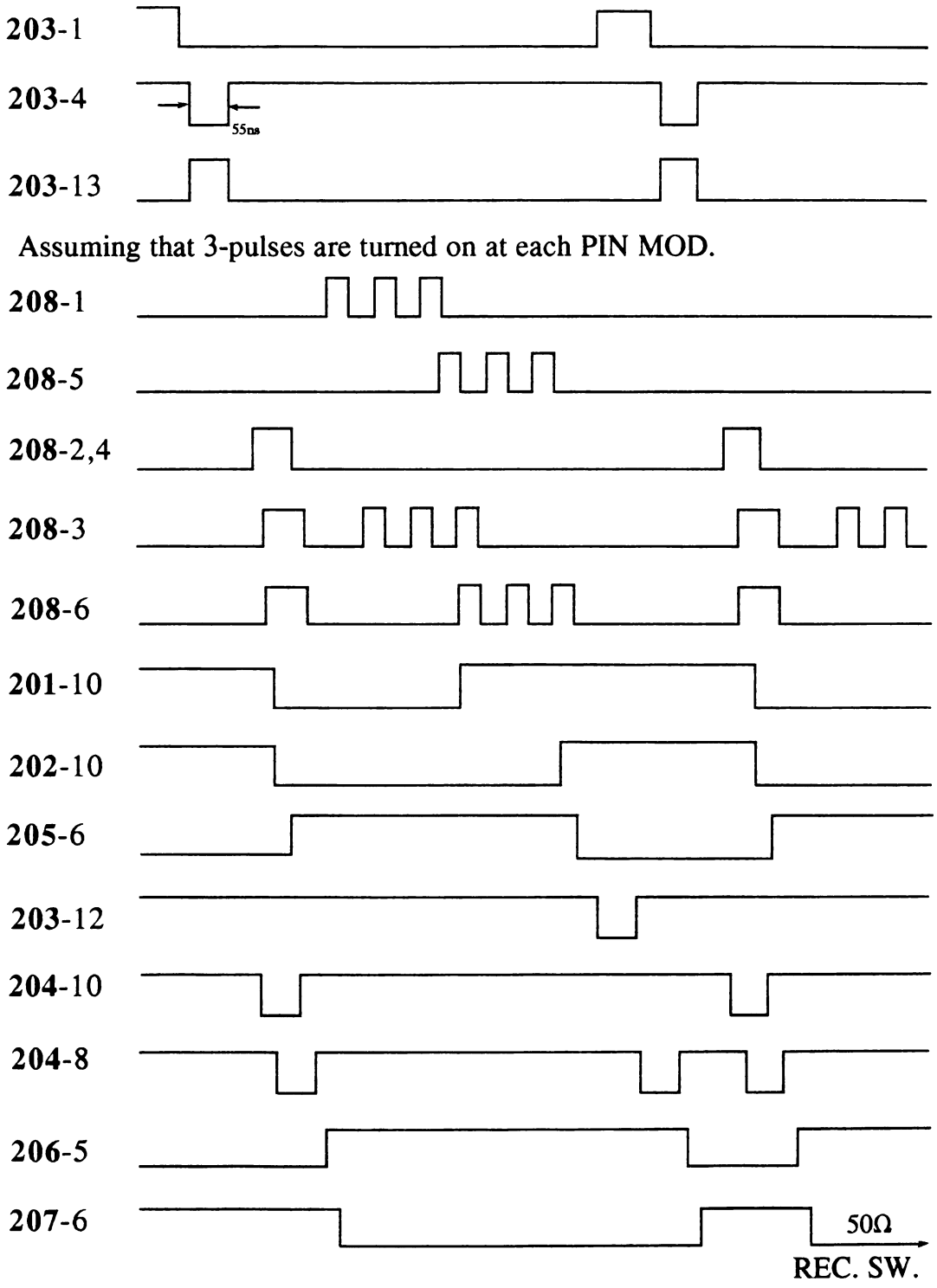

Figure A5-12. Timing diagram of receiver switch control circuit

A6. Computer Interfacing Programs for Performing 4-pulse ESEEM and HYSCORE (hyperfine sublevel correlation spectroscopy) Experiments

The programs are written in the C computer language. The main programs were written by myself. The subroutines were originally written by Professor J. McCracken for 2- and 3-pulse ESEEM experiments and modified for 4-pulse ESEEM and HYSCORE experiments when appropriate.

A6-1. Main Program for 4-Pulse ESEEM

```
/*
*   4-pulse.c - this routine will be used to govern the collection
*           of 4-pulse experiment data.
*
*
*   definition
*
*       limits(xmin,xmax,ymin,ymax,ixtic,iytic) - the box limit for the live
*
*      gpib0 - gpib controller
*      dg1   - dg535 pulse generator (#1)
*      dg2   - dg535 pulse generator (#2)
*      sri   - sr245 computer interface
*      mloc  - mouse location (pointer)
*
*   scan control parameters
*
*     cval[0] - tau                 (nsec)
*      cval[1] - starting T/2           (nsec)
*      cval[2] - T/2 increment          (nsec)
*       cval[3] - repetitions/time point
*      cval[4] - sequence repetition rate (Hz)
*      cavl[5] - plot scale factor
*      cval[6] - A timing shim          (nsec)
*      cval[7] - B timing shim          (nsec)
*      cval[8] - C timing shim          (nsec)
*      cval[9] - D timing shim          (nsec)
*      cval[10] - # of data
*   delay generator set up parameters
*
*      tpar[0] - trigger rate
*      tpar[1] - A delay time (tau)
*      tpar[2] - B delay time (tau + T/2)
*      tpar[3] - C delay time (tau + T)
*      tpar[4] - D delay time (2*tau +T)
*/

#include <stdio.h>
```

```
#include <console.h>
#include <string.h>
#include <stdlib.h>
#include "decl.h"
#include "matrix.h"

int  gpib0,dg1,dg2,sri;
char spr,pbuff[2];

typedef struct{int v,h;} POINT;
POINT *mloc;

main()
{
        int  i,limits[6],cval[11],tpar[5],specparm[4];
        int  *data,iopt,sizeofdata;
        float  fval[4],t1,dt1;
        char chopt[3];

        sizeofdata = -1 ;

        limits[0]=100;
        limits[1]=575;
        limits[2]=40;
        limits[3]=300;
        limits[4]=10;
        limits[5]=10;

        fval[0]=9.0;
        fval[1]=3000.0;
        fval[2]=50.0;
        fval[3]=4.2;

 /* set up console screen */

        pageset(stdout);

 /* read cval[] from time4p.dat */

   tparin4p(cval);

 /* open and clear gpib controller. Then open and clear sr245 and dg535 */

    if((gpib0=ibfind("gpib0"))<0)
 {
                printf("gpib0 not found\n\r");
                exit(-1);
 }

        if(ibsic(gpib0) & ERR) error();

        if((sri=ibfind("sr245"))<0)
        {
                printf("sr245 device not found\n\r");
                exit(-1);
        }

        if((dg1=ibfind("dg535"))<0)
        {
                printf(" first dg535 device not found\n\r");
                exit(-1);
        }

        if(ibclr(sri) & ERR) error();
```

```
        if(ibclr(dg1) & ERR) error();

/* get scanning parameters */

change: getparm4p(cval);

/* Initilize data array. */

if( sizeofdata > -1  ) free(data);
sizeofdata = cval[10] + 20;

data = ( int * ) calloc( sizeofdata , sizeof( int ) );


/* set up initial timing parameters */

  tpar[0]=cval[4];                          /* trigger rate */
  tpar[1]=cval[0]+cval[6];                  /* A delay time */
  tpar[2]=cval[0]+cval[1]+cval[7];          /* B delay time */
  tpar[3]=cval[0]+2*cval[1]+cval[8];        /* C delay time */
  tpar[4]=2*cval[0]+2*cval[1]+cval[9];      /* D delay time */

/* set up the scanning parameters for sr245 and dg535 devices */

  srsethy(cval[3]);

 repeat:dgsethy1(tpar);

/* set up the screen for data aquisition */

        eraseplot();

        lplabel4p(cval);

        box(limits);

/* set timing parameters for display */

  specparm[0]=cval[0];
  specparm[1]=cval[0]+cval[1];
  specparm[2]=cval[0]+2*cval[1];
  specparm[3]=2*cval[0]+2*cval[1];

  dgupdate4p(0,0,specparm[0]);
  dgupdate4p(1,0,specparm[1]);
  dgupdate4p(2,0,specparm[2]);
  dgupdate4p(3,0,specparm[3]);

/* data collection - the first point as collected from the integrator
*               is usually bad. the first twice to make up for this. 10 data
*              points are for baseline.
*/

        trstarthy1();               /* trigger start */
        data[0]=getpoint(sri,0);    /* data aquisition */
        trstophy1();                /* trigger stop */

 for(i=0;i<cval[10];i++)
 {
    cgotoxy(49,34,stdout);          /* put channel # on screen*/
        printf("%d",i);

        if(kbhit()) goto compl;     /* check for keystroke */
```

```
        trstarthy1();                   /* trigger start */

        data[i]=getpoint(sri,0);        /* data aquisition and type signal value */

        trstophy1();                    /* trigger stop */

        dplot4p(cval[5],i,cval[10]+20,data[i]);  /* plot data on screen */

        specparm[1]=dgupdate4p(1,cval[2],specparm[1]);    /* update delay generator */
        specparm[2]=dgupdate4p(2,2*cval[2],specparm[2]);  /* for 3rd, 4th pulses and */
        specparm[3]=dgupdate4p(3,2*cval[2],specparm[3]);  /* boxcar gate */

}

 /* get baseline points */

 specparm[3]=dgupdate4p(3,100,specparm[3]);

 for(i=cval[10];i<cval[10]+20;i++)
{
   cgotoxy(49,34,stdout);                       /* put channel # on screen*/
   printf("%d",i);

   trstarthy1();
    data[i]=getpoint(sri,0);
   trstophy1();

    dplot4p(cval[5],i,cval[10]+20,data[i]);
}

/* select exit option */

compl: iopt=0;

  cgotoxy(68,34,stdout);
 printf("1. save data set");
  cgotoxy(68,35,stdout);
 printf("2. repeat scan - same setting");
  cgotoxy(68,36,stdout);
 printf("3. repeat scan - change setting");
  cgotoxy(68,37,stdout);
 printf("4. manual scan");
  cgotoxy(68,38,stdout);
 printf("5. exit program");

again:

  cgotoxy(68,32,stdout);
printf("ENTER OPTION : ");
 gets(chopt);
  iopt=atoi(chopt);
 if(iopt<1 | iopt>5)
{
        cgotoxy(63,32,stdout);
        ccleol(stdout);
        goto again;
}

 if(iopt==1)
{
        savedata4p(cval,fval,data);     /* save comment,fval,cval,date,data */
        goto compl;
}
 if(iopt==2) goto repeat;
```

```
   if(iopt==3) goto change;
   if(iopt==4)
  {
          trstarthy1();
          ibloc(dg1);
          cgotoxy(68,39,stdout);
          printf("CLICK MOUSE WHEN FINISHED\r");
          SysBeep(1);
          for(;;)
          {
                  if(Button()) break;
          }
          dg1=ibfind("dg535");
          trstophy1();
          cgotoxy(63,32,stdout);
          ccleol(stdout);
          goto again;
  }

  free(data);
   ibonl(sri,0);
   ibonl(dg1,0);
   tparout4p(cval);
}

error()
{

          printf("GPIB function call error\n\r");
          printf("ibsta=0x%x, iberr = 0x%x\n\r",ibsta,iberr);
          printf("ibcnt=0x%x  \n\r",ibcnt);
          exit(-1);
}
```

A6-2. Main Program for HYSCORE

```
/*
*   hyscore1.c - this routine will be used to govern the collection
*         of HYSCORE (2-D ESEEM) data.
*
*           there are two different data collection scheme.
*
*         1st - direct detection
*                 (4-pulse sequence  <-- This program
*                 5-pulse sequence)
*         2nd - remote detection
*
*
*   definition
*
*       limits(xmin,xmax,ymin,ymax,ixtic,iytic) - the box limit for the live
*
*      gpib0 - gpib controller
*      dg1   - dg535 pulse generator (#1)
*      dg2   - dg535 pulse generator (#2)
*      sri   - sr245 computer interface
*      mloc  - mouse location (pointer)
*
*   scan control parameters
*
```

```
*     cval[0] - tau                (nsec)
*     cval[1] - starting t1        (nsec)
*     cval[2] - starting t2        (nsec)
*     cval[3] - t1 increment       (nsec)
*     cval[4] - t2 increment       (nsec)
*     cval[5] - long time [tL]     (nsec) [remote]
*     cval[6] - tauR               (nsec) [remote]
*     cval[7] - # of data points of t1
*     cval[8] - # of data points of t2
*     cval[9] - repetitions/time point
*     cval[10] - sequence repetition rate (Hz)
*     cavl[11] - plot scale factor
*     cval[12] - A timing shim     (nsec)
*     cval[13] - B timing shim     (nsec)
*     cval[14] - C timing shim     (nsec)
*     cval[15] - D timing shim     (nsec)
*     cval[16] - E timing shim     (nsec) [remote]
*     cval[17] - F timing shim     (nsec) [remote]
*     cval[18] - G timing shim     (nsec) [remote]
*
*   delay generator set up parameters
*
*     tpar[0] - trigger rate
*     tpar[1] - A delay time (tau)
*     tpar[2] - B delay time (tau + t1)
*     tpar[3] - C delay time (tau + t1 + t2)
*     tpar[4] - D delay time (2*tau +t1 + t2)          [direct - boxcar gate]
*                                                      [remote - 5th pulse]
*     tpar[5] - E delay time (2*tau + t1 + t2 + tL)    [remote]
*     tpar[6] - F delay time (2*tau + t1 + t2 + tL + tauR)  [rempte]
*     tpar[7] - G delay time (2*tau + t1 + t2 + tL + 2*tauR) [remote boxcar gate]
*/

#include <stdio.h>
#include <console.h>
#include <string.h>
#include <stdlib.h>
#include "decl.h"
#include "matrix.h"

int  gpib0,dg1,dg2,sri;
char spr,pbuff[2];

typedef struct{int v,h;} POINT;
POINT *mloc;

main()
{
        int  i,j,limits[6],cval[19],tpar[8],specparm[4];
        int  **data,iopt;
        float  fval[4],t1,dt1;
        char chopt[3];

        limits[0]=100;
        limits[1]=575;
        limits[2]=40;
        limits[3]=300;
        limits[4]=10;
        limits[5]=10;

        fval[0]=9.0;
        fval[1]=3000.0;
        fval[2]=50.0;
        fval[3]=4.2;
```

```
/* set up console screen */

        pageset(stdout);

/* read cval[] from timehy.dat */

  tparinhy(cval);

/* open and clear gpib controller. Then open and clear sr245 and dg535 */

  if((gpib0=ibfind("gpib0"))<0)
{
                printf("gpib0 not found\n\r");
                exit(-1);
}

        if(ibsic(gpib0) & ERR) error();

        if((sri=ibfind("sr245"))<0)
        {
                printf("sr245 device not found\n\r");
                exit(-1);
        }

        if((dg1=ibfind("dg535"))<0)
        {
                printf(" first dg535 device not found\n\r");
                exit(-1);
        }

        if(ibclr(sri) & ERR) error();
        if(ibclr(dg1) & ERR) error();

/* get scanning parameters */

change: getparmhy1(cval);

/* allocate data array */

  data=imatrix(cval[7],cval[8]+10);

/* set up initial timing parameters */

        tpar[0]=cval[10];                                   /* trigger rate */
        tpar[1]=cval[0]+cval[12];                           /* A delay time */
        tpar[2]=cval[0]+cval[1]+cval[13];                   /* B delay time */
        tpar[3]=cval[0]+cval[1]+cval[2]+cval[14];           /* C delay time */
        tpar[4]=2*cval[0]+cval[1]+cval[2]+cval[15];         /* D delay time */

/* set up the scanning parameters for sr245 and dg535 devices */

  srsethy(cval[9]);

repeat:dgsethy1(tpar);

/* set up the screen for data aquisition */

        eraseplot();

        lplabelhy1(cval);

        box(limits);
```

```
/* set timing parameters for display */

  specparm[0]=cval[0];
  specparm[1]=cval[0]+cval[1];
  specparm[2]=cval[0]+cval[1]+cval[2];
  specparm[3]=2*cval[0]+cval[1]+cval[2];

  dgupdatehy1(0,0,specparm[0]);
  dgupdatehy1(1,0,specparm[1]);
  dgupdatehy1(2,0,specparm[2]);
  dgupdatehy1(3,0,specparm[3]);

/* data collection - the first point as collected from the integrator
*             is usually bad. We will collect  cval[7]*(cval[8]+10)
*             points, the first twice to make up for this. 10 data
*             points are for baseline.
*/

        trstarthy1();                           /* trigger start */
        data[0][0]=getpoint(sri,0);             /* data aquisition */
        trstophy1();                            /* trigger stop */

        t1=cval[1];
        dt1=cval[3];
        t1=t1/1000.0;
        dt1=dt1/1000.0;

 for(i=0;i<cval[7];i++)                 /* t1 timing */
{



    cgotoxy(49,34,stdout);                      /* put channel # on screen*/
        printf("%d",i);

        cgotoxy(48,35,stdout);          /* put t1 (µsec) on screen */
        printf("%.3f",t1);
        t1+=dt1;

        for(j=0;j<cval[8];j++)                  /* t2 timing */
        {
                cgotoxy(56,34,stdout);      /* put channel # on screen*/
                printf("%d",j);

                if(kbhit()) goto compl;         /* check for keystroke */

                trstarthy1();                                   /* trigger start */

                data[i][j]=getpoint(sri,0);   /* data aquisition and type signal value */

                trstophy1();                                    /* trigger stop */

                dplothy(cval[11],j,cval[8]+10,data[i][j]);  /* plot data on screen */

                specparm[2]=dgupdatehy1(2,cval[4],specparm[2]); /* update delay generator */
                specparm[3]=dgupdatehy1(3,cval[4],specparm[3]); /* for 3rd pulse and gate */
        }

        /* get baseline points */

        specparm[3]=dgupdatehy1(3,100,specparm[3]);

    for(j=cval[8];j<cval[8]+10;j++)
        {
```

```
                cgotoxy(56,34,stdout);                  /* put channel # on screen*/
            printf("%d",j);

            trstarthy1();
             data[i][j]=getpoint(sri,0);
            trstophy1();

             dplothy(cval[11],j,cval[8]+10,data[i][j]);
          }

   eraseplot();                                         /* set up the screen for data aquisition */
                lplabelhy1(cval);
                box(limits);

  /* update for new t1 value */

     cgotoxy(28,33,stdout);
    printf("%d",specparm[0]);
     specparm[1]=dgupdatehy1(1,cval[3],specparm[1]);
      specparm[2]=dgback1(2,cval[8]*cval[4]-cval[3],specparm[2]);
      specparm[3]=dgback1(3,cval[8]*cval[4]+100-cval[3],specparm[3]);
}

/* display data[(cval[7]-1)][j] set (the last t1 set) */

        for(j=0;j<cval[8]+10;j++)  dplothy(cval[11],j,cval[8]+10,data[(cval[7]-1)][j]);

/* select exit option */

compl: iopt=0;

  cgotoxy(68,34,stdout);
  printf("1. save data set");
  cgotoxy(68,35,stdout);
  printf("2. repeat scan - same setting");
  cgotoxy(68,36,stdout);
  printf("3. repeat scan - change setting");
  cgotoxy(68,37,stdout);
  printf("4. manual scan");
  cgotoxy(68,38,stdout);
  printf("5. exit program");

again:

  cgotoxy(68,32,stdout);
 printf("ENTER OPTION : ");
  gets(chopt);
   iopt=atoi(chopt);
  if(iopt<1 | iopt>5)
 {
        cgotoxy(63,32,stdout);
        ccleol(stdout);
        goto again;
 }

  if(iopt==1)
 {
        savedatahy1(cval,fval,data);    /* save comment,fval,cval,date,data */
        free_imatrix(data,cval[7]);   /* dellocate data array */
        goto compl;
 }
  if(iopt==2) goto repeat;
  if(iopt==3) goto change;
  if(iopt==4)
```

```
  {
        trstarthy1();
        ibloc(dg1);
        cgotoxy(68,39,stdout);
        printf("CLICK MOUSE WHEN FINISHED\r");
        SysBeep(1);
        for(;;)
        {
                if(Button()) break;
        }
        dg1=ibfind("dg535");
        trstophy1();
        cgotoxy(63,32,stdout);
        ccleol(stdout);
        goto again;
  }

   ibonl(sri,0);
   ibonl(dg1,0);
   tparouthy(cval);
}

error()
{

        printf("GPIB function call error\n\r");
        printf("ibsta=0x%x, iberr = 0x%x\n\r",ibsta,iberr);
        printf("ibcnt=0x%x \n\r",ibcnt);
        exit(-1);
}
```

A6-3. Subprograms

```
/*************
*
*       box.c constructs a box with tick marks on the screen. The
*       characteristics of this box are governed by values placed in
*       an array of limits whose address is passed to box when called
*       from the main prog. The structure is an integer array with elements
*       defined as xmin, xmax, ymin, ymax, xtic, ytic
*
***************/

        box(plm)
        int *plm;
        {
        int i,xdel,ydel,xval,yval;
        int xmin,xmax,ymin,ymax,ixtic,iytic;

        xmin=*plm;
        xmax=*++plm;
        ymin=*++plm;
        ymax=*++plm;
        ixtic=*++plm;
        iytic=*++plm;
/*
*       draw the box
*/
        line(xmin,ymin,xmin,ymax);
        cont(xmax,ymax);
```

```
        cont(xmax,ymin);
        cont(xmin,ymin);

        xdel=(xmax-xmin)/ixtic;
        ydel=(ymax-ymin)/iytic;

/*      draw the tic marks */

        for(i=1;i<ixtic;i++){
                xval=xmin+i*xdel;
                line(xval,ymin,xval,ymin+xdel/10);
                line(xval,ymax,xval,ymax-xdel/10);
                };

        for(i=1;i<iytic;i++){
                yval=ymin+i*ydel;
                line(xmin,yval,xmin+ydel/5,yval);
                line(xmax,yval,xmax-ydel/5,yval);
                };
/*
*               return to calling routine
*/
        return;

        }


/*
*       cont.c - this function draws a line on the screen using quickdraw
*       routines
*
*       it is meant to take the place of the routine cont(x1,y1)
*       that existed in the unix library of think c3.0.
*/
        #include <console.h>

        cont(x1,y1)

                int x1,y1;

        {
                GrafPtr oldport;

                GetPort(&oldport);
                SetPort(stdout->window);

                LineTo(x1,y1);
                SetPort(oldport);

                return;
        }


/*
*       delaysethy.c - this function takes in the delay value and sets it using the
*       the cursor mode of the dg535. the routine assumes that prior
*       the function call the user has set the display to the approriate
*       channel and the the sursor is in position 16, the nanosecond
*       position.  upon return, the cursor is resored to the nanosecond.
*/

        #include "decl.h"
        extern int dg1;
```

```
        delaysethy(ival)
        int ival;
        {

        int i,k;
        long cval,temp;

/* ival can range from 1 nanosecond to 1msec, the leftmost digit is
*               tested first, and the dg535 cursor adusted if digit incrementation
*               is required.
*/
        ibwrt(dg1,"sc 10\r",6L);
        if(ibsta & ERR) error();

        cval=1000000;
        for(k=0;k<7;k++){
                temp=ival/cval;
                if(temp){
                        for(i=0;i<temp;i++){
                                ibwrt(dg1,"ic 1\r",5L);
                                if(ibsta & ERR) error();
                                };
                        };
                ival=ival-temp*cval;
                cval=cval/10;
                ibwrt(dg1,"MC 1\r",5L);
                if(ibsta & ERR) error();
                };

/* make sure cursor is left at position 16        */

        ibwrt(dg1,"sc 16\r",6L);
        if(ibsta & ERR) error();

        return;
        }


/*
*  dgback1.c - this routine makes delays of dg535 move backward for new
*          time set of t2 in HYSCORE (4-pulse), displays new time
*          position on mac, and put new time values into specparm
*          array. Assuming dg535 cursor is on nanosecond unit.
*
*     j = delay number
*               nd = moving backward by nd nanosecond
*     sp = specparm[j]
*/

#include "decl.h"
#include <console.h>

extern int dg1;

dgback1(j,nd,sp)

        int j,nd,sp;

{
        int msec,n100sec,n10sec,nsec,value,i;
        float fnd,fmsec,fn100sec,fn10sec;
        char s[12];
```

```
        s[0]='d';
        s[1]='l';
        s[2]=' ';
        s[3]='1';
        s[4]=',';
        s[5]='0';
        s[6]=',';
        s[7]=48+j;
        s[8]='\r';
        s[9]='\0';

/***************
*       select device and update it by nd nsec
*       note: the timing shims will be taken care of in the initialization
*       of the generators upon exiting from the setup table
***********/

        ibwrt(dg1,s,9L);
        if(ibsta & ERR) error();

 /* move backward on μ sec unit */

        fnd=nd;
        fnd=fnd/1000.0;
        msec=fnd;

        ibwrt(dg1,"MC 0;MC 0;MC 0\r",15L);
        if(ibsta & ERR) error();

        for(i=0;i<msec;i++)
        {
                ibwrt(dg1,"IC 0\r",5L);
                if(ibsta & ERR) error();
        }

 /* move backward on 100n sec unit */

        fmsec=msec;
        fnd=(fnd-fmsec)*10;
        n100sec=fnd;

        ibwrt(dg1,"MC 1\r",5L);
        if(ibsta & ERR) error();

        for(i=0;i<n100sec;i++)
        {
                ibwrt(dg1,"IC 0\r",5L);
                if(ibsta & ERR) error();
        }

 /* move backward on 10n sec unit */

        fn100sec=n100sec;
        fnd=(fnd-fn100sec)*10;
        n10sec=fnd;

        ibwrt(dg1,"MC 1\r",5L);
        if(ibsta & ERR) error();

        for(i=0;i<n10sec;i++)
        {
                ibwrt(dg1,"IC 0\r",5L);
                if(ibsta & ERR) error();
        }
```

```
/* move backward on n sec unit */

        fn10sec=n10sec;
        fnd=(fnd-fn10sec)*10;
        nsec=fnd;

        ibwrt(dg1,"MC  1\r",5L);
        if(ibsta & ERR) error();

        for(i=0;i<nsec;i++)
        {
                ibwrt(dg1,"IC  0\r",5L);
                if(ibsta & ERR) error();
        }

/* update specparm and display on mac */

        value=sp-nd;
        cgotoxy(28,33+j,stdout);
        printf("%d",value);

        return(value);
}


/*
*       dgsethy1.c - this rouitne is responsible for setting up the dg535
*                       delay and gate generator. It first finds and returns the
*                       integer descriptor for the device, then the device is
*                       cleared, the trigger rate is set, the outputs are changed
*                       to 50 ohms, the starting times are computed and set, the unit is
*                       placed in cursor mode for timing updates during a scan, and
*                       finally, the display is set to the appropriate channel so
*                       that the operator can monitor the progress of a scan from the
*                   front panel.
*
*                               the setup parameters are in an input array, that is passed
*                               to the routine in the call statement. the definitions of the
*                               5 values in this array are as follows
*
*                               tpar[0]  -  int trigger rate (Hz)
*                               tpar[1]  -  A delay time
*                               tpar[2]  -  B delay time
*                               tpar[3]  -          C delay time
*                               tpar[4]  -  D delay time
*
*/
        #include "decl.h"
        extern int dg1;
        extern char spr;

        dgsethy1(tpar)

        int *tpar;
        {
        int  trate,ast,bst,cst,dst;
        char s1[10],s[15];
        int i;
        long rcnt;

        trate=tpar[0];
        ast=tpar[1];
        bst=tpar[2];
```

```
        cst=tpar[3];
        dst=tpar[4];

/*      the device has been opened prior to calling this routine,
*       clear it by sending some caraiage returns
*/

        for(i=0;i<5;i++){
                ibwrt(dg1,"\r",1L);
                if(ibsta & ERR) error();
                };

        if(ibrsp(dg1,&spr) &ERR) error();

/* do a device clear and then set the internal trigger rate
*       and the to,a,b,c, and d outputs to 50 ohms
*/
        ibwrt(dg1,"cl\r",3L);
        if(ibsta & ERR) error();

        s[0]='t';
        s[1]='r';
        s[2]=' ';
        s[3]='0';
        s[4]=',';

        rcnt=stci_d(s1,trate,6);
        for(i=0;i<rcnt;i++){
                s[5+i]=s1[i];
                };

        s[rcnt+5]='\r';
        s[rcnt+6]='\0';

        rcnt=rcnt+6;

        ibwrt(dg1,s,rcnt);
        if(ibsta & ERR) error();

        ibwrt(dg1,"dl 0,1,0\r",9L);
        if(ibsta & ERR) error();

        ibwrt(dg1,"tz 1,0;tz 2,0;tz 3,0;tz 5,1;tz 6,1\r",35L);
        if(ibsta &ERR) error();

/* initialize delays to zero */

        ibwrt(dg1,"dt 2,1,0\r",9L);
        if(ibsta & ERR) error();

        ibwrt(dg1,"dt 3,1,0\r",9L);
        if(ibsta & ERR) error();

        ibwrt(dg1,"dt 5,1,0\r",9L);
        if(ibsta & ERR) error();

        ibwrt(dg1,"dt 6,1,0\r",9L);
        if(ibsta & ERR) error();

/*      set cursor mode and place c ursor on nsec digit */

        ibwrt(dg1,"dl 1,0,0\r",9L);
        if(ibsta & ERR) error();
```

```
        ibwrt(dg1,"cs 0;sc 16\r",11L);
        if(ibsta & ERR) error();

/*      now set initial delay values */

        if(ast) delaysethy(ast);

        ibwrt(dg1,"dl 1,0,1\r",9L);
        if(ibsta & ERR) error();

        if(bst) delaysethy(bst);

        ibwrt(dg1,"dl 1,0,2\r",9L);
        if(ibsta & ERR) error();

        if(cst) delaysethy(cst);

        ibwrt(dg1,"dl 1,0,3\r",9L);
        if(ibsta & ERR) error();

        if(dst) delaysethy(dst);

        return;
        }


/*
*       dgupdate4p.c - this function is responsible for updating the
*                      delay values of the 4 delay channels in the SRS dg535
*                      digital delay generator. It also updates the display with the new
*                      value and returns this value to the specparm array. the routine uses
*                      the dg535's cursor mode and assumes that the cursor is at
*                      the nanosecond digit prior to the function call.
*
*/
        #include "decl.h"
        #include <console.h>

        extern int dg1;

        dgupdate4p(j,nd,sp)

        int j,nd,sp;

/*      j: delay channel selected
*       nd: # of 1 nsec increments to be made
*       sp: specparm value
*/
        {
        int value,i;
        char s[12];

        s[0]='d';
        s[1]='l';
        s[2]=' ';
        s[3]='1';
        s[4]=',';
        s[5]='0';
        s[6]=',';
        s[7]=48+j;
        s[8]='\r';
        s[9]='\0';

/***************
```

```
*           select device and update it by nd nsec
*           note: the timing shims will be taken care of in the initialization
*                               of the generators upon exiting from the setup table
***********/

          ibwrt(dg1,s,9L);
          if(ibsta & ERR) error();

          for(i=0;i<nd;i++){
                    ibwrt(dg1,"IC  1\r",5L);
                    if(ibsta & ERR) error();
                    };

/*        update specparm and the display on mac          */

   value=sp+nd;
          cgotoxy(28,34+j,stdout);
          printf("%d",value);

          return(value);
          }


/*
*   dplot4p.c - plot 4-pulse ESEEM data point on screen
*
*       fmax  = maximum value of data set
*       fmin  = minimum value of data set
*       fi    = current data position on x-axis
*       fnum  = total data point #
*       fdata = current data value
*/

dplot4p(max,i,num,data)

          int  max,i,num,data;

{
   int x,y;
          float  fmax,fmin,fi,fnum,fdata,fx,fy;
          float  bxmax,bxmin,bymax,bymin,bdelx,bdely;

          bxmax=575;
          bxmin=100;
          bymax=300;
          bymin=40;
          bdelx=bxmax-bxmin;
          bdely=bymax-bymin;

          fmax=max;
          fmin=-fmax/5;
          fi=i;
          fnum=num;
          fdata=data;
          fdata=fdata-fmin;

 /* fraction of x,y axis */

          fdata=1-fdata/(fmax-fmin);
   fi=fi/(fnum-1.0);

 /* plot */

   fx=fi*bdelx+bxmin;
```

```
   fy=fdata*bdely+bymin;

   x=fx;
   y=fy;

    point(x,y);

   return;
}


/*
*       getpoint(sri,iarr) - gets data point from sr245 boxcar interface
*                                                       after the device has been triggered. The result is
*                                                       transmitted as a two byte string which is then
*                                                       assembled into integer form, displayed on the
screen
*                                                       and returned for storage in the approprite array.
*
*/
        #include <stdio.h>
        #include "decl.h"
        #include <console.h>

        extern char spr,pbuff[2];
        extern int sri,dg535;

        getpoint(sri,iarr)

        int iarr;
        {
        int value,sval,val1,val2;
        int rqs,cmpl,end;
        rqs=0x800;
        end=0x2000;
        cmpl=0x100;
        value=0;

/*      enable the running average on the sr250 by swinging sb2 high    */

        ibwrt(sri,"sb2=1\r",6L);
        if(ibsta & ERR) error();

/*      scan port 1 and set rqs after 1 trigger  */

        ibwrt(sri,"ss1:1\r",6L);
        if(ibsta & ERR) error();

/*      wait until rqs set on sr245   */

        ibwait(sri,rqs);

/*      read status byte and check data validity          */

        if(ibrsp(sri,&spr) & ERR) error();
        if(spr & 2) printf("data value out of range\n\r");

/*      read in value       */

        ibrd(sri,pbuff,2L);
        if(ibsta & ERR) error();

/*      clear the integrator running average   */
```

```
        ibwrt(sri,"sb2=0\r",6L);
        if(ibsta & ERR) error();

/*      reconstruct data value      */

        sval=1;
        val1=pbuff[1];
        val2=pbuff[0];
        if(val2 & 16) sval=-1;
        value=sval*((val2 & 15)*256+((val1>>4) & 15)*16+(val1 & 15));

/*      clear the status byte - check for scan end condition */

        for( ; ; ){
                ibrsp(sri,&spr);
                if(spr & 15) printf("sr245 error after read");
                if(spr & 16) break;
                };

/*      update the screen  */

        cgotoxy(10,34+iarr,stdout);
        printf("%d   ",value);
        return(value);
        }


/*
*       kbhit() - this function returns a non-zero result if the keyboard has been
*                                 depressed
*
*                                 It will be usd to prematurely stop data collection
*
*/
        kbhit()
        {
        EventRecord the_Event;

        EventAvail(40,&the_Event);

        return(the_Event.what);
        }

#include <stdlib.h>
#include <stdio.h>
#include "matrix.h"

void matrixerror(char *text)
{
        printf(text);
        exit(1);
}

int **imatrix(int row,int col)
{
        int i, **m;

        m = ( int **) malloc( (size_t)  row * sizeof(int*));
        if(!m) matrixerror(" Allocation Faliure For imatrix\n");

        for(i = 0; i < row; i++ ) {
                m[i]=(int*) malloc( (size_t) col*sizeof(int));
                if(!m[i]) matrixerror(" Allocation Faliure For imatrix\n");
        };
```

```
        return m;
}

void free_imatrix(int **m, int row)
{
        int i;

        for(i = 0; i < row; i++ )  free( m[i] );
        free( m );
}


/*
*   lplabel4p.c - labelling the grid for the dac live plot
*            in 4-pulse ESEEM experiment
*/

#include <console.h>

lplabel4p(cval)

        int *cval;

{
        int i;
        float  t,t2,t4,t8,n;
        char amp1[4]={'E','C','H','O'};
        char amp2[4]={' ','A','M','P'};
        char amp3[4]={'L','I','T','U'};
        char amp4[4]={'D','E',' ',' '};

        cgotoxy(45,2,stdout);
        printf("KEYSTROKE ABORTS SCAN");

 /* y-axis */

   for(i=0;i<=3;i++)
        {
                cgotoxy(5,9+i,stdout);
                printf("%.1s",&amp1[i]);
        }

        for(i=0;i<=3;i++)
        {
                cgotoxy(5,13+i,stdout);
                printf("%.1s",&amp2[i]);
        }

        for(i=0;i<=3;i++)
        {
                cgotoxy(5,17+i,stdout);
                printf("%.1s",&amp3[i]);
        }

        for(i=0;i<=3;i++)
        {
                cgotoxy(5,21+i,stdout);
                printf("%.1s",&amp4[i]);
        }

        cgotoxy(12,27,stdout);
        printf("%d",-cval[5]/5);
```

```
        cgotoxy(12,4,stdout);
        printf("%d",cval[5]);

/* x-axis */

        t2=cval[0];
        t4=cval[1];
        t8=cval[2];
        n=cval[10];

        t=(t2+2.0*t4)/1000.0;
        cgotoxy(15,29,stdout);
        printf("%.2f",t);

        t=(t2+2.0*t4+(n+19.0)*2.0*t8)/1000.0;
        cgotoxy(94,29,stdout);
        printf("%.2f",t);

        t=(2.0*t2+4.0*t4+(n+19.0)*2.0*t8)/2000.0;
        cgotoxy(54,29,stdout);
        printf("%.2f",t);

        cgotoxy(49,31,stdout);
        printf("tau + T (μsec)");

/* information */

  for(i=0;i<=3;i++)
 {
                cgotoxy(5,34+i,stdout);
                printf("S%d = ",i);
        }

        for(i=0;i<=3;i++)
 {
                cgotoxy(23,34+i,stdout);
                printf("T%d = ",i);
        }

        cgotoxy(41,34,stdout);
        printf("ch# = ");

        cgotoxy(1,1,stdout);

        return;
}



#include <stdlib.h>
#include <stdio.h>
#include "matrix.h"

void matrixerror(char *text)
{
        printf(text);
        exit(1);
}

int **imatrix(int row,int col)
{
        int i, **m;

        m = ( int **) malloc( (size_t)  row * sizeof(int*));
```

```
        if(!m) matrixerror(" Allocation Faliure For imatrix\n");

        for(i = 0; i < row; i++ ) {
                m[i]=(int*) malloc( (size_t) col*sizeof(int));
                if(!m[i]) matrixerror(" Allocation Faliure For imatrix\n");
        };

        return m;
}

void free_imatrix(int **m, int row)
{
        int i;

        for(i = 0; i < row; i++ ) free( m[i] );
        free( m );
}



/*
*  tparin4p.c - read cval[] from "time4p.dat"
*/

#include <stdio.h>

tparin4p(cval)

        int cval[];

{
   int i;
   FILE *fp,*fopen();

        if((fp=fopen("time4p.dat","r")) == '\0')
        {
                printf("file <time4p.dat> not found ! \n");
                for(i=0;i<=10;i++) cval[i]=0;
  }
  else
        {
           for(i=0;i<=10;i++) fscanf(fp,"%d\n",cval++);
        }

   fclose(fp);
   SysBeep(1);

   return;

}


/*
*       tparout4p.c - save timing parameters cval[] for 4-pulse
*               in time4p.dat file
*/

#include <stdio.h>
#include <console.h>

tparout4p(cval)

        int cval[];
```

```
{
  int i;
  FILE *fp,*fopen();

        if((fp=fopen("time4p.dat","r+")) == '\0')
        {
                printf("file <time4p.dat> not found ! \n");
                for(i=0;i<=10;i++) cval[i]=0;
  }
  else
        {
            for(i=0;i<=10;i++) fprintf(fp,"%d\n",cval[i]);
        }

  fclose(fp);

   cgotoxy(68,39,stdout);
  ccleol(stdout);
  printf("file <time4p.dat> updated");
   cgotoxy(1,1,stdout);

  SysBeep(1);

  return;
}


/*
*       trstarthy1.c - this routine starts the dg535 internal rate generator. it is
*                                   presumed that the trigger rate has already been appropriately
*                                   set by the user.
*/

        #include "decl.h"
        extern int dg1;

        trstarthy1()
        {
        ibwrt(dg1,"tm 0\r",5L);
        if(ibsta & ERR) error();

        return;
        }


/*
*       trstophy1.c - this function stops the internal rate generator on the dg535
*                           so that the unit is not triggered during an update
*/

        #include "decl.h"
        extern int dg1;

        trstophy1()
        {
        ibwrt(dg1,"tm 2\r",5L);
        if(ibsta & ERR) error();

        return;
        }
```

A7. Computer Programs for Searching Angle Sets from an Anisotropic EPR Spectrum to Interprete ESEEM Spectra

The computer program listed below was used to search the angle sets of samples excited by a microwave pulse from an anisotropic EPR spectrum of randomly oriented samples. The selected angle sets are used to interprete orientation selective ESEEM or ENDOR spectra. The program is written in MATLAB v.4.2 (Mathworks, Inc.).

A7-1. Main Program

```
%
% ansel.m - this generate selected theta and phi angle sets from g-anisotropic
%         and A (hyperfine enrgy)-anisotopic EPR pattern at some microwave
%         frequency and magnetic field strength
%
%    This finds out angle set (theta,phi) which satisfy the following
%    equation
%                hv - mI*A(theta,phi)
%           Hr = ----------------------
%                   betae*g(theta,phi)
%
%
%    Outputs of this subroutine are
%
%                    -I     -I+1 ....
%              angset(theta,phi,theta,phi,....)
%                | |  | |
%                columns
%
%           angset1 - angle sets which are symmetry of angset
%                about the center of sphere
%           nummi - vector : each culumn has the information of
%               the selected angle set number
%                of mI=-I,-I+1,...
%            prob - probabilities of each angle set for line integral
%               same row size , half culumn size as angset
%

global epr;

% rotate Hyperfine PAS to g-tensor axis by Euler rotation

AA=eulerA(epr(4:6),epr(7:9));

% loop for searching the theta and phi set

phi=-719:719;phi=pi*phi/180;
theta=0:180;theta=pi*theta/180;
```

```
theta(182)=theta(1);
icul=1;
nmi=0;
nummi=[0 0 0 0 0 0 0 0];
dphi=pi/180;
dphi2=pi/360;

for mi=-epr(12):epr(12),

 nmi=nmi+1;
 gop=1;
 theind=1;
 phiind=720;
 temp1=rescalc(AA,mi,theta(theind),phi(phiind));
 numset=0;

 while (gop>0) & (theind<182)
   theind=theind+1;
    temp2=rescalc(AA,mi,theta(theind),phi(phiind));
   gop=temp1*temp2;
   temp1=temp2;
 end

 if theind<182
   numset=numset+1;

   % the first angle set

    angset(numset,icul:icul+1)=[(theta(theind)+theta(theind-1))/2 phi(phiind)];
    angset1(numset,icul:icul+1)=[pi-angset(numset,icul) pi+angset(numset,icul+1)];

   % initiate the searching loop

   orst=[theind,0];
   phiind=phiind+1;
   nalphi=1;
   clor=[theind nalphi];
   iclopt=1;

   temp4=temp1;
    temp1=rescalc(AA,mi,theta(theind),phi(phiind));
    temp2=rescalc(AA,mi,theta(theind-1),phi(phiind));
    temp3=rescalc(AA,mi,theta(theind-1),phi(phiind-1));

   gop=temp1*temp2;

   if temp1*temp2<0 clopt=1;
   elseif temp2*temp3<0 clopt=2;
  else clopt=4;
  end

  probcalc;
   selangmvcell;

   % searching loop

    while orst(1)<clor(1)|orst(1)>clor(1)|orst(2)<clor(2)|orst(2)>clor(2)

    if iclopt==1
      temp4=temp1;
      temp3=temp2;
        temp1=rescalc(AA,mi,theta(theind),phi(phiind));
        temp2=rescalc(AA,mi,theta(theind-1),phi(phiind));
```

```
        if temp1*temp2<0 clopt=1;
        elseif temp2*temp3<0 clopt=2;
       else clopt=4;
      end

     elseif iclopt==2
       temp1=temp2;
       temp4=temp3;
         temp2=rescalc(AA,mi,theta(theind-1),phi(phiind));
         temp3=rescalc(AA,mi,theta(theind-1),phi(phiind-1));

        if temp1*temp2<0 clopt=1;
        elseif temp2*temp3<0 clopt=2;
       else clopt=3;
      end

     elseif iclopt==3
       temp1=temp4;
       temp2=temp3;
         temp3=rescalc(AA,mi,theta(theind-1),phi(phiind-1));
         temp4=rescalc(AA,mi,theta(theind),phi(phiind-1));

        if temp2*temp3<0 clopt=2;
        elseif temp3*temp4<0 clopt=3;
       else clopt=4;
      end

     else  % iclopt==4 case
       temp2=temp1;
       temp3=temp4;
         temp1=rescalc(AA,mi,theta(theind),phi(phiind));
         temp4=rescalc(AA,mi,theta(theind),phi(phiind-1));

        if temp1*temp2<0 clopt=1;
        elseif temp3*temp4<0 clopt=3;
       else clopt=4;
      end

    end

     probcalc;
     selangmvcell;

   end

    clopt=1; % probability calcuation for last angleset
   probcalc;

 end

 icul=icul+2;
 nummi(nmi)=numset;

end

return;
```

A7-2. Subprograms

```
%
```

```
% eprinput.m - EPR parameters which determine the EPR line shape
%

global epr;

epr=[2.0 2.0 2.5 20 20 400 0 0 0 3000 9.000 1.5];

fprintf('\n');
fprintf('-----------------------------------\n');
fprintf(' Type the number to be changed\n');
fprintf('-----------------------------------\n');
fprintf('1. gx              = %10.5f\n',epr(1));
fprintf('2. gy              = %10.5f\n',epr(2));
fprintf('3. gz              = %10.5f\n',epr(3));
fprintf('4. Ax(MHz)         = %10.5f\n',epr(4));
fprintf('5. Ay(MHz)         = %10.5f\n',epr(5));
fprintf('6. Az(MHz)         = %10.5f\n',epr(6));
fprintf('7. alpha(degree)   = %10.2f\n',epr(7));
fprintf('8. beta (degree)   = %10.2f\n',epr(8));
fprintf('9. gamma(degree)   = %10.2f\n',epr(9));
fprintf('10. field(G)       = %10.2f\n',epr(10));
fprintf('11. frequency(GHz) = %10.5f\n',epr(11));
fprintf('12. I(nuclear spin)= %10.1f\n',epr(12));
fprintf('13. list\n');
fprintf('14. calculation\n');
fprintf('-----------------------------------\n');
fprintf('\n');

n=0;

while n<14 | n>14
  n=input('number to be changed : ');
  if n==1 epr(1)=input('1. gx = ');
  elseif n==2 epr(2)=input('2. gy = ');
  elseif n==3 epr(3)=input('3. gz = ');
  elseif n==4 epr(4)=input('4. Ax (MHz) = ');
  elseif n==5 epr(5)=input('5. Ay (MHz) = ');
  elseif n==6 epr(6)=input('6. Az (MHz) = ');
  elseif n==7 epr(7)=input('7. alpha (degree) = ');
  elseif n==8 epr(8)=input('8. beta (degree) = ');
  elseif n==9 epr(9)=input('9. gamma (degree) = ');
  elseif n==10 epr(10)=input('10. field (G) = ');
  elseif n==11 epr(11)=input('11. frequency (GHz) = ');
  elseif n==12 epr(12)=input('12. I (nuclear spin) = ');
  elseif n==13
    fprintf('\n');
    fprintf('-----------------------------------\n');
    fprintf(' Type the number to be changed\n');
    fprintf('-----------------------------------\n');
    fprintf('1. gx              = %10.5f\n',epr(1));
    fprintf('2. gy              = %10.5f\n',epr(2));
    fprintf('3. gz              = %10.5f\n',epr(3));
    fprintf('4. Ax(MHz)         = %10.5f\n',epr(4));
    fprintf('5. Ay(MHz)         = %10.5f\n',epr(5));
    fprintf('6. Az(MHz)         = %10.5f\n',epr(6));
    fprintf('7. alpha(degree)   = %10.2f\n',epr(7));
    fprintf('8. beta (degree)   = %10.2f\n',epr(8));
    fprintf('9. gamma(degree)   = %10.2f\n',epr(9));
    fprintf('10. field(G)       = %10.2f\n',epr(10));
    fprintf('11. frequency(GHz) = %10.5f\n',epr(11));
    fprintf('12. I(nuclear spin)= %10.5f\n',epr(12));
    fprintf('13. list\n');
    fprintf('14. calculation\n');
    fprintf('-----------------------------------\n');
```

```
    fprintf('\n');
  end
end

epr(4)=epr(4)*1e6;
epr(5)=epr(5)*1e6;
epr(6)=epr(6)*1e6;
epr(7)=epr(7)*pi/180;
epr(8)=epr(8)*pi/180;
epr(9)=epr(9)*pi/180;
epr(11)=epr(11)*1e9;

return;


%
% eulerA.m - this rotate compin(1:3) in some axis system to compout(1:3,1:3)
%         in other axis by Euler rotation
%
%   input compin(1:3)
%         eulang(1:3) - alpha,beta,gamma
%   output compout(1:3,1:3)

function compout=eulerA(compin,eulang)

sint=sin(eulang);
cost=cos(eulang);

Rz1=[cost(1) sint(1) 0;-sint(1) cost(1) 0;0 0 1];
Ry=[cost(2) 0 -sint(2);0 1 0;sint(2) 0 cost(2)];
Rz2=[cost(3) sint(3) 0;-sint(3) cost(3) 0;0 0 1];

R=Rz1*Ry*Rz2;

compout=zeros(3);

for i=1:3,
compout(i,i)=compin(i);
end

compout=R'*compout*R;

return;


%
% probcalc.m - this calculates the line integral probability value
%          in angle selection ESEEM or ENDOR
%
%      prob=sqrt((dtheta/dphi)^2+sin(theta)^2)*dphi
%

if iclopt==1
  if clopt==4 | clopt==2
     prob(numset,(icul+1)/2)=sqrt(1+(sin(angset(numset,icul)))^2)*dphi2;
  else
     prob(numset,(icul+1)/2)=sqrt((sin(angset(numset,icul)))^2)*dphi;
  end
elseif iclopt==2
  if clopt==1 | clopt==3
     prob(numset,(icul+1)/2)=sqrt(1+(sin(angset(numset,icul)))^2)*dphi2;
  else
     prob(numset,(icul+1)/2)=0;
  end
```

```
elseif iclopt==3
  if clopt==2 | clopt==4
     prob(numset,(icul+1)/2)=sqrt(1+(sin(angset(numset,icul)))^2)*dphi2;
  else
     prob(numset,(icul+1)/2)=sqrt((sin(angset(numset,icul)))^2)*dphi;
  end
else
  if clopt==1 | clopt==3
     prob(numset,(icul+1)/2)=sqrt(1+(sin(angset(numset,icul)))^2)*dphi2;
  else
    prob(numset,(icul+1)/2)=0;
  end
end

return;


%
%  rescalc.m - calcuate the value of the following equation
%
%                 hv - mI*A(theta,phi)
%         f = Hr - ----------------------
%                    betae*g(theta,phi)
%
%         at some theta and phi value


function x=rescalc(AAin,miin,thetain,phiin)
global epr;

% calculate g(thetain,phiin)

 % direction cosines

  h=[sin(thetain)*cos(phiin)  sin(thetain)*sin(phiin)  cos(thetain)];

gh=epr(1:3).*h;
geff=sqrt(gh*gh');

% calcuate A(thetain,phiin)

Ah=gh*AAin;
Aeff=sqrt(Ah*Ah')/geff;

% calcualte gcalc

x=epr(10)-7.1448e-7*(epr(11)-miin*Aeff)/geff;

return;


%
%  selangmvcell.m - this stores the selected angle set and
%                   makes the cell, used in root finding of some function,
%                   move up,down,left or right.
%
%         Actually, this makes the origin of cell move.
%
%        x ------ x
%        |  2     |
%        | 3      1 | <----- cell
%        |          |          1,2,3,4 - side numbers
%        |  4     |
%         x ------ x <------origin
```

```
%

numset=numset+1;

if clopt==1
   angset(numset,icul:icul+1)=[(theta(theind)+theta(theind-1))/2 phi(phiind)];
   phiind=phiind+1;
   nalphi=nalphi+1;
elseif clopt==2
    angset(numset,icul:icul+1)=[theta(theind-1) (phi(phiind)+phi(phiind-1))/2];
   theind=theind-1;
elseif clopt==3
    angset(numset,icul:icul+1)=[(theta(theind)+theta(theind-1))/2 phi(phiind-1)];
   phiind=phiind-1;
   nalphi=nalphi-1;
else
    angset(numset,icul:icul+1)=[theta(theind) (phi(phiind)+phi(phiind-1))/2];
   theind=theind+1;
end

angset1(numset,icul:icul+1)=[pi-angset(numset,icul) pi+angset(numset,icul+1)];

iclopt=clopt;

if nalphi==360 nalphi=0;
end

clor=[theind nalphi];

return;
```

A8. Computer Programs for Calculating Orientation Selective Four-Pulse ESEEM Frequency Domain Spectrum for S=1/2 and I=1/2 Spin System

The computer program used to calculate orientation selective four-pulse ESEEM frequency domain spectra is listed below. The program is designed for a spin system described by anisotropic g- and/or metal hyperfine tensors. The ligand hyperfine interaction is assumed to be axial. First part of the program determines the selected angle sets (θ,ϕ) from EPR parameters (Appendix, A7) and the second part of the program generates the four-pulse ESEEM spectrum. The program is written in MATLAB v.4.2 (Mathworks, Inc.).

A8-1. Main Program

```
%
% ansel4ph.m - this program generate angle selection 4-pulse ESEEM frequency
%          domain spectrum for S=1/2 and I=1/2
%

% epr parameter input

global epr;
eprinput;

% angle selection - g anisotropic and A anisotropic

ansel;

eseem=[5.58566 2.0 2.5 0 0];
width=0.1;

eseopt=1;
while eseopt==1

% eseem parameter input

eseeminput;

% gaussian function for convolution

gaus;

% eseem frequency calculation

fpfrsp;
```

```
fpfrdspl;

end
```

A8-2. Subprograms

```
%
%  Acalc.m - calculate the superHyperfine matrix in g-tensor axis
%

% direction cosine of superhyperfine axis in g-axis

r=[sin(eseem(4))*cos(eseem(5)) sin(eseem(4))*sin(eseem(5)) cos(eseem(4))];

T=7.0692e-18*eseem(1)/(eseem(3))^3;

% superhyperfine matrix in g-axis

gmat=[epr(1) 0 0;0 epr(2) 0;0 0 epr(3)];
amat=eye(3)*eseem(2);
rmat=3*r'*r-eye(3);

A=-T*gmat*rmat+amat;

return;


%
%  eseeminput.m - gets eseem parameters for I=1/2 case
%
%       eseem(1) - nuclear g-value
%       eseem(2) - Aiso
%       eseem(3) - dipole-dipole distance
%       eseem(4) - theta-n
%       eseem(5) - phi-n
%

fprintf('\n');
fprintf('-----------------------------------\n');
fprintf('      type the number you want\n');
fprintf('-----------------------------------\n');
fprintf('1. gn                = %10.5f\n',eseem(1));
fprintf('2. Aiso (MHz)        = %8.3f\n',eseem(2));
fprintf('3. dipole distance (A) = %8.3f\n',eseem(3));
fprintf('4. theta-n (dgree)   = %7.2f\n',eseem(4));
fprintf('5. phi-n (dgree)     = %7.2f\n',eseem(5));
fprintf('6. gaussian band width = %7.2f\n',width);
fprintf('7. list\n');
fprintf('8. calculation\n');
fprintf('-----------------------------------\n');
fprintf('\n');

eseemopt=0;

while eseemopt<8 | eseemopt>8
  eseemopt=input('number to be changed : ');
  if eseemopt==1 eseem(1)=input('1. gn = ');
  elseif eseemopt==2 eseem(2)=input('2. Aiso (MHz) = ');
  elseif eseemopt==3 eseem(3)=input('3. dipole distance (A) = ');
  elseif eseemopt==4 eseem(4)=input('4. theta-n (dgree) = ');
```

```
  elseif eseemopt==5 eseem(5)=input('5. phi-n (dgree) = ');
  elseif eseemopt==6 width=input('6. gaussian band width = ');
  elseif eseemopt==7
     fprintf('\n');
     fprintf('-------------------------------\n');
     fprintf('     type the number you want\n');
     fprintf('-------------------------------\n');
     fprintf('1. gn              = %10.5f\n',eseem(1));
     fprintf('2. Aiso (MHz)      = %8.3f\n',eseem(2));
     fprintf('3. dipole distance (A) = %8.3f\n',eseem(3));
     fprintf('4. theta-n (dgree)     = %7.2f\n',eseem(4));
     fprintf('5. phi-n (dgree)       = %7.2f\n',eseem(5));
     fprintf('6. gaussian band width = %7.2f\n',width);
     fprintf('7. list\n');
     fprintf('8. calculation\n');
     fprintf('-------------------------------\n');
     fprintf('\n');
  end
end

eseem(2)=eseem(2)*1e6;
eseem(3)=eseem(3)*1e-8;
eseem(4)=eseem(4)*pi/180;
eseem(5)=eseem(5)*pi/180;

return;


%
% fpfrdspl.m - display 4-pulse (S=1/2,I=1/2) simulation  results
%


imin=1;
imax=n(2);

eseopt=0;

while eseopt==0

plot(2*fr(imin:imax),I(imin:imax));
xlabel('Frequency (MHz)');
ylabel('Amplitude');
%grid;

fprintf('\n');
fprintf('-------------------------\n');
fprintf('  Type the number you want\n');
fprintf('-------------------------\n');
fprintf('1. va\n');
fprintf('2. vb\n');
fprintf('3. v(a+b)\n');
fprintf('4. v(a-b)\n');
fprintf('5. va+vb\n');
fprintf('6. v(a+b)+v(a-b)\n');
fprintf('7. all\n');
fprintf('8. change max,min frequencies\n');
fprintf('9. tau effect (on)\n');
fprintf('10. tau effect (off)\n');
fprintf('11. change ESEEM parameters\n');
fprintf('12.  print\n');
fprintf('13. new plot window\n');
fprintf('14. Larmor frequency\n');
fprintf('15. tau suppression plot\n');
```

```
fprintf('16. quit\n');
fprintf('----------------------------\n');
fprintf('\n');

iopt=input('Type the number you want : ');

if iopt==1,
    Itot=Ia;
     I=Itot((nn(2)-1)/2+1:(nn(2)-1)/2+n(2));
     imin=1;imax=n(2);
  elseif iopt==2,
    Itot=Ib;
     I=Itot((nn(2)-1)/2+1:(nn(2)-1)/2+n(2));
     imin=1;imax=n(2);
  elseif iopt==3,
    Itot=Iapb;
     I=Itot((nn(2)-1)/2+1:(nn(2)-1)/2+n(2));
     imin=1;imax=n(2);
  elseif iopt==4,
    Itot=Iamb;
     I=Itot((nn(2)-1)/2+1:(nn(2)-1)/2+n(2));
     imin=1;imax=n(2);
  elseif iopt==5,
    Itot=Ia+Ib;
     I=Itot((nn(2)-1)/2+1:(nn(2)-1)/2+n(2));
     imin=1;imax=n(2);
  elseif iopt==6,
    Itot=Iapb+Iamb;
     I=Itot((nn(2)-1)/2+1:(nn(2)-1)/2+n(2));
     imin=1;imax=n(2);
  elseif iopt==7,
    Itot=Ia+Ib+Iamb+Iapb;
     I=Itot((nn(2)-1)/2+1:(nn(2)-1)/2+n(2));
     imin=1;imax=n(2);
  elseif iopt==8,
    imin=input('Minimum Frequency (MHz) :');
    imax=input('Maximum Frequency (MHz) :');
     imin=round((imin/2+10)*6000/60)+1;
     imax=round((imax/2+10)*6000/60)+1;
  elseif iopt==9,
    tau=input('tau (nsec) :');
    tau=tau*1e-9;

      ca=c2.*cos(2*pi*(frb-fra/2)*tau)+s2.*cos(2*pi*(frb+fra/2)*tau);
    ca=ca-cos(pi*fra*tau);
    ca=2*ca;
      cb=c2.*cos(2*pi*(fra-frb/2)*tau)+s2.*cos(2*pi*(fra+frb/2)*tau);
    cb=cb-cos(pi*frb*tau);
    cb=2*cb;
      cp=-4*c2.*sin(pi*tau*fra).*sin(pi*tau*frb);
      cm=-4*s2.*sin(pi*tau*fra).*sin(pi*tau*frb);

    Ia=zeros(size(fr));
    Ib=zeros(size(fr));
    Iapb=zeros(size(fr));
    Iamb=zeros(size(fr));

    n=size(fra);

    for i=1:n(2),
       Ia(nfra(i))=Ia(nfra(i))-k(i)/2*probfr(i)*ca(i);
       Ib(nfrb(i))=Ib(nfrb(i))-k(i)/2*probfr(i)*cb(i);
       Iamb(nframb(i))=Iamb(nframb(i))-k(i)/2*probfr(i)*cm(i);
       Iapb(nfrapb(i))=Iapb(nfrapb(i))-k(i)/2*probfr(i)*cp(i);
```

```
end

Ia=abs(Ia);
Ib=abs(Ib);
Iamb=abs(Iamb);
Iapb=abs(Iapb);

% convolution

Ia=conv(gau,Ia);
Ib=conv(gau,Ib);
Iapb=conv(gau,Iapb);
Iamb=conv(gau,Iamb);

Itot=Ia+Ib+Iapb+Iamb;

% rearrange the intensity vector due to convolution

nn=size(gau);
n=size(fr);

  I=Itot((nn(2)-1)/2+1:(nn(2)-1)/2+n(2));
 imin=1;imax=n(2);

elseif iopt==10;

Ia=zeros(size(fr));
Ib=zeros(size(fr));
Iapb=zeros(size(fr));
Iamb=zeros(size(fr));

n=size(fra);

ca=ones(size(k));
cb=ones(size(k));
cm=ones(size(k));
cp=ones(size(k));

for i=1:n(2),
    Ia(nfra(i))=Ia(nfra(i))-k(i)/2*probfr(i)*ca(i);
    Ib(nfrb(i))=Ib(nfrb(i))-k(i)/2*probfr(i)*cb(i);
    Iamb(nframb(i))=Iamb(nframb(i))-k(i)/2*probfr(i)*cm(i);
    Iapb(nfrapb(i))=Iapb(nfrapb(i))-k(i)/2*probfr(i)*cp(i);
end

Ia=abs(Ia);
Ib=abs(Ib);
Iamb=abs(Iamb);
Iapb=abs(Iapb);

% convolution

Ia=conv(gau,Ia);
Ib=conv(gau,Ib);
Iapb=conv(gau,Iapb);
Iamb=conv(gau,Iamb);

Itot=Ia+Ib+Iapb+Iamb;

% rearrange the intensity vector due to convolution

nn=size(gau);
n=size(fr);
```

```
      I=Itot((nn(2)-1)/2+1:(nn(2)-1)/2+n(2));
      imin=1;imax=n(2);

    elseif iopt==11
      eseem(2)=eseem(2)*1e-6;
      eseem(3)=eseem(3)*1e8;
      eseem(4)=eseem(4)*180/pi;
      eseem(5)=eseem(5)*180/pi;
      eseopt=1;
    elseif iopt==12 print;
    elseif iopt==13 figure;
    elseif iopt==14,
      fprintf('\n');
      fprintf('vn/2 = %7.2f MHz : vn = %7.2f MHz',vn*1e-6/2,vn*1e-6);
      fprintf('\n');
    elseif iopt==15,
      tau=input('tau (nsec) : ');
      tau=tau*1e-9;

        ca=c2.*cos(2*pi*(frb-fra/2)*tau)+s2.*cos(2*pi*(frb+fra/2)*tau);
      ca=ca-cos(pi*fra*tau);
      ca=2*ca;
        cb=c2.*cos(2*pi*(fra-frb/2)*tau)+s2.*cos(2*pi*(fra+frb/2)*tau);
      cb=cb-cos(pi*frb*tau);
      cb=2*cb;
        cp=-4*c2.*sin(pi*tau*fra).*sin(pi*tau*frb);
        cm=-4*s2.*sin(pi*tau*fra).*sin(pi*tau*frb);

      Ia=zeros(size(fr));
      Ib=zeros(size(fr));
      Iapb=zeros(size(fr));
      Iamb=zeros(size(fr));

      n=size(fra);

      for i=1:n(2),
        Ia(nfra(i))=Ia(nfra(i))+ca(i);
        Ib(nfrb(i))=Ib(nfrb(i))+cb(i);
        Iamb(nframb(i))=Iamb(nframb(i))+cm(i);
        Iapb(nfrapb(i))=Iapb(nfrapb(i))+cp(i);
      end

      Ia=abs(Ia);
      Ib=abs(Ib);
      Iamb=abs(Iamb);
      Iapb=abs(Iapb);

      I=Ia+Ib+Iapb+Iamb;

      nn=[1 1];
      n=size(fr);
      imin=1;imax=n(2);

    elseif iopt==16 eseopt=2;
  end
  end

  return;


  %
  % fpfrsp.m - generates 4-pulse frequency domain spectrum
  %
```

```
global epr;

Acalc;

% calculation of the superhyperfine frequency on the selected angle set

dummy=0;
frcnt=0;
fr=-10:0.01:50;          % frequency domain vector
Ia=zeros(size(fr));      % intensity vectors
Ib=zeros(size(fr));
Iapb=zeros(size(fr));
Iamb=zeros(size(fr));

for mi=-epr(12):epr(12),

  dummy=dummy+1;

   for angi=1:nummi(dummy),

     % direction cosine vector of g-tensor to magnetic field

      theang=angset(angi,dummy*2-1);
      phiang=angset(angi,dummy*2);

       h1=[sin(theang)*cos(phiang) sin(theang)*sin(phiang) cos(theang)];
      gh1=epr(1:3).*h1;
      gh1eff=sqrt(gh1*gh1');
     gh1A=gh1*A;
      vn=762.2591*eseem(1)*epr(10);

     % for ms=1/2 spin manifold

      ghA1=0.5*gh1A/gh1eff-vn*h1;
     frcnt=frcnt+1;
     fra(frcnt)=sqrt(ghA1*ghA1');      % alpha hyperfine frequency

     % for ms=-1/2 spin manifold

      ghA1=-0.5*gh1A/gh1eff-vn*h1;
     frb(frcnt)=sqrt(ghA1*ghA1');      % beta hyperfine frequency

  end
end

% counter partner of angle set - gives same frequencies

% combination band freqency vector

frapb=fra+frb;
framb=abs(fra-frb);

% probability vector for corresponding  frequency vector

dummy=0;

for mi=-epr(12):epr(12),

  if dummy==0,
     ininum=1;
     finnum=nummi(1);
  else
     ininum=ininum+nummi(dummy);
     finnum=finnum+nummi(dummy+1);
```

```
  end

  dummy=dummy+1;

  if finnum ~ 0,
     probfr(ininum:finnum)=prob(1:nummi(dummy),dummy);
  end

end

% calcuation of k and C vectors

probfr=probfr/sum(probfr); % normalization of probability

s2=abs(vn^2-0.25*(fra+frb).^2)./(fra.*frb);
c2=1-s2;
k=4*s2.*c2;

ca=ones(size(k));
cb=ones(size(k));
cm=ones(size(k));
cp=ones(size(k));

% calculation of Intensity of each frequency

nfra=round((fra/2+10e6)*6000/60e6)+1;
nfrb=round((frb/2+10e6)*6000/60e6)+1;
nframb=round((framb/2+10e6)*6000/60e6)+1;
nfrapb=round((frapb/2+10e6)*6000/60e6)+1;

n=size(fra);

for i=1:n(2),
   Ia(nfra(i))=Ia(nfra(i))-k(i)/2*probfr(i)*ca(i);       % divide 2 instead of
   Ib(nfrb(i))=Ib(nfrb(i))-k(i)/2*probfr(i)*cb(i);       % 4 because half of
    Iamb(nframb(i))=Iamb(nframb(i))-k(i)/2*probfr(i)*cm(i); % anglse set is
    Iapb(nfrapb(i))=Iapb(nfrapb(i))-k(i)/2*probfr(i)*cp(i); % calculated
end

Ia=abs(Ia);
Ib=abs(Ib);
Iamb=abs(Iamb);
Iapb=abs(Iapb);

% convolution

Ia=conv(gau,Ia);
Ib=conv(gau,Ib);
Iapb=conv(gau,Iapb);
Iamb=conv(gau,Iamb);


Itot=Ia+Ib+Iapb+Iamb;

% rearrange the intensity vector due to convolution

nn=size(gau);
n=size(fr);

I=Itot((nn(2)-1)/2+1:(nn(2)-1)/2+n(2));

return;
```

```
%
% gaus.m - generate gaussian function for convolution
%

%width=0.01; % for delbb=0.03 MHz in two-pulse scale
%width=0.123; % for delbb=0.4 MHz in two-pulse scale
%width=0.06; % for delbb=0.2  MHz in two-pulse scale

frgau=-0.25:0.01:0.25;
gau=exp(-frgau.^2/width^2);
gau=gau/sum(gau);

%plot(frgau,gau);
%grid

return;
```